

Electronic Thesis and Dissertation Repository

---

8-29-2016 12:00 AM

## Removal of Target PPCPs from Secondary Effluent Using AOPs and Novel Adsorbents

Venkateswara Reddy Kandlakuti  
*The University of Western Ontario*

Supervisor

Dr. Ernest K. Yanful  
*The University of Western Ontario*

Graduate Program in Civil and Environmental Engineering

A thesis submitted in partial fulfillment of the requirements for the degree in Doctor of Philosophy

© Venkateswara Reddy Kandlakuti 2016

Follow this and additional works at: <https://ir.lib.uwo.ca/etd>



Part of the [Environmental Engineering Commons](#)

---

### Recommended Citation

Kandlakuti, Venkateswara Reddy, "Removal of Target PPCPs from Secondary Effluent Using AOPs and Novel Adsorbents" (2016). *Electronic Thesis and Dissertation Repository*. 4090.

<https://ir.lib.uwo.ca/etd/4090>

This Dissertation/Thesis is brought to you for free and open access by Scholarship@Western. It has been accepted for inclusion in Electronic Thesis and Dissertation Repository by an authorized administrator of Scholarship@Western. For more information, please contact [wlsadmin@uwo.ca](mailto:wlsadmin@uwo.ca).

## Abstract

Atenolol ( $\beta$ -blocker), Clofibric Acid (Lipid regulators) and Diclofenac (Anti-inflammatory) are the drugs widely used and reported to have adverse effects on fish and other organisms. These drugs are found at trace levels in lakes, rivers, ground water and sewage treatment plants and conventional treatment plants are ineffective to eliminate these at those levels. A high resolution LC-MS/MS was used to quantify these drugs at low levels. Various advanced oxidation methods were used for the present research to eliminate these drugs from secondary effluent. Complete removal of selected PPCPs was achieved by synthesizing immobilized  $\text{TiO}_2$  on a stainless steel mesh and using a combination of  $\text{O}_3/\text{UV}/\text{TiO}_2$  a very powerful technique. Although individual advanced oxidation process or a combination of two AOPs were able to remove it to a lesser extent.  $\text{In}_2\text{O}_3$  porous microspheres, nanocubes, nanoplates and nano crystals were synthesized and used for treatment of secondary effluent. Results have shown that the complete removal of PPCPs was achieved in shorter duration in comparison to the various AOPs using  $\text{TiO}_2$ . Out of these four  $\text{In}_2\text{O}_3$  nano materials, porous microspheres exhibited higher activity compared to other nano materials. A deciduous wood biomass was subjected to slow pyrolysis at a rate of  $7^\circ\text{C}/\text{min}$  in the absence of oxygen to  $700^\circ\text{C}$  leading to the formation of biochar (BC). The produced biochar had increased surface area and micro porosity. Batch sorption studies were conducted using biochar, natural zeolite (Chabazite) and chemically activated biochar. It was observed that chemically activated biochar was highly efficient followed by biochar.

## Keywords

Wastewater, biochar, advanced oxidation process, adsorption, degradation rate, photodegradation

## Co-Authorship

Title: Preparation and characterization of homogeneous immobilized TiO<sub>2</sub> coatings on stainless steel mesh and its removal kinetics of PPCPs from wastewater by a combination of AOPs (O<sub>3</sub>/UV/TiO<sub>2</sub>) and its comparison with other techniques

Author: V.R. Kandlakuti

All literature survey was done by V.R. Kandlakuti under the guidance of advisor E.K. Yanful. All drafts of the manuscripts were written by V.R. Kandlakuti. Modification of the drafts was undertaken under the close supervision of thesis advisor E.K. Yanful.

Title: Preparation of Indium Oxide nanocubes, porous microspheres, nanoplates and nanocrystals, its characterization and application in degradation of PPCPs from wastewater

Author: V.R. Kandlakuti

All portions of experimental work and data analysis were undertaken by V.R. Kandlakuti under the guidance of advisor E.K. Yanful. All drafts of the manuscripts were written by V.R. Kandlakuti. Modification of the drafts was undertaken under the close supervision of thesis advisor E.K. Yanful.

Title: Preparation of Biochar, its characterization and application in removal of PPCPs from wastewater with comparison to natural zeolites

Author: V.R. Kandlakuti

All portions of experimental work and data analysis were undertaken by V.R. Kandlakuti under the guidance of advisor E.K. Yanful. All drafts of the manuscripts were written by V.R. Kandlakuti. Modification of the drafts was undertaken under the close supervision of thesis advisor E.K. Yanful.

## Acknowledgments

First of all, I want to thank almighty god for giving me strength and ability to successfully complete this work.

I would like to express my deep sense of gratitude to my supervisor, Professor Ernest K. Yanful for providing me the opportunity to work with him and whose encouragement, guidance, and support enabled me to develop an understanding of the subject. His wide knowledge and his logical way of thinking have been of great value for me and provided a good basis for the present thesis.

I am grateful to Dr. Mita Ray, Professor, Department of Chemical and Biochemical Engineering for providing lab facilities to conduct my research. I would also like to thank Professor and TWNER Program Director, Dr. George Nakhla, The Clean Technologies for Water Refining and Nutrient and Energy Recovery with Collaborative Research and Training Experience Program (TWNER - CREATE) sponsored by Natural Sciences and Engineering Research Council (NSERC).

I am sincerely grateful to the professors, technicians, and administrative assistants of the Department of Civil and Environmental Engineering and the Geotechnical Research Center at Western University for their support and help. The support of administrative and technical staffs Connie Walter, Cynthia Quintus, Stephanie Laurence, Kristen Edwards, Joanna Bloom, Tim Stephens, Caitlin Marshall, Fate Hashemi, Erol Tas, Souheil Afara, Brian Dennis, Mike Gaylard and Mike Mosley is highly appreciated. The valuable help of University Machine Services staff, Electronic Stores staff, Surface Science Western and Nano Fab is gratefully acknowledged.

I greatly acknowledge the enormous help and support from my friends and colleagues Sudhakar Yadlapalli, Dr. P. Venkateswarlu, Dr. Sidda Reddy Boyilla and their technical team who provided excellent services at FirstSource Laboratory Solution LLP, Anil Kumar Jhavar, Diego Velasquez, Amro Miqdadi, Ikrema Hassan, Kai Pisters, Elsayed Elbeshbishy and Saad Aldin at the University of Western Ontario and

Sudhakar Mamillapalli, Gopi Kiran Morla, Mahendra Reddy Thimmanagari, Murali Jupalli, Rama Rao Varanasi, Dr. Tad Venkateswarlu (Emeritus Professor), Dr. Sunil Parapuram, Sharath Bojja and Sashi Kiran who have all assisted me in various ways and I am sincerely grateful for their continued and untiring support during tough times.

In the last but not least, I owe my loving thanks to my parents, my wife Bhavani, my adorable kids Bhargav and Haran and other family members. Without their encouragement and understanding it would have been impossible for me to finish this work.

Dedication

To my beloved mother (late)

# Table of Contents

|   |      |
|---|------|
| Abstract.....   | ii   |
| Co-Authorship.....  | iii  |
| Acknowledgments.....  | iv   |
| Dedication.....   | vi   |
| Table of Contents.....                                      | vii  |
| List of Tables.....   | xiii |
| List of Appendices.....                                     | xxiv |
| Nomenclature.....   | xxvi |
| Chapter 1.....  | 1    |
| 1 Introduction.....   | 1    |
| 1.1 Background.....   | 1    |
| 1.2 Objectives of the study.....                            | 4    |
| 1.3 Contribution of the thesis.....                         | 5    |
| 1.4 Organization of the thesis.....                         | 5    |
| 1.5 References.....   | 7    |
| Chapter 2.....  | 10   |
| 2 Literature review.....                                    | 10   |
| 2.1 Introduction.....                                       | 10   |
| 2.1.1 Sources of PPCPs in the environment.....              | 10   |
| 2.1.2 Pathways of pharmaceuticals in the environment.....   | 12   |
| 2.1.3 Classification of PPCPs.....                          | 13   |
| 2.1.4 Fate of Pharmaceuticals in the environment.....       | 14   |
| 2.1.5 Occurrence of Pharmaceuticals in the environment..... | 15   |
| 2.1.6 Environmental Risk Assessment.....                    | 18   |

|           |   |    |
|-----------|---|----|
| 2.1.7     | Natural Organic Matter and Brominated species in natural waters .....   | 20 |
| 2.1.8     | Stages of a Wastewater Treatment Plant .....  | 21 |
| 2.1.9     | Comparison of various treatment technologies and percent removal of target PPCPs.....   | 24 |
| 2.1.10    | Physico-chemical properties of target PPCP compounds.....   | 28 |
| 2.2       | Advanced Oxidation Processes.....   | 34 |
| 2.2.1     | Advanced Oxidation Methods .....  | 35 |
| 2.2.1.1   | Ozonation .....   | 37 |
| 2.2.1.2   | UV .....  | 41 |
| 2.2.1.3   | Photocatalytic Metal Oxide (TiO <sub>2</sub> ).....   | 42 |
| 2.2.1.4   | Ozone–UV radiation (O <sub>3</sub> /UV).....  | 46 |
| 2.2.1.5   | Photocatalytic oxidation (UV/TiO <sub>2</sub> ).....  | 48 |
| 2.2.1.6   | Ozone + Catalyst (O <sub>3</sub> /TiO <sub>2</sub> ).....   | 50 |
| 2.2.1.7   | Hydrogen Peroxide (H <sub>2</sub> O <sub>2</sub> ).....   | 50 |
| 2.3       | Comparative operating costs of treatment for various AOPs .....   | 52 |
| 2.4       | Indium Oxide nano materials.....  | 53 |
| 2.5       | Biochar (BC).....   | 56 |
| 2.6       | References.....   | 61 |
| Chapter 3 | .....   | 80 |
| 3         | Preparation and characterization of homogeneous immobilized TiO <sub>2</sub> coatings on stainless steel mesh and its removal kinetics of PPCPs from wastewater by a combination of AOP (O <sub>3</sub> /UV/TiO <sub>2</sub> ) and its comparison with other techniques ..... | 80 |
| 3.1       | Introduction.....   | 80 |
| 3.2       | Materials and Methods.....  | 83 |
| 3.2.1     | Reagents and chemicals .....  | 83 |
| 3.2.2     | Raw water quality .....   | 85 |
| 3.2.3     | Sampling site and collection .....  | 85 |



|                |  |     |
|----------------|--|-----|
| 3.2.4          | Homogeneous Immobilized TiO <sub>2</sub> catalyst preparation on Stainless Steel mesh using Dip-Coat method.....   | 86  |
| 3.2.5          | Characterization of Immobilized TiO <sub>2</sub> Catalyst .....  | 87  |
| 3.2.6          | Experimental protocol.....   | 90  |
| 3.2.6.1        | Experiments conducted with wastewater samples .....  | 90  |
| 3.2.6.2        | Reactor setup .....  | 91  |
| 3.3            | PPCP method setup by LC-MS/MS (High Resolution).....   | 94  |
| 3.4            | PPCP analysis in wastewater samples .....  | 99  |
| 3.5            | Results and Discussion .....   | 99  |
| 3.5.1          | Effect of TiO <sub>2</sub> loading.....  | 100 |
| 3.5.2          | Effect of AOP .....  | 104 |
| 3.5.3          | Effect of pH.....  | 111 |
| 3.5.4          | Effect of Natural Organic Matter and Bromine .....   | 117 |
| 3.5.5          | Identification of UV-transformation products .....   | 123 |
| 3.5.5.1        | Degradation products of Atenolol .....   | 123 |
| 3.5.5.2        | Degradation products of Clofibric acid .....   | 129 |
| 3.5.5.3        | Degradation products of Diclofenac.....  | 131 |
| 3.6            | Conclusions.....   | 133 |
| 3.7            | References.....  | 134 |
| Chapter 4..... |  | 140 |
| 4              | Preparation of Indium Oxide nanocubes, porous microspheres, nanoplates and nanocrystals, its characterization and application in degradation of PPCPs from wastewater..... | 140 |
| 4.1            | Introduction.....  | 140 |
| 4.2            | Materials and Methods.....   | 144 |
| 4.2.1          | Reagents and chemicals .....   | 144 |
| 4.2.2          | Experimental Methodology .....   | 144 |

|           |   |     |
|-----------|---|-----|
| 4.2.2.1   | Synthesis of $\text{In}_2\text{O}_3$ from $\text{In}(\text{NO}_3)_3 \cdot 4.5\text{H}_2\text{O}$ via $\text{In}(\text{OH})_3$ by Solvothermal process.....  | 145 |
| 4.2.2.2   | Formation of $\text{In}_2\text{O}_3$ nanocubes, nanoplates and porous microspheres.....   | 146 |
| 4.2.2.3   | Preparation of $\text{In}_2\text{O}_3$ nanocrystals from $\text{In}(\text{NO}_3)_3 \cdot 4.5\text{H}_2\text{O}$ by a simple co-precipitation method .....   | 148 |
| 4.2.2.4   | Characterization.....   | 149 |
| 4.2.2.5   | Photocatalytic procedures.....  | 150 |
| 4.2.2.6   | Quantification of PPCPs by LC-MS/MS.....  | 151 |
| 4.3       | Results and discussion .....  | 152 |
| 4.3.1     | Morphology and crystal structure of calcined $\text{In}_2\text{O}_3$ samples.....   | 152 |
| 4.3.2     | FTIR spectra of calcined and AOP treated samples .....  | 155 |
| 4.3.3     | Energy Dispersive X-ray (EDX) Spectroscopy .....  | 162 |
| 4.3.4     | Decomposition of PPCPs using various photocatalytic $\text{In}_2\text{O}_3$ nano particles.....   | 167 |
| 4.3.5     | Comparison of photocatalytic decomposition between distilled water and secondary effluent at pH 7 .....   | 171 |
| 4.3.6     | Effect of pH.....   | 173 |
| 4.3.7     | Comparison of various $\text{In}_2\text{O}_3$ nano structures with AOPs .....   | 177 |
| 4.4       | Conclusion .....  | 182 |
| 4.5       | References.....   | 183 |
| Chapter 5 | .....   | 187 |
| 5         | Preparation and characterization of Biochar and its application in the removal of PPCPs from wastewater and comparison to removals by natural zeolites..... | 187 |
| 5.1       | Introduction.....   | 187 |
| 5.2       | Experimental Methods .....  | 195 |
| 5.2.1     | Materials and Reagents.....   | 195 |
| 5.2.2     | Synthesis of biochar.....   | 195 |

|           |   |     |
|-----------|---|-----|
| 5.2.3     | Characterization .....                                  | 197 |
| 5.2.4     | Wastewater collection.....                              | 201 |
| 5.2.5     | Sorption studies on biochar.....                        | 202 |
| 5.2.6     | Use of Natural Zeolite for adsorption studies.....      | 203 |
| 5.2.7     | Use of Activated Carbon for comparison studies .....    | 203 |
| 5.2.8     | Pre-conditioning of Biochar with 0.1N NaCl .....        | 203 |
| 5.2.9     | Chemical Activation of Biochar using KOH .....          | 203 |
| 5.2.10    | Quantification of PPCPs by LC-MS/MS .....               | 204 |
| 5.2.11    | Adsorption models .....                                 | 204 |
| 5.3       | Results and Discussion .....                            | 206 |
| 5.3.1     | Morphology and structure of BC samples by FE-SEM.....   | 206 |
| 5.3.2     | Energy Dispersive X-ray (FE-SEM/EDX) Spectroscopy.....  | 208 |
| 5.3.3     | FTIR spectra of BC samples .....                        | 210 |
| 5.3.4     | <sup>13</sup> C NMR spectra of BC samples.....          | 213 |
| 5.3.5     | CHNS analysis of BC samples .....                       | 214 |
| 5.3.6     | BET analysis of BC samples.....                         | 215 |
| 5.3.7     | Adsorption of target PPCPs compounds.....               | 215 |
| 5.3.7.1   | Effect of pH on biochar .....                           | 216 |
| 5.3.7.1.1 | Effect of pH at constant PPCP concentration of 10ppm    | 216 |
| 5.3.7.1.2 | Effect of pH at constant PPCP concentration of 20ppm    | 219 |
| 5.3.7.1.3 | Effect of pH at constant PPCP concentration of 30ppm    | 221 |
| 5.3.7.2   | Effect of pH on biochar : Chb .....                     | 224 |
| 5.3.7.3   | Effect of PPCPs concentration at constant pH 9.0 .....  | 227 |
| 5.3.7.4   | Effect of Pre-conditioning on Sorbent Performance ..... | 229 |
| 5.3.7.5   | Effect of Chemical conditioning .....                   | 231 |

|  |     |
|--|-----|
| 5.3.8 Comparison of various adsorption methods with varying pH ..... | 232 |
| 5.3.9 Isotherms.....   | 237 |
| 5.4 Conclusions.....   | 244 |
| 5.5 References.....  | 245 |
| Chapter 6.....   | 259 |
| 6 Conclusions and Recommendations .....                              | 259 |
| 6.1 Conclusions.....   | 259 |
| 6.2 Recommendations.....   | 261 |
| Appendices.....  | 263 |
| Curriculum Vitae .....   | 274 |

## List of Tables

|   |    |
|---|----|
| Table 2.1. Concentrations of Pharmaceuticals in Sludges, Biosolids and Groundwater, reported in the literature since 2004.....                                      | 16 |
| Table 2.2. Concentration of Pharmaceuticals in Wastewater Influent, Effluents and Surface Water, reported in the literature since 2004.....                         | 16 |
| Table 2.3. Comparison of various treatment technologies and their removal efficiency from various types of water matrices for the three target PPCP compounds ..... | 25 |
| Table 2.4. Test compounds with its IUPAC names and chemical structure.....  | 28 |
| Table 2.5. Physico-chemical properties of test compounds.....   | 29 |
| Table 2.6. Uses, toxicity and byproduct/degradation products for test compounds .....   | 30 |
| Table 2.7. Log Kow versus Sorption Potential .....  | 32 |
| Table 2.8. Some oxidizing species with their relative oxidation power (Carey, 1992 and Techcommentary, 1996) .....  | 33 |
| Table 2.9. Organic compounds with reaction rate constants of ozone vs. hydroxyl radical (The UV/Oxidation Handbook) .....   | 34 |
| Table 2.10. Photolysis of ozone and H <sub>2</sub> O <sub>2</sub> leading to the formation of ·OH (Techcommentary, 1996).....                                       | 47 |
| Table 2.11. Comparative operating costs of some AOPs ((Techcommentary, 1996). ....  | 52 |
| Table 2.12. Operating costs of advanced oxidation processes <sup>a</sup> (Yonar et al., 2005). ....   | 52 |
| Table 3.1. Physico-Chemical properties of ATN, CFA and DCF .....  | 82 |
| Table 3.2: Properties of TiO <sub>2</sub> powder as per manufacturer .....  | 84 |
| Table 3.3: Semi-quantitative EDX Results for TiO <sub>2</sub> .....   | 90 |

|   |     |
|---|-----|
| Table 3.4: Water quality parameters of secondary effluent .....   | 91  |
| Table 3.5: Gradient program for LC-MS/MS .....  | 97  |
| Table 3.6: Source parameters for LC-MS/MS .....   | 97  |
| Table 3.7: Multiple Reaction Monitoring parameters for LC-MS/MS .....   | 98  |
| Table 3.8: Effect of TiO <sub>2</sub> loadings of ATN, CFA and DCF in SE [rate constant k and correlation coefficient R <sup>2</sup> , Co = 10mg/L, UV = 13W, O <sub>3</sub> = 2mg/L, pH = 7, T = 23 ± 1°C] .....   | 103 |
| Table 3.9: Comparison of various AOPs with their degradation parameters (rate constant k and correlation coefficient R <sup>2</sup> ) of ATN, CFA and DCF in SE [Co = 10mg/L, TiO <sub>2</sub> = 1g/m <sup>2</sup> , UV = 13W, O <sub>3</sub> = 2mg/L, pH = 7.0, T = 23 ± 1°C]..... | 110 |
| Table 3.10: Comparison of various AOPs with pH (rate constant k and correlation coefficient R <sup>2</sup> ) of ATN in SE [Co = 10 mg/L, TiO <sub>2</sub> = 1 g/m <sup>2</sup> , UV = 13W, O <sub>3</sub> = 2 mg/L, T = 23 ± 1°C] .....   | 115 |
| Table 3.11: Comparison of various AOPs on degradation of PPCPs in presence of varying concentrations of NOM and Br with their k and R <sup>2</sup> values .....   | 119 |
| Table 4.1. Comparison of various types of In <sub>2</sub> O <sub>3</sub> nanostructures produced by different methods comprising of all three phases, namely, the solution, solid and vapor phase and their properties .....  | 142 |
| Table 4.2. Characterization of various types of In <sub>2</sub> O <sub>3</sub> using various equipment types  | 149 |
| Table 4.3. Comparison of FTIR spectra of microsphere peaks with literature values (Tom Tague). .....  | 158 |
| Table 4.4. Comparison of FTIR spectra of nano cube peaks with literature values (Tom Tague). .....  | 159 |
| Table 4.5. Comparison of FTIR spectra of nano plate peaks with literature values (Tom Tague). .....   | 160 |

|   |     |
|---|-----|
| Table 4.6. Comparison of FTIR spectra of nano crystal peaks with literature values (Tom Tague). .....   | 161 |
| Table 4.7. EDX results in duplicate for In <sub>2</sub> O <sub>3</sub> microspheres after calcination. ....   | 163 |
| Table 4.8. EDX results in duplicate for In <sub>2</sub> O <sub>3</sub> nano plates after calcination .....  | 164 |
| Table 4.9. EDX results in duplicate for In <sub>2</sub> O <sub>3</sub> nano cubes after calcination.....  | 165 |
| Table 4.10. EDX results in duplicate for In <sub>2</sub> O <sub>3</sub> nano crystals after calcination.....  | 166 |
| Table 4.11. Rate constants (k, min <sup>-1</sup> ) of various nano particles with their correlation coefficient (R <sup>2</sup> ) values for ATN, CFA and DCF for SE.....                     | 171 |
| Table 4.12. Rate constants (k, min <sup>-1</sup> ) of various AOPs with their correlation coefficient (R <sup>2</sup> ) values for ATN, CFA and DCF for SE (Chapter 3. V.R. Kandlakuti). .... | 180 |
| Table 5.1. Physico-chemical properties of the selected PPCPs .....  | 198 |
| Table 5.2. Physical properties of the tested Natural Zeolites (Gallant et al., 2009) .....  | 201 |
| Table 5.3. EDX spectroscopy results of three spots scanned on the BC sample at 10kV .....   | 209 |
| Table 5.4. FTIR spectra of BC peaks with literature values (Tom Tague).....   | 211 |
| Table 5.5. CHNS results of biochar analyzed by CHNS analyzer.....   | 214 |
| Table 5.6. Freundlich and Langmuir isotherm constants for ATN adsorption onto BC with their correlation coefficient, R <sup>2</sup> at different dosages .....                                | 242 |
| Table 5.7. Freundlich and Langmuir isotherm constants for CFA adsorption onto BC with their correlation coefficient, R <sup>2</sup> at different dosages .....                                | 243 |
| Table 5.8. Freundlich and Langmuir isotherm constants for DCF adsorption onto BC with their correlation coefficient, R <sup>2</sup> at different dosages .....                                | 243 |

## List of Figures

|  |    |
|--|----|
| Figure 2.1. Occurrence of pharmaceutical and its metabolite residues showing possible sources and pathways in the aquatic environment (Heberer and Adam, 2002a). Residues of animal excretions reaching surface waters or municipal STPs are represented by astrick..... | 13 |
| Figure 2.2. Physical processes that affect the environmental concentrations of PPCPs (Meade H. R., 1995, U.S. Geological Survey Circular 1133, p. 114-135).....  | 15 |
| Figure 2.3. Various stages of a conventional wastewater treatment plant (Sherry S., and Karl A., 2006) .....   | 22 |
| Figure 2.4. Adelaide wastewater treatment plant, London, ON, Canada .....  | 23 |
| Figure 2.5. Classification of Advanced Oxidation Processes into Homogeneous and Heterogeneous Processes (Poyatos et al., 2009).....  | 36 |
| Figure 2.6. Ozone production from corona-discharge (Oxidation technologies, 2014) .....  | 38 |
| Figure 2.7. Reactions of ozone and dissolved solids * .....  | 39 |
| Figure 2.8. Double-layer model for ozone mass transfer (ESCO International) .....  | 40 |
| Figure 2.9. Schematic diagram of an irradiated TiO <sub>2</sub> semiconductor particle with photo-physical and photo-chemical process (Giwa et al., 2012) .....  | 43 |
| Figure 2.10. Schematic illustrations in the dark and under UV light irradiation on TiO <sub>2</sub> film showing reversible changes in amount of hydroxyl groups (Sakai et al., 2003).....   | 45 |
| Figure 2.11. Ozone dissociation with UV irradiation (Spartan Environmental Technologies, 2014).....  | 47 |
| Figure 2.12. Photocatalytic oxidation process (Conee Orsal, 2015).....   | 49 |
| Figure 2.13. Crystalline In <sub>2</sub> O <sub>3</sub> – Bixbyite structure (Buchholz et al., 2014) .....   | 54 |



|  |     |
|--|-----|
| Figure 2.14. Schematic for solution-processed In <sub>2</sub> O <sub>3</sub> thin-films by a hydroxyl radical-assisted (HRA) method (Sabri et al., 2015) .....                             | 55  |
| Figure 2.15. Schematic illustrations showing metastable states induced by the hydroxyl-radical assisted oxidation (Sabri et al., 2015). .....  | 56  |
| Figure 2.16. Production and application of biochar for wastewater treatment as an effective adsorbent (Tan, X. et al., 2015). .....  | 57  |
| Figure 2.17. Summarized adsorption mechanisms proposed on biochars by heavy metals (Tan, X. et al., 2015).....   | 58  |
| Figure 2.18. Summarized adsorption mechanisms proposed on biochars by organic contaminants (Tan, X. et al., 2015).....   | 60  |
| Figure 3.1. Chemical structures of target Pharmaceuticals (ChemIDplus, 2014) .....   | 83  |
| Figure 3.2. Dip coatings of homogeneous immobilized 2%, 4% and 20% of Degussa P25 TiO <sub>2</sub> supported on SS plates .....  | 86  |
| Figure 3.3. SEM image of dried film at 10kV .....  | 88  |
| Figure 3.4. EDX spectroscopy of dried film at 10kV .....   | 88  |
| Figure 3.5. SEM image of calcined TiO <sub>2</sub> film at 10kV .....  | 89  |
| Figure 3.6 EDX spectroscopy of calcined TiO <sub>2</sub> film at 10kV .....  | 89  |
| Figure 3.7. Experimental Reactor Setup for AOP .....   | 93  |
| Figure 3.8. Mechanism of ion formation in Turbo V <sup>TM</sup> ESI ion source equipped with QTRAP before entering LC-MS/MS region (Mohamad, A., 2010 and AB Sciex, Ontario, Canada) ..... | 96  |
| Figure 3.9. Effect of catalyst loading on SE (a) ATN (b) CFA and (c) DCF [Co = 10mg/L each, O <sub>3</sub> = 2ppm, UV = 13W, pH = 7.0, T = 23 ± 1°C].....                                  | 102 |

|  |     |
|--|-----|
| Figure 3.10. Effect of different oxidation process on relative concentration profiles (a) ATN (b) CFA and (c) DCF [Co = 10mg/L, TiO <sub>2</sub> = 1g/m <sup>2</sup> , pH = 7.0, T = 23 ± 1°C] ...   | 106 |
| Figure 3.11. Percent Reduction under influence of various AOPs a) ATN, b) CFA and c) DCF [Co = 10mg/L, O <sub>3</sub> = 2mg/L, UV = 13W, TiO <sub>2</sub> = 1g/m <sup>2</sup> , pH = 7.0, T = 23 ± 1°C] .....  | 108 |
| Figure 3.12. Relative concentration profiles with various AOPs a) ATN, b) CFA and c) DCF [Co = 10mg/L, O <sub>3</sub> = 2mg/L, UV = 13W, TiO <sub>2</sub> = 1g/m <sup>2</sup> , pH = 7.0, T = 23 ± 1°C]  | 110 |
| Figure 3.13. Relative concentration profiles of pH on ATN (a) UV/TiO <sub>2</sub> (b) O <sub>3</sub> /TiO <sub>2</sub> and (c) O <sub>3</sub> /UV/TiO <sub>2</sub> [Co = 10mg/L, TiO <sub>2</sub> = 1g/m <sup>2</sup> , O <sub>3</sub> = 2 mg/L, UV = 13W, T = 23 ± 1°C] .....   | 112 |
| Figure 3.14. Percent removal of ATN at varying pH (a) UV/TiO <sub>2</sub> (b) O <sub>3</sub> /TiO <sub>2</sub> and (c) O <sub>3</sub> /UV/TiO <sub>2</sub> [Co = 10mg/L, TiO <sub>2</sub> = 1g/m <sup>2</sup> , O <sub>3</sub> = 2mg/L, UV = 13W, T = 23 ± 1°C] ..   | 115 |
| Figure 3.15. Relative concentration of ATN at varying pH (a) UV/TiO <sub>2</sub> (b) O <sub>3</sub> /TiO <sub>2</sub> and (c) O <sub>3</sub> /UV/TiO <sub>2</sub> [Co = 10mg/L, TiO <sub>2</sub> = 1g/m <sup>2</sup> , O <sub>3</sub> = 2mg/L, UV = 13W, T = 23 ± 1°C] .....   | 117 |
| Figure 3.16. Effect of varying concentrations of NOM and Br on ATN, CFA and DCF a) UV/TiO <sub>2</sub> (b) O <sub>3</sub> /TiO <sub>2</sub> and (c) O <sub>3</sub> /UV/TiO <sub>2</sub> [Co = 10mg/L, TiO <sub>2</sub> = 1g/m <sup>2</sup> , O <sub>3</sub> = 2 mg/L, UV = 13W, T = 23 ± 1°C] .....  | 121 |
| Figure 3.17. Determination of rate constant k, min <sup>-1</sup> at varying concentrations of NOM and Br on ATN, CFA and DCF using UV/TiO <sub>2</sub> (b) O <sub>3</sub> /TiO <sub>2</sub> and (c) O <sub>3</sub> /UV/TiO <sub>2</sub> [Co = 10mg/L, TiO <sub>2</sub> = 1g/m <sup>2</sup> , O <sub>3</sub> = 2 mg/L, UV = 13W, T = 23 ± 1°C]. ..... | 122 |
| Figure 3.18. (a) to (m) Spectrum of ATN and its transformation products by MS/MS with its proposed structure and molecular ion [M+H] <sup>+</sup> .....  | 129 |
| Figure 3.19. Various oxidative and reductive pathways for degradation of CFA .....   | 130 |
| Figure 3.20. (a) and (b) Spectrum of DCF and its transformation products by MS/MS with its proposed structure and molecular ion [M+H] <sup>+</sup> .....   | 132 |

|   |     |
|---|-----|
| Figure 4.1. Stainless steel autoclave used to synthesize nanocubes, nanoplates and porous microspheres in Parr reactor at $180^{\circ}\text{C} \pm 2^{\circ}\text{C}$ for 16h .....               | 145 |
| Figure 4.2. Precipitates of 1) porous microspheres (MS) 2) nanocubes (NC) and 3) nanoplates (NP), obtained after autoclaving in Parr reactor at $180^{\circ}\text{C} \pm 1^{\circ}\text{C}$ ..... | 146 |
| Figure 4.3. Formation of $\text{In}_2\text{O}_3$ after calcination at $500^{\circ}\text{C}$ for 2h producing 1) MS, 2) NC and 3) NP.....  | 147 |
| Figure 4.4. White precipitate of $\text{In}(\text{NO}_3)_3 \cdot 4.5\text{H}_2\text{O}$ after co-precipitation followed by drying at $80^{\circ}\text{C}$ for 24h.....                            | 148 |
| Figure 4.5. Yellow $\text{In}_2\text{O}_3$ nanocrystals obtained after calcination at $400^{\circ}\text{C}$ for 2h. ....  | 149 |
| Figure 4.6. (a, b, c and d). Leo (Zeiss) 1540XB FIB/SEM images of microspheres....  | 152 |
| Figure 4.7. (a and b). Leo (Zeiss) 1540XB FIB/SEM images of nano cubes at 1kV ...   | 153 |
| Figure 4.8. (a and b). Leo (Zeiss) 1540XB FIB/SEM images of nano plates.....  | 154 |
| Figure 4.9. (a, b, c and d) Leo (Zeiss) 1540XB FIB/SEM images of nano crystals .....  | 154 |
| Figure 4.10. FTIR spectra of $\text{In}_2\text{O}_3$ microspheres calcined at $500^{\circ}\text{C}$ for 2h (a) before AOP treatment and (b) after AOP treatment of PPCPs. ....                    | 155 |
| Figure 4.11. FTIR spectra of $\text{In}_2\text{O}_3$ nano cubes calcined at $500^{\circ}\text{C}$ for 2h (a) before AOP treatment and (b) after AOP treatment of PPCPs. ....                      | 156 |
| Figure 4.12. FTIR spectra of $\text{In}_2\text{O}_3$ nano plates calcined at $500^{\circ}\text{C}$ for 2h (a) before AOP treatment and (b) after AOP treatment of PPCPs. ....                     | 157 |
| Figure 4.13. FTIR spectra of $\text{In}_2\text{O}_3$ nano crystals calcined at $400^{\circ}\text{C}$ for 2h (a) before AOP treatment and (b) after AOP treatment of PPCPs. ....                   | 157 |
| Figure 4.14. Spot EDX spectra of $\text{In}_2\text{O}_3$ microspheres calcined at $500^{\circ}\text{C}$ for 2h.....   | 162 |
| Figure 4.15. Spot EDX spectra of $\text{In}_2\text{O}_3$ nano plates calcined at $500^{\circ}\text{C}$ for 2h .....   | 164 |

|  |     |
|--|-----|
| Figure 4.16. Spot EDX spectra of In <sub>2</sub> O <sub>3</sub> nano cubes calcined at 500°C for 2h .....  | 165 |
| Figure 4.17. Spot EDX spectra of In <sub>2</sub> O <sub>3</sub> nano crystals calcined at 400°C for 2h .....   | 166 |
| Figure 4.18. Photocatalytic decomposition of ATN, CFA and DCF by In <sub>2</sub> O <sub>3</sub> microsphere at pH 7 for SE at 23 ± 1°C (a) C/Co (b) % Reduction and (c) ln Co/C .  | 167 |
| Figure 4.19. Photocatalytic decomposition of ATN, CFA and DCF by In <sub>2</sub> O <sub>3</sub> nano plates at pH 7 for SE at 23 ± 1°C (a) C/Co (b) % Reduction and (c) ln Co/C .....  | 168 |
| Figure 4.20. Photocatalytic decomposition of ATN, CFA and DCF by In <sub>2</sub> O <sub>3</sub> nano cubes at pH 7 for SE at 23 ± 1°C (a) C/Co (b) % Reduction and (c) ln Co/C .....   | 169 |
| Figure 4.21. Photocatalytic decomposition of ATN, CFA and DCF by In <sub>2</sub> O <sub>3</sub> nano crystals at pH 7 for SE at 23 ± 1°C (a) C/Co (b) % Reduction and (c) ln Co/C .....  | 170 |
| Figure 4.22. A comparison of photocatalytic decomposition of ATN, CFA and DCF by In <sub>2</sub> O <sub>3</sub> NCY at pH 7, 23 ± 1°C between DW and SE.....   | 172 |
| Figure 4.23. Percent reduction of ATN, CFA and DCF by In <sub>2</sub> O <sub>3</sub> NCY at pH 7, 23 ± 1°C between DW and SE .....   | 172 |
| Figure 4.24. Percent reduction of ATN by NCY on SE at pH 3, 5 and 7 .....  | 173 |
| Figure 4.25. Percent reduction of CFA by NCY on SE at pH 3, 5 and 7 .....  | 174 |
| Figure 4.26. Percent reduction of DCF by NCY on SE at pH 3, 5 and 7 .....  | 174 |
| Figure 4.27. Rate constants of ATN, CFA and DCF by NCY on SE at pH 3 .....   | 175 |
| Figure 4.28. Rate constants of ATN, CFA and DCF by NCY on SE at pH 5 .....   | 176 |
| Figure 4.29. Rate constants of ATN, CFA and DCF by NCY on SE at pH 7 .....   | 176 |
| Figure 4.30. Comparison of photocatalytic decomposition of MS, NP, NC and NCY In <sub>2</sub> O <sub>3</sub> versus UV/TiO <sub>2</sub> , O <sub>3</sub> /TiO <sub>2</sub> and O <sub>3</sub> /UV/TiO <sub>2</sub> for SE at pH = 7, T = 23 ± 1°C (a) ATN (b) CFA and (c) DCF..... | 178 |

|  |     |
|--|-----|
| Figure 4.31. Comparison of removal efficiency of MS, NP, NC and NCY In <sub>2</sub> O <sub>3</sub> versus UV/TiO <sub>2</sub> , O <sub>3</sub> /TiO <sub>2</sub> and O <sub>3</sub> /UV/TiO <sub>2</sub> for SE at pH = 7, T = 23 ± 1°C (a) ATN (b) CFA and (c) DCF..... | 180 |
| Figure 5.1. Carbonization of Wood .....  | 190 |
| Figure 5.2. Probable mechanisms of the interactions of organic contaminants with biochar (Ahmad, M. et al., 2013).....   | 191 |
| Figure 5.3. Representation of the Chabazite structure with O atoms represented by red lines and Si (or Al) bonds to O represented by yellow lines. ....  | 193 |
| Figure 5.4. Distribution sizes of various pores and its adsorption phenomena in activated carbon. ....   | 194 |
| Figure 5.5. Production of biochar, biooil and syngas from thermochemical decomposition of waste biomass by a process of pyrolysis.....   | 196 |
| Figure 5.6. Biochar obtained after slow pyrolysis at 700°C with a ramp temperature of 7°C/min for 1h.....  | 197 |
| Figure 5.7. Chemical structures of targeted PPCPs compounds.....   | 199 |
| Figure 5.8. SEM images scanned at 200, 120, 60 and 37.5 μm of biochar at 10 kV ...   | 206 |
| Figure 5.9. SEM images scanned at 30 and 20μm of biochar at 10kV .....   | 207 |
| Figure 5.10. SEM images of three spots scanned at 300μm of biochar at 10kV .....   | 208 |
| Figure 5.11. EDX images scanned at 300μm of biochar at 10kV .....  | 209 |
| Figure 5.12. FTIR spectra of BC sample after pyrolysis at 700°C .....  | 210 |
| Figure 5.13. Structure of straight chain Alkanes with Methylene group (CH <sub>2</sub> ) (Tom Tague) .....   | 212 |
| Figure 5.14. Structure of C-O-C symmetric stretch (Tom Tague) .....  | 213 |

|   |     |
|---|-----|
| Figure 5.15. Comparison of various spectra using $^{13}\text{C}$ NMR.....   | 213 |
| Figure 5.16. Effect of pH in percent removal onto BC (a) ATN, (b) CFA and (c) DCF<br>[ $C_0 = 10 \text{ mg/L}$ , adsorbent dosage = 1, 2, 5, 10 and 20 g/L] .....                             | 218 |
| Figure 5.17. Effect of pH in percent removal onto BC a) ATN, (b) CFA and (c) DCF<br>[ $C_0 = 20\text{mg/L}$ , adsorbent dosage = 1, 2, 5, 10 and 20 g/L] .....                                | 220 |
| Figure 5.18. Effect of pH in percent removal onto BC (a) ATN, (b) CFA and (c) DCF<br>[ $C_0 = 30\text{mg/L}$ , adsorbent dosage = 1, 2, 5, 10 and 20 g/L] .....                               | 222 |
| Figure 5.19. Percent removal efficiency of PPCPs from a mixture of BC:Chb (a) ATN,<br>(b) CFA and (c) DCF [ $C_0 = 10 \text{ mg/L}$ , dosage = 1, 2, 5, 10 and 20 g/L] .....                  | 226 |
| Figure 5.20. Effect of concentration onto BC and its removal efficiency (a) ATN, (b)<br>CFA and (c) DCF [pH = 9, adsorbent dosage = 1, 2, 5, 10 and 20 g/L].....                              | 228 |
| Figure 5.21. Effects of biochar pre-conditioning with 0.1N NaCl at pH 3, 6 and 9 (a)<br>ATN (b) CFA and (c) DCF [ $C_0 = 10 \text{ mg/L}$ ].....  | 230 |
| Figure 5.22. Effects of chemical activation of BC in removal efficiency at varying<br>concentration of KOH [ $C_0 = 10\text{mg/L}$ , pH = 9, adsorbent dosage = 1, 2, 5, 10, 20 g/L]<br>..... | 231 |
| Figure 5.23. Comparison of various adsorption methods at varying pH onto BC and its<br>removal efficiency for ATN [ $C_0 = 10\text{mg/L}$ , dosage = 1, 2, 5, 10, 20g/L] .....                | 233 |
| Figure 5.24. Comparison of various adsorption methods at varying pH onto BC and its<br>removal efficiency for CFA [ $C_0 = 10\text{mg/L}$ , dosage = 1, 2, 5, 10, 20g/L] .....                | 234 |
| Figure 5.25. Comparison of various adsorption methods at varying pH onto BC and its<br>removal efficiency for DCF [ $C_0 = 10\text{mg/L}$ , dosage = 1, 2, 5, 10, 20g/L] .....                | 235 |
| Figure 5.26. ATN equilibrium adsorption isotherm onto BC [pH = 9; $C_0 = 10, 20,$<br>$30\text{mg/L}$ ; dosage = 1, 2, 5, 10, 20g/L] .....   | 238 |

|   |     |
|---|-----|
| Figure 5.27. Freundlich plot for ATN adsorption onto BC [pH = 9; Co = 10, 20, 30mg/L; dosage = 1, 2, 5, 10, 20g/L] .....  | 238 |
| Figure 5.28. Langmuir plot for ATN adsorption onto BC [pH = 9; Co = 10, 20, 30mg/L; dosage = 1, 2, 5g/L] .....            | 239 |
| Figure 5.29. CFA equilibrium adsorption isotherm onto BC [pH = 9; Co = 10, 20, 30mg/L; dosage = 1, 2, 5, 10g/L] .....     | 239 |
| Figure 5.30. Freundlich plot for CFA adsorption onto BC [pH = 9; Co = 10, 20, 30mg/L; dosage = 1, 2, 5, 10, 20g/L] .....  | 240 |
| Figure 5.31. Langmuir plot for CFA adsorption onto BC [pH = 9; Co = 10, 20, 30mg/L; dosage = 1, 2, 5, 10g/L] .....        | 240 |
| Figure 5.32. DCF equilibrium adsorption isotherm onto BC [pH = 9; Co = 10, 20, 30mg/L; dosage = 1, 2, 5, 10, 20g/L] ..... | 241 |
| Figure 5.33. Freundlich plot for DCF adsorption onto BC [pH = 9; Co = 10, 20, 30mg/L; dosage = 1, 2, 5, 10, 20g/L] .....  | 241 |
| Figure 5.34. Langmuir plot for DCF adsorption onto BC [pH = 9; Co = 10, 20, 30mg/L; dosage = 1, 2, 5 g/L] .....           | 242 |

## List of Appendices

|  |     |
|--|-----|
| Appendix 1. Average monthly water quality (raw and treated) reported by Adelaide Wastewater Treatment Plant, 2014.....             | 263 |
| Appendix 2. BET Surface Area for TiO <sub>2</sub> film after calcination .....   | 264 |
| Appendix 3. Reactor setup showing the wastewater spiked with PPCP compounds subjected to O <sub>3</sub> /UV/TiO <sub>2</sub> ..... | 265 |
| Appendix 4. Agilent 6460 LC-MS/MS (High Resolution).....   | 265 |
| Appendix 5. A five point calibration curve for Atenolol with conc. of 10, 20, 50, 75 and 100 ng/ml .....                           | 266 |
| Appendix 6. A five point calibration curve for Clofibric acid with conc. of 10, 20, 50, 75 and 100 ng/ml .....                     | 266 |
| Appendix 7. A five point calibration curve for Diclofenac with conc. of 10, 20, 50, 75 and 100 ng/ml .....                         | 267 |
| Appendix 8. A comparison of various AOPs with their percent removal .....  | 267 |
| Appendix 9. Effect of pH on the percent removal of ATN using various AOPs .....  | 268 |
| Appendix 10. Comparison of various AOPs on degradation of PPCPs in presence of varying concentrations of NOM and Br.....           | 268 |
| Appendix 11. Crystal Structure of Chabazite .....  | 269 |
| Appendix 12. BET Surface Area plot for Biochar sample pyrolyzed at 700oC.....  | 269 |
| Appendix 13. BET Surface Area Report with pore volume for Biochar samples.....   | 270 |
| Appendix 14. A six point calibration curve for Atenolol with conc. of 10, 20, 50, 75, 100 and 200 ng/ml .....                      | 271 |



|   |     |
|---|-----|
| Appendix 15. A six point calibration curve for Clofibric Acid with conc. of 10, 20, 50, 75, 100 and 200 ng/ml ..... | 271 |
| Appendix 16. A six point calibration curve for Diclofenac with conc. of 10, 20, 50, 75, 100 and 200 ng/ml .....     | 272 |
| Appendix 17. Blank Milli-Q water chromatogram by LC-MS/MS.....  | 272 |
| Appendix 18. Secondary Effluent chromatogram by LC-MS/MS (baseline study)....                                       | 273 |

## Nomenclature

|                               |   |
|-------------------------------|---|
| ACR                           | Acute to Chronic Ratio                          |
| AOP                           | Advanced Oxidation Process                      |
| APCI                          | Atmospheric Pressure Chemical Ionization        |
| APIs                          | Active Pharmaceutical Ingredients               |
| AC                            | Activated Carbon                                |
| ATN                           | Atenolol  |
| Ave                           | Average concentration                           |
| BC                            | Biochar   |
| BET                           | Brunauer-Emmett-Teller                          |
| BOD                           | Biochemical Oxidation Demand                    |
| BPA                           | Bis Phenol A                                    |
| CAS                           | Chemical Abstract Service                       |
| CAT                           | Catalyst  |
| Ce                            | Equilibrium Concentration (mg/L)                |
| CFA                           | Clofibric Acid                                  |
| Chb                           | Chabazite                                       |
| CHNS                          | Carbon, Hydrogen, Nitrogen and Sulfur Analyzer  |
| Cl <sup>·</sup>               | Chlorine radical                                |
| Cl <sub>2</sub> <sup>·-</sup> | dichloride anion radical                        |
| C <sub>0</sub>                | Initial Solute Concentration                    |
| CO <sub>3</sub> <sup>2-</sup> | Carbonates                                      |
| COD                           | Chemical Oxygen Demand                          |
| COX1/2                        | Cyclo-Oxygenase enzyme(s)                       |
| <sup>13</sup> C-NMR           | <sup>13</sup> Carbon Nuclear Magnetic Resonance |

|                  |   |
|------------------|---|
| DBPs             | Disinfection By-Products                    |
| DCF              | Diclofenac                                  |
| D/DBP            | Disinfectants and Disinfection By-Products  |
| DI               | Deionized Water                             |
| DNA              | Deoxyribo Nucleic Acid                      |
| DOM              | Dissolved Organic Matter                    |
| DW               | Distilled Water                             |
| EDC              | Endocrine-disrupting compounds              |
| EDX              | Energy-dispersive X-ray Spectroscopy        |
| EPA              | Environmental Protection Agency             |
| EPR              | Electron Paramagnetic Resonance             |
| ERA              | Environmental Risk Assessment               |
| ESI              | Electrospray ionization                     |
| $\epsilon$       | Molar Extinction Coefficient                |
| FE-SEM           | Field Emission Scanning Electron Microscopy |
| FA               | Fulvic acid                                 |
| FAC              | Fiber Activated Carbon                      |
| FIB              | Focused Ion Beam                            |
| FTIR             | Fourier Transform Infrared Spectroscopy     |
| $\text{Fe}^{2+}$ | Ferrous ion                                 |
| GAC              | Granular Activated Carbon                   |
| HA               | Humic Acid                                  |
| HAA              | Haloacetic Acid                             |
| Hc               | Henry's Law Constant                        |
| $\text{HCO}_3^-$ | Bicarbonates                                |
| $\text{HO}\cdot$ | Hydroxyl radical                            |

|                                   |   |
|-----------------------------------|---|
| HOBr                              | Hypobromous acid  |
| H <sub>2</sub> O <sub>2</sub>     | Hydrogen peroxide   |
| HPLC                              | High Performance Liquid Chromatography                    |
| H <sub>2</sub> S                  | Hydrogen Sulfide  |
| HTC                               | Hydrothermal Carbonization                                |
| In(OH) <sub>3</sub>               | Indium Hydroxide  |
| In <sub>2</sub> O <sub>3</sub>    | Indium Oxide  |
| In(NO <sub>3</sub> ) <sub>3</sub> | Indium Nitrate  |
| ISC                               | Inter System Crossing                                     |
| k                                 | Rate Constant   |
| K <sub>F</sub>                    | Freundlich Sorption Coefficient                           |
| K <sub>L</sub>                    | Langmuir Constant (L/mg)                                  |
| KOH                               | Potassium Hydroxide                                       |
| K <sub>ow</sub>                   | Octanol-Water Partition Coefficient                       |
| kV                                | Kilovolt  |
| LC-MS/MS                          | Liquid Chromatography Triple Quadrupole Mass Spectrometry |
| LD <sub>50</sub>                  | Lethal Dose   |
| LOEC                              | Lowest Observed Effect Concentration                      |
| LPM                               | Liters per minute   |
| M                                 | Mass of Adsorbent in g                                    |
| MAO                               | Monoamine oxidase   |
| MBR                               | Membrane Bio Reactor                                      |
| MDL                               | Method detection limit                                    |
| [M-H] <sup>-</sup>                | Deprotonized molecular ion                                |
| Mn                                | Million   |
| MRM                               | Multiple Reaction Monitoring                              |

|                              |  |
|------------------------------|--|
| MS                           | Microsphere                                |
| m/z                          | Mass to Charge Ratio                       |
| N                            | Normality                                  |
| nd                           | Not Detected                               |
| NA                           | Not Available                              |
| NC                           | Nano Cubes                                 |
| NCY                          | Nano Crystals                              |
| NOM                          | Natural Organic Matter                     |
| NO <sub>3</sub> <sup>-</sup> | Nitrates                                   |
| NP                           | Nano Plates                                |
| NSAIDs                       | Non - Steroidal Anti - Inflammatory Drugs  |
| NTU                          | Nephlo Turbidimetric Units                 |
| O <sub>2</sub> <sup>•-</sup> | Superoxide radical                         |
| OM                           | Organic Matter                             |
| PAC                          | Powdered Activated Carbon                  |
| PBT                          | Persistence, Bioaccumulation and Toxic     |
| PEC                          | Predicted Environmental Concentration      |
| PFOA                         | Perfluorooctanoic acid                     |
| pKa                          | Acid dissociation constant                 |
| pH <sub>zpc</sub>            | Zero point charge                          |
| PNEC                         | Predicted no - effect concentration        |
| PPCPs                        | Pharmaceuticals and Personal Care Products |
| psi                          | Pounds per square inch                     |
| PTFE                         | Polytetrafluoroethylene                    |
| qe                           | Equilibrium adsorbed concentration (mg/g)  |

|                  |  |
|------------------|--|
| q <sub>max</sub> | Maximum mass adsorbed at saturated adsorption capacity of adsorbent (mg/g) |
| RAPET            | Reaction under the Autogenic Pressure at Elevated Temperature              |
| R <sup>2</sup>   | Correlation Coefficient  |
| ROS              | Reactive Oxygen Species  |
| RPM              | Revolutions Per Minute   |
| RSD              | Relative Standard Deviation  |
| SAF-MBR          | Staged Anaerobic Fluidized Membrane Bioreactor                             |
| SE               | Secondary Effluent   |
| SEM              | Scanning Electron Microscope   |
| SS               | Stainless Steel  |
| TCOs             | Transparent Conducting Oxides  |
| TDS              | Total Dissolved Solids   |
| THMs             | Trihalomethanes  |
| TiO <sub>2</sub> | Titanium Dioxide   |
| TOC              | Total organic carbon   |
| TSS              | Total Suspended Solids   |
| UVGI             | Ultraviolet germicidal irradiation   |
| USGS             | United States Geological Survey  |
| US FDA           | Food and Drug Administration   |
| WTW              | Wastewater Treatment Works   |
| WWTP             | Wastewater Treatment Plant   |
| WHO              | World Health Organization  |
| β                | Beta   |

## Chapter 1

### 1 Introduction

#### 1.1 Background

The presence of pharmaceuticals in drinking water, rivers and wastewaters of Switzerland, United Kingdom, Italy, Germany (Kreuzinger et al., 2004 and Heberer et al., 2004) and the United States (Bruchet et al., 2005) is a major concern as most of the data was generated by conducting studies in these countries. Among pharmaceuticals and personal care products (PPCPs), Atenolol, Clofibric Acid and Diclofenac are in the top 20 drugs sold and widely used in the world (Fierce Pharma, 2014, Global Market Sales, 2014 and NDC Health, USA, 2015). These PPCPs are non-regulated and the risk of their long term exposure at low concentrations to aquatic life can have adverse effects. For example, the exposure of the anti-inflammatory and arthritis drug, diclofenac, between 2000 and 2007 has resulted in the death of 95% of India's Gyps vultures and 90% of Pakistan's due to renal failure. Diclofenac was sold worldwide in more than 3 dozen different brand names. Scientists have found that in the environment, combinations of compounds are commonly found together. For example, it was found that although low concentrations of fluoxetine, an antidepressant, and clofibric acid do not have any effect on water fleas individually, they killed more than half of water fleas when they were exposed to the two compounds simultaneously (Sonia Shah, 2010).

It was observed that concentrations of diclofenac, clofibric acid and atenolol in wastewater treatment plant (WWTP) influent, effluent, groundwater and surface-water follows the order of diclofenac>atenolol>clofibric acid whereas diclofenac and clofibric acid has been observed in sludge and biosolids.

One of the most pressing global environmental issues of present and future is the protection and conservation of precious water resources. Water reclamation efficiency from various effluents and source water protection is the long-term sustainability of

clean water supply. Increasing interest in water reuse and public health concerns about micropollutants originating from a variety of PPCPs and common household chemical agents has raised concerns about the fate and transformation of these chemicals and their removal from water. Around 65 to 80 mg/L of bromide concentrations has been observed in confined areas of seawater (Al-Mutaz, 2000), while fresh waters show trace amounts to about 0.5 mg/L concentration. In U.S, daily dietary intake from fish, grains and nuts accounts to 2-8mg of bromide (Nielsen and Dunn, 2009).

Drinking water should be safe from emerging contaminants, including Endocrine Disrupting Compounds (EDCs), PPCPs, Natural Organic Matter (NOM) and Bromine (Br). The problem is that most of these EDCs and PPCPs compounds are not regulated, so neither utilities nor the public know what “safe” is. Therefore, until the regulations catch up with the research, we aim to remove or reduce the levels of contaminants or their biological activity in our waters.

Many EDCs and PPCPs are low molecular weight compounds that are relatively hydrophilic, and are thus not suited for removal by traditional treatments. Many studies have indicated that conventional water and sewage treatment plants can remove less than 75% of most EDCs and PPCPs (although this varies widely with chemical properties and treatment processes). To avoid the potential dangerous accumulation of pharmaceuticals in the aquatic environment, research is being proposed to determine the efficacy of powerful oxidation techniques to remove these compounds from conventionally treated wastewater prior to release to receptors (e.g. rivers), source water and drinking water.

Several treatment processes were used in the past to remove atenolol from wastewater by conventional biological treatment (Castiglioni et al., 2006), membrane bioreactor (MBR) (Kim et al., 2014) and staged anaerobic fluidized membrane bioreactor (SAF-MBR) (Dutta et al., 2014). Atenolol was also removed from secondary effluent by ferrate VI (Zhou and Jiang, 2015). For diclofenac the treatment process employed were photo-Fenton (Pe´rez-Estrada et al., 2005), H<sub>2</sub>O<sub>2</sub>/UV and ozonation (Vogna et al., 2004 and Huber et al., 2003), activated sludge (Clara et al., 2005), flotation (Carballa et al.,



2005), membrane bioreactor and conventional treatment (Radjenovic et al., 2007), heterogeneous catalytic oxidation with  $\text{H}_2\text{O}_2$  (Hofmann et al., 2007), solar irradiation (Bartels et al., 2007 and Aguiñera et al., 2005), granular activated carbon, ultrafiltration, coagulation/flocculation and reverse osmosis were also employed. Diclofenac was also removed from wastewater by using adsorption techniques such as micelle–clay complex (Karaman et al., 2012). Another study involved removal of diclofenac from contaminated water by the usage of silica gel synthesized by sol-gel process as an adsorbent (Benavent et al., 2009). Similarly, clofibrac acid was removed from water and wastewater by  $\text{O}_3/\text{H}_2\text{O}_2$  (Zwiener and Frimmel, 2000), Ozonation (Ternes et al., 2002 and Andreozzi et al., 2003),  $\text{H}_2\text{O}_2/\text{UV}$  (Andreozzi et al., 2003),  $\text{TiO}_2/\text{UV}$  (Doll et al., 2004), MBR and conventional treatment (Radjenovic et al., 2007) techniques.

Organic compounds have been treated in drinking water using advanced oxidation processes (AOPs) at several sites across the United States and Canada over the past ten years or so. AOPs are chemical oxidation techniques able to produce in situ reactive free radicals, mainly the hydroxyl radical ( $\bullet\text{OH}$ ), by means of different reacting systems. The concept was originally established by Glaze et al., (1987) as ‘Oxidation processes which generate hydroxyl radical in sufficient quantity to affect water treatment’.

Unlike air stripping and adsorption, which are phase-transfer processes, AOPs are destructive processes that break down organic contaminants directly in the water through chemical reaction, as opposed to simply transferring them from the liquid phase to gas phase (in the case of air stripping) or solid phase (in the case of powdered activated carbon and resins). However, despite this advantage, there are significant limitations and challenges in the full-scale application of AOPs. These include (a) the complex nature of the chemical and physical processes involved in oxidation reactions, and (b) the influence of background water quality on contaminant removal. For example, the presence of high bromide concentrations or natural organic matter can result in the formation of regulated oxidation by-products that may cause water quality to deteriorate beyond its initial state of contamination; and (c) the non-selective nature of oxidation processes leads to the potential for significant interference.

To compensate for these limitations, more energy or higher chemical dosages may be required, which can potentially result in higher costs. In general, though, AOPs can be employed to achieve total degradation of PPCPs and their by-products, thereby avoiding their dangerous accumulation in the aquatic environment. Even partial degradation and transformation of the parent compounds may attenuate their toxicity.

The commonly used AOPs include homogeneous or heterogeneous processes which include photodissociation of hydrogen peroxide and ultraviolet ( $\text{H}_2\text{O}_2/\text{UV}$ ), photolysis of ozone ( $\text{O}_3/\text{UV}$ ), Fenton reaction (Ferrous,  $\text{Fe}^{2+}/\text{H}_2\text{O}_2$ ), photo-Fenton reaction ( $\text{Fe}^{2+}/\text{H}_2\text{O}_2/\text{UV}$ ), photocatalysis (Titanium dioxide,  $\text{TiO}_2/\text{UV}$ ), etc.

Each method has its own merits and limitations, and the efficiency of each process depends on the ease with which it can be operated, the cost effectiveness, the extent of mineralization achieved and finally the reaction time. Most of these methods are effective in bringing about the complete oxidation of organic pollutants, thus achieving the lowest level of pollution.

## 1.2 Objectives of the study

Broadly the objectives of this research were to select the best technologies for complete removal of the PPCPs compounds from wastewater. The main objectives of the study are: a) preparation and characterization of homogeneous immobilized  $\text{TiO}_2$  coatings on stainless steel mesh and its PPCPs removal kinetics in wastewater by a combination of AOPs ( $\text{O}_3/\text{UV}/\text{TiO}_2$ ) and its comparison to other techniques; b) preparation of Indium Oxide ( $\text{In}_2\text{O}_3$ ) nano cubes, porous microspheres, nano plates and nano crystals, its characterization and application in degradation of PPCPs from wastewater and c) preparation of biochar, its characterization and application in removal of PPCPs from wastewater with comparison to natural zeolites.

### 1.3 Contribution of the thesis

To date, various treatment technologies have been used in the removal of PPCPs from drinking water, distilled water and surface water but very few studies have been conducted on wastewater and sludge. Although some of the AOPs were able to remove these PPCPs completely in water but were not efficient in complete removal in wastewater due to its complex water matrix such as the presence of natural organic matter, color, odor, suspended solids, ions, etc. Some of the key contributions of this research helped in improving the methods of removal of PPCPs from wastewater as follows:

- a) Extensive wastewater sampling, laboratory experiments and data analysis by high resolution Liquid Chromatography Triple Quadrupole Mass Spectrometry (LC-MS/MS)
- b) A study of the combination of  $O_3$ /UV/ $TiO_2$  AOP has improved the removal of PPCP from wastewater
- c) Use of  $In_2O_3$  in the removal of PPCP from wastewater was conducted for the first time as no published work to date has dealt with removal of these compounds
- d) Although activated carbon has been used in the removal of various organics and PPCPs, biochar was used for the first time to remove PPCPs from wastewater
- e) A combination of biochar and zeolite was studied to compare the removal efficiencies of PPCPs from wastewater

### 1.4 Organization of the thesis

The thesis is written in an integrated-article format with each of the articles in individual chapters containing separate introduction, tables, figures, results, discussion and references. It is divided into six chapters and one appendix.

Chapter 1 consists of background, objectives and contribution.

Chapter 2 presents a review of literature on PPCPs (atenolol, clofibric acid and diclofenac) model compounds, various advanced oxidation processes (ozonation, UV, TiO<sub>2</sub>, O<sub>3</sub>/UV, UV/TiO<sub>2</sub>, O<sub>3</sub>/TiO<sub>2</sub> and H<sub>2</sub>O<sub>2</sub>), semi-conductor photocatalysis (immobilization of TiO<sub>2</sub> into thin films), and the applications of AOPs, Indium Oxide and Biochar in degradation of PPCPs from wastewater.

Chapter 3 deals with PPCPs removal from wastewater by using advanced oxidation process of O<sub>3</sub>/UV/TiO<sub>2</sub> and its comparison with other AOPs. This chapter discusses sampling procedure, wastewater characterization, methodology of LC-MS/MS, adsorbent preparation on support medium by coating procedures and characterization of the TiO<sub>2</sub> films, influence of pH, variation of the concentration of TiO<sub>2</sub> coatings, the effect of the presence of natural organic matter and bromine in wastewater on PPCPs removal, and the kinetics of the removal of the individual compounds.

Chapter 4 deals with the preparation and characterization of In<sub>2</sub>O<sub>3</sub> in the form of porous microspheres, nanocubes, nanoplates and nanocrystals and their application to PPCPs (atenolol, clofibric acid and diclofenac) removal from wastewater and, the comparison of the performance of microspheres, nanocubes, nanoplates and nanocrystals with that of O<sub>3</sub>/UV/TiO<sub>2</sub>, O<sub>3</sub>/TiO<sub>2</sub> and UV/TiO<sub>2</sub>.

Chapter 5 deals with the preparation and characterization of biochar and its application to PPCPs (atenolol, clofibric acid and diclofenac) removal from wastewater and its comparison with natural zeolite and activated biochar at varying pH and zeolite concentration at varying adsorbent ratios.

Chapter 6 deals with conclusions from the study and recommendations for application of O<sub>3</sub>/UV/TiO<sub>2</sub>, In<sub>2</sub>O<sub>3</sub> and biochar for removal of PPCPs.

## 1.5 References

- Al-Mutaz I.S., 2000. Water desalination in the Arabian Gulf region. In: Goosen MFA, Shayya WH, eds. Water management, purification and conservation in arid climates. Vol. 2. Water purification. Basel, Technomic Publishing, pp. 245–265.
- Agüera, A., Pérez-Estrada, L.A., Ferrer, I., Thurman, E.M., Malato, S., Fernández-Alba, A.R., 2005. Application of time-of-flight mass spectrometry to the analysis of phototransformation products of diclofenac in water under natural sunlight. *J. Mass Spectrom.* 40:908–15.
- Andreozzi, R., Raffaele, M., and Nicklas, P., 2003. Pharmaceuticals in STP effluents and their solar photodegradation in aquatic environment. *Chemosphere.* 50 (10), 1319–1330.
- Bartels, P., von Tümpling, Jr. W., 2007. Solar radiation influence on the decomposition process of diclofenac in surface waters. *Science of the Total Environment.* 374, 143–155.
- Benavent, M.S., Zhang, Y.- J., Geissen, S. U., 2009. Adsorption of pharmaceuticals on a synthesized silica and its regeneration with ozone. Masters student in Chemical Engineering, Universitat Rovira I Virgili, Tarragona, Spain and Department of Environmental Technology, Chair of Environmental Process, Technical University of Berlin, Germany. pp.2-5.
- Bruchet, A., Hochereau, C., Picard, C., Decottignies, V., Rodrigues, J.M., and Janex-Habibi, M.L., 2005. Analysis of drugs and personal care products in French source and drinking waters: The analytical challenge and examples of application. *Water Science and Technology.* 52 (8), 53–61.
- Carballa, M., Omil, F., and Lema, J.M., 2005. Removal of cosmetic ingredients and pharmaceuticals in sewage primary treatment. *Water Res.*39, 4790–4796.
- Castiglioni, S., Bagnati, R., Fanelli, R., Pomati, F., Calamari, D., and Zuccato, E., 2006. Removal of pharmaceuticals in sewage treatment plants in Italy. *Environ. Sci. Technol.* 40, 357–363.
- Clara, M., Strenn, B., Gans, O., Martinez, E., Kreuzinger, N., Kroiss, H., 2005. Removal of selected pharmaceuticals, fragrances and endocrine disrupting compounds in a membrane bioreactor and conventional wastewater treatment plants. *Water Research.* 39, 4797-4807.
- Doll, T.E., Frimmel, F.H., 2004. Kinetic study of photocatalytic degradation of carbamazepine, clofibrac acid, iomeprol and iopromide assisted by different TiO<sub>2</sub> materials—determination of intermediates and reaction pathways. *Water Research.* 38, 955–964.

Dutta, K., Lee, M.Y., Lai, W.W.P., Lee, C.H., Lin, A.Y.C., Lin, C.F., Lin, J.G., 2014. Removal of pharmaceuticals and organic matter from municipal wastewater using two-stage anaerobic fluidized membrane bioreactor. *Bioresource Technology*. 165, 42–49.

Glaze, W.H., Kang, J.W., and Chapin, D.H., 1987. The Chemistry of water treatment processes involving ozone, hydrogen peroxide and ultraviolet radiation. *Ozone Science and Engineering*. 9, 335-352.

Heberer, T., Mechlinski, A., Fanck, B., Knappe, A., Massmann, G., Pekdeger, A., and Fritz, B., 2004. Field studies on the fate and transport of pharmaceutical residues in bank filtration. *Ground Water Monitoring and Remediation*. 24 (2), 70–77.

Hofmann, J., Freier, U., Wecks, M., Hohmann, S., 2007. Degradation of diclofenac in water by heterogeneous catalytic oxidation with H<sub>2</sub>O<sub>2</sub>. *Appl. Catal. B*. 70:447–451.

[https://www.imshealth.com/files/imshealth/Global/North%20America/Canada/Home%20Page%20Content/Pharma%20Trends/Top20GlobalTherapyAreas\\_EN\\_14.pdf](https://www.imshealth.com/files/imshealth/Global/North%20America/Canada/Home%20Page%20Content/Pharma%20Trends/Top20GlobalTherapyAreas_EN_14.pdf) (Date retrieved: 18th Oct, 2015).

<http://www.fiercepharma.com/special-report/top-20-generic-molecules-worldwide>. (Date retrieved: 26th May, 2014).

Huber, M.M., Canonica, S., Park, G.-Y., and von Gunten, U., 2003. Oxidation of pharmaceuticals during ozonation and advanced oxidation processes. *Environ. Sci. Technol.* 37, 1016–1024.

Karaman, R., Khamis, M., Quried, M., Halabieh, R., Makharzeh, I., Manassra, A., Abbadi, J., Qtait, A., Bufo, S.A., Nasser, A., 2012. Removal of diclofenac potassium from wastewater using clay-micelle complex. *Environ. Technol.* pp. 1279-1287.

Kim, M., Guerra, P., Shah, A., Parsa, M., Alae, M., and Smyth, S.A., 2014. Removal of pharmaceuticals and personal care products in a membrane bioreactor wastewater treatment plant. *Water Science & Technology*. 69.11, 2221-2229.

Kreuzinger, N., Clara, M., Strenn, B., and Vogel, B., 2004. Investigation on the behaviour of selected pharmaceuticals in the groundwater after infiltration of treated wastewater. *Water Science and Technology*. 50 (2), 221–228.

NDC Health, USA, 2010. [homepage.ntlworld.com/bhandari/Imperial/Atenolol/Introduction.Htm](http://homepage.ntlworld.com/bhandari/Imperial/Atenolol/Introduction.Htm) (Date retrieved: 2015/07/09).

Nielsen, F.H., Dunn, M., 2009. Bromine. In: *Other trace elements*. Bethesda, MD, American Society for Nutrition (<http://jn.nutrition.org/nutinfo/content/trace.shtml>). (Date retrieved: 2016/08/30).

Perez-Estrada, L.A., Malato, S., Gernjak, W., Aguera, A., Thurman, E.M., Ferrer, I., and Fernandez-Alba, A.R., 2005. Photo-fenton degradation of diclofenac: Identification of main intermediates and degradation pathway. *Environmental Science & Technology*. 39 (21), 8300–8306.

Radjenovic', J., Petrovic', M., Barcelo', D., 2007. Analysis of pharmaceuticals in wastewater and removal using a membrane bioreactor. *Anal. Bioanal. Chem.* 387 (4), 1365–1377.

Sonia Shah, 2010. As Pharmaceutical Use Soars, Drugs Taint Water and Wildlife. *Yale environment 360*, article 15 Apr. 2010. (Date retrieved: 2014/04/23).

Ternes, T.A., Meisenheimer, M., McDowell, D., Sacher, F., Brauch, H.J., Gulde, B.H., Preuss, G., Wilme, U., and Seibert, N.Z., 2002. Removal of pharmaceuticals during drinking water treatment. *Environmental Science & Technology*. 36 (17), 3855–3863.

Vogna, D., Marotta, R., Napolitano, A., Andreozzi, R., and d'Ischia, M., 2004. Advanced oxidation of the pharmaceutical drug diclofenac with UV/H<sub>2</sub>O<sub>2</sub> and ozone. *Water Res.* 38(2), 414–422.

Zhou, Z., and Jiang, J.Q., 3-5 September 2015. Removal of selected pharmaceuticals spiked in the secondary effluent of a wastewater treatment plant (WWTP) by potassium ferrate (VI). *Proceedings of the 14th International Conference on Environmental Science and Technology, Rhodes, Greece*. CEST2015\_00043.

Zwiener, C., and Frimmel, F.H., 2000. Oxidative treatment of pharmaceuticals in water. *Water Res.* 34, 1881–1885.

## Chapter 2

### 2 Literature review

#### 2.1 Introduction

##### 2.1.1 Sources of PPCPs in the environment

The presence of pharmaceuticals in surface waters of Europe (particularly in Switzerland, United Kingdom, Italy and Germany) and the United States has encouraged several other scientists across the globe to investigate the presence of such chemicals in lakes, streams, rivers and reservoirs in their regions. These studies have further fueled interest beyond surface water studies to other water resources and environmental systems such as groundwater, sediments, landfill leachates and biosolids.

Over \$800 billion dollars of drugs were sold in 2008 worldwide, and the total audited and unaudited Global Pharmaceutical Market sales during 2005-2014 increased from US \$608 billion to US \$1057 billion dollars (IMS Health May, 2015). In addition, more than 150 different human and veterinary medicines (including prescription and over the counter medications) and drug metabolites were detected in the waters of Europe, USA and as far as the Arctic region, which were discharged into the aquatic environment on a continual basis from domestic and industrial sewage. Also, a federal study conducted on 74 waterways found that 53 of these waterways that provide drinking water in 25 states were contaminated with traces of one or more pharmaceuticals. Although there are no federal regulations of pharmaceuticals that exist for drinking water or wastewater, only 12 of them are currently on the Environmental Protection Agency's list of drinking water standards (Bienkowski, 2013). Sampling performed by the United States Geological Survey (USGS) has found that 80% of the streams and a quarter of the groundwater resources in the United States are contaminated with a variety of medications. The average American uses more than 10 prescription drugs per year and



consumes approximately 17 grams of antibiotics alone, which is more than three times the per capita rate of consumption in European countries such as Germany. Also, farmers dispense approximately 11,000 metric tons of antimicrobial medications every year to promote livestock growth (Sonia Shah, 2010).

Non-steroidal anti-inflammatory drugs (NSAIDs), Lipid regulator agents, Beta-blockers and Antiepileptics are among the various categories of pharmaceuticals often found as persistent toxic waste and are most widely used drugs in the world. For example, based on 3.05 billion prescriptions for Atenolol, it is considered on 3<sup>rd</sup> rank as the best selling hypertension drug in the world (NDC Health, USA, 2015), While Diclofenac 2011 sales were at \$1.61 billion putting it at 12<sup>th</sup> rank in the top 20 generic molecules worldwide (Fierce Pharma, 2014). Clofibric acid, a metabolite of the lipid regulator clofibrate was the first drug to be detected in water which enabled to detect concentration of other PPCP compounds in water. Clofibric acid has been detected at a concentration of 103ng/L at A.H. Weeks Water Treatment Plant inlet in Windsor, Ontario, Canada, a city that relies on the Detroit River for its drinking water source. Similar findings have been reported for European surface waters (Stan et al., 1994; Stumpf et al., 1996; Ternes, 1998; Daughton and Ternes, 1999). Due to the decline in the use of clofibrate in the United States (WHO, 1996), clofibric acid is not present in Mississippi River and Lake Pontchartrain waters (Boyd et al., 2003).

Increasing interest in water reuse and public health concerns about micro-pollutants originating from a variety of pharmaceuticals, personal care products and common household chemical agents has raised concerns about the fate and transformation of these chemicals and their removal from water.

Increasing quantities of PPCPs are entering the environment due to growing use by humans and domestic animals. In addition to antibiotics and steroids, over 100 individual PPCPs have been identified (as of 2007) in environmental samples and drinking water. Sewage systems are not equipped for PPCP removal. Currently, there are no municipal sewage treatment plants that are engineered specifically for PPCP removal or for other unregulated contaminants. Effective removal of PPCPs from

treatment plants varies based on the type of chemical and on the individual sewage treatment facilities. The risks are uncertain. While the major concerns have been the resistance to antibiotics and disruption of aquatic endocrine systems by natural and synthetic sex steroids, many other PPCPs have unknown consequences. There are no known human health effects from such low-level exposures in drinking water, but special scenarios (one example being fetal exposure to low levels of medications that a mother would ordinarily be avoiding) require more investigation. Most pharmaceuticals retain their chemical structure in order to exert therapeutic effect. This characteristic, along with the continuous release of pharmaceuticals into the environment, may enable them to persist in the environment for extended periods of time (Ternes, 2000).

### 2.1.2 Pathways of pharmaceuticals in the environment

Pharmaceuticals from biosolids are leached into surface water and groundwater by rainfall and snowmelt (Ternes et al., 2004). Veterinary pharmaceuticals enter into the environment either by seepage from manure lagoons or deposited onto the ground directly from manures. Studies conducted on pharmaceuticals come from Europe (Kreuzinger et al., 2004 and Heberer et al., 2004) followed by those that in United States (Bruchet et al., 2005). These studies have produced most of the data on the presence of pharmaceuticals in drinking water, rivers and wastewaters.

Figure 2.1 depicts number of sources and pathways through which pharmaceutical substances enter into the environment mainly from wastewater treatment plants (WWTPs) discharges or land application of animal manure and sewage sludge that are used in human and veterinary medicine. Transformation of most of these active ingredients occurs partially in the body and gets excreted into the sewage systems as a mixture of bioactive and metabolites forms.

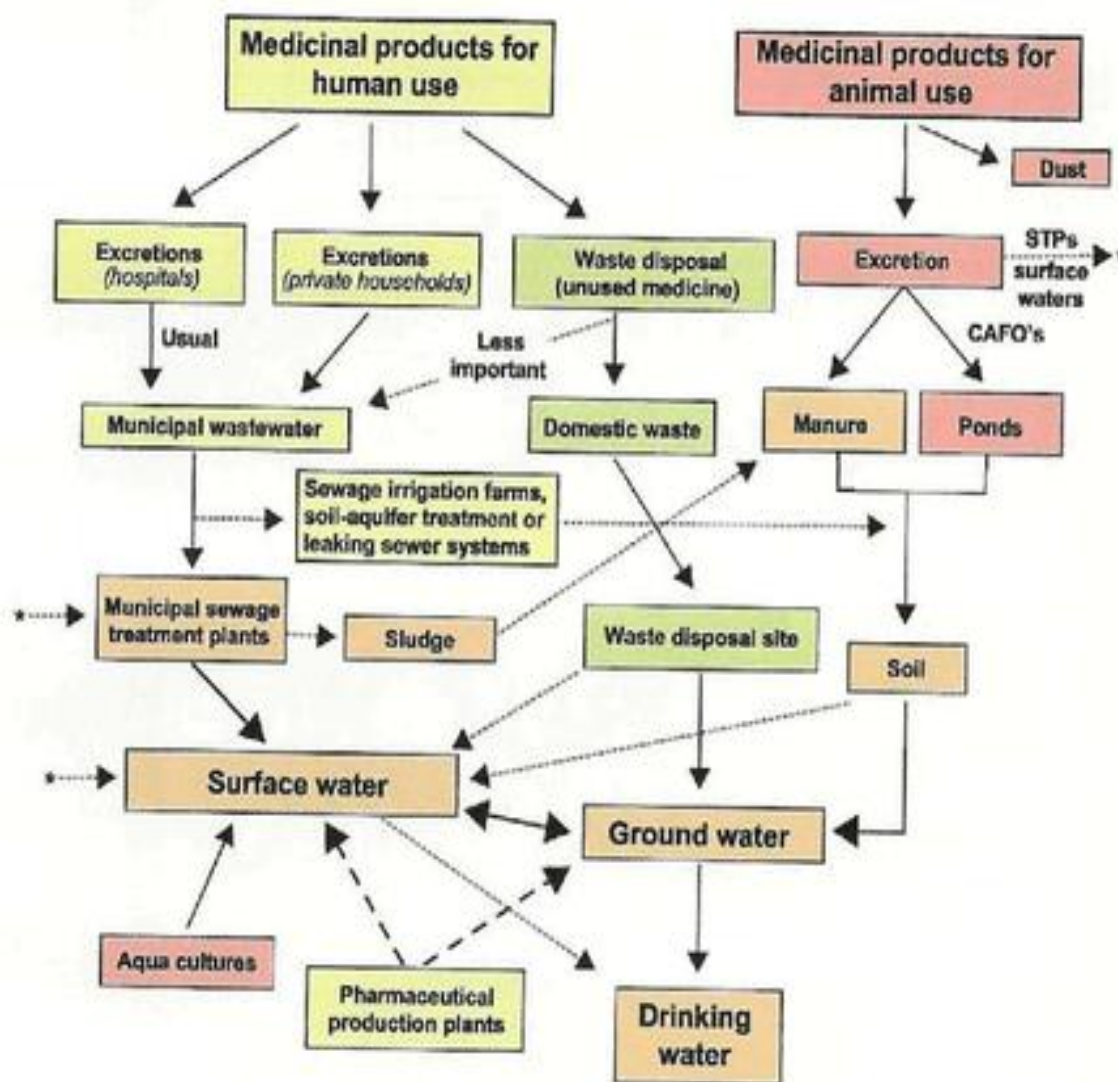


Figure 2.1. Occurrence of pharmaceutical and its metabolite residues showing possible sources and pathways in the aquatic environment (Heberer and Adam, 2002a). Residues of animal excretions reaching surface waters or municipal STPs are represented by astrick.

### 2.1.3 Classification of PPCPs

The various categories of PPCPs that are classified based on their therapeutical groups are Analgesics (diclofenac, naproxen, ibuprofen, ketoprofen and paracetamol/acetaminophen), antibiotics/antimicrobials (sulfamethoxazole, triclosan,

trimethoprim, erythromycin and ciprofloxacin), antihyperlipidemics (clofibrilic acid, bezafibrate and gemfibrozil), sun-screen products (e.g., methylbenzylidene camphor), diagnostic agents (e.g., x-ray contrast media), cosmetics, fragrances (musks, tonalide and galaxolide), nutraceuticals (e.g., vitamins), excipients (or inert ingredients used in manufacturing and formulation of PPCPs) and other compounds (caffeine, bisphenol A and carbamazepine). Many of the sources of these PPCPs are derived from human activity, residues from hospitals and pharmaceutical manufacturing, antibiotics and steroids, illicit drugs and agribusiness. PPCPs find their routes to (a) both surface water (rivers, lakes, marine, streams) and groundwater; (b) solids (soils including agricultural lands and sediments), (c) biota, and (d) air. Most of these drugs have insufficient vapor pressures but gain entry to air while sorbed to fine particulates through dispersal (e.g., use of medicated feed dusts in confined animal feeding operations) (Daughton 2007).

#### 2.1.4 Fate of Pharmaceuticals in the environment

The concentrations of PPCPs in surface water are higher than in groundwater by a factor of 10 (Susan et al., 2008). Several physicochemical processes in water systems play an important role in altering the pharmaceutical persistence and concentration in the environment regardless of its entry route (Gurr and Reinhard, 2006). The fate of PPCPs is divided into transport, sequestration and degradation categories: a) transport of particulate and dissolved constituents from the point of entry; b) sequestration of PPCPs in various environmental compartments; and c) deposition of particles, bioconcentration and sorption without degradation of pharmaceuticals and stored temporarily in other matrices or compartments.

Biodegradation (Snyder et al., 2004), (Quintana et al., 2005), (Perez et al., 2005, Kim et al., 2005, Carucci et al., 2006, Lindberg et al., 2006), photolysis (Perez-Estrada et al., 2005, Lin et al., 2005, Andreatti et al., 2003, Kwon et al., 2005, Lam et al., 2005, Packer et al., 2003) and hydrolysis (Quintana et al., 2005) are three processes in the aquatic environment that most likely mineralize or transform PPCPs as shown in Figure 2.2.

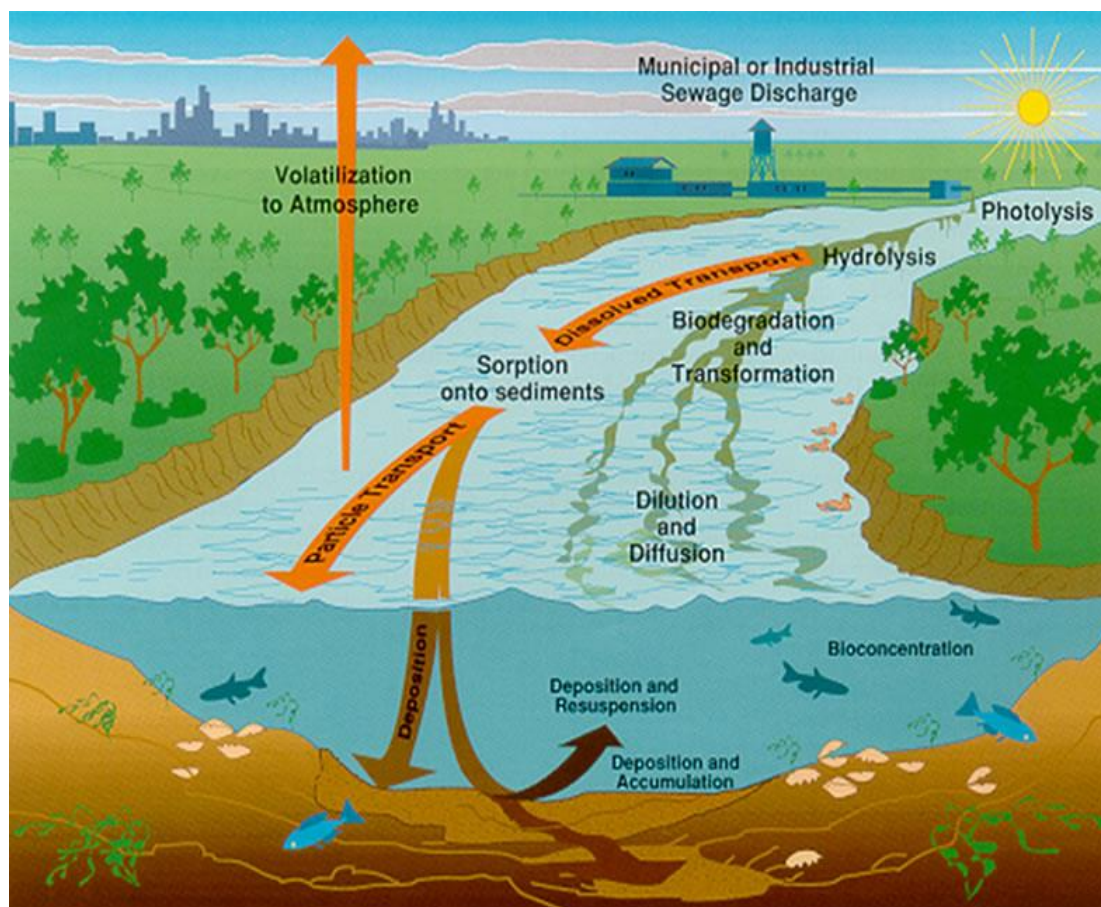


Figure 2.2. Physical processes that affect the environmental concentrations of PPCPs (Meade H. R., 1995, U.S. Geological Survey Circular 1133, p. 114-135)

### 2.1.5 Occurrence of Pharmaceuticals in the environment

Pharmaceuticals have been detected frequently in the environment even after incomplete removal from wastewater treatment or additional removal after discharge as shown in Table 2.1 and Table 2.2, which also presents the concentrations of 124 compounds found in surface-water samples. These chemicals are moderated either by dilution, biological degradation, sorption to the solid particles settled out of the waste stream or oxidation by disinfection in wastewater treatment (Ternes et al., 2004). The concentrations of these pharmaceuticals range from low parts-per-billion (low micrograms-per-liter ( $\mu\text{g/L}$ )) to high parts-per-trillion (nanograms-per-liter ( $\text{ng/L}$ )) in liquid effluents, whereas in biosolids they occur at parts-per-million (milligrams-per-kilogram ( $\text{mg/kg}$ )) level (Table 2.1 and 2.2).

Table 2.1. Concentrations of Pharmaceuticals in Sludges, Biosolids and Groundwater, reported in the literature since 2004

| Compound              | Sludge and Biosolid Concentration mg/kg | References          | Groundwater Concentration µg/L | References              |
|-----------------------|---|---------------------|--------------------------------|-------------------------|
| <b>Clofibric acid</b> | 0.087 only                              | Ternes et al., 2004 | nd - 0.29                      | Scheytt et al., 2004    |
|                       |   |                     | nd - 0.125                     | Heberer et al., 2004    |
| <b>Diclofenac</b>     | 0.31 - 7.02                             | Ternes et al., 2004 | nd - 0.05                      | Scheytt et al., 2004    |
|                       |   |                     | nd - 0.9                       | Kreuzinger et al., 2004 |
|                       |   |                     | nd - 0.035                     | Heberer et al., 2004    |

Table 2.2. Concentration of Pharmaceuticals in Wastewater Influent, Effluents and Surface Water, reported in the literature since 2004

| Compound              | WWTP Influent Conc., µg/L | WWTP Effluent Conc., µg/L | Surface Water Conc., µg/L | Reference                |
|-----------------------|---------------------------|---------------------------|---------------------------|--------------------------|
| <b>Atenolol</b>       | nd - 0.74                 | nd - 1.15                 | nd - 0.25                 | Gros et al., 2006        |
|                       | 0.03 only                 | 0.16 only                 | 0.06 max                  | Bendz et al., 2005       |
|                       |                           | 0.466 med                 | 0.017 med                 | Zuccato et al., 2005     |
|                       |                           |                           | 0.042 max                 | Castiglioni et al., 2004 |
|                       |                           | 0.19 med                  |                           | Paxeus et al., 2004      |
| <b>Clofibric Acid</b> | nd - 0.36                 | 0.02 - 0.03               | 0.01 - 0.02               | Gros et al., 2006        |
|                       | 0.163 ave                 | 0.109 ave                 | 0.279 ave                 | Quintana et al., 2004    |
|                       |                           |                           | nd - 0.022                | Wiegel et al., 2004      |
|                       | nd - 0.651                | nd - 0.044                |                           | Zhang et al., 2007       |
|                       | 0.34 only                 |                           |                           | Wolf et al., 2004        |
|                       |                           | nd - 0.038                |                           | Brun et al., 2006        |
|                       |                           |                           | 0.003 - 0.027             | Roberts et al., 2006     |

| <b>Compound</b>   | <b>WWTP<br/>Influent Conc.,<br/>µg/L</b> | <b>WWTP<br/>Effluent Conc.,<br/>µg/L</b> | <b>Surface<br/>Water Conc.,<br/>µg/L</b> | <b>Reference</b>       |
|-------------------|--|--|--|------------------------|
| <b>Diclofenac</b> | 0.16 only                                | 0.12 only                                | 0.12 max                                 | Bendz et al., 2005     |
|                   | 0.05 – 0.54                              | nd – 0.39                                | nd – 0.06                                | Gros et al., 2006      |
|                   | 2.333 ave                                | 1.561 ave                                | 0.272 ave                                | Quintana et al., 2004  |
|                   |  |  | nd – 0.069                               | Kosjek et a., 2005     |
|                   | 0.46 ave                                 | 0.4 ave                                  |  | Vieno et al., 2005     |
|                   | 0.28 ave                                 | 1.9 ave                                  | nd – 0.282                               | Quintana et al., 2005  |
|                   | 0.905 – 4.11                             | 0.78 – 1.68                              |  | Clara et al., 2005     |
|                   | 0.901 – 1.036                            | 0.261 – 0.598                            |  | Roberts et al., 2006   |
|                   | 0.14 med                                 | 0.14 med                                 |  | Lishman et al., 2006   |
|                   | 0.05 – 2.45                              | 0.07 – 0.25                              |  | Lee et al., 2005       |
|                   |  | nd - 2.349                               |  | Ashton et al., 2004    |
|                   | 0.33 – 0.49                              |  |  | Thomas et al., 2005    |
|                   |  | nd - 0.5                                 |  | Brun et al., 2006      |
|                   |  | 0.01 - 0.04                              |  | Lindqvist et al., 2005 |
|                   | 4.1 only                                 |  |  | Wolf et al., 2004      |
|                   |  | 0.29 med                                 | nd – 0.089                               | Paxeus et al., 2004    |
|                   |  | 0.032 – 0.457                            |  | Verenitch et al., 2006 |
|                   | 0.06 - 1.9                               | nd – 0.003                               | Gomez et al., 2006                       |                        |

nd = not detected; concentration reported: max = maximum concentration; med = median concentration; only = only measured concentration and ave = average concentration

Over 120 chemicals have been reported in the literature between 2004 and 2006 as shown in Table 2.1 and Table 2.2 for the concentrations of atenolol, clofibric acid and diclofenac in all the major compartments of wastewater influent and effluent, surface water, ground water, sludge and biosolids. In water and sludge, 67 chemicals in wastewater influents, 22 in biosolids and 105 in WWTP effluents have been detected, while 35 each have been detected in groundwater and drinking water, 4 in sediments and 124 in surface water samples.

Wastewater treatment produces about 50% of the biosolids that are spread as a soil amendment on agricultural lands and land reclamation with the remainder destroyed through incineration or disposed of in landfills (USEPA 1999 and 2003).

### 2.1.6 Environmental Risk Assessment

Low biodegradability and relatively persistent compounds and break-down products of pharmaceuticals have been found in water, so further research is needed in this area. There is need for predictive models to predict fate and effects. Other areas requiring further investigation include expanded environmental studies on environmental concentrations; laboratory and field studies on chronic effects and Acute to Chronic Ratio (ACR); field studies on population effects; improved exposure scenarios; and effect of mixtures on aquatic and terrestrial species. There is also a need to consider best practices, e.g., new technologies for wastewater treatment plants, good veterinary and agricultural practices, good manufacturing practices, and disposal programs. The Environmental risk assessment (ERA) for pharmaceutical substances consists of two phases. If exposure assessment in surface water triggers  $PEC_{\text{water}} > 0.01 \mu\text{g/L}$  in Phase I then they are extended to Phase II tests which consists of two tiers. Studies are conducted in surface water and in wastewater treatment plants for acute ecotoxicological tests and its fate in Tier A while bioaccumulations, chronic effects, sorption onto soils and transformation are investigated further in Tier B. Therefore ERA has been prioritized for targeted monitoring based upon their predicted environmental concentration (PEC), predicted no-effect concentration (PNEC) and



persistence, bioaccumulation and toxic (PBT) properties for regulatory purposes (Carlsson et al., 2006a). Further in Phase II, based on Tier A results, an action plan is generated. For example, if  $PEC_{\text{surface water}}/PNEC_{\text{water}} < 1.0$  then it requires no further aquatic testing and if  $PEC_{\text{surface water}}/PNEC_{\text{water}} > 1.0$  or  $PEC/PNEC_{\text{Groundwater}} > 1.0$  or  $PEC_{\text{SurfaceWater}}/PNEC_{\text{Microorganism}} > 0.1$  then it requires Tier B assessment (Merrington et al., 2014).

Climate changes especially in poor and arid countries where there is insufficient water and few resources, recycling of wastewater into drinking water enriches the concentrations of contaminants and pharmaceuticals within a closed cycle (Klaus Kummerer, 2014). Human health can also be affected due to our drugged environment especially antibiotics in the environment. For example, scientists have found that antibiotic-resistant bacteria population is 70% more common where livestock in dairy farms are treated and from lakes that receive hospital effluents compared to uncontaminated environment (Joakim Larsson, 2010). Similarly, low concentrations of antibiotics such as triclosan, erythromycin and trimethoprim if exposed to water fleas simultaneously will result in skewing of sex ratios in water fleas, but have no adverse effect as individual compounds. Similarly Ketoprofen, an arthritis drug is also known to be toxic to birds.

Many PPCPs have the potential to produce acute or chronic adverse effects on ecosystems and humans. Therefore there is a need to develop effective technologies for their removal from water. Acute effects of pharmaceuticals exposure focuses on environmental toxicology rather than chronic effects. Exposure risks and effects on aquatic organisms are much greater than those for humans. Aquatic organisms have multi-generational, continual and high concentration exposures of PPCPs and their low dose effects in untreated water.

### 2.1.7 Natural Organic Matter and Brominated species in natural waters

Presence of a heterogeneous mixture of natural organic matter (NOM) in water supplies is another great concern (Boyer and Singer 2008; Sharp et al., 2006) as it comprises of fulvic acid (FA), humic acid (HA), proteins, carbohydrates and lignins (Chen et al., 2002; Her et al., 2002). Properties such as taste, color and odor are affected in water by the presence of NOM as it is an important factor which determines doses that are needed for disinfectant and coagulation. Compounds such as atrazine, also competes with NOM (Li et al., 2003a). Disinfection byproducts (DBPs) are produced when NOM reacts with disinfectants that are harmful to human beings (Ivancev-Tumbas et al., 1999); The operability and effectiveness of the treatment processes is strongly impacted by the presence of NOM. Fouling of membranes takes place due to NOM (Lee et al., 2005); Pore blocking is enhanced by NOM as its decreases the adsorption capacity of powdered activated carbon/granular activated carbon (Li et al., 2003b). Hence in most water purification systems the priority is to remove NOM. Ozonation (Selcuk et al., 2007), adsorption, and coagulation (Ho and Newcombe 2005), biodegradation (Leiknes et al., 2005), membrane filtration and ion exchange (Bolto et al., 2002) are some of the current options for the removal of NOM. Almost 90% removal of NOM was observed by Wang et al., 2010 in 15min using carbonaceous nanoparticles and alum coagulation. The two main mechanisms of coagulation are sweep flocculation and charge neutralization (Duan and Gregory 2003). Many factors aid in the removal of NOM which include concentration of NOM, pH or hydrogen ion concentration, coagulants dosage, alkalinity of raw water and intensity of mixing (Franceschi et al., 2002; Volk et al., 2000).

Further, chlorination of drinking water reacts with dissolved organic carbon (DOC) and bromide resulting in the formation of halogenated disinfection by-products (DBPs) which are more harmful than chlorinated counterparts (Attias et al., 1995; Plewa et al., 2002). The free chlorine (HOCl) oxidizes bromide forming hypobromous acid (HOBr) which react with natural organic matter (NOM) forming DBPs, haloacetic acids (HAA) and trihalomethanes (THMs). Currently these are regulated under the Stage 1

Disinfectants and Disinfection By-Products (D/DBP) by US Environmental Protection Agency (US EPA, 1998). As per Oliver, 1983; Symons et al., 1993, more brominated species of DBP will form due to high dose ratios of  $\text{Br}^-/\text{Cl}_2$  and  $\text{Br}^-/\text{DOC}$ . Nanofiltration, enhanced coagulation and activated carbon adsorption were used to remove DBP prior to chlorination but that lead to removal of DOC. An expensive technology involving membrane processes such as reverse osmosis or anion exchangers may be used to remove DBP to protect human health. During water treatment, oxidizing agents generate bromate anions from bromide anions present in water resources (U. von Gunten, 2003) that are highly toxic to humans. The maximum concentration of bromated anions permitted in drinking water is  $25\mu\text{g/L}$  as per World Health Organization (WHO).

### 2.1.8 Stages of a Wastewater Treatment Plant

Figure 2.3 shows various stages of primary, secondary and tertiary treatments in a wastewater treatment facility. Primary treatment or mechanical treatment is the first stage of the treatment process which includes screening to trap large objects, suspended and floating solids from raw sewage followed by grit channel which allows grit, stones and sand to settle at the bottom of channel. The grits and larger objects are taken to landfill site for disposal. The sewage then passes through the sedimentation tanks or primary clarifiers where suspended solids are removed by gravity through addition of chemicals to accelerate the process and the floating oil and grease is skimmed off. Around 20-30% BOD and 50-60% total suspended solids (TSS) are removed in the first stage of treatment process. Secondary or biological treatment is the second stage of the treatment process where microbes consumes organic matter as food that escapes primary treatment and convert them to carbon dioxide, water and energy. In the aeration tank, vigorous mixing of air with wastewater in presence of microorganisms can work more efficiently and more of the suspended solids are removed by additional settling tanks where 90% organics are removed by processes that include trickling filters, activated sludge, biotowers, oxidation ditches and other forms that break down organic matter utilizing biological activity.

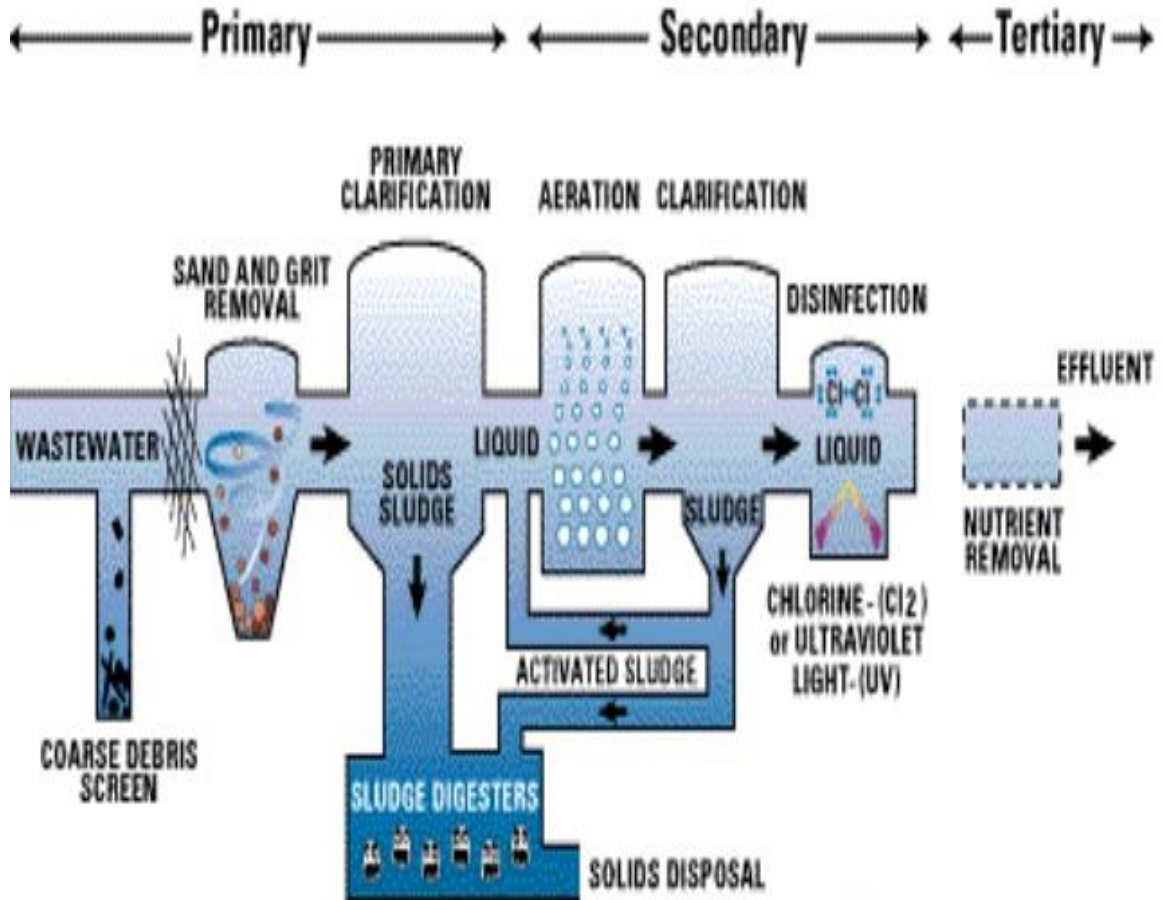


Figure 2.3. Various stages of a conventional wastewater treatment plant (Sherry S., and Karl A., 2006)

The water is pumped to secondary clarifier after biological treatment where any remaining microorganisms or solids settle at the bottom and continues on to disinfection. Tertiary treatment is an additional and advanced treatment technique that produces an effluent equivalent to drinking water quality which removes almost 99% of all impurities including nitrogen and phosphorus from sewage. Before effluent is discharged, disinfection with chlorine, ultraviolet radiation or ozone can be the final step to reduce the number of microorganisms in the water that is discharged back into the environment.

According to Roberts and Thomas (2006), up to 90% of ibuprofen was removed by wastewater treatment works (WTW) in UK. Data obtained from the final treated effluent collected from Canadian WWTP during the period 1999-2002 showed

concentration of selected acidic PhACs from Whitby, Ontario by Miao et al. (2002), eighteen WWTPs in fourteen municipalities showed prescription and non-prescription drugs in small residues by Metcalfe et al. (2003a), and acidic and neutral drugs from WWTP effluents for the cities of Windsor, Peterborough and Burlington, Ontario Hua et al. (2006), Metcalfe et al. (2003b). Miao et al. (2002), Metcalfe et al. (2003a) and Hua et al. (2006) reported maximum concentrations of 28.4  $\mu\text{g/L}$  of Diclofenac and 0.076  $\mu\text{g/L}$  of Clofibric Acid in treated effluent samples collected from Canadian WWTPs. Similarly 0.194  $\mu\text{g/L}$  of Diclofenac and 0.175  $\mu\text{g/L}$  of Clofibric acid were reported in surface waters of Lake Erie, Lake Ontario and Great Lakes Basin in Canada adjacent to discharges of effluent from sewage treatment plant effluents during 1999-2002. According to Ternes 1998 and Heberer 2002 a,b the maximum concentrations of drugs in Canada appeared to be greater compared to Switzerland or Germany in final effluents of WWTP for Ibuprofen, salicylic acid, naproxen and anti-inflammatory drugs.



Figure 2.4. Adelaide wastewater treatment plant, London, ON, Canada

For the present study, among the six STPs, the target waters were secondary effluent from Adelaide wastewater treatment plant, London, ON, Canada shown in Figure 2.4. The present research aims at exploring and validating an advanced oxidation method (photocatalysis of  $\text{TiO}_2/\text{O}_3/\text{UV}$ ) for the degradation of Diclofenac, Clofibric acid and Atenolol which are widely consumed in high amounts in industrialized countries as well as around the world. The research will also focus on kinetic studies that are needed to identify the degradation of Diclofenac, Clofibric acid and Atenolol to obtain data for the evaluation of their post treatment toxicity in a future study.

### 2.1.9 Comparison of various treatment technologies and percent removal of target PPCPs

A comparison of different literature studies shown in Table 2.3 shows maximum percent removal by various treatment methods adopted for various types of water. Most of the previous studies have been conducted on the removal of ATN, CFA and DCF from drinking water, double distilled water, Milli Q, river and lake water

In wastewater, the studies have been limited and it was found that the maximum removal efficiency by conventional treatment was 50.1% (MBR 87.4%) for diclofenac, 27.7% (MBR 86%) for clofibric acid, and 55% (staged anaerobic fluidized membrane bioreactor (SAF-MBR, 98-100%) for atenolol. Hence the hypothesis for the present research will be based on further studies in wastewater using a combination of different techniques.

Table 2.3. Comparison of various treatment technologies and their removal efficiency from various types of water matrices for the three target PPCP compounds

| Compound                            | Type of Water  | Treatment Method  | % Removal                                    | References               |
|-------------------------------------|--|---|--|--------------------------|
| <b>Atenolol<br/>(Beta-blockers)</b> | Wastewater   | Conventional biological treatment   | 10% in winter months<br>55% in summer months | Castiglioni et al., 2006 |
|                                     | Wastewater   | MBR   | 77%  | Kim et al., 2014         |
|                                     | Wastewater   | SAF-MBR   | 98-100%                                      | Dutta et al., 2014       |
|                                     | Secondary Effluent   | Ferrate VI (Conc. 5mg/L at pH 6)  | 28.4%  | Zhou and Jiang, 2015     |
|                                     | Milli-Q Ultrapure Water  | Solar 1kW lamp (Xe-OP)/TiO <sub>2</sub>   | 80% in 120min at pH 8                        | Ioannou et al., 2011     |
|                                     | Secondary Treated Effluent   | H <sub>2</sub> O <sub>2</sub> /Degussa P25 (250mg/L)<br>TiO <sub>2</sub> = 2g/L | 76% in 120min<br>17% in 30min                |                          |
| Milli-Q Water                       | High pressure mercury lamp= 125W, TiO <sub>2</sub> =2g/L<br>Conc.=37.6μM | Completed in 60min  | Ji et.al., 2013                              |                          |

|  |                               |  |        |                           |
|--|-------------------------------|--|--------|---------------------------|
| <b>Diclofenac<br/>(Anti-inflammatory drug)</b> | Wastewater                    | NA   | 69%    | Ternes et al., 1998       |
|  | Distilled and drinking water  | O <sub>3</sub> /H <sub>2</sub> O <sub>2</sub>    | 100%   | Zwiener and Frimmel, 2000 |
|  | Distilled water               | Ozonation  | 100%   | Zwiener and Frimmel, 2000 |
|  | Milli Q, river and lake water | Ozonation  | 97%    | Huber et al., 2003        |
|  | Different samples             | NA   | 53-74% | Clara et al., 2005        |
|  | Wastewater                    | Activated Sludge                                 | 7-29%  | Clara et al., 2005        |
|  | Doubly distilled water        | H <sub>2</sub> O <sub>2</sub> /UV<br>(17 W lamp) | 100%   | Vogna et al., 2004        |
|  | Wastewater                    | Flotation  | 45%    | Carballa et al., 2005     |
|  | Wastewater                    | NA   | -34%   | Lishman et al., 2006      |
|  | Wastewater                    | MBR  | 87.4%  | Radjenovic et al., 2007   |
|  | Wastewater                    | Conventional Treatment                           | 50.1%  | Radjenovic et al., 2007   |

NA = Not Available



|   |  |   |   |                           |
|---|--|---|---|---------------------------|
| <b>Clofibric acid<br/>(Lipid regulators,<br/>Antiphlogistics)</b> | Distilled and drinking water                                     | O <sub>3</sub> /H <sub>2</sub> O <sub>2</sub> | 97.9%   | Zwiener and Frimmel, 2000 |
|   | Wastewater   | Pilot WWTP and biofilm reactor                | 5%  | 2003                      |
|   | Distilled and drinking water                                     | Ozonation (0.5mg/L O <sub>3</sub> dose)       | 10-15%  | Ternes et al., 2002       |
|   |  | (2.5- 3.0mg/L O <sub>3</sub> dose)            | 40% (20 min)  |                           |
|   | Aqueous solution   | Ozonation                                     | 100% in 20 min (34% mineralization) & 60 min (48% mineralization) | Andreozzi et al., 2003    |
|   | Aqueous solution   | H <sub>2</sub> O <sub>2</sub> /UV (17W lamp)  | 100% (60 min)   | Andreozzi et al., 2003    |
|   | Ultrapure water  | Photocatalysis (TiO <sub>2</sub> /Solar)      | 99.7% (50 min)  | Doll and Frimmel, 2005    |
|   | Wastewater   | MBR   | 71.80%  | Radjenovic et al., 2007   |
|   | Wastewater   | MBR<br>Conventional Activated Sludge          | 72-86%<br>26-51%  | Radjenovic et al., 2009   |
| Wastewater  | Conventional WWTP<br>Tertiary treatment (chemical + sand filter) | 55%<br>61%                                    | Zorita et al., 2009   |                           |

### 2.1.10 Physico-chemical properties of target PPCP compounds

Table 2.4. Test compounds with its IUPAC names and chemical structure

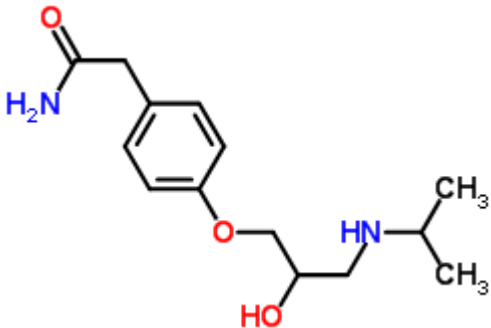
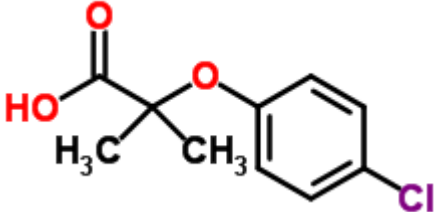
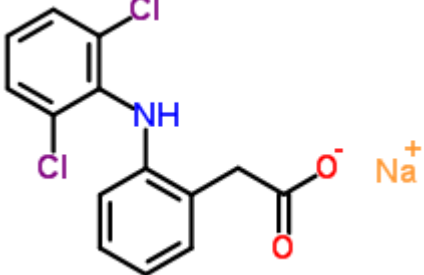
| Compound   | Structure  |
|--|--|
| <p><b>Atenolol</b></p> <p><b>IUPAC:</b> 2-[4-[2-hydroxy-3-(propan-2-ylamino) propoxy] phenyl]acetamide</p> |    |
| <p><b>Clofibric Acid</b></p> <p><b>IUPAC:</b> 2-(4-Chlorophenoxy)-2-methyl propanoic acid</p>              |   |
| <p><b>Diclofenac</b></p> <p><b>IUPAC:</b> Sodium;2-[2-(2,6-dichloroanilino) phenyl] acetate</p>            |  |

Table 2.4 shows the chemical structure of the target PPCP compounds (ChemSpider). Atenolol shows methyl, amino and hydroxyl moieties while methyl and carboxylic acid moieties exist for Clofibric Acid whereas Diclofenac shows acetic acid, amino and phenyl moieties. Presence of various heteroatoms such as N, Cl, O and Na in these organic compounds determines its solubility with various solvents by the interaction of these specific heteroatoms causing high polarizability (Zilnik et al., 2007).

Table 2.5. Physico-chemical properties of test compounds

| Properties  | Atenolol                    | Clofibric Acid                                 | Diclofenac Sodium                            |
|---|-----------------------------|--|--|
| <b>Therapeutical Group</b>  | $\beta$ -blocker            | Lipid regulator and Cholesterol lowering drugs | Non-Steroidal Anti-Inflammatory Drug         |
| <b>Brand Name</b>   | Tenormin, Normiten, Blokium | Atromid-S                                      | Cambia, Zipsor, Cataflam, Voltaren, Zorvolex |
| <b>CAS Number</b>   | 29122-68-7                  | 882-09-7                                       | 15307-79-6                                   |
| <b>Category</b>   | Basic                       | Acidic   | Acidic                                       |
| <b>Chemical Formula</b>   | $C_{14}H_{22}N_2O_3$        | $C_{10}H_{11}ClO_3$                            | $C_{14}H_{11}Cl_2NO_2.Na$                    |
| <b>Molecular Weight (g/mol)</b>                                   | 266.34                      | 214.65   | 318.13                                       |
| <b>Vapor Pressure (mm Hg)</b>                                     | $2.92 \times 10^{-10}$      | $1.13 \times 10^{-4}$                          | $4.75 \times 10^{-14}$                       |
| <b>Water Solubility at 20°C (mg/L)*</b>                           | 26500 at 37°C               | 583  | 2370   |
| <b>pKa at 20°C</b>  | 9.6                         | 3.2  | 4.15   |
| <b>log Kow</b>  | 0.16                        | 2.57   | 4.51<br>0.7 (DCF-Na)                         |
| <b>Henry's Law Constant (atm-m<sup>3</sup>/mole)</b>              | $1.37 \times 10^{-18}$      | $2.19 \times 10^{-8}$                          | $4.73 \times 10^{-12}$ (DCF)                 |
| <b>Atmospheric OH Rate Constant (cm<sup>3</sup>/molecule-sec)</b> | $1.38 \times 10^{-10}$      | $7.75 \times 10^{-12}$                         | $1.64 \times 10^{-10}$                       |

\* Benner et al., 2009

Table 2.5 shows a summary of some of the physico-chemical properties of Atenolol, Clofibric Acid and Diclofenac (ChemID Plus). The physical and chemical properties

helps to determine if a compound is most likely to concentrate in the atmospheric environmental or aquatic or terrestrial compartments based on pKa, log Kow, Henry's Law constant or vapor pressure. Non-ionized or ionized chemical form is determined by the compounds pKa and pH of the medium. For the present study, three different therapeutic groups categorized into basic and acidic drugs were chosen. The acid dissociation constant (pKa) values ranged from 3.2 to 9.6 and the octanol water partition coefficient (log Kow) ranged from 0.16 to 4.51.

Table 2.6. Uses, toxicity and byproduct/degradation products for test compounds

| Compound                | Uses  | Side effects/Toxicity  | By Products/Degradation  |
|-------------------------|---|--|--|
| <b>Atenolol</b>         | Treat angina (chest pain), high blood pressure (hypertension), irregular heart beat (cardiac dysrhythmias) and reduction of heart complication following heart attack (myocardial infarction) | Tiredness, dizziness, drowsiness, depression, lightheadedness, nausea, diarrhea, unusual weight gain, swelling of the hands, feet, ankles or lower legs  | 3-(isopropylamino) propane-1,2-diol;<br>p-hydroxyphenyl acetamide<br>4-[2-hydroxy-3-(isopropyl amino) propoxy] benzaldehyde<br>(Ji et al., 2013) |
| <b>Clofibrilic Acid</b> | Decreases triglycerides and cholesterol production. Plant growth regulator against plant hormone auxin  | anorexia; nausea; gastric discomfort; stomatitis; headache; dizziness; skin reaction; myotoxicity; fatigue; alopecia; vertigo; vomiting; impotence; anaemia; leucopenia; diarrhoea; thrombocytopenia; weight gain; flatulence; drowsiness; hepatomegaly. Increased incidence of cholecystitis, gallstones and pancreatitis | hydroquinone, 4-chlorophenol and isobutyric acid<br>(Doll and Frimmel, 2004)   |

|                   |   |  |  |
|-------------------|---|--|--|
| <b>Diclofenac</b> | Treat Cancer, musculoskeletal complaints, reduce inflammation, pain and stiffness from menstrual cramps | Gastrointestinal, cardiac, renal, hepatic. Toxicity: Oral (LD50): Acute: 53 mg/kg [Rat], 95 mg/kg [Mouse], 157 mg/kg [Rabbit]. Degeneration of tubular epithelial cells, hyaline droplets and interstitial nephritis | 2-chloroaniline; 2,6-Dichloro phenol; 2,6-dichloroaniline; 1-(2,6-dichlorophenyl)indolin-2-one; 2-(2-chlorophenylamino) benzaldehyde; 2,6dichloro-N-o-tolylbenzenamine; 9H-carbazole-1-carbaldehyde; 8-chloro-9H-carba zole-1-carbalde hyde; 2-(2,6-dichlorophenylamino) benzaldehyde (Bartels et al., 2007) |
|-------------------|---|--|--|

Table 2.6 provides a summary on therapeutical uses, toxicity and by product or degradation products formed for the target compounds through various treatment processes. PPCP compounds find several applications. For example Diclofenac, a NSAID compound is used to reduce inflammation, pain and stiffness from menstrual cramps, arthritis, and similar conditions. Clofibrac acid, a fibrate drug under an antihyperlipidemics decreases triglycerides and cholesterol production and increases high-density lipoprotein production, and Atenolol a beta-blocker is used in the treatment of hypertension and angina (chest pain) and prevents heart attack.

Based on Henry's Law constant ( $H_c$ ) and  $K_{ow}$ , during wastewater treatment volatilization losses of organic compounds can be estimated using the following empirically defined categories:

$H_c > 1 \times 10^{-4}$  and  $H_c/K_{ow} > 1 \times 10^{-9}$       High-volatilization potential

$H_c < 1 \times 10^{-4}$  and  $H_c/K_{ow} < 1 \times 10^{-9}$       Low-volatilization potential

As per Table 2.4,  $H_c$  values of ATN, CFA and DCF are very low and is lesser than  $1 \times 10^{-4}$  and the ratio of  $H_c/K_{ow}$  is also less than  $1 \times 10^{-9}$  which indicates that the selected PPCP compounds exhibit very low-volatilization potential.

Table 2.7. Log K<sub>ow</sub> versus Sorption Potential

| <b>Log K<sub>ow</sub></b>      | <b>Sorption Potential</b> |
|--------------------------------|---------------------------|
| log K <sub>ow</sub> <2.5       | Low                       |
| 2.5 < log K <sub>ow</sub> <4.0 | Medium                    |
| log K <sub>ow</sub> >4.0       | High                      |

Based on Table 2.7, compounds with log K<sub>ow</sub> higher than 4.0 may have a higher tendency to sorb to soil or sludge and are more hydrophobic as in the case of diclofenac the log Kow values are 4.51, while a medium sorption is observed for compounds exhibiting log Kow between 2.5 and 4.0 as in the case of Clofibrac acid with log Kow values of 2.57 and low sorption potential is observed for compounds with log Kow less than 2.5 as in the case of Atenolol with log Kow values of 0.16. Based on these values, either an electrostatic attraction or repulsion can take place between the solute and the adsorbent.

In order to oxidize most of the organic and inorganic compounds from water, there is a need to study various oxidizing species that could generate high oxidation power to degrade the contaminants. Therefore a comparison among the relative oxidation power of various oxidizing species, are represented in Table 2.8. Among all the oxidizing species, hydroxyl radical and TiO<sub>2</sub><sup>+</sup> exhibit highest oxidation power. The hydroxyl radicals ( $\cdot\text{OH}$ ) are generated in Advanced Oxidation Processes which will act rapidly with most of the organic compounds due to its relative high oxidation power of 2.05 which acts as a powerful, non-selective chemical oxidant.

Table 2.8. Some oxidizing species with their relative oxidation power (Carey, 1992 and Techcommentary, 1996)

| Oxidizing species             | Relative oxidation power |
|-------------------------------|--------------------------|
| Chlorine                      | 1.00                     |
| Hypochlorous acid             | 1.10                     |
| Hydrogen Peroxide             | 1.31                     |
| Ozone                         | 1.52                     |
| Atomic oxygen                 | 1.78                     |
| Hydroxyl radical              | 2.05                     |
| TiO <sub>2</sub> <sup>+</sup> | 2.35                     |

Table 2.9 provides the reaction rate constants which vary widely in the range from 0.01 to  $10^3 \text{ M}^{-1} \text{ s}^{-1}$  of molecular ozone and hydroxyl radicals with different organic compounds. All organic compounds are aggressively attacked by the generated hydroxyl radicals typically million to a billion times faster compared to hydrogen peroxide and ozone. The treatment costs are thus greatly reduced including system size. Addition and hydrogen abstraction are the two types of possible initial attacks that take place by hydroxyl radicals depending on the nature of organic species. For the first type, hydroxyl radicals add to the contaminants such as aromatic or olefins leading to mineralization or abstraction of hydrogen atom from alkanes or alcohols leading to formation of water. Thus the destruction rate of contaminant is directly proportional to contaminant rate constant with hydroxyl radical. As shown in Table 2.9, alkanes are very difficult to be oxidized due to their smaller rate constants whereas chlorinated alkenes due to presence of double bond are attacked most efficiently by hydroxyl radicals.

Table 2.9. Organic compounds with reaction rate constants of ozone vs. hydroxyl radical (The UV/Oxidation Handbook)

| <b>Compound</b>              | <b>O<sub>3</sub></b><br><b>(k, M<sup>-1</sup> s<sup>-1</sup>)</b> | <b>·OH</b><br><b>(k, M<sup>-1</sup> s<sup>-1</sup>)</b> |
|------------------------------|---|---|
| <b>Chlorinated alkenes</b>   | 10 <sup>-1</sup> – 10 <sup>3</sup>                                | 10 <sup>9</sup> - 10 <sup>11</sup>                      |
| <b>Phenols</b>               | 10 <sup>3</sup>   | 10 <sup>9</sup> - 10 <sup>10</sup>                      |
| <b>N-containing Organics</b> | 10 – 10 <sup>2</sup>  | 10 <sup>8</sup> - 10 <sup>10</sup>                      |
| <b>Aromatics</b>             | 1 – 10 <sup>2</sup>   | 10 <sup>8</sup> - 10 <sup>10</sup>                      |
| <b>Ketones</b>               | 1   | 10 <sup>9</sup> - 10 <sup>10</sup>                      |
| <b>Alcohols</b>              | 10 <sup>-2</sup> - 1  | 10 <sup>8</sup> – 10 <sup>9</sup>                       |
| <b>Alkanes</b>               | 10 <sup>-2</sup>  | 10 <sup>6</sup> – 10 <sup>9</sup>                       |

## 2.2 Advanced Oxidation Processes

Advanced Oxidation Process (AOP) refers to the removal of organic and inorganic materials by oxidation from water and wastewater by chemical treatment procedures. The aim of AOP procedure is the purification of wastewater to such an extent that the receiving streams get cleaned wastewater after reduction of the chemical contaminants. AOP involves generation of highly reactive in situ hydroxyl radicals by a combination of one or more of the following oxidants such as UV, H<sub>2</sub>O<sub>2</sub>, O<sub>3</sub>, H<sub>2</sub>O<sub>2</sub>/Fe<sup>2+</sup>, UV/O<sub>3</sub>, UV/H<sub>2</sub>O<sub>2</sub>, etc (Mustranta and Viikari (1993); Pere et al., (1993); Bowers et al., (1991), and Sarikaya and Al-Marshoud (1993)).



Some of the applications of AOPs are reduction of COD in wastewater and removal of chlorinated hydrocarbons from drinking water, biodegradability improvement of harmful substances and aqueous solution detoxification (Wedekamp, 1994; Ince, 1999; Wenzel et al., 1999). In the present work, pretreatment of wastewater using various AOPs such as  $O_3$ , UV, UV/ $O_3$ ,  $TiO_2$ , UV/ $TiO_2$  and  $H_2O_2$  will be described.

### 2.2.1 Advanced Oxidation Methods

The main mechanism of AOPs function is the generation of highly reactive free radicals.  $\bullet OH$  is a non-selective oxidant that is able to oxidize a wide range of organic molecules with rate constants usually in the order of  $10^6$ - $10^9 M^{-1} s^{-1}$  (Andreozzi et al., 1999). The  $\bullet OH$  radical is among the strongest oxidizing species used in water and wastewater treatment and offers the potential to greatly accelerate the rates of contaminant oxidation (Zhou et al., 2001). Once generated, the hydroxyl radicals can attack organic chemicals by radical addition, hydrogen abstraction and electron transfer (Ray et al., 2006). The reaction of hydroxyl radical with organic pollutants leads to the complete mineralization to  $CO_2$  and  $H_2O$ .

Figure 2.5 depicts both photochemical and non-photochemical methods generating  $\bullet OH$  radicals. A homogeneous process may or may not utilize energy to generate  $\bullet OH$  radicals. UV radiation alone or a combination of UV such as UV/ $O_3$ , UV/ $H_2O_2$ , UV/ $O_3$ / $H_2O_2$  and Photo-Fenton (UV/ $H_2O_2$ / $Fe^{2+}$ ) or Ultrasound (US) such as  $O_3$ /US and  $H_2O_2$ /US or Electrical such as electro-fenton, anodic oxidation and electrochemical oxidation utilize energy to generate  $\bullet OH$  radicals in solution. While some of the reactions such as ozonation in the alkaline medium (at pH >8.5), ozone combined with hydrogen peroxide and hydrogen peroxide with catalyst utilizes no energy. For a heterogeneous process, catalytic ozonation, photocatalytic ozonation and heterogeneous photocatalysis reactions are involved.

For the present study, the secondary effluent will be subjected to both homogeneous and heterogeneous processes such as  $O_3$ , UV, UV/TiO<sub>2</sub>,  $O_3$ /UV,  $O_3$ /TiO<sub>2</sub> and  $O_3$ /UV/TiO<sub>2</sub> to generate ·OH radicals in solution for degradation of PPCPs.

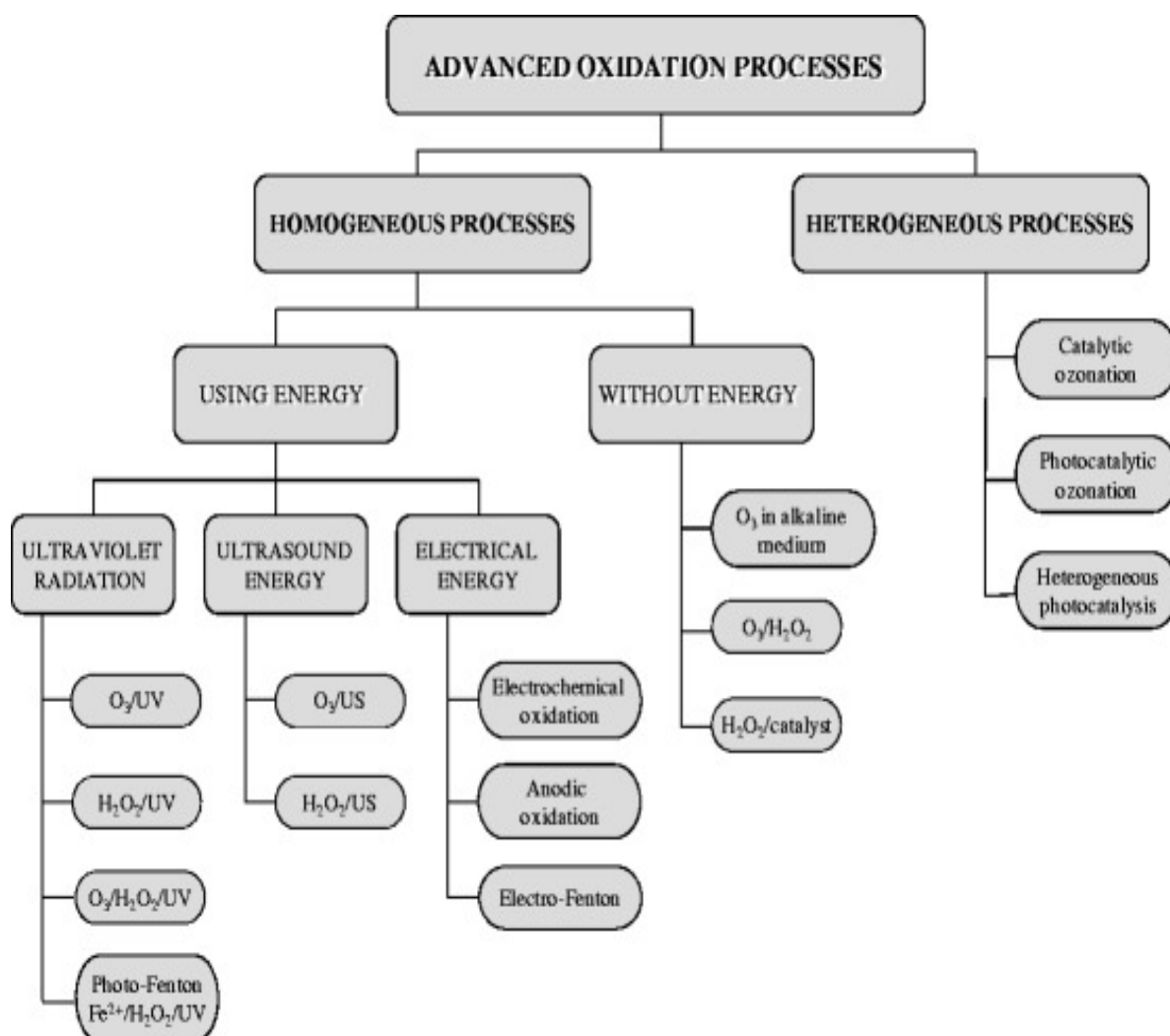


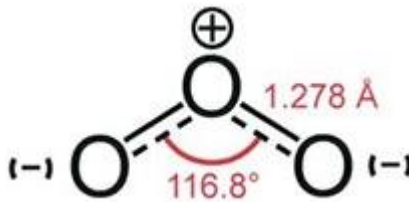
Figure 2.5. Classification of Advanced Oxidation Processes into Homogeneous and Heterogeneous Processes (Poyatos et al., 2009)

### 2.2.1.1 Ozonation

Ozone is a colorless or pale blue gas consisting of three oxygen atoms with distinctively pungent smell and an allotrope of oxygen that are very unstable with a short half-life as per the following reaction mechanism:



The structure of ozone is a bent molecule and is a polar molecule with double bond on one side and single bond on the other side with the following bond angles.



In the presence of organic pollutants in water, ozone undergoes three reactions: 1, 3-dipole (cyclo addition, a Criegee mechanism), a nucleophilic and an electrophilic. Ozone is a very strong oxidant and its solubility in water increases by increasing air pressure (oxygen) and ozone concentration in the air (oxygen) and decreasing pH, amount of solute, excess of UV-light and water temperature.

The corona discharge element present in the ozone generator provides a capacitive load which ruptures the stable oxygen molecule forming two oxygen radicals that further combine with oxygen molecules to form ozone. A dielectric controls and maintains the electrical discharge in glass or ceramic and is often cooled by air or cooling water to remove the excessive heat from the electrodes shown in Figure 2.6 (Oxidation technologies, 2014). Pure oxygen supplied from an oxygen generator is used for the production of ozone.

Air dryers, air and dust filters are used to condition this. Ozone destructors are used to break down the left over of ozone after use, such as magnesium oxide catalyst which accelerates decomposition of ozone into oxygen. Over 90% of the power supplied to the

ozone generator is utilized to produce sound, light and primary heat, which is a very energy-intensive process. Inlet gas oxygen concentration, purity and humidity of the inlet gas, electrical parameters and cooling water temperature are some of the important factors optimized to influence high ozone generation and minimize energy usage (Lenntech, 2007).

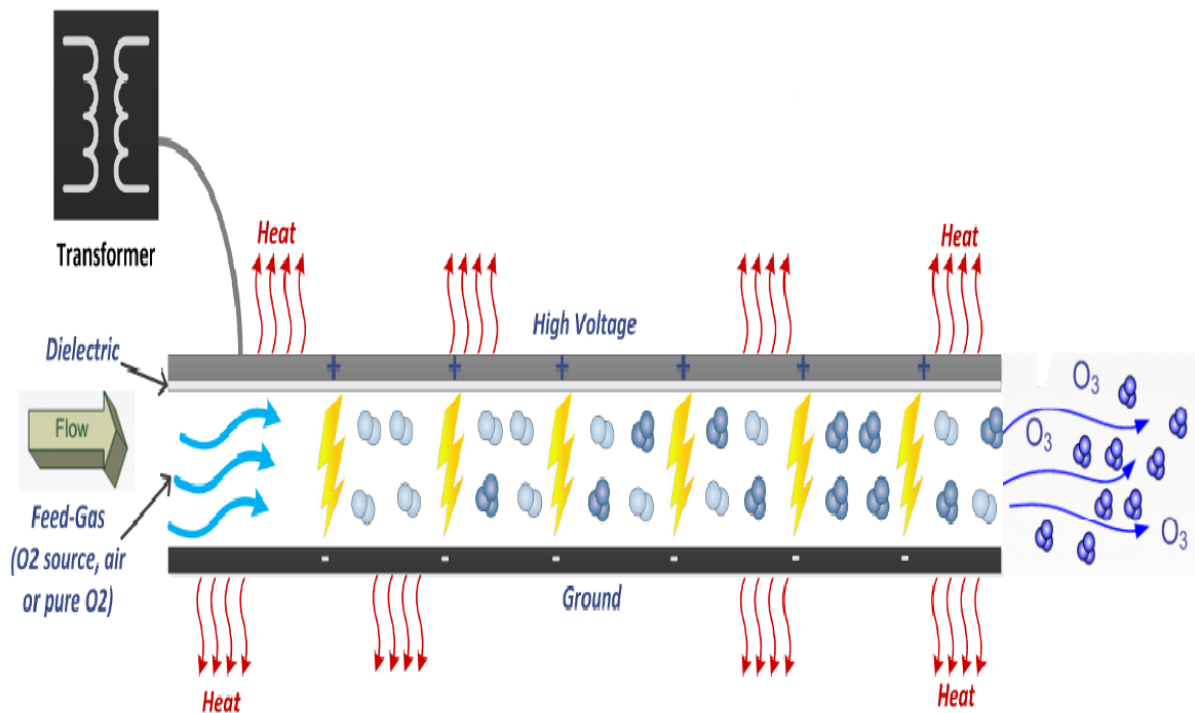


Figure 2.6. Ozone production from corona-discharge (Oxidation technologies, 2014)

In natural waters, the ozone decay into OH-radicals is characterized by a fast initial decrease of ozone which is followed by first order kinetics where ozone decreases in the second phase (Arooj et al., 2014). The half-life of ozone varies from seconds to hours depending on the quality of water, and the factors that influence ozone decomposition are pH, temperature, UV light, concentrations and environment of dissolved matter. For example, at higher temperature, ozone is less stable and the solubility of ozone decreases. The half-life of ozone in water is shorter at pH 7, i.e., at 15°C is 30 min, at 20°C is 20 min, at 25°C is 15 min and at 30°C is 12 min. The formation of OH<sup>-</sup> radicals increases as the pH value increases. In water, ozone

decomposes into OH-radicals. Based on the nature of dissolved constituents, substances can slow down or inhibit the reaction (scavenging capacity) in decaying of ozone or accelerate (promote chain reaction).

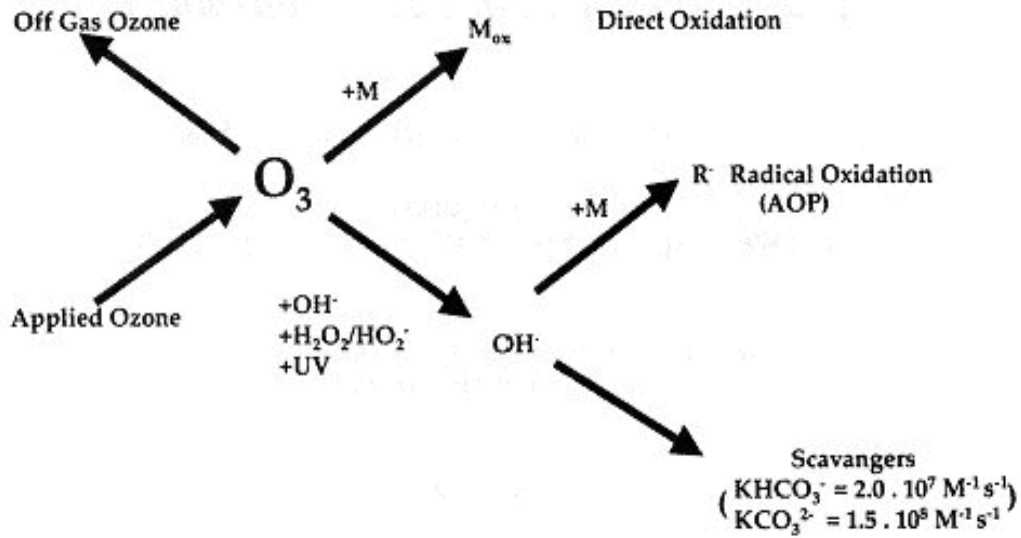


Figure 2.7. Reactions of ozone and dissolved solids \*

The scavenging capacity of carbonate ( $\text{CO}_3^{2-}$ ) ions is much stronger (reaction speed  $\text{CO}_3^{2-}$ :  $k = 4.2 \times 10^8 \text{ M}^{-1} \text{ s}^{-1}$ ) than that of bicarbonate ( $\text{HCO}_3^-$ ) ions (reaction speed  $\text{HCO}_3^-$ :  $k = 1.5 \times 10^7 \text{ M}^{-1} \text{ s}^{-1}$ ) as defined in Figure 2.7 (Lopez et al., 1999).

$$k_{\text{OH-DOC}}[\text{DOC}] + k_{\text{OH-HCO}_3^-}[\text{HCO}_3^-] + k_{\text{OH-CO}_3^{2-}}[\text{CO}_3^{2-}] \quad \text{Eq. (2.2)}$$

The mass transfer rate of ozone follows a double-layer model and depends on the physical properties of gas and liquid, turbulence and concentration difference across the surface. The following stages are processed during the transfer of ozone from gas to liquid: ozone diffusion across the gas/liquid phase, dissolving into liquid and diffusion

into liquid as shown in Figure 2.8. In the liquid phase, Ozone alone can produce hydroxyl radicals or can combine with other AOPs to generate hydroxyl radicals that react with pollutants and break down partially or completely to harmless intermediates and end-products such as carbon dioxide, halide ions and carboxylic acids. Diffuser and Venturi are the most common techniques used to inject ozone in water (Lennetech, 2007).

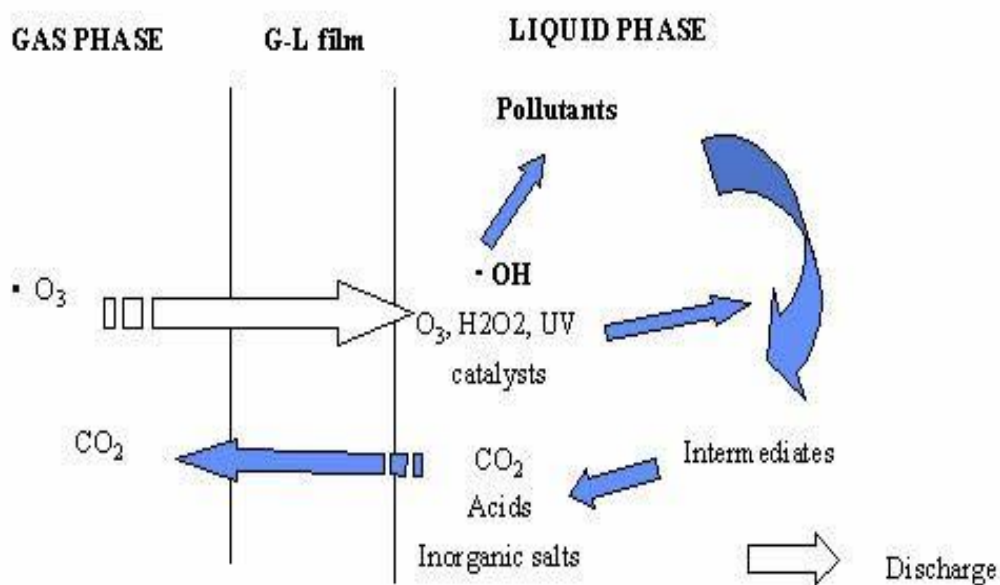
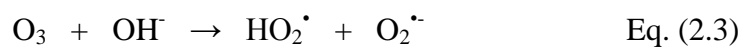
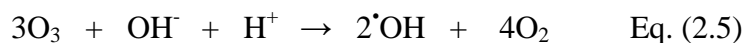


Figure 2.8. Double-layer model for ozone mass transfer (ESCO International)

Ozone decomposition rate increases in water as the pH rises and the half-life of ozone is less than 1 min at pH 10. A combination of molecular ozone with  $\cdot\text{OH}$  radical reactions may lead to the oxidation of organic species.





Hydroperoxyl radical  $\text{HO}_2\cdot$  and super-oxide anion radical  $\text{O}_2^{\cdot-}$  are formed by the reaction between hydroxide ions and ozone. This ozone further undergoes reaction with super-oxide anion radical forming the ozonide anion radical  $\text{O}_3^{\cdot-}$  which decomposes immediately leading to the formation of  $\cdot\text{OH}$  radical. The above equation shows the formation of two  $\cdot\text{OH}$  radicals from three ozone molecules (Gottschalk, 2000)

Ozone finds several applications as it is used to reduce acute toxicity of effluents and destroys bacteria in the pulp and paper industry (Zmolek, 1977), decoloration of wastewater in textile industry (Gough, 1993), effective at dibenzofuran and dibenzo-p-dioxin destructive oxidation (Hostachy, et al., 1993), treating landfill leachates (Wable et al., 1993) and so on.

### 2.2.1.2 UV

UV technology has been used for over 25 years. It destroys 99.99% of harmful microorganisms without the addition of chemicals or a change in the water's taste or odor, and is considered a safe and cost-effective technology to purify water. It is one of the four methods of disinfection approved by the United States FDA. Ultraviolet germicidal irradiation (UVGI), kills or inactivates microorganisms, such as viruses, bacteria, pathogens and molds, by disrupting their DNA or destroying their nucleic acids. This UVGI uses short-wavelength UV-C light and has been used since the mid - 20<sup>th</sup> century and finds several applications to disinfection primarily in sterile work facilities and medical sanitation, apart from drinking and wastewater treatment facilities, and as air purifier. UV is also more effective to both *Cryptosporidium* and *Giardia*, unlike chlorine, and does not form chemical disinfection by products (DBPs) and is easy to maintain with an annual lamp and filter replacements.

In water treatment applications, U.S. EPA suggests UV effectiveness based on its transmittance (light reaching the target), flow rate (contact time), outages or fouling or lamp age (reduction in UV intensity) and turbidity (cloudiness) rather than measuring UV dose. Direct photolysis by UV leads to degradation of organic compounds by light absorption.

### 2.2.1.3 Photocatalytic Metal Oxide (TiO<sub>2</sub>)

TiO<sub>2</sub> an N-type semiconductor has been used widely since past few years to remove organic pollutants from wastewater due to its high photocatalytic activity, low energy, environmentally safe and non-toxic (Chen X., and Selloni, A., 2014). Anatase, Rutile and Brookite are the three distinct forms of Titanium Dioxide in nature and most widely used in industry as a photocatalyst, catalyst or catalyst support. Preparation of thin films could be achieved due to its high refractive index in the visible range. Among these three, anatase phase is quite unstable at higher temperatures and has an energy band gap of 3.2 eV when activated by UV upto a wavelength of 387.5 nm (Martin 1995). The optical and electronic properties have been studied well for rutile phase because of its most stability and having an energy band gap of 3.0 eV while phase of brookite occurs rarely. There are some disadvantages despite many advantages of using TiO<sub>2</sub> due to its band-gap energy which can just be activated by UV light and constitutes 4-5% in sunlight. Another disadvantage is to resolve photo-generated electron-hole pairs during recombination.

An aqueous suspension of TiO<sub>2</sub> (metal oxide photocatalyst) in aqueous solutions induces very significant generation of HO• due to excitation at or near UV wavelength by irradiation of sunlight. The behaviour of aqueous suspensions of TiO<sub>2</sub> in the presence of DOM is reported in a general scheme of HO• photo-production (Konstantinou and Albanis 2004; Murov et al., 1993; Tseng and Haung 1991; Fox 1993; Chen et al., 2001; Han et al., 2009).



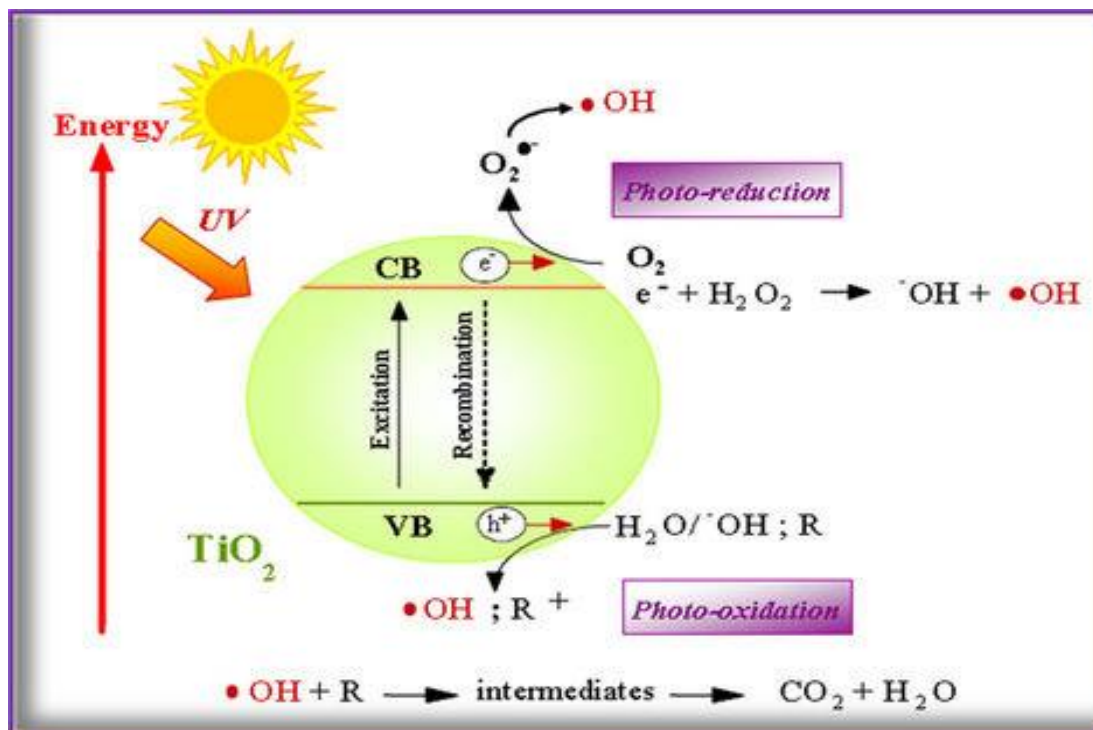


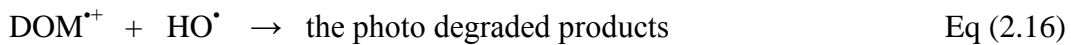
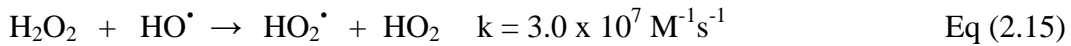
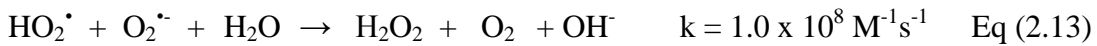
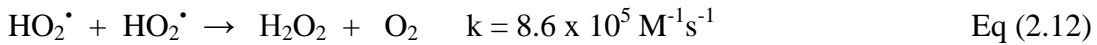
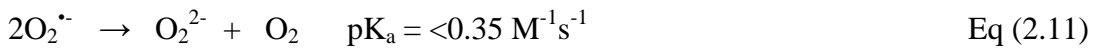
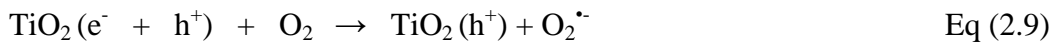
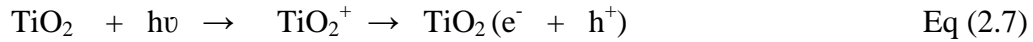
Figure 2.9. Schematic diagram of an irradiated TiO<sub>2</sub> semiconductor particle with photo-physical and photo-chemical process (Giwa et al., 2012)

Upon irradiation, a semiconductor photocatalyst generates electron/hole pairs with positive holes in the valence band and free electrons produced in the conduction band (Bard 1979; Schiavello 1987). Depending on the ambient conditions, the lifetime of an electron/hole pair varies from few nano-seconds to few hours (Pleskov and Gurevich 1986).

The ability of TiO<sub>2</sub> to split water depends on the photogenerated hole lifetime in TiO<sub>2</sub> which is measured over a range of excitation intensities using transient absorption spectroscopy. Depending on the light intensity used from below 1 sun equivalent to nearly 1 sun equivalent, the production of quantum yield of oxygen production can be estimated (Junwang Tang et al., 2008).

Organic compounds react with HO• radical (surface-bound or in solution) resulting in heterogeneous photocatalytic degradation of organic contaminants in solution (Sun and

Bolton 1996; Ullah et al., 1998; Konstantinou and Albanis 2004; Tseng and Haung 1991; Fox 1993; Han et al., 2009; Prousek 1996; Vione et al., 2001; Munoz et al., 2006; Saquib et al., 2008).



Absorption of photons by the functional groups of DOM leads to formation of  ${}^1\text{DOM}^*$  (singlet excited states) which is further converted into the  ${}^3\text{DOM}^*$  (triplet state) by intersystem crossing (ISC) (Eq. 2.6). Similarly absorption of photons by  $\text{TiO}_2$  (Eq. 2.7) leads to the formation of  $\text{TiO}_2^+$  generating  $\text{TiO}_2(e^- + h^+)$ . The valence-band holes ( $h^+$ ) get trapped by surface  $\text{Ti-OH}^-$  groups to yield  $\text{Ti-HO}^{\bullet}$  radical species (surface-bound  $\text{HO}^{\bullet}$  or  $\text{HO}_{\text{ads}}^{\bullet}$ ) upon UV irradiation of  $\text{TiO}_2$  whereas surface and sub-surface  $\text{Ti}^{\text{III}}$  species are formed by trapping of electrons ( $e^-$ ) in the conduction-band. The latter produces perhydroxy radicals ( $\text{HO}_2^{\bullet}$ ) after reacting with  $\text{O}_2^{\bullet-}$  (Eq. 2.9 and 2.10). The

photoexcited DOM reacts with oxygen generating superoxide radical anion ( $O_2^{\bullet-}$ ) which further leads to formation of perhydroxyl radical ( $HO_2^{\bullet}$ ) in equilibrium with its conjugate acid (Eq. 2.8 and 2.10). The  $O_2^{\bullet-}$  and  $HO_2^{\bullet}$  disproportionates to produce  $H_2O_2$  and gives  $HO^{\bullet}$  in solution after photolysis (Murov et al., 1993; Tseng and Haung 1991; Fox 1993; Sakugawa et al. 1990) (Eq. 2.11 – 2.13). Eq. 2.13 shows faster reaction due to the presence of  $O_2^{\bullet-}$  with  $HO_2^{\bullet}$  than Eq. 2.12 which involves  $HO_2^{\bullet}$  with  $HO_2^{\bullet}$  and the termination reaction is too slow of the two  $O_2^{\bullet-}$  radicals (Clark et al., 2009). Clark et al., 2009; Cabelli 1997 studied the generation of perhydroxyl radical ( $HO_2^{\bullet}$ ) with  $pK_a = 4.8$ , in coastal waters. Eq. 2.14 shows the photolysis of  $H_2O_2$  producing  $2HO^{\bullet}$  (Sakugawa et al. 1990) which further reacts with hydrogen peroxide generating perhydroxyl radicals (Eq. 2.15). The photoinduced generated hydroxyl radical further degrades  $DOM^{\bullet+}$  to produce photo degraded products (Eq. 2.16).

Figure 2.10 illustrates photogenerated holes that are produced under UV light irradiation are mainly responsible for highly hydrophilic conversion but not the electrons as per the mechanism. The photogenerated holes produced diffuse to the surface that were produced in the bulk of  $TiO_2$  and gets trapped at sites of lattice oxygen.

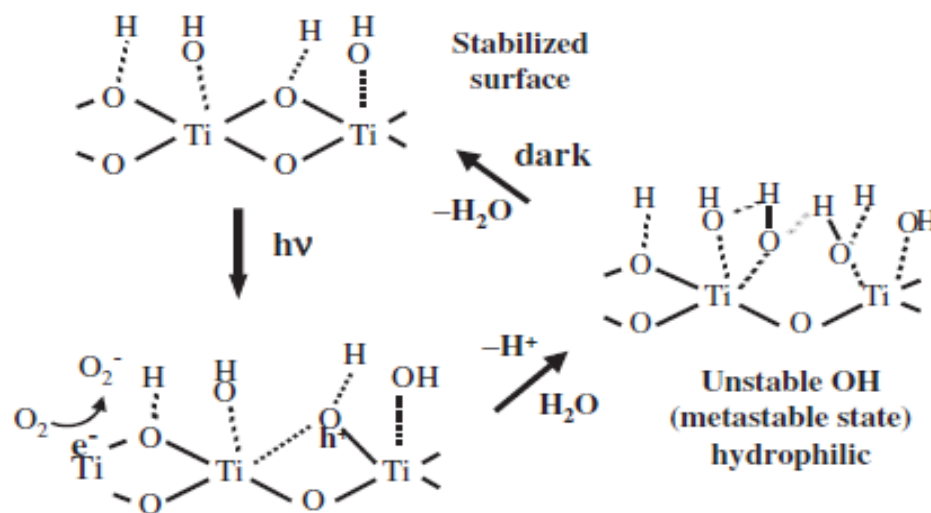


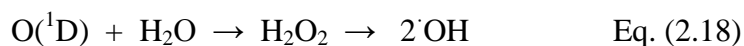
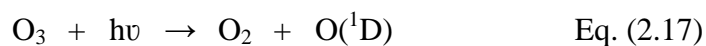
Figure 2.10. Schematic illustrations in the dark and under UV light irradiation on  $TiO_2$  film showing reversible changes in amount of hydroxyl groups (Sakai et al., 2003).

Most of the trapped holes that were consumed produce OH radicals after reacting with adsorbed water or adsorbed organics directly. At the titanium site, coordination of water molecules occurs due to breakage of bond between oxygen ions and lattice titanium by a small portion of trapped hole reacting with TiO<sub>2</sub> itself.

Number of newly OH groups formation increases at the surface due to release of proton for charge compensation by the coordinated water molecules. Compared to initial doubly coordinated OH groups, the produced singly coordinated new OH groups are thermodynamically less stable by UV light irradiation. The TiO<sub>2</sub> surface covered with the initial OH groups will have less surface energy than that of the surface of TiO<sub>2</sub> covered with the thermodynamically less stable OH groups. Compared to domains of hydrophilic or hydrophobic, the water droplet are larger and resembles a two dimensional capillary phenomenon as it spreads instantaneously on such a surface completely.

#### 2.2.1.4 Ozone–UV radiation (O<sub>3</sub>/UV)

According to Gottschalk, et al., (2000), UV radiation at 254 nm wavelength with its extinction coefficient  $\epsilon_{254 \text{ nm}} = 3300 \text{ M}^{-1}\text{cm}^{-1}$  is readily absorbed by ozone resulting in production of oxygen molecule and free oxygen atom (Eq. 2.17) depicted in Figure 2.11. The free oxygen atom further reacts with water forming an intermediate H<sub>2</sub>O<sub>2</sub> that decomposes to ·OH radicals (Eq. 2.18).



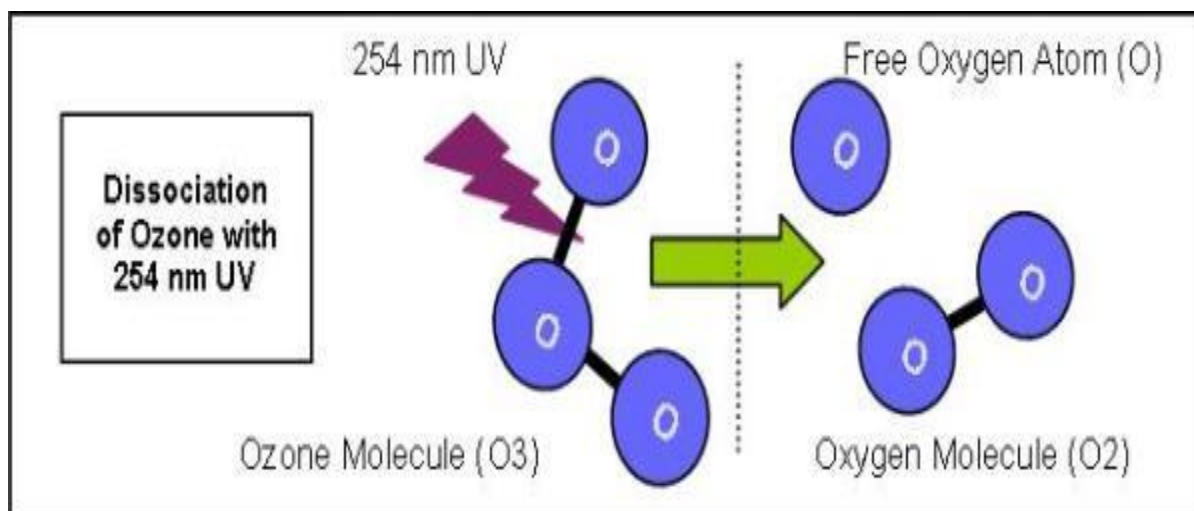


Figure 2.11. Ozone dissociation with UV irradiation (Spartan Environmental Technologies, 2014).

It appears that photolysis of ozone seems to be an expensive way to produce hydrogen peroxide as over 80% of UV energy generated by low pressure mercury lamps shows lower molecular absorptivity of  $\text{H}_2\text{O}_2$  ( $\epsilon_{254 \text{ nm}} = 18.6 \text{ M}^{-1}\text{cm}^{-1}$ ) at that wavelength resulting in limited  $\cdot\text{OH}$  yield. It can be seen in Table 2.10, that the photolysis of ozone yields more radicals per incident photon compared to UV/ $\text{H}_2\text{O}_2$  process. Using UV lamps with lower wavelengths, the absorptivity of  $\text{H}_2\text{O}_2$  can be increased but requires UV lamps in kilowatts for hydrogen peroxide photolysis compared to ozone photolysis where the power requirement is in watts range.

Table 2.10. Photolysis of ozone and  $\text{H}_2\text{O}_2$  leading to the formation of  $\cdot\text{OH}$  (Techcommentary, 1996).

| Oxidant                | $\epsilon_{254 \text{ nm}},$<br>$\text{M}^{-1}\text{cm}^{-1}$ | Stoichiometry                                      | $\cdot\text{OH}$ formed per<br>incident photon |
|------------------------|---|--|--|
| $\text{H}_2\text{O}_2$ | 20  | $\text{H}_2\text{O}_2 \rightarrow 2\cdot\text{OH}$ | 0.09   |
| $\text{O}_3$           | 3300  | $3\text{O}_3 \rightarrow 2\cdot\text{OH}$          | 2.00   |

Screening of ozone occurs by strong absorption of UV light by optically active organic compounds in water such as 5-methylresorcinol, xylenols, phenol, etc that does not give any additional effect to ozone from UV radiation (Munter et al., 1995 and Trapido et al., 2000). Complete mineralization to CO<sub>2</sub> and H<sub>2</sub>O is uncommon even though ozone oxidizes phenolic compounds very easily such as 2, 3-xyleneol, *p*-cresol, 3, 4-xyleneol, phenol). According to Gurol & Vatistas, 1987 and Takahashi, 1990, complete mineralization could be achieved by O<sub>3</sub>/UV system for glyoxylic acid, formic acid, glyoxal and oxalic acid due to the presence of shorter molecular chain. Compared to only photolysis and ozonation, Peyton et al., (1982) demonstrated removal of C<sub>2</sub>Cl<sub>4</sub> from water due to the efficiency of O<sub>3</sub>/UV system.

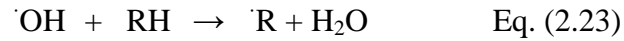
Ozonation at elevated pH values is of limited use. Although the O<sub>3</sub>/UV combination seems difficult to implement on a large scale, it can be successfully used for lower flow rates etc. Peyton et al., (1982) presented a kinetic model of the O<sub>3</sub>/UV process. The model takes into consideration the radiation flux, ozone concentration in the liquid phase, and the ozonation reaction rate constant.

### 2.2.1.5 Photocatalytic oxidation (UV/TiO<sub>2</sub>)

An absorption of electromagnetic radiation by a TiO<sub>2</sub> semiconductor results in the photo-excitation in the near UV spectrum on the basis of photocatalysis.

Mathews (1986) observed that when this material was excited by photons that possess energies of sufficient magnitude produces conduction band electrons and valence band holes which induce oxidation or reduction by these charge carriers and react with absorbed species on the surface of the TiO<sub>2</sub> particle as shown in Eq. 2.19 to 2.24.





All the chemicals are oxidized due to the positive oxidation potential possessed by holes. Eq. 2.25 shows the formation of hydroxyl radicals resulting from even a single electron oxidation of water making it energetically feasible. These generated hydroxyl radicals destroys bacteria and other microorganisms and disintegrate harmful substances into harmless end products such as  $CO_2$  and  $H_2O$  as depicted in Figure 2.12.

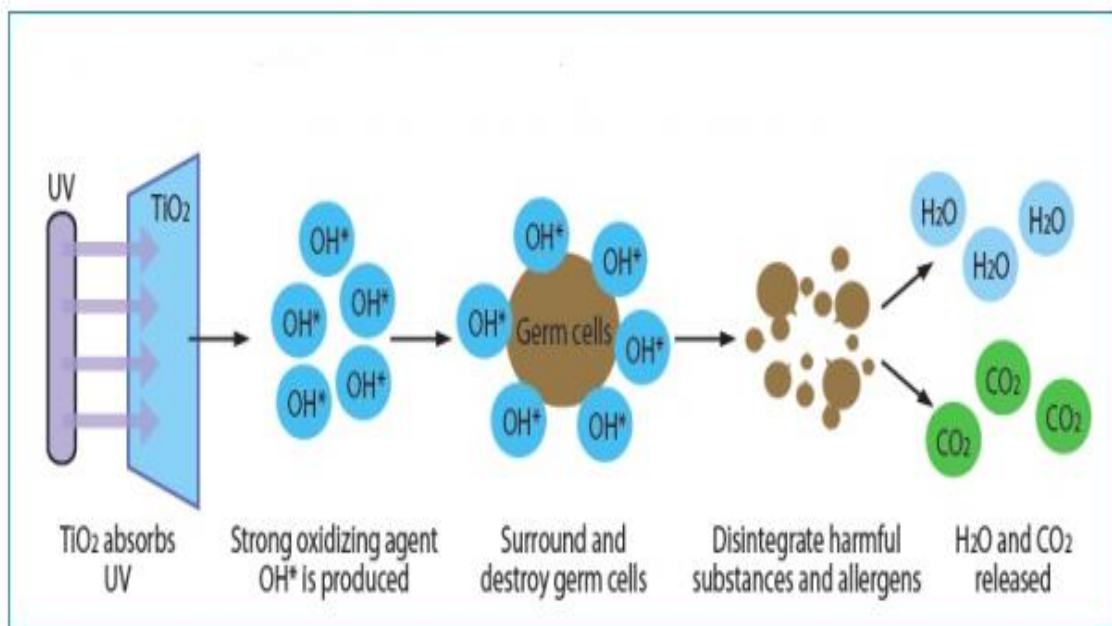
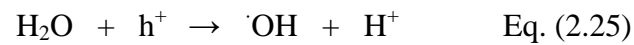


Figure 2.12. Photocatalytic oxidation process (Conee Orsal, 2015).

Titanium dioxide is being used in various applications such as paints, outdoor building material, cement, and also in removal of volatile organic compounds and oxides of nitrogen among other applications.

#### 2.2.1.6 Ozone + Catalyst ( $O_3/TiO_2$ )

Decomposition of target compound can also be accelerated by use of homogeneous or heterogeneous catalysts such as metal ions ( $Mn^{2+}$ ,  $Fe^{3+}$ ,  $Fe^{2+}$ ) and/or metal oxides ( $TiO_2-Me$ ,  $Al_2O_3-Me$ ,  $Ru/CeO_2$ ,  $MnO_2$ ,  $Fe_2O_3$ ) along with ozonation although the reaction mechanism is unclear in most of the cases. Legube et al., (1996) observed the catalytic ozonation process for the model compound, salicylic acid by using clay as the support for  $TiO_2$  in its anatase form where complete removal of organics was possible compared to unassisted ozonation by TOC measurements. Paillard et al., (1991) observed that the process efficiency of catalytic ozonation ( $O_3/TiO_2$ ) was preferable compared to  $O_3/H_2O_2$  or ozonation ( $O_3$ ) for the target oxalic acid compound in terms of TOC reduction.

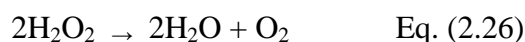
Jans & Hoigne (1998) reported that a radical-type chain reaction can be initiated forming  $\cdot OH$  radicals in aqueous phase by the addition of a few milligrams of carbon black or activated carbon per litre of water containing ozone.

#### 2.2.1.7 Hydrogen Peroxide ( $H_2O_2$ )

$H_2O_2$  has an additional oxygen atom with chemical formula ( $H-O-O-H$ ) which is a universal constituent of the hydrosphere occurring in seawater, freshwater, mineral water, air, rain, snow, dew, cloud and all living organisms and finds its application in treatment processes. In the aquatic environment,  $H_2O_2$  acts as useful indicator of



abiotic, biological and photoinduced processes and undergoes dismutation into water and oxygen:



$\text{H}_2\text{O}_2$  finds numerous applications as a

- natural tracer in mixing zone of surface water (Johnson et al., 1989; Sikorsky and Zika 1993a, b; Sarthou et al., 1997; Scully and Vincent 1997)
- in biota/living cells, due to its elevated reactivity,  $\text{H}_2\text{O}_2$  is involved in oxidative stress by both oxidation and reduction (Berlett and Stadtman 1997; Paradies et al., 2000; Blokhina et al., 2003; Richard et al., 2007)
- acts as an indicator of photoinduced activity generated through irradiation of various dissolved organic matter in natural waters (Cooper and Zika 1983; Zika et al., 1985a, b; Mostofa and Sakugawa 2009; Obernosterer et al., 2001; Fujiwara et al., 1993; Moore et al., 1993; Scully et al., 1996)
- helpful in the identification of biological activity (Fujiwara et al., 1993; Moffett and Zafiriou 1990; Cooper and Zepp 1990; Petasne and Zika 1997)
- useful tracer of the convective overturn or vertical advective transport (Johnson et al., 1989; Sarthou et al., 1997; Scully and Vincent 1997; Yuan and Shiller 2001)

Jacks Lake surface water, Ontario, Canada, has  $\text{H}_2\text{O}_2$  concentration of 10-800nM, Lake Erie surface water has  $\text{H}_2\text{O}_2$  concentration ranges 50-200 nM, Lake Ontario surface water has 100nM whereas rainwater from North Bay, Ontario (Jan-Feb) has  $\text{H}_2\text{O}_2$  between 500-5000nM (Sakugawa et al., 1990), at 44°N latitude (diurnal with no lightning varies between 4400-29600nM and with lightning has 34000nM) Cooper and Lean (1992).

The production rate of  $\text{H}_2\text{O}_2$  by using Quartz Halogen Lamp at Lake Ontario (43°N) varies between 161 to 234nM/h and the DOC varies between 225 to 292  $\mu\text{MC}$  whereas Hamilton Harbor ((43°N) has a  $\text{H}_2\text{O}_2$  production rate of 790nM/h and DOC 325  $\mu\text{MC}$  (Scully et al., 1996).

## 2.3 Comparative operating costs of treatment for various AOPs

Based on type, flow rate and concentration of contaminants present in wastewater and their required degree of removal by various processes such as O<sub>3</sub>/H<sub>2</sub>O<sub>2</sub>, UV/TiO<sub>2</sub>, H<sub>2</sub>O<sub>2</sub>/UV and/or O<sub>3</sub>/UV depends on capital, operating and treatment cost. Table 2.11 and 2.12 presents a comparison of the operating costs of various AOPs and the treatment costs.

Table 2.11. Comparative operating costs of some AOPs ((Techcommentary, 1996).

| Process                                       | Cost of Oxidant | Cost of UV     |
|---|-----------------|----------------|
| O <sub>3</sub> /UV                            | High            | Medium         |
| O <sub>3</sub> /H <sub>2</sub> O <sub>2</sub> | High            | 0              |
| H <sub>2</sub> O <sub>2</sub> /UV             | Medium          | High           |
| UV/TiO <sub>2</sub>                           | Very low        | Medium to high |

Table 2.12. Operating costs of advanced oxidation processes<sup>a</sup> (Yonar et al., 2005).

| Process  | Treatment cost (\$/m <sup>3</sup> ) |
|--|-------------------------------------|
| Ozone  | 5.35                                |
| Ozone/UV <sup>b</sup>                                | 8.68                                |
| H <sub>2</sub> O <sub>2</sub> /UV <sup>b</sup>       | 4.56                                |
| Ozone/H <sub>2</sub> O <sub>2</sub> /UV <sup>b</sup> | 11.25                               |

<sup>a</sup>Cost of labor not included

<sup>b</sup>Optimum lamp life: 2,000 h. Operating costs calculated on the basis of 90% COD removal

## 2.4 Indium Oxide nano materials

Indium is very soft crystalline, malleable and ductile metal that possess the most stable oxidation state of three-charged indium cation ( $\text{In}^{3+}$ ) belonging to Group 13 element with spherical symmetry of electron shell ( $d^{10}$ ).  $\text{In}^{3+}$  has an ionic radius of 92 pm (Emsley, J., 1991 and 1993). Indium forms strong bonds with O, N and F and stable complexes with Cl, I, Br, S and P forming coordination compounds that finds application in biology and medicine. For example, aqueous solutions of indium complexes are administered to patient's body for diagnostic and therapeutic medicaments in medical practices (Petrosyants and Ilyukhin, 2011). At cryogenic temperatures, indium retains its plastic properties and thus increases hardness of an alloy, resistance to corrosion and strength and is used in dental alloys, low pressure sodium lamps, semiconductors, electrical contacts and alkaline dry batteries (Habashi, 1997).

Concentrations of environmental and hazardous gases are measured by sensors of metal oxide films that interact with atoms or molecules producing variation in film conductivity. Among binary oxide compounds,  $\text{TiO}_2$ ,  $\text{SnO}_2$ ,  $\text{In}_2\text{O}_3$  and  $\text{ZnO}$  are being used as Transparent Conducting Oxides (TCOs). Based on the properties of the used material, both oxidizing and reducing species can be detected (Himmerlich et al., 2012).  $\text{In}_2\text{O}_3$  has been attracted by many researchers in recent years due to its indirect band gap of 2.8 eV and acts as an efficient sensitizer for photocatalyst extending its absorption spectra from UV into the visible region (Lv et al., 2010) and because of its high mobility of  $\sim 10 - 65 \text{ cm}^2 \text{ V}^{-1} \text{ s}^{-1}$  is one of the most studied materials as channel layers (Nakazawa). Trapping, mobility, relatively cheaper, lower toxicity and higher electron production are some of the specific characteristics of indium (Tahir and Amin, 2013).

Figure 2.13 represents the crystalline structure of indium oxide, bixbyite structure existing as fluorite-type structure with anions missing on one-quarter and producing structural vacancies. The six oxygen atoms ( $c\text{-N}_{\text{In-O}} = 6$ ) are octahedrally coordinated around indium cations with two structural vacancies sitting along the face diagonal (d-

site, represents 75% of octahedra) or along the body diagonal (b-site, represents 25% of octahedra). In crystalline  $\text{In}_2\text{O}_3$ , the  $\text{InO}_6$  octahedra are linked together by structural vacancies giving rise to two configurations. The first is corner sharing by an oxygen and a structural vacancy shared between adjacent polyhedral and the second edge sharing by two oxygens along the entire edge between adjacent polyhedra (Buchholz et al., 2014).

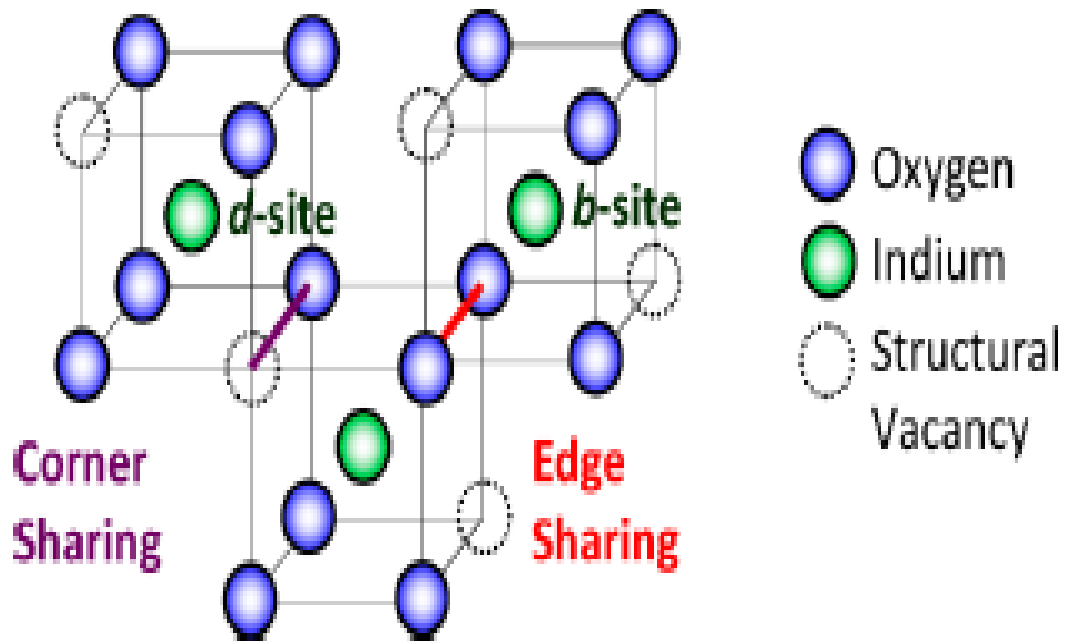


Figure 0.1. Crystalline  $\text{In}_2\text{O}_3$  – Bixbyite structure (Buchholz et al., 2014)

The stability and electrical performance of  $\text{In}_2\text{O}_3$  thin film transistors (TFTs) is based on its fabrication and depends on the hydroxyl radical-assisted (HRA) decomposition and oxidation as shown in Figure 2.14. All TFTs fabricated contains a bottom-gate and top-contact configuration ( $\text{SiO}_2/\text{p}^+\text{-Si}$  gate dielectrics/gate). Upon UV irradiation,  $\text{H}_2\text{O}_2$  generates two  $\text{OH}^\cdot$  per molecule of  $\text{H}_2\text{O}_2$  caused by photocatalytic cleavage after absorbing wavelengths at  $\leq 350\text{nm}$  (Harbour et al., 1974; Ghassemzadeh, et al., 2013; Jones, C. W., 1999).

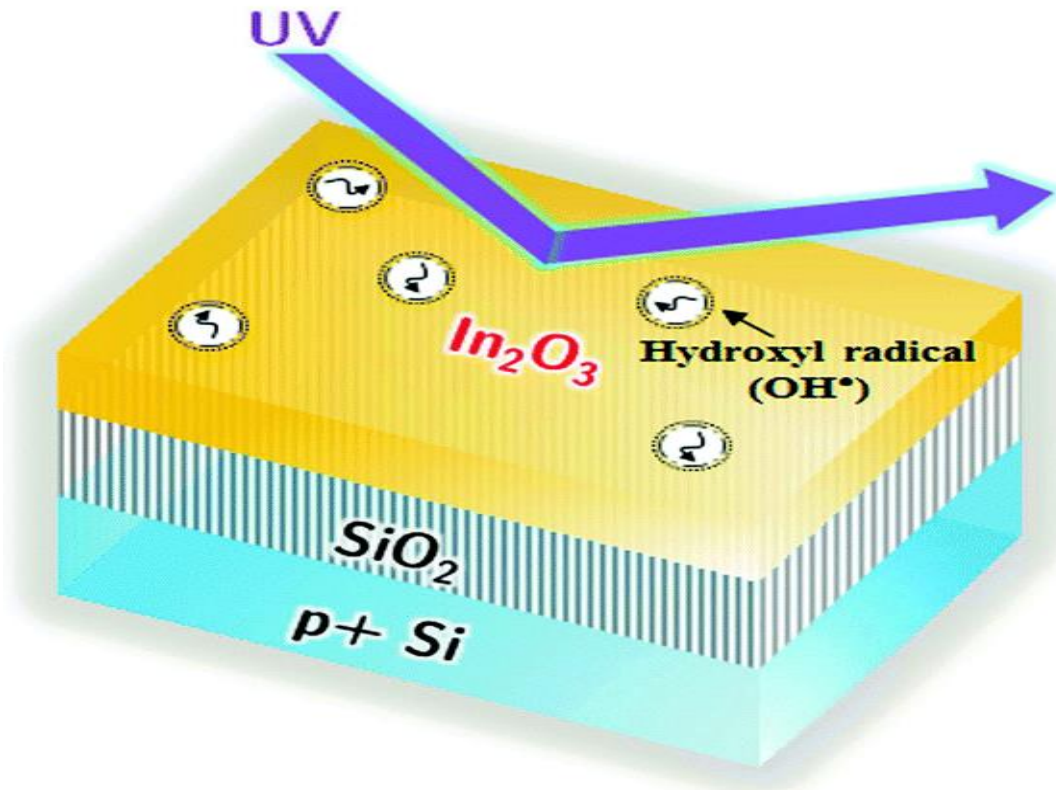


Figure 0.2. Schematic for solution-processed  $\text{In}_2\text{O}_3$  thin-films by a hydroxyl radical-assisted (HRA) method (Sabri et al., 2015)

$\text{OH}^\bullet$  in amorphous oxides, oxidizes sub-gap states from a near conduction band minimum (CBM) that consists of electron-donor states occupied at a neutral charge provide electrons by ionization to shallow states (metastable) as illustrated in Figure 2.15. The near-valence band maximum (VBM) is located below CBM (near-VBM) (Nomura, et al., 2011) and consists of oxygen sites occupied by electron-acceptors with low valence cations ( $\text{In}^{3+}$  from In 4d and 5s) (Murat and Medvedeva, 2012). Due to high density of oxygen sites just below and very close to CBM has  $\text{V}_o$  in  $\text{In}_2\text{O}_3$  that are donors and binds two electrons by exhibiting inward relaxation.

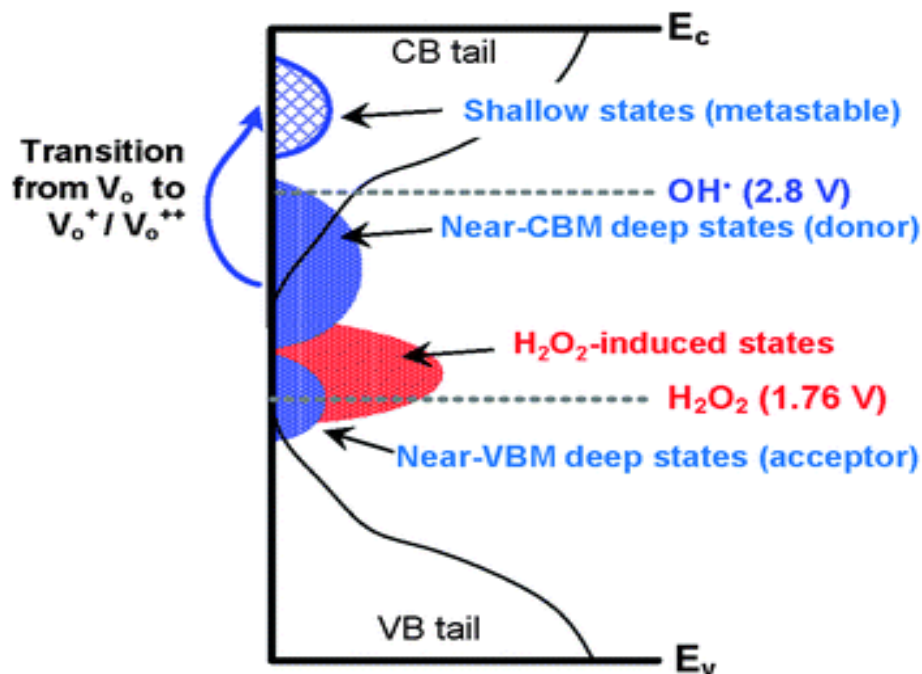


Figure 0.3. Schematic illustrations showing metastable states induced by the hydroxyl-radical assisted oxidation (Sabri et al., 2015).

The incorporation of  $\text{H}_2\text{O}_2$  for  $\text{In}_2\text{O}_3\text{-H}_2\text{O}_2$ , induces electron acceptors located near-VBM. In contrast, the incorporation of high density  $\text{OH}^\cdot$ , ionizes the neutral  $\text{V}_o$  chemically to single ( $\text{V}_o^+$ ) and double ( $\text{V}_o^{++}$ ) ionized states due to its strong oxidation potential for  $\text{In}_2\text{O}_3\text{-HRA}$  (Jones, C.W., 1999). Both of the ionized states are located above the CBM and capable of trapping and donating electrons as they are metastable. (Noh, et al., 2011). Thus the hydroxyl radicals induce formation of metastable states and reduce carbon impurities during thin film formation.

## 2.5 Biochar (BC)

Biochar has garnered attention in recent years as it appears to be an effective adsorbent produced with lower energy requirements and cheaper (Cao et al., 2009; Zheng et al., 2010; Karakoyun et al., 2011; Ahmad et al., 2012; Lu et al., 2012). Compared to biochar, the production of activated carbon requires higher temperature and additional

activation process. Biochar is carbon-rich possessing differing physical and chemical properties such as enriched surface mineral components and functional groups, large specific surface area and porous structure based on feedstock and pyrolysis temperatures.



Figure 0.4. Production and application of biochar for wastewater treatment as an effective adsorbent (Tan, X. et al., 2015).

Figure 2.16 shows production of biochar from a number of different feedstocks that includes wood biomass, crop residues, solid wastes, animal litters, etc by various thermochemical processes such as fast pyrolysis, slow pyrolysis, flash carbonization, gasification, hydrothermal carbonization (HTC) and torrefaction. Biochar finds several applications in removal of organic, inorganic, heavy metals and other pollutants from

aqueous solutions and possess even better or comparable adsorption capacity compared to activated carbon (Karakoyun et al., 2011; Xue et al., 2012; Zhang et al., 2012; Yang et al., 2014b). Studies have shown some of the benefits of using biochar results in enhanced crop yield, soil amendment, carbon storage and mitigating global warming (Whitman et al., 2011; Abit et al., 2012; Mao et al., 2012; Sohi, 2012; Khare and Goyal, 2013; Verheijen et al., 2014).

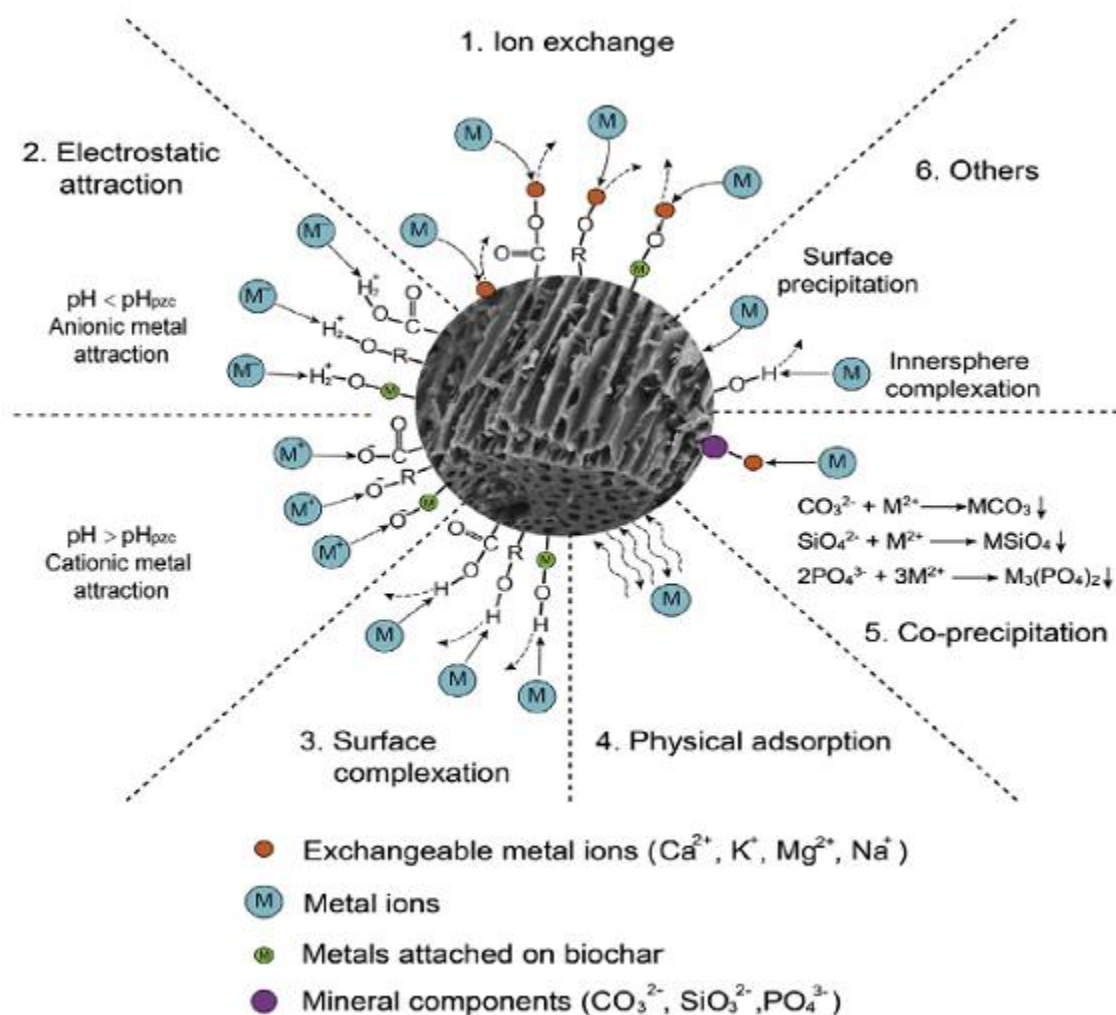


Figure 0.5. Summarized adsorption mechanisms proposed on biochars by heavy metals (Tan, X. et al., 2015).



Interaction of biochar with heavy metals involved several kinds of adsorption mechanisms including physical adsorption, electrostatic attraction, precipitation, surface complexation and ion-exchange as summarized in Figure 2.17. For example, Cr (VI) was effectively removed by sugar beet tailing biochar by electrostatic attraction (Dong et al. 2011), while Lu et al. (2012) proposed Pb removal by adsorption onto sludge derived biochar via functional group. Similarly, Sun et al. (2014) used corn straw biochar for adsorption of Cd (II) whereas Kong et al. (2011) used soybean stalk-based biochar as efficient adsorption of Hg (II).

Similarly Figure 2.18 summarizes various adsorption interaction mechanisms that bind organic contaminants to biochar including hydrophobic effect, electrostatic interaction, partition, pore-filling and hydrogen bonds. Since surface properties of biochar is heterogeneous due to presence of non-carbonized and co-existed carbonized fractions, the specific adsorption mechanisms are also different for different organic pollutants.

Han et al. (2013) and Inyang et al. (2014) reported adsorption of methylene blue and phenol from water onto biochar was via pore-filling effect. Similarly, Inyang et al. (2014) observed that most of the adsorption was via electrostatic attraction of organic contaminants onto biochars followed by other contributing adsorption mechanisms. Qiu et al. (2009) observed  $\pi - \pi$ , intermolecular hydrogen bonding and electrostatic attraction/repulsion mechanism of interaction between dye and straw based biochar whereas methyl violet showed adsorption mechanism via electrostatic attraction between dye and biochar (Xu et al., 2011). Similarly adsorption of atrazine and carbaryl on biochars derived from pig-manure showed adsorption mechanism via  $\pi - \pi$  electron donor-acceptor, hydrophobic effect and pore-filling interactions (Zhang et al., 2013b) whereas adsorption of sulfonamides by different biochars showed  $\pi - \pi$  electron-donor-acceptor interactions (Xie et al., 2014).

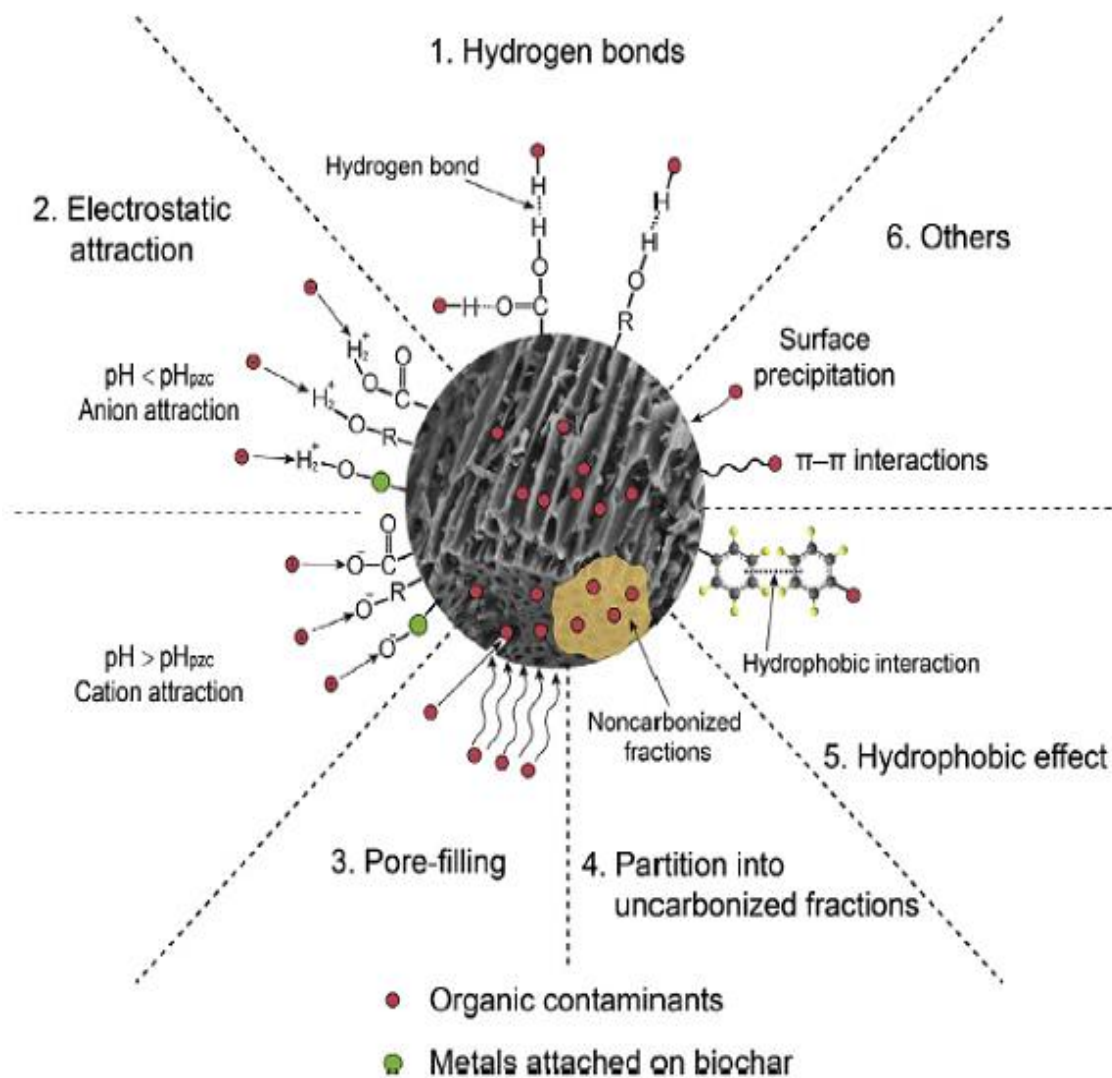


Figure 0.6. Summarized adsorption mechanisms proposed on biochars by organic contaminants (Tan, X. et al., 2015).

As per Ahmad et al., 2013b, very few articles review the removal of pollutants in water by the use of biochar while, studies on the removal of PPCPs in wastewater by the use of biochar is minimal. Hence further research on the applications of biochar for the purification of water and wastewater is urgently needed.

## 2.6 References

Abit, S.M., Bolster, C.H., Cai, P., Walker, S.L., 2012. Influence of feedstock and pyrolysis temperature of biochar amendments on transport of *Escherichia coli* in saturated and unsaturated soil. *Environ. Sci. Technol.* 46, 8097–8105.

Ahmad, M., Lee, S.S., Dou, X., Mohan, D., Sung, J.K., Yang, J.E., Ok, Y.S., 2012. Effects of pyrolysis temperature on soybean stover-and peanut shell-derived biochar properties and TCE adsorption in water. *Bioresour. Technol.* 118, 536–544.

Ahmad, M., Rajapaksha, A.U., Lim, J.E., Zhang, M., Bolan, N., Mohan, D., Vithanage, M., Lee, S.S., Ok, Y.S., 2013b. Biochar as a sorbent for contaminant management in soil and water: a review. *Chemosphere* 99, 19–33.

Andreozzi, R., Caprio, V., Insola, A. and Marotta, R., 1999. Advanced oxidation processes (AOP) for water purification and recovery”. *Catalysis Today*. 53: 51-59.

Andreozzi, R., Raffaele, M., and Nicklas, P., 2003. Pharmaceuticals in STP effluents and their solar photodegradation in aquatic environment. *Chemosphere*. 50 (10), 1319–1330.

Arooj, F., Ahmad N., and Chaudhry, M. N., 2015. A Pilot-Scale Application of Ozone to Bleach Raw Cotton Fabric Using Various Additives. *Ozone: Science and Engineering: The journal of the International Ozone Associations*. Volume 37, Issue 3, 203-215.

Ashton, D., Hilton, M., and Thomas, K.V., 2004. Investigating the environmental transport of human pharmaceuticals to streams in the United Kingdom. *Science of the Total Environment*. 333 (1–3), 167–184.

Attias, L., Contu, A., Loizzo, A., Massiglia, M., Valente, P., Zapponi, G.A., 1995. Trihalomethanes in drinking water and cancer risk: risk assessment an integrated evaluation of available data, in animals and humans. *The Science of the Total Environment*. 171 (1), 61–68.

Barber, L.B., Leenheer, J.A., Pereira, W.E., Noyes, T.I., Brown, G.K., Tabor, C.F., and Writer, J.H., *Organic Contamination of the Mississippi River from Municipal and Industrial Wastewater*, in *Contaminants in the Mississippi River*, US Geological Survey Circular 1133, Meade, R.H., U.S. Geological Survey, Reston, VA, 1995, <http://pubs.usgs.gov/circ/circ1133>.

Bard, A.J., 1979. Photoelectro chemistry and heterogeneous photocatalysis at semiconductors. *J. Photochem.* 10:59–75.

Bendz, D., Paxeus, N.A., Ginn, T.R., and Loge, F.J., 2005. Occurrence and fate of pharmaceutically active compounds in the environment, a case study: Hoje River in Sweden. *Journal of Hazardous Materials*. 122 (3), 195–204.

Berlett, B.S., Stadtman, E.R., 1997. Protein oxidation in aging, disease, and oxidative stress. *J. Biol. Chem.* 272:20313–20316.

Bienkowski, B., 2013. Only about half of the prescription drugs and other newly emerging contaminants in sewage are removed by treatment plants. Nov 22, 2013. *Environmental Health News*. (Date retrieved: 2014/02/05).

Blokhina, O., Virolainen, E., Fagerstedt, K. V., 2003. Antioxidants, oxidative damage and oxygen deprivation stress: a review. *Ann. Bot.* 91:179–194.

Bolto, B., Dixon, D., Eldridge, R., King, S., and Linge, K., 2002. “Removal of natural organic matter by ion exchange.” *Water Res.* 36(20), 5057–5065.

Bowers, A.R., Cho, S.H. and Singh, A., 1991. Chemical oxidation of aromatic compounds: comparison of  $H_2O_2$ ,  $KMnO_4$  and  $O_3$  for toxicity reduction and improvements in biodegradability. In: *Proceedings of the First International Symposium Chemical Oxidation Technologies for the Nineties*, Eckenfelder, W.W., Bowers, A.R. and Roth, J.A. (eds). Vanderbilt University, Nashville, Tennessee, USA, pp. 11-25.

Boyd, G.R., Reemstma, H., Grimm, D.A., and Mitra, S., 2003. Pharmaceuticals and personal care products (PPCPs) in surface and treated waters of Louisiana, USA, and Ontario Canada. *Sci. Total Environ.* 311:135.

Boyer, T. H., and Singer, P. C., 2008. “Stoichiometry of removal of natural organic matter by ion exchange.” *Environ. Sci. Technol.* 42(2), 608–613.

Bruchet, A., Hochereau, C., Picard, C., Decottignies, V., Rodrigues, J.M., and Janex-Habibi, M.L., 2005. Analysis of drugs and personal care products in French source and drinking waters: The analytical challenge and examples of application. *Water Science and Technology.* 52 (8), 53–61.

Brun, G.L., Bernier, M., Losier, R., Doe, K., Jackman, P., and Lee, H.B., 2006. Pharmaceutically active compounds in Atlantic Canadian sewage treatment plant effluents and receiving waters, and potential for environmental effects as measured by acute and chronic aquatic toxicity. *Environmental Toxicology and Chemistry.* 25, 2163–2176.

Buchholz, D. B., Ma, Q., Alducin, D., Ponce, A., Jose-Yacaman, M., Khanal, R., Medvedeva, J.E., and Chang, R.P.H., 2014. The Structure and Properties of Amorphous Indium Oxide. [dx.doi.org/10.1021/cm502689x](https://doi.org/10.1021/cm502689x) | *Chem. Mater.* 26, 5401–5411.

Cabelli, D.E., 1997. The reactions of  $HO_2/O_2^-$  radicals in aqueous solution. In: Alfassi ZB (ed) *Peroxyl radicals*. Wiley, New York, pp 407–437.

Cao, X., Ma, L., Gao, B., Harris, W., 2009. Dairy-manure derived biochar effectively sorbs lead and atrazine. *Environ. Sci. Technol.* 43, 3285–3291.

Carballa, M., Omil, F., and Lema, J.M., 2005. Removal of cosmetic ingredients and pharmaceuticals in sewage primary treatment. *Water Res.* 39, 4790–4796.

Carey, J. H., 1992. An introduction to AOP for destruction of organics in wastewater. *Water Pollut. Res. J. Can.*, 27, 1–21.

Carlsson, C., Johansson, A. K., Alvan, G., Bergman, K., Kuehler, T., 2006a. Are pharmaceuticals potent environmental pollutants? Part I: Environmental risk assessments of selected active pharmaceutical ingredients. *Sci. Total Environ.* 364, 67–87.

Carucci, A., Cappai, G., and Piredda, M., 2006. Biodegradability and toxicity of pharmaceuticals in biological wastewater treatment plants. *Journal of Environmental Science and Health Part A—Toxic/Hazardous Substances & Environmental Engineering.* 41 (9), 1831–1842.

Castiglioni, S., Bagnati, R., Fanelli, R., Pomati, F., Calamari, D., and Zuccato, E., 2006. Removal of pharmaceuticals in sewage treatment plants in Italy. *Environ. Sci. Technol.* 40, 357–363.

Castiglioni, S., Fanelli, R., Calamari, D., Bagnati, R., and Zuccato, E., 2004. Methodological approaches for studying pharmaceuticals in the environment by comparing predicted and measured concentrations in River Po, Italy. *Regulatory Toxicology and Pharmacology.* 39 (1), 25–32.

Chen, C., Li, X., Ma, W., Zhao, J., Hidaka, H., Serpone, N., 2001. Effect of transition metal ions on the TiO<sub>2</sub>-assisted photodegradation of dyes under visible irradiation: a probe for the interfacial electron transfer process and reaction mechanism. *J. Phys. Chem. B.* 106:318–324.

Chen, J., Gu, B. H., LeBoeuf, E. J., Pan, H. J., and Dai, S., 2002. “Spectroscopic characterization of the structural and functional properties of natural organic matter fractions.” *Chemosphere.* 48(1), 59–68.

Chen X., and Selloni, A., 2014. Introduction: Titanium Dioxide (TiO<sub>2</sub>) nanomaterials. *Chem. Rev.* 114, 9281–9282.

Clara, M., Strenn, B., Gans, O., Martinez, E., Kreuzinger, N., and Kroiss, H., 2005. Removal of selected pharmaceuticals, fragrances and endocrine disrupting compounds in a membrane bioreactor and conventional wastewater treatment plants. *Water Research.* 39 (19), 4797–4807.

Clark, C.D., De Bruyn, W.J., Jones, J.G., 2009. Photochemical production of hydrogen peroxide in size-fractionated Southern California coastal waters. *Chemosphere.* 76:141–146.

Cooper, W.J., Lean, D.R.S., 1992. Hydrogen peroxide dynamics in marine and fresh water systems. *Encyclopedia of Earth system science.* Academic Press Inc. 2:527–535.

Cooper, W.J., Zepp, R.G., 1990. Hydrogen peroxide decay in waters with suspended soils: evidence for biologically mediated processes. *Can J Fish Aquat Sci* 47:888–893.

Cooper, W.J., Zika, R.G., 1983. Photochemical formation of hydrogen peroxide in surface and ground waters exposed to sunlight. *Science*. 220:711–712.

Daughton, C.G. and Ternes, T.A., 1999. Pharmaceuticals and personal care products in the environment: Agents of subtle change? *Environmental Health Perspectives*. 107, 907–938.

Daughton, C.G., 2007. Pharmaceuticals in the environment: sources and their management. In: Petrovic M., Barcelo D., editors. *Analysis, Fate and Removal of Pharmaceuticals in the Water Cycle*: Elsevier Science. P 1-58. Available: [http://www.epa.gov/nerlesd1/bios/daughton/Chap1\\_Petrovic&Barcelo.pdf](http://www.epa.gov/nerlesd1/bios/daughton/Chap1_Petrovic&Barcelo.pdf).

Doll, T.E. and Frimmel, F.H., 2005. Photocatalytic degradation of carbamazepine, clofibrac acid and iomeprol with P25 and Hombikat UV100 in the presence of natural organic matter (NOM) and other organic water constituents. *Water Res.* 39(2–3), 403–411.

Dong, X., Ma, L.Q., Li, Y., 2011. Characteristics and mechanisms of hexavalent chromium removal by biochar from sugar beet tailing. *J. Hazard. Mater.* 190, 909–915.

Duan, J. M., and Gregory, J., 2003. “Coagulation by hydrolysing metal salts.” *Adv. Colloid Interface Sci.* 100–102, 475–502.

Dutta, K., Lee, M.Y., Lai, W.W.P., Lee, C.H., Lin, A.Y.C., Lin, C.F., Lin, J.G., 2014. Removal of pharmaceuticals and organic matter from municipal wastewater using two-stage anaerobic fluidized membrane bioreactor. *Bioresource Technology*. 165, 42–49.

Emsley, J., 1991 and 1993. *The Elements*, 2nd ed. (Clarendon, 1991; Mir, Moscow. 1993).

Fox, M.A., 1993. The role of hydroxyl radicals in the photocatalyzed detoxification of organic pollutants—pulse-radiolysis and time-resolved diffuse-reflectance measurements. In: Ollis D.F., Alekabi, H., (eds). *Trace metals in the environment*. 3, pp 163–167.

Fujiwara, K., Ushiroda, T, Takeda, K., Kumamoto, Y., Tsubota, H., 1993. Diurnal and seasonal distribution of hydrogen peroxide in seawater of Seto Inland Sea. *Geochem. J.* 27:103–115.

Franceschi, M., Girou, A., Carro-Diaz, A. M., Maurette, M. T., and Puech-Costes, E., 2002. “Optimisation of the coagulation-flocculation process of raw water by optimal design method.” *Water Res.* 36(14), 3561–3572.

Ghassemzadeh, L., Peckham, T.J., Weissbach, T., Luo, X., and Holdcroft, S., 2013. *J. Am. Chem. Soc.*, 2013, 135, 15923–15932.

- Giwa, A., Nkeonye, P. O., Bello, K.A., Kolawole, K. A., 2012. Photocatalytic Decolourization and Degradation of C. I. Basic Blue 41 Using TiO<sub>2</sub> Nanoparticles. *Journal of Environmental Protection*. Vol. 3 No. 9, Article ID: 22707, 7 pages DOI:10.4236/jep.2012.39124.
- Gomez, M.J., Petrovic, M., Fernandez-Alba, A.R., and Barcelo, D., 2006. Determination of pharmaceuticals of various therapeutic classes by solid-phase extraction and liquid chromatography-tandem mass spectrometry analysis in hospital effluent wastewaters. *Journal of Chromatography A*. 1114 (2), 224–233.
- Gottschalk, C., Libra, J. A. & Saupe, A, 2000. *Ozonation of Water and Waste Water*. Wiley-VCH.
- Gough, A. J., 1993. The use of ozone to remove colour from wastewater. In *Proc. Intl. Symp. On Ozone-Oxidation Methods for Water and Wastewater Treatment*, Berlin, Germany, 1993, II.2.1–II.2.14.
- Gros, M., Petrovic, M., and Barcelo, D., 2006. Development of a multi-residue analytical methodology based on liquid chromatography-tandem mass spectrometry (LC-MS/MS) for screening and trace level determination of pharmaceuticals in surface and wastewaters. *Talanta*. 70, 678–690.
- Gurul, M. D. & Vatistas, R., 1987. Oxidation of phenolic compounds by ozone and ozone/UV radiation: A comparative study. *Water Res.* 21, 895–903.
- Gurr, C. J. and Reinhard, M., 2006. Harnessing natural attenuation of pharmaceuticals and hormones in rivers, *Environmental Science & Technology* 40 (9), 2872–2876.
- Habashi, F., 1997. In: *Handbook of Extractive Metallurgy*. Wiley-VCH, New York, p. 1997, vol. I, p. 488.
- Han. F., Kambala, V.S.R., Srinivasan, M., Rajarathnam, D., Naidu, R., 2009. Tailored titanium dioxide photocatalysts for the degradation of organic dyes in wastewater treatment: a review. *Appl. Catal. A. Gen.* 359:25–40.
- Han, Y., Boateng, A.A., Qi, P.X., Lima, I.M., Chang, J., 2013. Heavy metal and phenol adsorptive properties of biochars from pyrolyzed switchgrass and woody biomass in correlation with surface properties. *J. Environ. Manage.* 118, 196–204.
- Harbour, J.R., Chow, V., and Bolton, J.R., 1974. *Can. J. Chem.*, 1974, 52, 3549–3553.
- Heberer, T., 2002a. Occurrence, fate and removal of pharmaceutical residues in the aquatic environment: a review of recent research data, *Toxicology Letters*. 131, 5-17.
- Heberer, T., 2002b. Tracking persistent pharmaceutical residues from municipal sewage to drinking water, *Journal of Hydrology*. 266 (3-4), 175–189.

Heberer, T., Mechlinski, A., Fanck, B., Knappe, A., Massmann, G., Pekdeger, A., and Fritz, B., 2004. Field studies on the fate and transport of pharmaceutical residues in bank filtration. *Ground Water Monitoring and Remediation*. 24 (2), 70–77.

Her, N., Amy, G., Foss, D., and Cho, J. W., 2002. “Variations of molecular weight estimation by HP-size exclusion chromatography with UVA versus online DOC detection.” *Environ. Sci. Technol.* 36(15), 3393–3399.

Himmerlich, M., Wang, Ch. Y., Cimalla, V., Ambacher, O., and Krischok, S., 2012. Surface properties of stoichiometric and defect-rich indium oxide films grown by MOCVD. *Journal of Applied Physics*. 111, 093704.

Ho, L., and Newcombe, G., 2005. “Effect of NOM, turbidity and floc size on the PAC adsorption of MIB during alum coagulation.” *Water Res.*, 39(15), 3668–3674.

Hostachy, J. C., Lachenal, D., Coste, C. & Richard, Y. Ozonation of bleaching effluents in order to reduce AOX, COD, BOD, acute toxicity and chlorophenolic derivatives. In *Proc.11th Ozone World Congress of IOA, 1993, San Francisco, Vol. 2, S-10-13–S-10-23*.

<http://born2invest.com/cdn/the-honda-fujishima-effect-using-titanium-dioxide-as-a-photocatalyst/>By Conee Orsal on May 29, 2015. (Date Retrieved: 21st July, 2015).

<http://www.escouk.com/processes/advanced-oxidation-process/> (Date Retrieved: 24th August, 2012).

<http://www.oxidationtech.com/ozone/ozone-production/corona-discharge.html> (Date Retrieved: 7th May, 2014).

<http://www.spartanwatertreatment.com/UV-ozone-destruction.html> (Date Retrieved: 7th May, 2014).

<http://water.worldbank.org/shw-resource-guide/infrastructure/menu-technical-options/wastewater-treatment>. (Date Retrieved: 11<sup>th</sup> June, 2013).

[http://ipc.chem.demokritos.gr/index.php?option=com\\_content&view=article&id=302%3Acatalytic&catid=68%3Aresearchpro&lang=el](http://ipc.chem.demokritos.gr/index.php?option=com_content&view=article&id=302%3Acatalytic&catid=68%3Aresearchpro&lang=el). (Date Retrieved: 4<sup>th</sup> Aug. 2012).

<http://www.lenntech.com/library/ozone/disinfection/ozone-disinfection-mechanism.htm>. (Date retrieved: 26th May, 2014).

<http://www.fiercepharma.com/special-report/top-20-generic-molecules-worldwide>. (Date retrieved: 26th May, 2014).

Hua, W., Bennett, E.R., Letcher, R.J., 2006. Ozone treatment and the depletion of detectable pharmaceuticals and atrazine herbicide in drinking water sourced from the upper Detroit River, Ontario, Canada. *Water Research*. 40 (12), 2259-2266.



Huber, M.M., Canonica, S., Park, G.-Y., and von Gunten, U., 2003. Oxidation of pharmaceuticals during ozonation and advanced oxidation processes. *Environ. Sci. Technol.* 37, 1016–1024.

IMS Health MIDAS, 2015. (Date retrieved: 12<sup>th</sup>, November, 2015).

Ince, N.H., 1999. Critical effect of hydrogen peroxide in photochemical dye degradation. *Water Res.* 33(4), 1080-1084.

Inyang, M., Gao, B., Zimmerman, A., Zhang, M., Chen, H., 2014. Synthesis, characterization, and dye sorption ability of carbon nanotube–biochar nanocomposites. *Chem. Eng. J.* 236, 39–46.

Ioannou, L.A., Hapeshi, E., Vasquez, M.I., Mantzavinos, D., Fatta-Kassinos, D., 2011. Solar/TiO<sub>2</sub> photocatalytic decomposition of  $\beta$ -blockers atenolol and propranolol in water and wastewater. *Solar Energy.* 85, 1915–1926.

Ivancev-Tumbas, I., Dalmacija, B., Tamas, Z., and Karlovic, E., 1999. “The effect of different drinking water treatment processes on the rate of chloroform formation in the reactions of natural organic matter with hypochlorite.” *Water Res.*, 33(18), 3715–3722.

Jans, U. & Hoigne, J. 1998. Activated carbon and carbon black catalyzed transformation of aqueous ozone into ·OH radicals. *Ozone: Sci. Eng.* 20, 67–90.

Ji, Y., Zeng, C., Ferronato, C., Chovelon, J.-M., Yang, X., 2012. Nitrate-induced Photodegradation of atenolol in aqueous solution: Kinetics, toxicity and degradation pathways. *Chemosphere.* 88, 644–649.

Johnson, K.S., Willason, S.W., Wiesenburg, D. A., Lohrenz, S. E., Arnone, R.A., 1989. Hydrogen peroxide in the western Mediterranean Sea: a tracer for vertical advection. *Deep-Sea Res.* 36:241–254.

Jones, C.W., 1999. *Applications of Hydrogen Peroxide and Derivatives*, Royal Society of Chemistry, 1999.

Karakoyun, N., Kubilay, S., Aktas, N., Turhan, O., Kasimoglu, M., Yilmaz, S., Sahiner, N., 2011. Hydrogel-biochar composites for effective organic contaminant removal from aqueous media. *Desalination* 280, 319–325.

Khare, P., Goyal, D.K., 2013. Effect of high and low rank char on soil quality and carbon sequestration. *Ecol. Eng.* 52, 161–166.

Kim, M., Guerra, P., Shah, A., Parsa, M., Alaei, M., and Smyth, S.A., 2014. Removal of pharmaceuticals and personal care products in a membrane bioreactor wastewater treatment plant. *Water Science & Technology.* 69.11, 2221-2229.

Kim, S., Eichhorn, P., Jensen, J.N., Weber, A.S., and Aga, D.S., 2005. Removal of antibiotics in wastewater: Effect of hydraulic and solid retention times on the fate of

tetracycline in the activated sludge process. *Environmental Science & Technology*. 39 (15), 5816–5823.

Kong, H., He, J., Gao, Y., Wu, H., Zhu, X., 2011. Co-sorption of phenanthrene and mercury (II) from aqueous solution by soybean stalk-based biochar. *J. Agric. Food. Chem.* 59, 12116–12123.

Konstantinou, I.K., Albanis, T.A., 2004. TiO<sub>2</sub>-assisted photocatalytic degradation of azo dyes in aqueous solution: kinetic and mechanistic investigations: a review. *Appl. Catal. B Environ.* 49:1–14.

Kosjek, T., Heath, E., and Krbavcic, A., 2005. Determination of non-steroidal anti-inflammatory drug (NSAIDs) residues in water samples. *Environment International*. 31(5), 679–685.

Kreuzinger, N., Clara, M., Strenn, B., and Vogel, B., 2004. Investigation on the behaviour of selected pharmaceuticals in the groundwater after infiltration of treated wastewater. *Water Science and Technology*. 50 (2), 221–228.

Kümmerer Klaus. University of Freiburg environmental chemist and leading green-pharmacy advocate *Yale environment 360*, article 15 Apr. 2010 (Date retrieved: 2014/04/23).

Kwon, J.W. and Armbrust, K.L., 2005. Degradation of citalopram by simulated sunlight. *Environmental Toxicology and Chemistry*. 24 (7), 1618–1623.

Lam, M.W. and Mabury, S.A., 2005. Photodegradation of the pharmaceuticals atorvastatin, carbamazepine, levofloxacin and sulfamethoxazole in natural waters. *Aquatic Sciences*. 67 (2), 177–188.

Larsson Joakim. “Selection machines for resistant bacteria,” says University of Gothenburg physiology professor. *Yale environment 360*, article 15 Apr. 2010 (Date retrieved: 2014/04/23).

Lee, H.B., Peart, T.E., and Svoboda, M.L., 2005. Determination of endocrine-disrupting phenols, acidic pharmaceuticals, and personal-care products in sewage by solid-phase extraction and gas chromatography-mass spectrometry. *Journal of Chromatography A*. 1094 (1–2), 122–129.

Lee, S., Cho, J. W., and Elimelech, M., 2005. “Combined influence of natural organic matter NOM and colloidal particles on nanofiltration membrane fouling.” *J. Membr. Sci.* 262(1–2), 27–41.

Legube, B., Delouane, B., Karpel Vel Leitner, N. & Luck, F. Catalytic ozonation of salicylic acid in aqueous solution: Efficiency and mechanisms. In *Proc. Reg. Conf. Ozone, UV-light, AOPs Water Treatm.* September 24–26, 1996, Amsterdam, Netherlands, 509–514.

- Leiknes, T., Lazarova, M., and Odegaard, H., 2005. "Development of a hybrid ozonation biofilm-membrane filtration process for the production of drinking water." *Water Sci. Technol.*, 51(6–7), 241–248.
- Li, Q. L., Snoeyink, V. L., Mariaas, B. J., and Campos, C., 2003a. "Elucidating competitive adsorption mechanisms of atrazine and NOM using model compounds." *Water Res.*, 37(4), 773–784.
- Li, Q. L., Snoeyink, V. L., Marinas, B. J., and Campos, C., 2003b. "Pore blockage effect of NOM on atrazine adsorption kinetics of PAC: The roles of PAC pore size distribution and NOM molecular weight." *Water Res.*, 37(20), 4863–4872.
- Lin, A.Y.C. and Reinhard, M., 2005. Photodegradation of common environmental pharmaceuticals and estrogens in river water, *Environmental Toxicology and Chemistry* 24 (6), 1303–1309.
- Lindberg, R.H., Olofsson, U., Rendahl, P., Johansson, M.I., Tysklind, M., and Andersson, B.A.V., 2006. Behavior of fluoroquinolones and trimethoprim during mechanical, chemical, and active sludge treatment of sewage water and digestion of sludge. *Environmental Science & Technology*. 40 (3), 1042–1048.
- Lindqvist, N., Tuhkanen, T., and Kronberg, L., 2005. Occurrence of acidic pharmaceuticals in raw and treated sewages and in receiving waters. *Water Research*. 39 (11), 2219–2228.
- Lishman, L., Smyth, S.A., Sarafin, K., Kleywegt, S., Toito, J., Peart, T., Lee, B., Servos, M., Beland, M., and Seto, P., 2006. Occurrence and reductions of pharmaceuticals and personal care products and estrogens by municipal wastewater treatment plants in Ontario, Canada. *Science of the Total Environment*. 367 (2–3), 544–558.
- Lopez, A., Ricco G, Ciannarella R., 1999. Textile wastewater reuse: Ozonation of membrane concentrated secondary effluent. *Water Sci. technol.* 40, 99-105.
- Lu, H., Zhang, W., Yang, Y., Huang, X., Wang, S., Qiu, R., 2012. Relative distribution of  $Pb^{2+}$  sorption mechanisms by sludge-derived biochar. *Water Res.* 46, 854–862.
- Lv, J., Kako, T., Li, Z.S., Zou, Z., Ye, J., 2010. Synthesis and photocatalytic activities of  $NaNbO_3$  rods modified by  $In_2O_3$  nanoparticles. *Journal of Physical Chemistry C*. Volume 114, Issue 13, 6157-6162.
- Mao, J.D., Johnson, R., Lehmann, J., Olk, D., Neves, E., Thompson, M., Schmidt-Rohr, K., 2012. Abundant and stable char residues in soils: implications for soil fertility and carbon sequestration. *Environ. Sci. Technol.* 46, 9571–9576.
- Martin, C., Martin, I. & Rives, V., 1995. Effect of sulfate removal on the surface texture and acid-base properties of  $TiO_2$  (anatase). *J. Math. Sci.*, 30, 3847–3852.

- Matthews, R. W., 1986. Photo-oxidation of organic material in aqueous suspensions of titanium dioxide. *Water Res.* 20, 569–578.
- Meade, H. R., 1995. USGS Circular, 1133, p. 114-135, Reston Virginia. [http://toxics.usgs.gov/regional/emc/transport\\_fate.html](http://toxics.usgs.gov/regional/emc/transport_fate.html) (Date Retrieved: 20th Dec. 2014).
- Merrington G., Taylor, D., Gross, M., Leverett D., 2014. SETAC Asia-Pacific – Adelaide, Pharmaceutical era [gm2]. The prioritisation and environmental risk assessment of pharmaceuticals: Experiences in Europe.
- Metcalf, C.D., Koenig, B.G., Bennie, D.T., Servos, M., Ternes, T.A., Hirsch, R., 2003a. Occurrence of neutral and acidic drugs in the effluents of Canadian sewage treatment plants, *Environmental Toxicology and Chemistry*. 22 (12), 2872-2880.
- Metcalf, C.D., Miao, X.-S., Koenig, B.G., Struger, J., 2003b. Distribution of acidic and neutral drugs in surface waters near sewage treatment plants in the Lower Great Lakes, Canada, *Environmental Toxicology and Chemistry*. 22 (12), 2881-2889.
- Miao, X.-S., Koenig, B. G., Metcalfe, C. D., 2002. Analysis of acidic drugs in the effluent of sewage treatment plants using liquid chromatography-electrospray ionization tandem mass spectrometry, *Journal of Chromatography A*. 952, 139-147.
- Moffett, J.W., Zafiriou, O.C., 1990. An Investigation of hydrogen peroxide chemistry in surface waters of Vineyard sound with  $H_2^{18}O_2$  and  $^{18}O_2$ . *Limnol Oceanogr.* 35:1221–1229.
- Moore, C.A., Farmer, C.T., Zika, R.G., 1993. Influence of the Orinoko river on hydrogen peroxide distribution and production in the Eastern Caribbean. *J. Geophys. Res.* 98(C2):2289–2298.
- Mostofa, K.M.G., Sakugawa, H., 2009. Spatial and temporal variations and factors controlling the concentrations of hydrogen peroxide and organic peroxides in rivers. *Environ. Chem.* 6:524–534.
- Munoz, I., Rieradevall, J., Torrades, F, Peral, J., Dome`nech, X., 2006a. Environmental assessment of different advanced oxidation processes applied to a bleaching kraft mill effluent. *Chemosphere.* 62:9–16.
- Munoz, I., Rieradevall, J., Torrades, F., Peral, J., Dome`nech, X., 2006b. Environmental assessment of different advanced oxidation processes applied to a bleaching kraft mill effluent. *Chemosphere.* 62:9–16.
- Munter, R., Kallas, J., Preis, S., Kamenev, S., Trapido, M. & Veressinina, Y., 1995. Comparative studies of AOP for aromatic and PAH destruction. In Proc. 12th World Ozone Congr., May 15–18, 1995, Lille, France, **1**, 395–406.
- Murat, A., and Medvedeva, J.E., 2012. *Phys. Rev. B: Condens. Matter Mater. Phys.* 86, 085123.

- Murov, S.L., Carmichael, I., Hug, G.L., 1993. Handbook of photochemistry, 2nd edn. Marcel Dekker, New York, pp 299–305.
- Mustranta, A., and Viikari, L., 1993. Dewatering of activated sludge by an oxidative treatment. *Water Sci Technol.* 28(1): 213–221.
- Nakazawa, H., Ito, Y., Matsumoto, E., Adachi, K., Aoki, N., and Ochiai, Y., 2006. *J. Appl. Phys.* 100, 093706.
- Noh, H.-K., Chang, K., Ryu, B., and Lee, W.-J., 2011. *Phys. Rev. B: Condens. Matter Mater. Phys.* 84, 115205.
- Nomura, K., Kamiya, T., Ikenaga, E., Yanagi, H., Kobayashi K., and Hosono, H., 2011. *J. Appl. Phys.* 109, 073726.
- NDC Health, USA, 2010. [homepage.ntlworld.com/bhandari/Imperial/Atenolol/Introduction.Htm](http://homepage.ntlworld.com/bhandari/Imperial/Atenolol/Introduction.Htm) (Date retrieved: 2015/07/09).
- Oliver, B.G., 1983. Dihaloacetonitriles in drinking water: algae and fulvic acid as precursors. *Environmental Science & Technology.* 17 (2), 80–83.
- Obernosterer, I., Ruardij, P., Herndl, G.J., 2001. Spatial and diurnal dynamics of dissolved organic matter (DOM) fluorescence and H<sub>2</sub>O<sub>2</sub> and the photochemical oxygen demand of surface water DOM across the subtropical Atlantic Ocean. *Limnol. Oceanogr.* 46:632–643.
- Packer, J.L., Werner, J.J., Latch, D.E., McNeill, K., and Arnold, W.A., 2003. Photochemical fate of pharmaceuticals in the environment: Naproxen, diclofenac, clofibric acid, and ibuprofen. *Aquatic Sciences.* 65 (4), 342–351.
- Paillard, H., Dore, M. & Bourbigot, M. Prospect concerning applications of catalytic ozonation in drinking water treatment. In *Proc. 10th Ozone World Congr.*, March, 1991, Monaco, 1, 313–331.
- Paradies, G., Petrosillo, G., Pistolese, M., Ruggiero, F.M., 2000. The effect of reactive oxygen species generated from the mitochondrial electron transport chain on the cytochrome C oxidase activity and on the cardiolipin content in bovine heart submitochondrial particles. *FEBS. Lett.* 466:323–326.
- Paxeus, N., 2004. Removal of selected non-steroidal anti-inflammatory drugs (NSAIDs) gemfibrozil, carbamazepine, beta-blockers, trimethoprim and triclosan in conventional wastewater treatment plants in five EU countries and their discharge to the aquatic environment. *Water Science and Technology.* 50 (5), 253–260.
- Pere, J., Alen, R., Viikari, L., Eriksson, L., 1993. Characterization and dewatering of activated sludge from the pulp and paper industry. *Water Sci. Technol.* 28, 193-201.

Perez, S., Eichhorn, P., and Aga, D.S., 2005. Evaluating the biodegradability of sulfamethazine, sulfamethoxazole, sulfathiazole, and trimethoprim at different stages of sewage treatment. *Environmental Toxicology and Chemistry*. 24 (6), 1361–1367.

Perez-Estrada, L.A., Malato, S., Gernjak, W., Aguera, A., Thurman, E.M., Ferrer, I., and Fernandez-Alba, A.R., 2005. Photo-fenton degradation of diclofenac: Identification of main intermediates and degradation pathway. *Environmental Science & Technology*. 39 (21), 8300–8306.

Petasne, R.G., Zika, R.G., 1997. Hydrogen peroxide lifetimes in south Florida coastal and offshore waters. *Mar. Chem.* 56:215–225.

Petrosyants, S. P., and Ilyukhin, A. B., 2011. Indium(III) Coordination Compounds. ISSN 0036-0236, *Russian Journal of Inorganic Chemistry*. Vol. 56, No. 13, pp. 2047–2069.

Peyton, G. R., Huang, F. Y., Burleson, J. L. & Glaze, W. H., 1982. Destruction of pollutants in water with ozone in combination with UV radiation. *Environ. Sci. Technol.* 16, 448–453.

Pleskov, Y.V., Gurevich, Y.Y., 1986. Semiconductor photoelectron chemistry. Consultants Bureau, New York, p 29.

Plewa, M.J., Kargalioglu, Y., Vankerk, D., Minear, R.A., Wagner, E.D., 2002. Mammalian cell cytotoxicity and genotoxicity analysis of drinking water disinfection byproducts. *Environmental and Molecular Mutagenesis*. 40 (2), 134–142.

Poyatos, J.M., Munio, M.M., Almecija, M.C., Osorio, F., 2009. Advanced Oxidation Processes for Wastewater Treatment: State of the Art. *Water, Air and Soil Pollution* 205(1):187-204.

Prousek, J., 1996. Advanced oxidation processes for water treatment photochemical processes. *Chem. Listy*. 90:307–315.

Qiu, Y., Zheng, Z., Zhou, Z., Sheng, G.D., 2009. Effectiveness and mechanisms of dye adsorption on a straw-based biochar. *Bioresour. Technol.* 100, 5348–5351.

Quintana, J.B., and Reemtsma, T., 2004. Sensitive determination of acidic drugs and triclosan in surface and wastewater by ion-pair reverse-phase liquid chromatography/tandem mass spectrometry. *Rapid Communications in Mass Spectrometry*. 18 (7), 765–774.

Quintana, J.B., Weiss, S., and Reemtsma, T., 2005. Pathways and metabolites of microbial degradation of selected acidic pharmaceutical and their occurrence in municipal wastewater treated by a membrane bioreactor. *Water Research*. 39 (12), 2654–2664.

Radjenovic, J., Sirtori, C., Petrovic, M., Barcelo, D., Malato, S., 2009. Solar photocatalytic degradation of persistent pharmaceuticals at pilot-scale: kinetics and characterization of major intermediate products. *Appl. Catal. B-Environ.* 89, 255–264.

Radjenovic, J., Petrovic, M., Barcelo, D., 2007. Analysis of pharmaceuticals in wastewater and removal using a membrane bioreactor. *Anal. Bioanal. Chem.* 387 (4), 1365–1377.

Ray, M.B., Chen, J.P., Wang, L.K., and Pehkonen, S.O., 2006. Advanced oxidation processes". In: *Handbook of Environmental Engineering, Vol. 4. Advanced Physicochemical Treatment Processes*, Chapter 14 Ed. L.K. Wang et al., The Humana.

Richard, L.E., Peake, B.M., Rusak, S.A., Cooper, W.J., Burritt, D.J., 2007. Production and decomposition dynamics of hydrogen peroxide in freshwater. *Environ. Chem.* 4:49–54. doi:101071/EN06068.

Roberts, P.H. and Thomas, K.V., 2006. The occurrence of selected pharmaceuticals in wastewater effluent and surface waters of the lower Tyne catchment. *Science of the Total Environment.* 356 (1–3), 143–153.

Sabri, M.M., Jung, J., Yoon, D. H., Yoon, S., Tak, Y. J., and Kim, H. J., 2015. *J. Mater. Chem. C.* 3, 7499.

Sakai, N., Fujishima, A., Watanabe, T., and Hashimoto, K., 2003. *J. Phys. Chem. B.* 107, 1028.

Sakugawa, H., Kaplan, I.R., Tsai, W., Cohen, Y., 1990. Atmospheric hydrogen peroxide. *Environ. Sci. Technol.* 24:1452–1462.

Sandra Pérez and Barceló, D., 2008. *Advances in the Analysis of Pharmaceuticals in the Aquatic Environment (Chapter 2). Fate of Pharmaceuticals in the Environment and in Water Treatment Systems.*

Saquib, M., Tariq, M.A., Haque, M.M., Muneer, M., 2008. Photocatalytic degradation of disperse blue 1 using UV/TiO<sub>2</sub>/H<sub>2</sub>O<sub>2</sub> process. *J. Environ. Manag.* 88:300–306.

Sarikaya, H.Z., and Al-Marshoud S., 1993. Improvement of Dewatering Characteristics of Aerobically Digested Sludges. *Water Science and Technology.* 28(1):47-51.

Sarthou, G., Jeandel, C., Brisset, L., Amouroux, D., Besson, T., Donard, O.F.X., 1997. Fe and H<sub>2</sub>O<sub>2</sub> distributions in the upper water column in the Indian sector of the Southern Ocean Earth. *Planetary Sci. Lett.* 147:83–92.

Scheytt, T., Mersmann, P., Leidig, M., Pekdeger, A., and Heberer, T., 2004. Transport of pharmaceutically active compounds in saturated laboratory columns. *Ground Water.* 42 (5), 767–773.

- Schiavello, M., 1987. Basic concepts in photocatalysis. In: Schiavello, M., (ed). Photocatalysis and environmental trends and applications. Kluwer Academic Publishers, The Netherlands. pp 351–360.
- Scully, N.M., McQueen, D.J., Lean, D.R.S., Cooper, W.J., 1996. Hydrogen peroxide formation: the interaction of ultraviolet radiation and dissolved organic carbon in lake waters along a 43–75°N gradient. *Limnol. Oceanogr.* 41:540–548.
- Scully, N.M., McQueen, D.J., Lean, D.R.S., Cooper, W.J., 1996. Hydrogen peroxide formation: the interaction of ultraviolet radiation and dissolved organic carbon in lake waters along a 43–75°N gradient. *Limnol. Oceanogr.* 41:540–548.
- Scully, N.M., Vincent, W.F., 1997. Hydrogen peroxide: a natural tracer of stratification and mixing processes in subarctic lakes. *Arch. Hydrobiol.* 139:1–15.
- Selcuk, H., Rizzo, L., Nikolaou, A. N., Meric, S., Belgiorno, V., and Bekbolet, M., 2007. “DBPs formation and toxicity monitoring in different origin water treated by ozone and alum/PAC coagulation.” *Desalination.* 210(1–3), 31–43.
- Sharp, E. L., Parson, S. A., and Jefferson, B., 2006. “Coagulation of NOM: Linking character to treatment.” *Water Sci. Technol.* 53(7), 67–76.
- Sherry, S., and Karl, A., 2006. <http://www.sheffy6marketing.com/index.php?page=test-child-page>. (Date Retrieved: 10<sup>th</sup> Oct. 2013).
- Sikorsky, R.J., Zika, R.G., 1993a. Modeling mixed-layer photochemistry of H<sub>2</sub>O<sub>2</sub>: optical and chemical modeling of production. *J. Geophys. Res.* 98:2315–2328.
- Sikorsky, R.J., Zika, R.G., 1993b. Modeling mixed-layer photochemistry of H<sub>2</sub>O<sub>2</sub>: physical and chemical modeling of distribution. *J. Geophys. Res.* 98:2329–2340.
- Snyder, S.A., Leising, J., Westerhoff, P., Yoon, Y., Mash, H., and Vanderford, B., 2004. Biological and physical attenuation of endocrine disruptors and pharmaceuticals: Implications for water reuse. *Ground Water Monitoring and Remediation.* 24 (2), 108–118.
- Sohi, S.P., 2012. Carbon storage with benefits. *Science* 338, 1034–1035.
- Sonia Shah, 2010. As Pharmaceutical Use Soars, Drugs Taint Water and Wildlife. *Yale environment* 360, article 15 Apr. 2010. (Date retrieved: 2014/04/23).
- Stan, H.J., Heberer, Th., and Linkerhägner, M., 1994. Occurrence of clofibric acid in the aquatic system – Is their therapeutic use responsible for the loads found in surface, ground- and drinking water? *Vom Wasser.* 83, 57–68.
- Stumpf, M., Ternes, T.A., Haberer, K., Seel, P., and Baumann, W., 1996. Nachweis von Arzneimittelrückständen in Klaranlagen und Fliesgewässern. *Vom Wasser.* 86, 291.



Sun, J., Lian, F., Liu, Z., Zhu, L., Song, Z., 2014. Biochars derived from various crop straws: characterization and Cd (II) removal potential. *Ecotoxicol. Environ. Saf.* 106, 226–231.

Sun, L., Bolton, J.R., 1996. Determination of the Quantum Yield for the Photochemical Generation of Hydroxyl Radicals in TiO<sub>2</sub> Suspensions. *J. Phys. Chem.* 100:4127-4134.

Susan, T. G., Dana, W. K., Edward, T. F., and Michael, J. F. Environmental Presence and Persistence of Pharmaceuticals. An Overview. Diana S. A., 2008. Fate of pharmaceuticals in the environment and in water treatment systems.

Symons, J.M., Krasner, S.W., Simms, L.A., Scilimenti, M.J., 1993. Measurement of THM and precursor concentrations revisited: the effect of bromide ion. *Journal of AWWA.* 85 (1), 51–62.

Tahir, M., Amin, N.S., 2013. Photocatalytic CO<sub>2</sub> reduction and kinetic study over In/TiO<sub>2</sub> nanoparticles supported microchannel monolith photoreactor. *Appl. Catal. A: Gen.* 467, 483–496.

Takahashi, N., 1990. Ozonation of several organic compounds having low molecular weight under UV irradiation. *Ozone: Sci. Eng.* 12, 1–18.

Tang, J., Durrant, J.R., Klug, D.R., 2008. Mechanism of photocatalytic water splitting in TiO<sub>2</sub>. Reaction of water with photoholes, importance of charge carrier dynamics, and evidence for four-hole chemistry. *Journal of the American Chemical Society.* 130 (42), 13885-13891.

Techcommentary, 1996. Advanced Oxidation Processes for Treatment of Industrial Wastewater. An EPRI Community Environmental Center Publ. No. 1.

Ternes, T.A. and Hirsch, R.A. 2000. Occurrence and behaviour of X-ray contrast media in sewage facilities and the aquatic environment. *Environ. Sci. Technol.* 34:2741.

Ternes, T.A., 1998. Occurrence of drugs in German sewage treatment plants and rivers. *Water Research.* 32 (11), 3245–3260.

Ternes, T.A., Joss, A., and Siegrist, H., 2004. Scrutinizing pharmaceuticals and personal care products in wastewater treatment. *Environmental Science & Technology.* 38 (20), 392A-399A.

Ternes, T.A., Meisenheimer, M., McDowell, D., Sacher, F., Brauch, H.J., Gulde, B.H., Preuss, G., Wilme, U., and Seibert, N.Z., 2002. Removal of pharmaceuticals during drinking water treatment. *Environmental Science & Technology.* 36 (17), 3855–3863.

The UV/Oxidation Handbook, 1994. Solarchem Environmental Systems, Markham, Ontario, Canada.

- Thomas, P.M. and Foster, G.D., 2005. Tracking acidic pharmaceuticals, caffeine, and triclosan through the wastewater treatment process. *Environmental Toxicology and Chemistry*. 24(1), 25–30.
- Tan, X., Liu, Y., Zeng, G., Wang, X., Hu, X., Gu, Y., Yang, Z., 2015. Application of biochar for the removal of pollutants from aqueous solutions. *Chemosphere*. 125, 70–85.
- Trapido, M. & Kallas, J., 2000. Advanced oxidation processes for the degradation and detoxification of 4-nitrophenol. *Environ. Technol.* 21, 799–808.
- Tseng, J.M., Haung, C.P., 1991. Removal of chlorophenols from water by photocatalytic oxidation. *Water Sci. Technol.* 23:377–387.
- U.S. Environmental Protection Agency, 1998. National primary drinking water regulations: disinfectants and disinfection byproducts. *Federal Register*. 63 (241), 69289.
- Ullah, S.S., Khan, M.G.M., Rahman, A.B.M.S., 1998. Photocatalytic decomposition of phenols by titanium dioxide under sunlight and UV. *J. Bang. Acad. Sci.* 22:29–37.
- USEPA, 1999. Biosolids generation, use and disposal in the United States. US EPA-530-R-99-009.
- USEPA, 2003. <http://www.epa.gov/owm/mtb/biosolids/genqa.htm>. (Date Retrieved: 13<sup>th</sup> Feb. 2011).
- Verenitch, S.S., Lowe, C.J., and Mazumder, A., 2006. Determination of acidic drugs and caffeine in municipal wastewaters and receiving waters by gas chromatography-ion trap tandem mass spectrometry. *Journal of Chromatography A*. 1116 (1–2), 193–203.
- Verheijen, F., Graber, E., Ameloot, N., Bastos, A.C., Sohi, S., Knicker, H., 2014. Biochars in soils: new insights and emerging research needs. *Eur. J. Soil Sci.* 65, 22–27.
- Vieno, N.M., Tuhkanen, T., and Kronberg, L., 2005. Seasonal variation in the occurrence of pharmaceuticals in effluents from a sewage treatment plant and in the recipient water. *Environmental Science & Technology*. 39 (21), 8220–8226.
- Vione, D., Maurino, V., Minero, C., Pelizzetti, E., 2001a. Phenol photolysis upon UV irradiation of nitrite in aqueous solution II: effects of pH and TiO<sub>2</sub>. *Chemosphere*. 45:903–910.
- Vione, D., Maurino, V., Minero, C., Pelizzetti, E., 2001b. Phenol photolysis upon UV irradiation of nitrite in aqueous solution II: effects of pH and TiO<sub>2</sub>. *Chemosphere*. 45:903–910.

- Vogna, D., Marotta, R., Napolitano, A., Andreozzi, R. and d'Ischia, M., 2004. Advanced oxidation of the pharmaceutical drug diclofenac with UV/H<sub>2</sub>O<sub>2</sub> and ozone. *Water Res.* 38(2), 414–422.
- Volk, C., Bell, K., Ibrahim, E., Verges, D., Amy, G., and Lechevallier, M., 2000. “Impact of enhanced and optimized coagulation on removal of organic matter and its biodegradable fraction in drinking water.” *Water Res.* 34(12), 3247–3257.
- von Gunten, U., 2003. Review: Ozonation of drinking water: Part II. Disinfection and by-product formation in presence of bromide, iodide or chlorine. *Water Research.* 37, 1469–1487.
- Wable, O., Jousset, M., Courant, P. & Duguet, J.-P. Oxidation of landfill leachates by ozone and hydrogen peroxide: A French example. In *Proc. Intl. Symp. on Ozone Oxidation Methods for Water and Wastewater Treatment*, Paris, 1993, II.6.1–II.6.11.
- Wang, H., Keller, A. A., ASCE, M., and Li, F., 2010. Natural Organic Matter Removal by Adsorption onto Carbonaceous Nanoparticles and Coagulation. *J. Environ. Eng.* 136:1075-1081.
- Watanabe, T., Hashimoto K., and Fujishima A., 1993: in *Photocatalytic Purification and Treatment of Water and Air*, eds. Ollis, D. F., and Al-Ekabi, H. (Elsevier, Amsterdam).
- Wedekamp H., and Schwammlein, K., 1994. "Disinfection of Drinking-Water with UV-Light results from full-size tests". *Journal of Information Recording Materials.* 21(5-6), pp. 487-490.
- Wenzel, A., Gahar, A., and Niessner, R., 1999. TOC-removal and degradation of pollutants in leachate using a thin-film photoreactor. *Water Res.* 33(4) 937-946.
- Whitman, T., Nicholson, C.F., Torres, D., Lehmann, J., 2011. Climate change impact of biochar cook stoves in Western Kenyan farm households: system dynamics model analysis. *Environ. Sci. Technol.* 45, 3687–3694.
- Wiegel, S., Aulinger, A., Brockmeyer, R., Harms, H., Löffler, J., Reincke, H., Schmidt, R., Stachel, B., Von Tumpling, W., and Wanke, A., 2004. Pharmaceuticals in the river Elbe and its tributaries. *Chemosphere.* 57 (2), 107–126.
- Wolf, L., Held, I., Eiswirth, M., and Hotzl, H., 2004. Impact of leaky sewers on groundwater quality. *Acta Hydrochimica Et Hydrobiologica.* 32 (4–5), 361–373.
- Xie, M., Chen, W., Xu, Z., Zheng, S., Zhu, D., 2014. Adsorption of sulfonamides to demineralized pine wood biochars prepared under different thermochemical conditions. *Environ. Pollut.* 186, 187–194.

Xu, R.K., Xiao, S.C., Yuan, J.H., Zhao, A.Z., 2011. Adsorption of methyl violet from aqueous solutions by the biochars derived from crop residues. *Bioresour. Technol.* 102, 10293–10298.

Xue, Y., Gao, B., Yao, Y., Inyang, M., Zhang, M., Zimmerman, A.R., Ro, K.S., 2012. Hydrogen peroxide modification enhances the ability of biochar (hydrochar) produced from hydrothermal carbonization of peanut hull to remove aqueous heavy metals: batch and column tests. *Chem. Eng. J.* 200, 673–680.

Yang, Y., Wei, Z., Zhang, X., Chen, X., Yue, D., Yin, Q., Xiao, L., Yang, L., 2014b. Biochar from *Alternanthera philoxeroides* could remove Pb(II) efficiently. *Bioresour. Technol.* 171, 227–232.

Yonar, T., Yonar, G.K., Kestioglu, K., & Azbar, N., 2005. Decolorisation of Textile Effluent Using Homogeneous Photochemical Oxidation Processes. *Colour. Technol.* Vol.121, pp. 258-264, ISSN 1472-3581.

Yuan, J., Shiller, A.M., 2001. The distribution of hydrogen peroxide in the southern and central Atlantic ocean. *Deep-Sea Res. II* 48:2947–2970.

Zhang, S., Zhang, Q., Darisaw, S., Ehie, O., and Wang, G., 2007. Simultaneous quantification of polycyclic aromatic hydrocarbons (PAHs), polychlorinated biphenyls (PCBs), and pharmaceuticals and personal care products (PPCPs) in Mississippi River water, in New Orleans, Louisiana. *Chemosphere.* 66, 1057–1069.

Zhang, M., Gao, B., Yao, Y., Xue, Y., Inyang, M., 2012. Synthesis of porous MgO biochar nanocomposites for removal of phosphate and nitrate from aqueous solutions. *Chem. Eng. J.* 210, 26–32.

Zhang, P., Sun, H., Yu, L., Sun, T., 2013b. Adsorption and catalytic hydrolysis of carbaryl and atrazine on pig manure-derived biochars: impact of structural properties of biochars. *J. Hazard. Mater.* 244, 217–224.

Zheng, W., Guo, M., Chow, T., Bennett, D.N., Rajagopalan, N., 2010. Sorption properties of greenwaste biochar for two triazine pesticides. *J. Hazard. Mater.* 181, 121–126.

Zhou, H., and Smith, D.W., 2001. Advanced technologies in water and wastewater treatment. *Can. J. Civ. Eng.* 28(Suppl. 1): 49-66.

Zhou, Z., and Jiang, J.Q., 3-5 September 2015. Removal of selected pharmaceuticals spiked in the secondary effluent of a wastewater treatment plant (WWTP) by potassium ferrate (VI). Proceedings of the 14th International Conference on Environmental Science and Technology, Rhodes, Greece. CEST2015\_00043.

Zika, R.G., Moffett, W., Petasne, R.G., Cooper, W.J., Saltzman, E.S., 1985a. Spatial and temporal variations of hydrogen peroxide in Gulf of Mexico waters. *Geochim. Cosmochim. Acta.* 49:1173–1184.

Zika, R.G., Saltzman, E.S., Cooper, W.J., 1985b. Hydrogen peroxide concentrations in the Peru upwelling area. *Mar. Chem.* 17:265–275.

Zilnik, L. F., Jazbinsek, A., Hvala, A., Vrečer, F., Klamt, A., 2007. Solubility of sodium diclofenac in different solvents. *Fluid Phase Equilibria.* 261, 140-145.

Zmolek, C. R. Ultra pure water for integrated circuits processing. *Ind. Water Eng.*, 1977, 12, 6–11.

Zorita, S., Mårtensson, L., and Mathiasson, L., 2009. Occurrence and removal of pharmaceuticals in a municipal sewage treatment system in the south of Sweden. *Science of The Total Environment.* 407 (8) 2760-2770.

Zuccato, E., Chiabrando, C., Castiglioni, S., Calamari, D., Bagnati, R., Schiarea, S., and Fanelli, R. 2005. Cocaine in surface waters: a new evidence-based tool to monitor community drug abuse. *Environ. Health: A Glob. Acc. Sci. Source* 4:14.

Zwiener, C. and Frimmel, F.H., 2000. Oxidative treatment of pharmaceuticals in water. *Water Res.* 34, 1881–1885.

Zwiener, C. and Frimmel, F.H., 2003. Short-term tests with a pilot sewage plant and biofilm reactors for the biological degradation of the pharmaceutical compounds clofibrac acid, ibuprofen, and diclofenac. *Science of the Total Environment.* 309, 201–211.

## Chapter 3

### 3 Preparation and characterization of homogeneous immobilized TiO<sub>2</sub> coatings on stainless steel mesh and its removal kinetics of PPCPs from wastewater by a combination of AOP (O<sub>3</sub>/UV/TiO<sub>2</sub>) and its comparison with other techniques

#### 3.1 Introduction

Pharmaceutical and personal care products (PPCPs) are non-regulated water pollutants that may be grouped into a plethora of other classes such as antidepressants, antibiotics, steroids, painkillers, narcotics, tranquilizers, antiseptics, oral contraceptives, insect repellents, fragrances, shampoos, sunscreens, food supplements, nicotine and caffeine. Among these, two therapeutic classes, antibiotics and steroidal hormones, have received the most attention due to their potential for selective resistance to certain pathogens. Municipal sewage containing PPCPs may discharge into receiving waters and the impact would depend on the types and relative abundances of the individual constituent PPCPs.

Most of the drugs in the human body get metabolized by either phase I and/or phase II reactions to a certain extent while entering the environment before leaving the body. Reduction, oxidation and hydroxylation are phase I reactions that produce water-soluble reactive compounds that expose functional groups enhancing further reactions (Halling-Sorensen et al., 1998; Josephy and Mannervik, 2006). Methylation, sulfation, acetylation, glucuronide conjugation and glutathione conjugation are phase II or conjugated reactions that bind functional groups to the compound, thus enhancing its water solubility and increasing its elimination from the body (Josephy and Mannervik, 2006).

Lipid Regulators ranks 9<sup>th</sup> as one of the top 20 Global Therapy Areas in 2014 with sales of US\$ 28,412Mn where the Global Market sales stands with a total of US\$ 936,511Mn in 2014 with quarterly exchange rates for the top 20 therapy areas of usage (IMS, 2014).

These PPCPs are referred to as pseudo-persistent chemicals as they are introduced to the aquatic realm via sewage leading to continual and multigenerational exposure for aquatic organisms despite their short half-lives. For instance, when diclofenac in surface waters is exposed to natural sunlight, rapid decomposition takes place as shown by several authors (Packer et al., 2003 and Bartels et al., 2007). It was also seen that in natural environment, CFA was hardly biodegraded and in aquatic system, the fate of CFA was only a minimal due to adsorption and abiotic losses (Winkler et al., 2001).

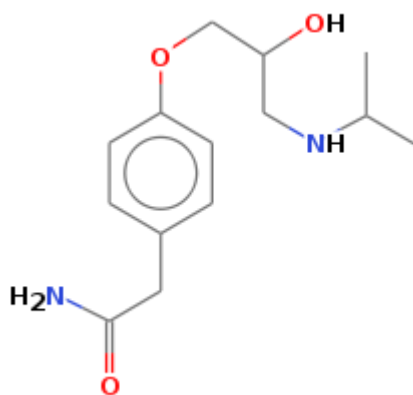
Certain drugs gain intracellular access via active transport in aquatic tissues from ambient water despite their low lipid solubility's. For instance, estrogen has a concentration of 60,000x in fish bile, 113x in fish tissue due to gemfibrozil, fluoxetine gets concentrated in brain, liver and muscle of fish whereas diclofenac gets concentrated in fish. Due to their low octanol-water partition coefficients, most of the PPCPs prevent bio-concentration. However, sunscreen filters, triclosan, synthetic musks, parabens and triclocarban are subjected to bio-concentration (Daughton, C., 2005).

Analgesics and anti-inflammatory drugs are among the major pharmaceutical pollutants found in surface waters at concentrations of up to  $\mu\text{g/L}$  levels as they are ubiquitous in effluents from municipal WWTPs. These groups of drugs show pKa values between 3.6 and 4.9 and are acidic in nature because of the presence of one or two phenolic hydroxyl groups and carboxylic moieties. Table 3.1 represents some of the physico-chemical properties of  $\beta$ -blockers, lipid regulators and anti-inflammatory drugs that were selected for the present degradation studies and their chemical structures are shown in Figure 3.1. A detailed explanation on the physico-chemical properties are described in Chapter 2, Table 2.5 of this thesis (V.R. Kandlakuti).

Table 3.1. Physico-Chemical properties of ATN, CFA and DCF

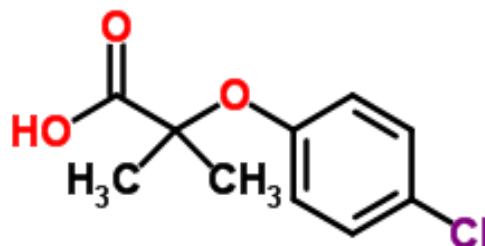
| Property                          | Atenolol (ATN)  | Clofibric Acid (CFA)                             | Diclofenac Sodium (DCF)   |
|-----------------------------------|---|--|---|
| Molecular Formula                 | C <sub>14</sub> H <sub>22</sub> N <sub>2</sub> O <sub>3</sub> | C <sub>10</sub> H <sub>11</sub> ClO <sub>3</sub> | C <sub>14</sub> H <sub>11</sub> C <sub>12</sub> NO <sub>2</sub> |
| CAS Number                        | 29122-68-7  | 882-09-7   | 15307-79-6  |
| Category                          | Basic   | Acidic   | Acidic  |
| Therapeutic group                 | β-blockers  | Lipid regulators                                 | Anti-inflammatory   |
| Molecular Weight (g/mol)          | 266.34  | 214.65   | 318.134   |
| Vapor Pressure (mm Hg)            | 2.92 x 10 <sup>-10</sup>                                      | 1.13 x 10 <sup>-4</sup>                          | 4.75 x 10 <sup>-14</sup>  |
| Water Solubility * (mg/L at 20°C) | 26500 at 37°C   | 583  | 2370  |
| pKa at 20°C                       | 9.6   | 3.2  | 4.15  |
| log Kow                           | 0.16  | 2.57   | 4.51  |

\* Benner et al., 2009

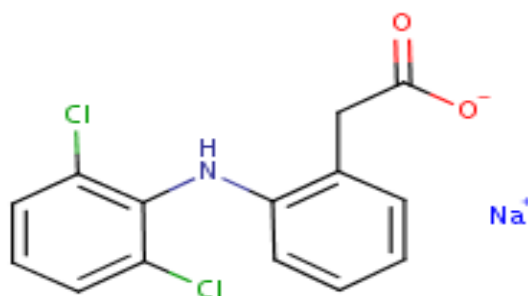


a) Atenolol (β-blocker)





b) Clofibric acid (Lipid regulators)



c) Diclofenac (Anti-inflammatory)

Figure 3.1. Chemical structures of target Pharmaceuticals (ChemIDplus, 2014)

## 3.2 Materials and Methods

### 3.2.1 Reagents and chemicals

Atenolol, (RS)-2-[4-[2-Hydroxy-3-(propan-2-ylamino)propoxy]phenyl]acetamide, Clofibric Acid, 2-(4-chlorophenoxy)-2-methylpropanoic acid and Diclofenac Sodium, 2-[2-(2,6-dichloroanilino) phenyl]acetic acid, Sodium Bromide,  $\geq 99.99\%$ , Humic Acid, Titanium Dioxide Degussa P25, hydrochloric acid, sodium hydroxide and nitrocellulose membrane filters (pore size  $0.22\mu\text{m}$  and diameter  $47\text{mm}$ ) were purchased

from Sigma Aldrich whereas AISI 316L Stainless Steel was purchased from McMaster Carr, USA. High purity water was produced with a Thermo Scientific Barnstead Nanopure system (Thermo Fisher Scientific, Waltham, MA, USA).

Table 3.2: Properties of TiO<sub>2</sub> powder as per manufacturer

| <b>Catalyst Properties</b>                      | <b>Degussa P25</b>    |
|---|-----------------------|
| <b>Density (20°C)</b>                           | 3.8 g/cm <sup>3</sup> |
| <b>Particle Size</b>                            | 20-25nm               |
| <b>BET surface area (m<sup>2</sup>/g)*</b>      | 50 ± 1                |
| <b>Langmuir Surface Area (m<sup>2</sup>/g)*</b> | 86.7949 ± 2           |
| <b>Crystal Form – Anatase</b>                   | 80%                   |
| <b>Rutile</b>                                   | 20%                   |

\* BET surface area is shown in appendix A.3

Exactly 10000 mg/L of individual stock solutions of ATN and CFA and 1000 mg/L of DCF target PPCPs were prepared in ultrapure water and stored at -20<sup>0</sup>C. A 10mg/L working solution was obtained by spiking a known aliquot of stock solution to 1L of secondary effluent. For another batch of experiments, 100mg/L of individual stock solutions of sodium bromide and natural organic matter were prepared with ultrapure water and stored at -20<sup>0</sup>C. A known aliquot from the stock solutions of sodium bromide and natural organic matter were spiked into 1L of secondary effluent to obtain a final concentration of 0.1 and 0.3ppm of bromine and a concentration of 4 and 8ppm of natural organic matter.

### 3.2.2 Raw water quality

On sample collection days, general monitoring data was recorded, including daily flow rates, retention time and chemical dosages. Temperature, pH and turbidity were also recorded for the water samples as well as free chlorine, combined chlorine and total chlorine concentrations of the treated water samples.

### 3.2.3 Sampling site and collection

Adelaide Wastewater Treatment Plant has an annual average flow of 24,780 cubic meters per day. In 2014, the daily average peak flow was 70,281 cubic meters per day. In 2013, the precipitation levels were observed to be at an average of 956 mm.

In 2014, the total sludge generated at Adelaide Wastewater Treatment Plant was 97,258 cubic metres. The thickened waste activated sludge contributed to 55,779 cubic metres whereas the primary sludge contribution was 41,479 cubic metres. This total sludge was incinerated at Greenway Pollution Control Centre.

Twenty liters (20 L) of grab samples of secondary effluent from secondary clarifier was collected from Adelaide Pollution Control Plant, London, ON, Canada. The samples were filtered through 0.22  $\mu\text{m}$  filters and collected in 1 L amber glass containers. The bottle was shaken to mix the contents and the samples were stored at 4°C until subjected to various advanced oxidation processes. The secondary effluent was analyzed for the selected PPCP compounds by LC-MS/MS and the results obtained showed that the effluent had no trace levels of these PPCP compounds collected from Adelaide Treatment Plant as shown in Appendix 17 and 18. All the reactions were conducted at pH 7.0 at room temperature (22°C) by adjusting the pH with 1N HCl.

### 3.2.4 Homogeneous Immobilized TiO<sub>2</sub> catalyst preparation on Stainless Steel mesh using Dip-Coat method

A comparison among photocatalysts such as Degussa P25, Aldrich rutile, Hombikat UV100 and Millennium PC500 showed that the photocatalytic activity in oxidizing ATN and its intermediate products by Degussa P25 was the highest (Ioannou, et al., 2011). Based on its highest photocatalytic activity, a 2%, 4% and 20% of Degussa P25 TiO<sub>2</sub> were prepared in pure water by weighing a known amount of TiO<sub>2</sub> into a 500mL Erlenmeyer flask. The solutions were shaken vigorously for 2 hours using a magnetic stirrer. A dimension of 10 x 10 cm of AISI 316L stainless steel wire mesh were used as substrates with openings of 3 mm x 3 mm by dipping the plates with 2%, 4% and 20% of TiO<sub>2</sub> solution by a process of dip-coat method. The plates were immersed in the solution following each coating and withdrawn at a speed of 6 cm/min to avoid cracking. The coated plates were dried at 100°C in an oven.

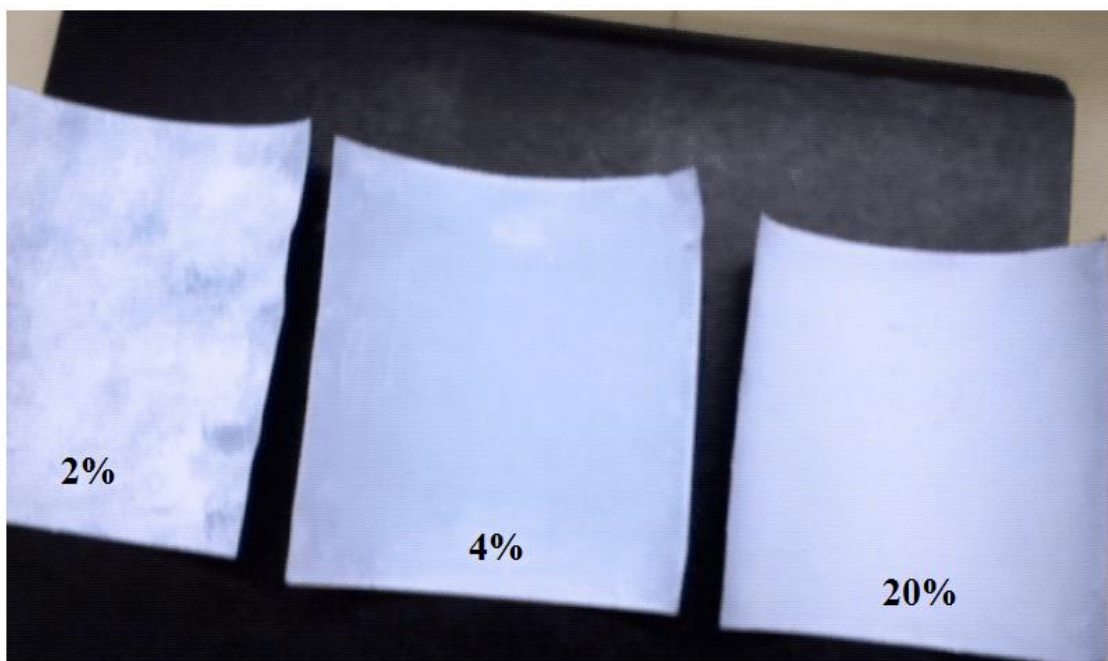


Figure 3.2. Dip coatings of homogeneous immobilized 2%, 4% and 20% of Degussa P25 TiO<sub>2</sub> supported on SS plates

Dipping and drying were continued until the coatings weight was approximately  $0.75\text{g/m}^2$ ,  $1.0\text{g/m}^2$  and  $1.25\text{g/m}^2$  respectively. Over 20 dipping and drying cycles were performed on each stainless steel mesh and took longer time for 2% and 4% of coating weights of  $0.75\text{g/m}^2$  and  $1.0\text{g/m}^2$  while around 10 cycles were enough with 20% of  $\text{TiO}_2$  to get a coating of  $1.25\text{g/m}^2$ . The obtained films were annealed by raising the temperature slowly from room temperature to  $500^\circ\text{C}$  at a rate of approximately  $1^\circ\text{C}/\text{min}$  in a muffle furnace and kept for 1 hour after reaching the set temperature. The obtained films were allowed to cool to room temperature gradually as shown in Figure 3.2.

### 3.2.5 Characterization of Immobilized $\text{TiO}_2$ Catalyst

The homogeneous immobilized  $\text{TiO}_2$  films were characterized for SEM and EDX after scrapping of some particles from the surface of coatings. A comparison between before and after calcination is made.

For the high magnification SEM imaging of the samples, small portions of the dried and calcined films of  $\text{TiO}_2$  samples were placed in clean glass vials containing acetone and sonicated to disperse the particles. A small drop of the samples along with acetone was placed on clean silicon wafers and the acetone was allowed to evaporate in air. Once dried, the samples were platinum coated to alleviate charging and analyzed by scanning electron microscopy coupled with energy dispersive X-ray (SEM/EDX) spectroscopy using the upper detector on Hitachi S-4500 Field Emission SEM equipped with a Quartz PCI XOne SSD X-ray Analyzer at an accelerating voltage of 10kV. The obtained images are shown in Figures 3.3 and 3.5. The EDX analysis of the dried and calcined films was analyzed similarly and the obtained spectra are shown in figures 3.4 and 3.6.

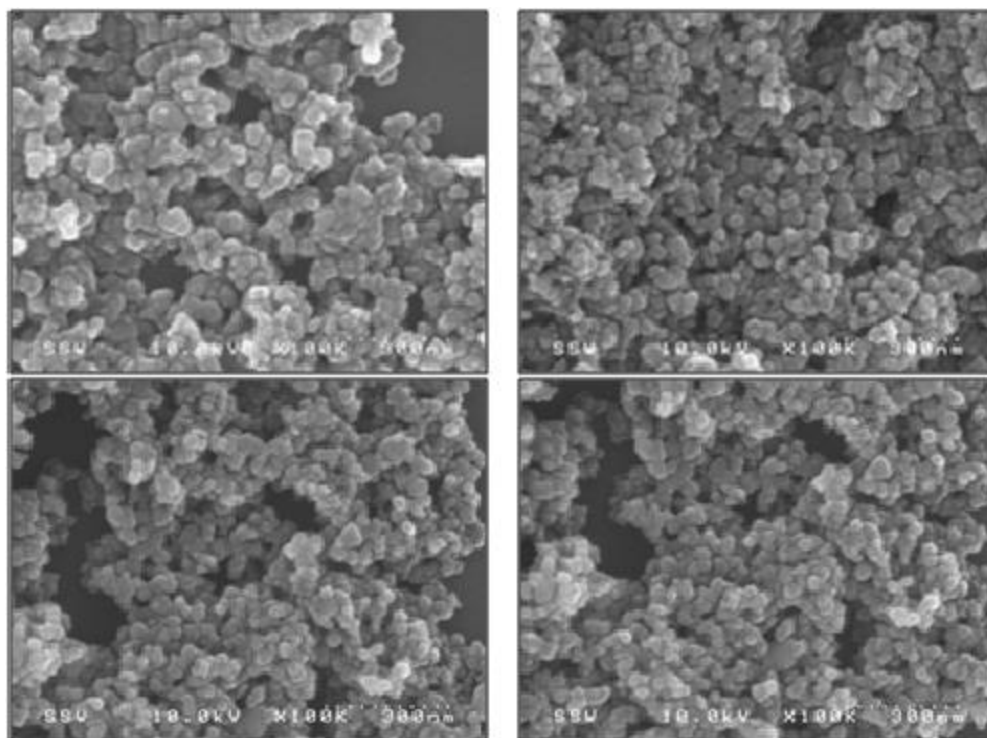


Figure 3.3. SEM image of dried film at 10kV

The morphologies of the coatings were investigated by use of SEM analysis. Figure 3.3 shows that immobilized  $\text{TiO}_2$  stainless steel mesh dried at  $100^\circ\text{C}$  has particles that are closely located which indicates that there exists a built up of P25 between them.

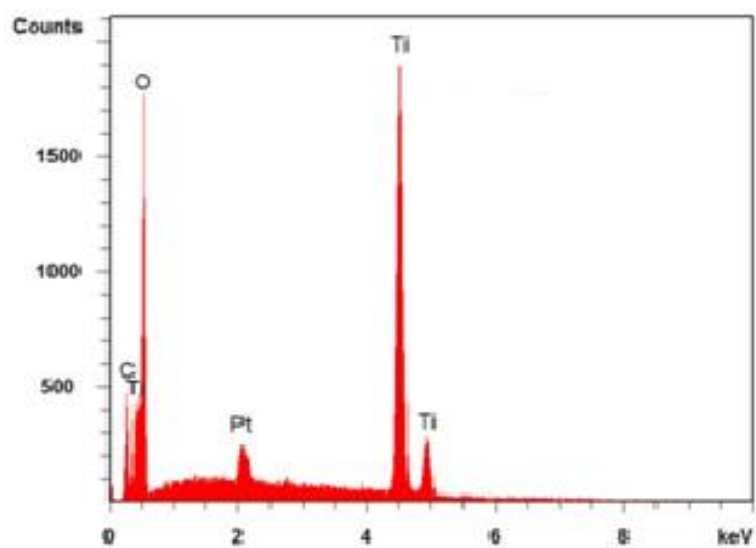


Figure 3.4. EDX spectroscopy of dried film at 10kV

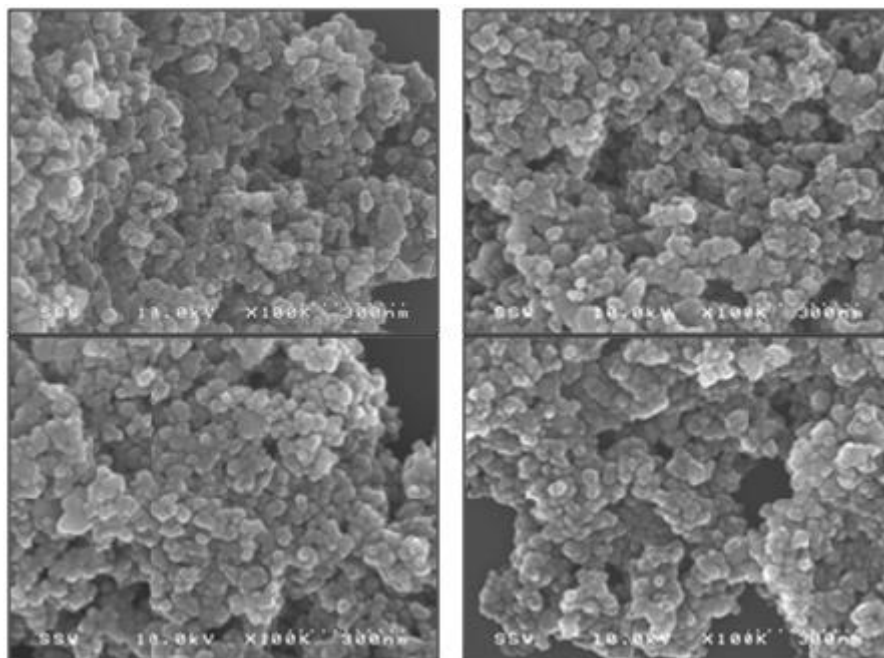


Figure 3.5. SEM image of calcined TiO<sub>2</sub> film at 10kV

After calcination of TiO<sub>2</sub> stainless steel mesh as can be seen in Figure 3.5, the particles had smooth surface with even distribution of aggregates.

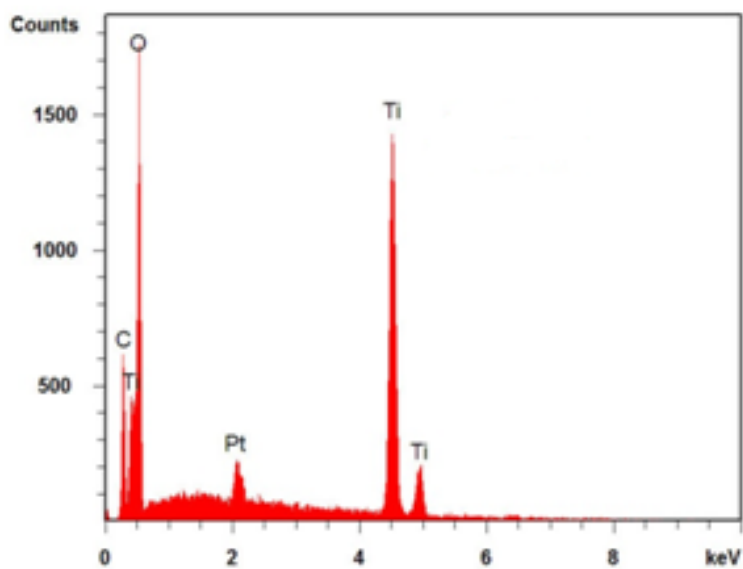


Figure 3.6 EDX spectroscopy of calcined TiO<sub>2</sub> film at 10kV

As can be seen from Figures 3.4 and 3.6, the EDX images shows the composition of before and after calcination with slight variation in the peaks due to changes that took place after calcining at 500°C.

Table 3.3: Semi-quantitative EDX Results for TiO<sub>2</sub>

| <b>EDX Results, in weight %</b> | <b>C</b> | <b>O</b> | <b>Ti</b> |
|---------------------------------|----------|----------|-----------|
| <b>Dried film</b>               | 5.5      | 34.3     | 60.3      |
| <b>Calcined film</b>            | 8.7      | 38.2     | 53.1      |

The weight percentage of carbon, oxygen and Titanium changed slightly between dried film and the calcined film and the results are shown in Table 3.3.

### 3.2.6 Experimental protocol

#### 3.2.6.1 Experiments conducted with wastewater samples

The water quality parameters of the secondary effluent that were characterized as per standard methods of APHA, 2004 are shown in Table 3.4. Orion pH meter was used to measure the pH and temperature, HACH Turbidimeter was used to measure Turbidity, Shimadzu TOC-V<sub>CPN</sub> analyzer with an ANSI-V auto sampler was used to measure total organic carbon (TOC) while nitrate and phosphate were measured using Dionex Ion Chromatograph ICS 3000. Hach reactor was used to measure chemical oxygen demand and ammonia by using HACH vials. Total suspended solids and total dissolved solids were measured by gravimetric method whereas BOD was measured during 5 days of incubation at 20°C.



Table 3.4: Water quality parameters of secondary effluent

| <b>Parameters</b>                            | <b>Results, mg/L</b> |
|--|----------------------|
| <b>pH</b>                                    | 7.3 ± 0.2            |
| <b>Temperature, °C</b>                       | 19 ± 1               |
| <b>Turbidity, NTU</b>                        | 11.5                 |
| <b>Total Suspended Solids (TSS)</b>          | 25.9                 |
| <b>Total Dissolved Solids (TDS)</b>          | 384                  |
| <b>Chemical Oxygen Demand (COD)</b>          | 39                   |
| <b>Biochemical Oxygen Demand (BOD)</b>       | 14                   |
| <b>Total Organic Carbon (TOC)</b>            | 10.8                 |
| <b>Ammonia</b>                               | 2.7                  |
| <b>Nitrate as NO<sub>3</sub><sup>-</sup></b> | 20.6                 |
| <b>Phosphorus</b>                            | 0.82                 |

Note: All the above values are reported in mg/L except pH, Temperature and Turbidity

### 3.2.6.2 Reactor setup

A bench scale annular reactor of 1.5 L capacity was used to conduct the AOP experiments as shown in Figure 3.7. Prior to starting the reaction, 1 L of wastewater was allowed to achieve thermal equilibrium by maintaining it at a constant temperature of 23 ± 1°C with continuous stirring by a magnetic stirrer and using stir bars to complete mixing. Once the sample reached to room temperature, the immobilized TiO<sub>2</sub>

on stainless steel mesh was suspended into the reactor before irradiation for 15 min in dark to reach adsorption-desorption equilibrium. A known aliquot of the stock solution was also brought to room temperature to spike a known concentration of the individual stock solution.

The reaction volume was kept at 1 L in all experiments and the temperature of the reaction vessel was kept constant by circulating cooling water at 20°C. The initial pH of the sample was measured to be 7.3. The pH of the secondary effluent was adjusted to 7, 8 and 9 using 0.1N hydrochloric acid or 0.1N sodium hydroxide to study the variation of pH effect on degradation of Atenolol while pH 7 was maintained for all the other studies.

Ozone was produced by an ozone generator (model TG-40, Ozone Solutions, Hull, Iowa, US) with compressed air tank fed oxygen (99.8% purity) to the generator at a pressure of 15 psi. 2 mg/L of ozone produced was measured by ozone analyzer (model UV-100, Eco Sensors, Newark, California, USA). Ozone feeding into the reactor was maintained at 1.2 LPM.

A low pressure Hg lamp of 13 W with monochromatic light at 254 nm and surrounded by a quartz protective sleeve (model Philips TUV PL-S, 1000 Bulbs.com, Texas, US) was used as the light source. The UV lamp was turned on at least 15min prior to start of the experiment for stabilization.

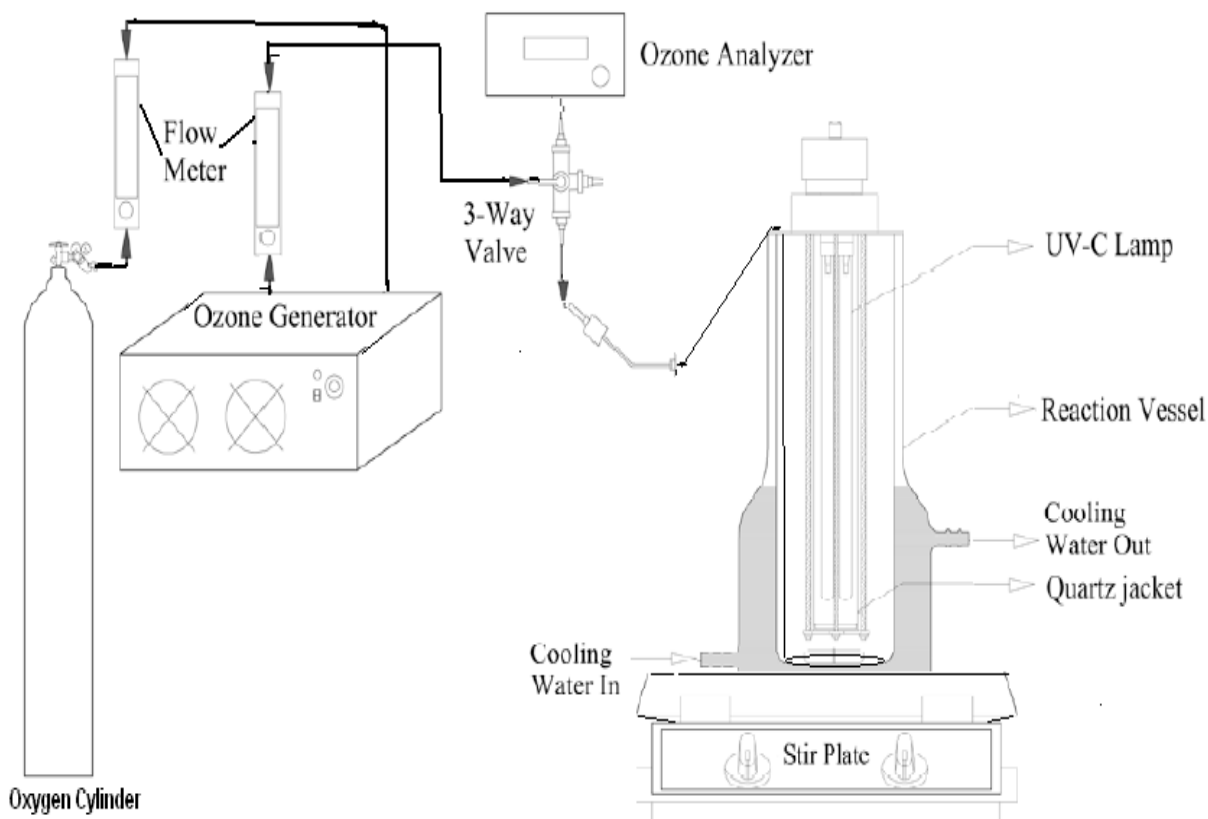


Figure 3.7. Experimental Reactor Setup for AOP

Exactly 1mL of stock standard of target PPCP compound was spiked into the 1L reactor and stirred for few minutes before the reactor was subjected to AOP treatment technologies such as UV. 10mL of sample was withdrawn immediately at intervals of 0, 5, 15, 30, 60 and 90 min.

Similarly other experiments were conducted using  $O_3$ , UV/ $O_3$ , UV/ $TiO_2$ ,  $O_3$ / $TiO_2$  and  $O_3$ /UV/ $TiO_2$  by following the same procedure as above on secondary effluent. Several batch experiments were conducted by spiking the secondary effluent with 0.1ppm and 0.3ppm of bromine (Br) from a stock solution of 100ppm of bromide prepared by using sodium bromide, 4ppm and 8ppm of Natural Organic Matter (NOM) and finally suspending  $0.75g/m^2$ ,  $1g/m^2$  and  $1.25g/m^2$  of immobilized  $TiO_2$  into the reactor and subjected to UV/ $TiO_2$ ,  $O_3$ / $TiO_2$  and  $O_3$ /UV/ $TiO_2$ .

Another set of experiments were also conducted to study the effect of pH on the Atenolol removal in wastewater. As soon as the AOP reaction was started, 10mL of sample was withdrawn at regular intervals of 0, 5, 15, 30, 60 and 90 minutes respectively into amber glass vials, spiked with 2-3 drops of sodium thiosulfate and stored under  $-20^{\circ}\text{C}$  for further LC-MS/MS (Liquid Chromatography Coupled with Triple Quadrupole Mass Spectrometer) analysis to detect the degradation and transformation products of atenolol, clofibric acid and diclofenac from secondary effluent samples after AOP treatment.

### 3.3 PPCP method setup by LC-MS/MS (High Resolution)

Most recent studies in environmental waters on acidic herbicides and their degradation products has garnered attention on the use of high flow pneumatically assisted atmospheric pressure chemical ionization (APCI) and electrospray ionization (ESI) interfaces as the best choices among other LC-MS interfaces (Crescenzi et al., 1995, Otsuka et al., 1998 and Puig et al., 1997). Both ESI and APCI produce positive or negative ions when polar substances are introduced through a needle into the stream of HPLC eluent. Application of high electric fields to the needle promotes ionization in the case of ESI. With the aid of a nebulizer gas, a spray of charged droplets that are formed from the liquid phase shrinks as the solvent evaporates due to vaporizer gas thus increases the repulsion forces between the charged ions. Due to high repulsion forces or explosion of droplets, they become unstable and dissociate further into smaller droplets resulting in separation of ions from the surface after several repeated cycles thus forming gas phase ions.

A capillary orifice separates the spray chamber from the vacuum region of the mass spectrometer. In presence of curtain gas, the precursor ions entering into  $Q_0$  region via the capillary orifice are responsible for declustering of ions and protecting curtain plate from striking by these ions. A declustering potential aids in inducing and controlling fragmentation and accumulates the ions enhancing their concentration at  $Q_0$  region before entering the  $Q_1$  region. The ions from  $Q_1$  region are introduced further to

collision cell a Q2 region where further fragmentation takes place to produce characteristic product or fragment ions by a collision or inert gas. The collision energy and the pressure of the collision gas are directly proportional to the degree of fragmentation. The product ions enter Q3 region after fragmentation where trapping of ions by linear ion trap (LIT) is used to enhance sensitivity before scanning by mass spectrometer (Mohamad, A., 2010).

Some of the factors that were optimized which affect the higher separation efficiency, sensitivity, selectivity, specificity and reproducibility was improved by choosing proper flow rate, column selection, pH of the mobile phase, electrolyte in the buffer, exit voltage and selection of ionization source technique for determination of PPCPs by Agilent 6460 LC-MS/MS (Liquid Chromatography Triple Quadrupole Mass Spectrometer) in wastewater.

The analytical methodology of LC-MS/MS (Figure 3.8) has been used in the present study as a powerful technique for identification and structural elucidation of PPCPs in secondary effluent before and after AOP treatment. The main advantage of LC-MS/MS is its high sensitivity and selectivity. Using of narrow bore columns produced less matrix effects and higher separation efficiency and sensitivity. In stationary phase of the column, retention is based on the VanderWaals interaction with hydrophobic components. Similarly acetonitrile was used as mobile phase for the PPCP compounds for the chromatographic separation because of its relatively high vapor pressure and low viscosity. Matrix effects are greatly reduced by using electrospray ionization (ESI) as the choice of interface. Also using a T-connection at the post-column reduces the flow rate thus reducing matrix effects that is delivered to the ESI interface. Specificity of the analyses was increased by increasing the exit voltage of the capillary interface in the electrospray ion source to produce fragment ions, Cahill et al., (2004).

The main components of LC-MS/MS comprises of HPLC (Agilent 1290), Ion Source, Mass Analyzer (6460) and Detector with HiP Sampler (G4226A), Binary Pump (G4220A) and Column Comp. (G1316C).

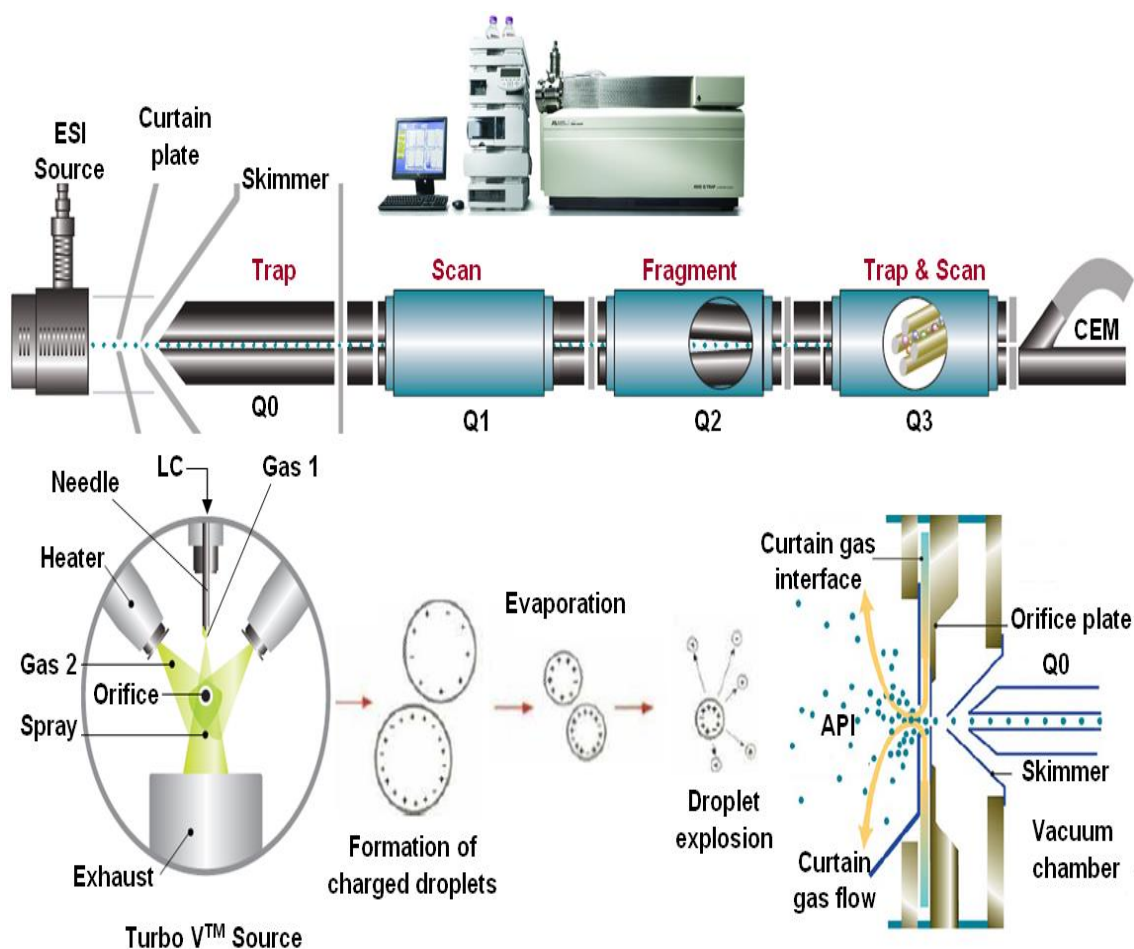


Figure 3.8. Mechanism of ion formation in Turbo V™ ESI ion source equipped with QTRAP before entering LC-MS/MS region (Mohamad, A., 2010 and AB Sciex, Ontario, Canada)

LC instrumental conditions for acidic and basic compounds, ESI+ and ESI-

Auto sampler: Injection volume 5  $\mu$ L

Column: Poroshell 120 EC- C18 (3.0 x 150 mm, 2.7 $\mu$ m)

Mobile phase: A (10mM ammonium formate and 0.1% formic acid in water) and  
B (0.1% formic acid in acetonitrile)

Flow Rate: 0.35 mL/min

Run Time: 5 min

Table 3.5: Gradient program for LC-MS/MS

| <b>S. No.</b> | <b>Time (min)</b> | <b>% Composition of mobile phase A</b> | <b>% Composition of mobile phase B</b> |
|---------------|-------------------|--|--|
| <b>1</b>      | 0.0               | 90                                     | 10                                     |
| <b>2</b>      | 1.0               | 90                                     | 10                                     |
| <b>3</b>      | 2.0               | 10                                     | 90                                     |
| <b>4</b>      | 3.0               | 10                                     | 90                                     |
| <b>5</b>      | 4.0               | 90                                     | 10                                     |
| <b>6</b>      | 5.0               | 90                                     | 10                                     |

Table 3.6: Source parameters for LC-MS/MS

| <b>Parameter</b>               | <b>Value (+)</b>                 | <b>Value (-)</b> |
|--------------------------------|----------------------------------|------------------|
| <b>Gas Temp (°C)</b>           | 250                              | 250              |
| <b>Gas Flow (l/min)</b>        | 10                               | 10               |
| <b>Nebulizer (psi)</b>         | 30                               | 30               |
| <b>Sheath Gas Heater</b>       | 350                              | 350              |
| <b>Sheath Gas flow (L/min)</b> | 11                               | 11               |
| <b>Capillary (V)</b>           | 3500                             | 3000             |
| <b>VCharging</b>               | 0                                | 0                |
| <b>MRM</b>                     | 2 transitions for every compound |                  |

Table 3.7: Multiple Reaction Monitoring parameters for LC-MS/MS

| <b>Compound Name</b>   | <b>Precursor Ion</b> | <b>Product Ion</b> | <b>Dwell (ms)</b> | <b>Fragmentor Voltage (V)</b> | <b>Collision Energy (V)</b> | <b>Cell Accelerator Voltage</b> | <b>Polarity</b> |
|------------------------|----------------------|--------------------|-------------------|-------------------------------|-----------------------------|---------------------------------|-----------------|
| <b>Atenolol-1</b>      | 267.2                | 145                | 200               | 100                           | 20                          | 7                               | Positive        |
| <b>Atenolol-2</b>      | 267.2                | 190                | 200               | 100                           | 10                          | 7                               | Positive        |
| <b>Clofibric Acid-</b> | 213                  | 127                | 100               | 60                            | 10                          | 7                               | Negative        |
| <b>Clofibric Acid-</b> | 213                  | 85.2               | 100               | 60                            | 5                           | 7                               | Negative        |
| <b>Diclofenac-1</b>    | 293.9                | 249.9              | 100               | 60                            | 5                           | 7                               | Negative        |
| <b>Diclofenac-2</b>    | 293.9                | 214.1              | 100               | 60                            | 10                          | 7                               | Negative        |

Apart from the above set conditions, some of the optimized parameters are summarized and shown as Table 3.5 for gradient program of mobile phase A and B, Table 3.6 for source parameters and Table 3.7 for multiple reaction monitoring (MRM) parameters that were used for LC-MS/MS.

Computer based software, Mass Hunter Version B.05.01, was used to process the data by peak area method for the acquired chromatograms. The concentration of the unknown is calculated from the following equation using regression analysis of calibration standard.

$$y = mx + c$$

Where, x = concentration of analyte

m = slope of calibration curve

y = peak area of analyte

c = y-axis intercept of the calibration curve



### 3.4 PPCP analysis in wastewater samples

Secondary effluent samples were analyzed for selected PPCPs by LC-MS/MS without any extraction procedure. The performance of the LC-MS/MS method was evaluated for method detection limit (MDL), relative standard deviation (RSD) and percent recovery. By using linear regression, a five-point calibration curve was developed for each compound ranging from 0 to 200ng/mL.  $R^2$  values had linearity range between 0.99 – 0.999 for all the compounds with RSD values lower than 10%. Percent recoveries ranged from 90 to 100 % for the effluent matrix. The Milli-Q water had MDLs of 0.5ug/L for atenolol and clofibric acid and 2ug/L for diclofenac respectively whereas effluent samples had MDLs of 2ug/L for atenolol and clofibric acid and 5ug/L for diclofenac respectively. The concentration of the unknown is calculated by using regression analysis of calibration standard.

Performance of water matrix was evaluated by calculating the recovery of spiked samples by using

$$\% \text{ Recovery} = \frac{(\text{Concentration of Spiked Sample} - \text{Concentration in Sample})}{\text{Concentration of Spiked Value}} \times 100$$

### 3.5 Results and Discussion

All the experiments are conducted in triplicate and the values reported are the average values as shown in figures. Degradation rates for the target compounds ATN, CFA and DCF were examined by varying the effect of  $\text{TiO}_2$  loadings, comparison of various AOPs, effect of pH on ATN removal, and in the presence of NOM and Br at varying concentrations. Some of the degradation products were also elucidated by LC-MS/MS for ATN, CFA and DCF.

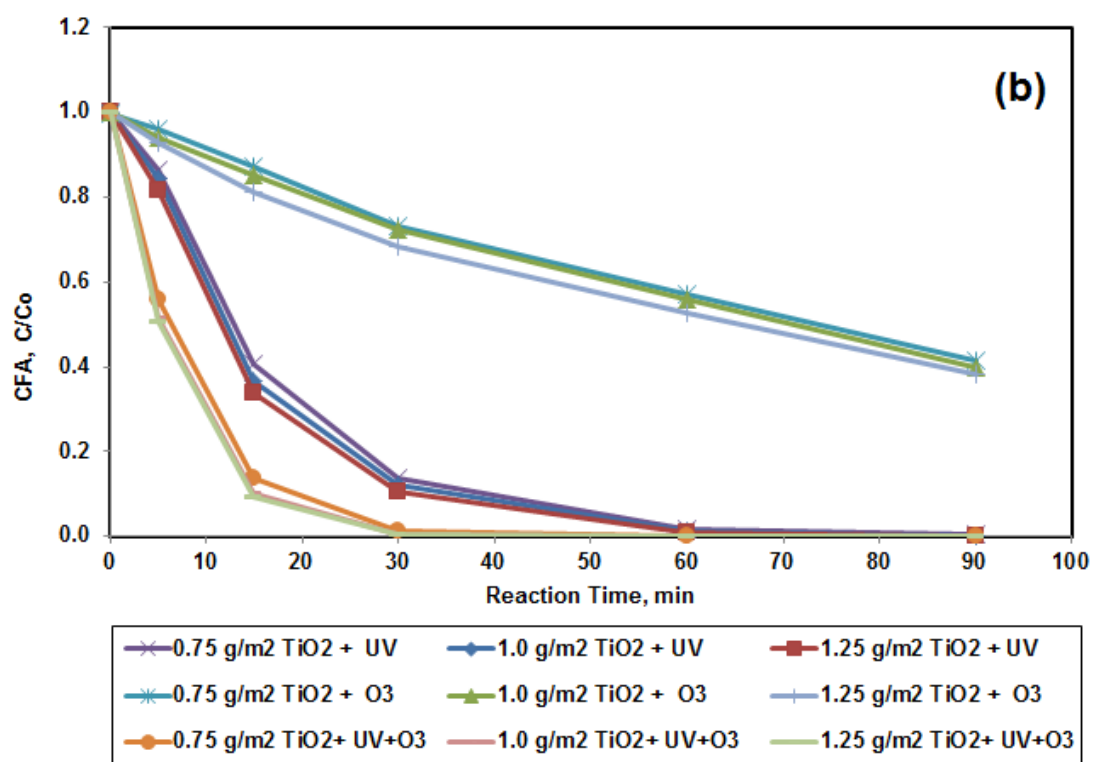
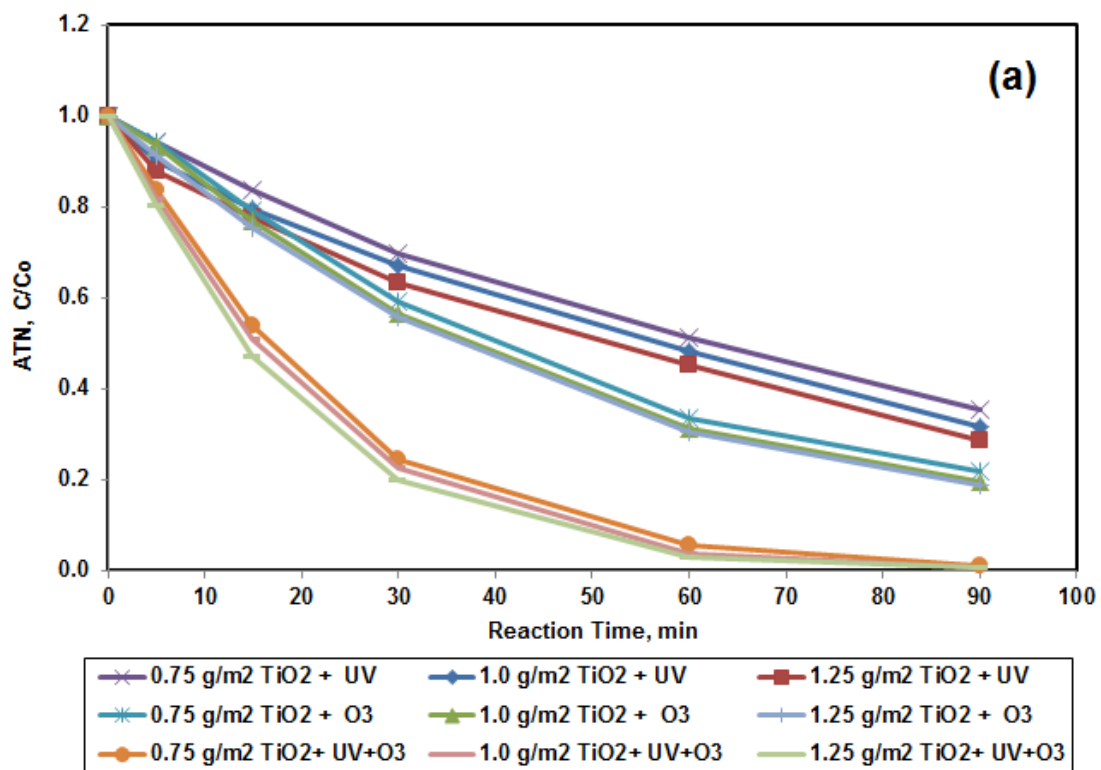
### 3.5.1 Effect of TiO<sub>2</sub> loading

The structural and surface properties of TiO<sub>2</sub> semiconductor depends on several factors that are responsible for the photocatalytic activity such as surface area, porosity, crystal composition, surface hydroxyl density, particle size distribution and band gap (Ryu and Choi, 2008; Haque et al., 2006). Some of the catalyst properties are shown in Table 3.2.

Based on several studies in the past, the photocatalytic activity of Degussa P25 was found to be substantially more active because of slower electron/hole recombination that takes place on the surface (Martin et al., 1994; Emilio et. al., 2006) and also as its structure contains a mixture of both anatase and rutile compared to other individual pure crystalline phases of TiO<sub>2</sub> photocatalysts (Bickley et al., 1991). The rutile disperses into the matrix of anatase thus showing higher photocatalytic activity due to electronic interactions between the two phases (Haque et al., 2006).

The increased activity of anatase over rutile is due to its larger surface areas particularly due to slow electron/hole recombination where the rates of electron transfer amongst reactants, electrons and holes increase with increase in surface areas (Kaneko and Okura, 2002). Presence of higher density of superficial hydroxyl groups in anatase shows increased aptitude to photo adsorb oxygen and also attributed to various positions of the conduction band (Sclafani and Herrmann, 1996; Chatzisyneon et al., 2008).

Initial screening experiments were performed on 0.75g/m<sup>2</sup>, 1.0 g/m<sup>2</sup> and 1.25 g/m<sup>2</sup> of immobilized TiO<sub>2</sub> calcined on stainless steel mesh to assess the photocatalytic activity of ATN, CFA and DCF at an initial concentration, Co of 10mg/L each. Figure 3.9 shows the removal efficiency of all the three PPCPs at different loadings subjected to UV/TiO<sub>2</sub>, O<sub>3</sub>/TiO<sub>2</sub> and O<sub>3</sub>/UV/TiO<sub>2</sub> at pH 7.



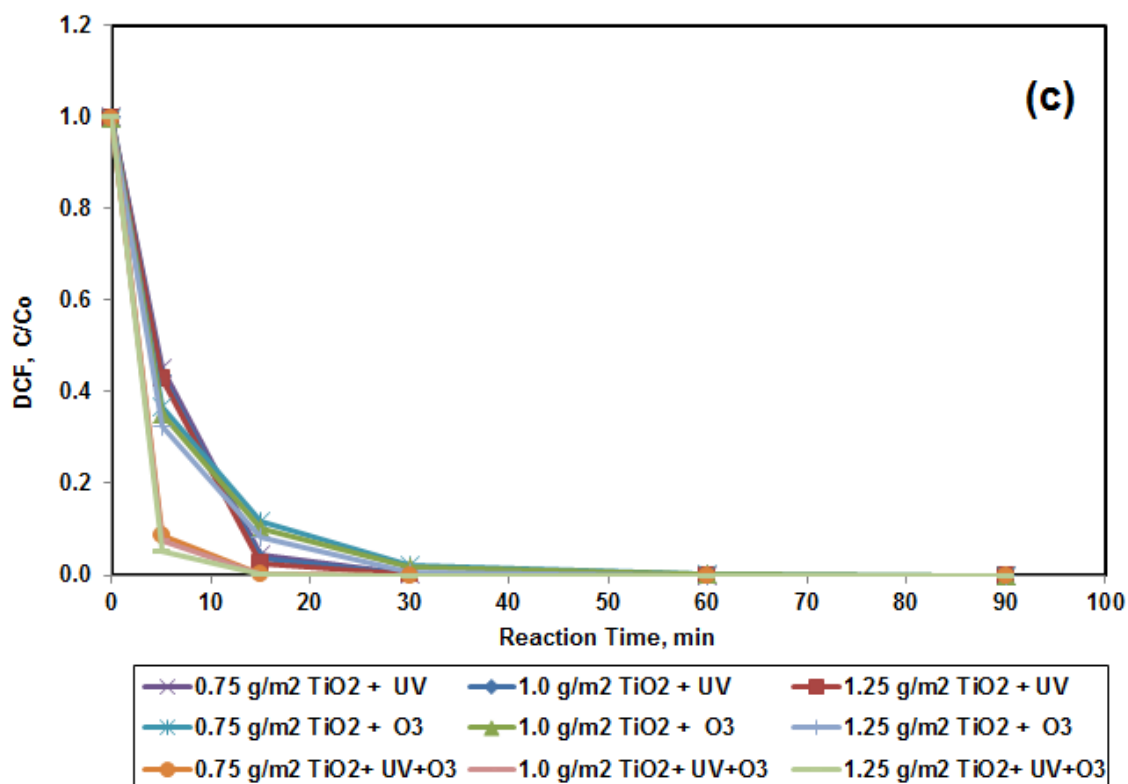


Figure 3.9. Effect of catalyst loading on SE (a) ATN (b) CFA and (c) DCF [ $C_0 = 10\text{mg/L}$  each,  $O_3 = 2\text{ppm}$ ,  $UV = 13\text{W}$ ,  $pH = 7.0$ ,  $T = 23 \pm 1^\circ\text{C}$ ]

Initial screening experiments were performed on  $0.75\text{g/m}^2$ ,  $1.0\text{g/m}^2$  and  $1.25\text{g/m}^2$  of immobilized  $\text{TiO}_2$  calcined on stainless steel mesh to assess the photocatalytic activity of ATN, CFA and DCF at an initial concentration,  $C_0$  of  $10\text{mg/L}$  each. Figure 3.9 shows the removal efficiency of all the three PPCPs at different loadings subjected to  $UV/\text{TiO}_2$ ,  $O_3/\text{TiO}_2$  and  $O_3/UV/\text{TiO}_2$  at  $pH 7$ . Table 3.8 and 3.9 provides the  $k$  values for various  $\text{TiO}_2$  loadings. It was observed that as the catalyst loadings increased from  $0.75\text{g/m}^2$  to  $1.25\text{g/m}^2$ , the removal efficiency increased with least  $k$  values observed for ATN followed by CFA and the highest for DCF and followed the order  $DCF > CFA > ATN$ . Further  $k$  values depended on type of AOP applied and followed the order  $O_3/UV/\text{TiO}_2 > O_3/\text{TiO}_2 > UV/\text{TiO}_2$  for ATN whereas  $k$  values for CFA and DCF followed the trend in the order  $O_3/UV/\text{TiO}_2 > UV/\text{TiO}_2 > O_3/\text{TiO}_2$ . It was also observed that as the  $\text{TiO}_2$  loadings increased, the removal efficiency of ATN, CFA and DCF

increased more between  $0.75\text{g/m}^2$  and  $1.0\text{g/m}^2$  when compared to  $1.0\text{g/m}^2$  and  $1.25\text{g/m}^2$ . Based on these studies, the effect of AOP was performed using  $1.0\text{g/m}^2$   $\text{TiO}_2$  catalyst with 20% coatings.

Table 3.8: Effect of  $\text{TiO}_2$  loadings of ATN, CFA and DCF in SE [rate constant  $k$  and correlation coefficient  $R^2$ ,  $\text{Co} = 10\text{mg/L}$ ,  $\text{UV} = 13\text{W}$ ,  $\text{O}_3 = 2\text{mg/L}$ ,  $\text{pH} = 7$ ,  $T = 23 \pm 1^\circ\text{C}$ ]

| <b><math>0.75\text{ g/m}^2\text{ TiO}_2</math></b>    |   |                         |   |                         |   |                         |
|---|---|-------------------------|---|-------------------------|---|-------------------------|
| <b>PPCP</b>   | <b>ATN</b>  |                         | <b>CFA</b>  |                         | <b>DCF</b>  |                         |
| <b>AOP</b>  | <b><math>k</math> in <math>\text{min}^{-1}</math></b> | <b><math>R^2</math></b> | <b><math>k</math> in <math>\text{min}^{-1}</math></b> | <b><math>R^2</math></b> | <b><math>k</math> in <math>\text{min}^{-1}</math></b> | <b><math>R^2</math></b> |
| <b>UV/<math>\text{TiO}_2</math></b>                   | 0.0115  | 0.999                   | 0.0652  | 0.9974                  | 0.2018  | 0.9973                  |
| <b><math>\text{O}_3/\text{TiO}_2</math></b>           | 0.0173  | 0.9969                  | 0.0097  | 0.9983                  | 0.1278  | 0.9944                  |
| <b><math>\text{O}_3/\text{UV}/\text{TiO}_2</math></b> | 0.0503  | 0.9967                  | 0.1461  | 0.9933                  | 0.4493  | 0.9983                  |
| <b><math>1.25\text{ g/m}^2\text{ TiO}_2</math></b>    |   |                         |   |                         |   |                         |
| <b>UV/<math>\text{TiO}_2</math></b>                   | 0.0139  | 0.9925                  | 0.0774  | 0.9982                  | 0.2246  | 0.9942                  |
| <b><math>\text{O}_3/\text{TiO}_2</math></b>           | 0.019   | 0.9984                  | 0.0109  | 0.9913                  | 0.1656  | 0.9929                  |
| <b><math>\text{O}_3/\text{UV}/\text{TiO}_2</math></b> | 0.0578  | 0.9982                  | 0.1774  | 0.992                   | 0.5113  | 0.9926                  |

The surface of  $\text{TiO}_2$  gets hydroxylated readily when it is in contact with water. In presence of UV, electron-hole pairs in the semiconductor are formed. Formation of  $\bullet\text{OH}$  is thermodynamically favoured when hydroxylated  $\text{TiO}_2$  oxidation potential lies above the semiconductor valence band forming holes due to the oxidation of surface-bound  $\text{OH}^-$  and  $\text{H}_2\text{O}$  (Turchi et al., 1990).

Thus immobilized TiO<sub>2</sub> favors removal of PPCPs from secondary effluent as it is easy to dispose of water without filtration after treatment unlike TiO<sub>2</sub> suspension in water where increase of loadings have negative effect due to obstruction of UV light and requires filtration before disposal.

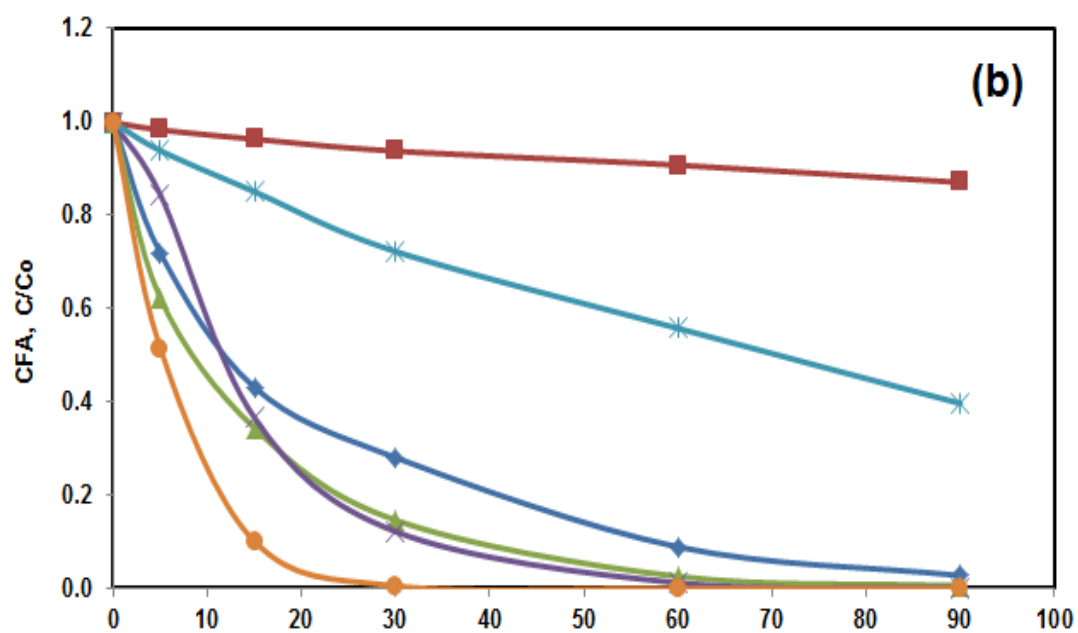
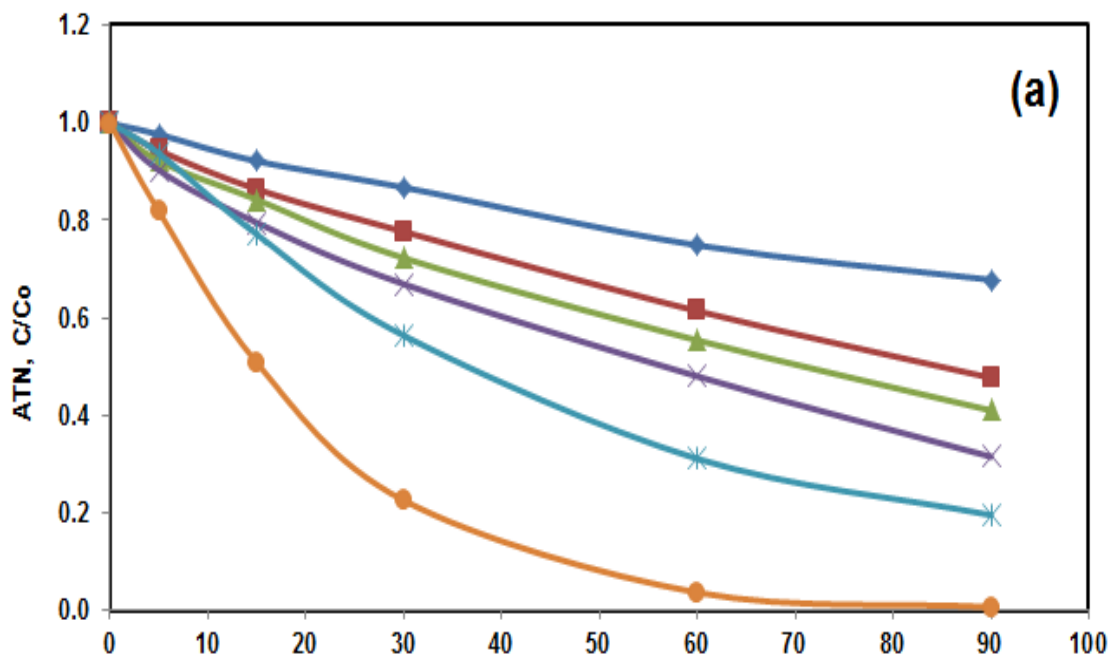
### 3.5.2 Effect of AOP

Various AOP treatments such as O<sub>3</sub>, UV, UV/O<sub>3</sub>, UV/TiO<sub>2</sub>, O<sub>3</sub>/TiO<sub>2</sub> and O<sub>3</sub>/UV/TiO<sub>2</sub>, were conducted to degrade atenolol, clofibric acid and diclofenac in secondary effluent. A comparison of the various removal rates and AOP techniques used are shown in Table 3.9.

For ATN oxidation, UV showed the least efficiency whereas for CFA oxidation, O<sub>3</sub> showed the least efficiency and for DCF, UV/O<sub>3</sub> showed the least efficiency while O<sub>3</sub>/UV/TiO<sub>2</sub> showed the maximum efficiency for all the three compounds. Among the 3 compounds at pH 7, diclofenac showed the fastest degradation rates and the least by atenolol and follows the order diclofenac > clofibric acid > atenolol. Among these six AOPs, O<sub>3</sub>/UV/TiO<sub>2</sub> showed better photocatalytic ozonation compared to other AOPs as it generates large number of .OH and acts as a promising oxidation method for refractory organic compounds (Agustina, et al., 2005; Beltran, et al., 2005; Li, et al., 2005; Farre, et al., 2005).

There was significant effect of the concentration of TiO<sub>2</sub> on kinetics which confirms a positive influence on the increased number of active sites on TiO<sub>2</sub>. Using O<sub>3</sub>/TiO<sub>2</sub>, the degradation of ATN was faster compared to UV/TiO<sub>2</sub>, UV/O<sub>3</sub>, UV and O<sub>3</sub> while the efficiency decreased by almost 20% for CFA. Whereas the photocatalytic activity of UV/TiO<sub>2</sub> was faster for CFA compared to ATN because as per literature, a slow electron/hole recombination rate takes place for P25 which promotes charge pair separation inhibiting recombination due to rutile/anatase combination. Suppose to this electron/hole pairs formation, if a slow adsorption/desorption of PPCPs is compared, then electron/hole pairs will have longer lifetimes and P25 is considered the best photocatalyst for ATN. While a reverse trend can also be followed for PPCPs, where

adsorption/desorption is faster and electron and hole recombination is prevented due to the reactions of holes with adsorbed pollutants and reaction of electrons with suitable electron acceptors.



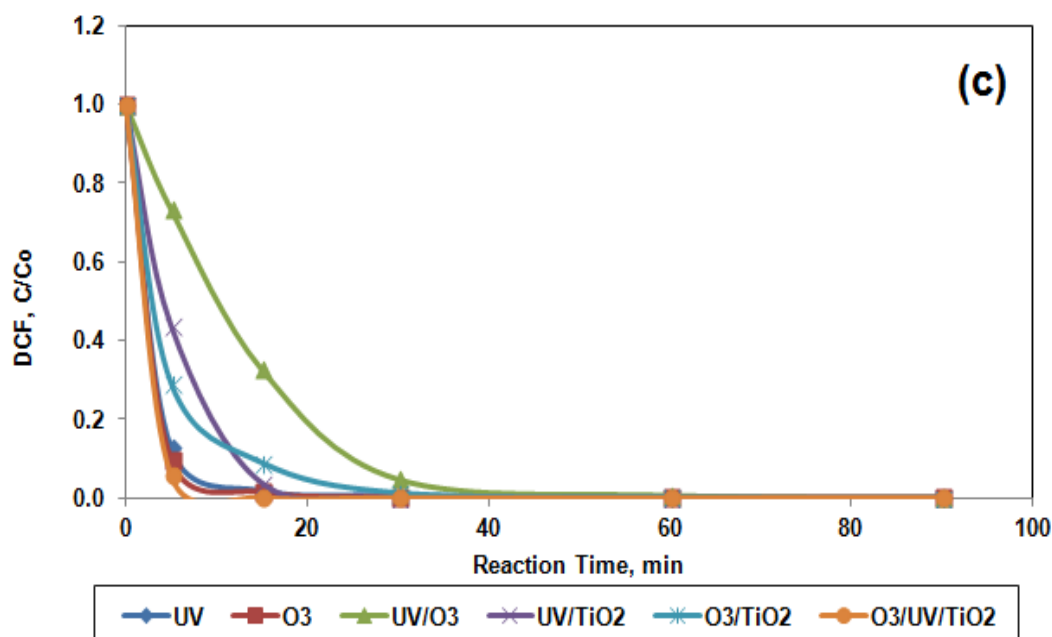


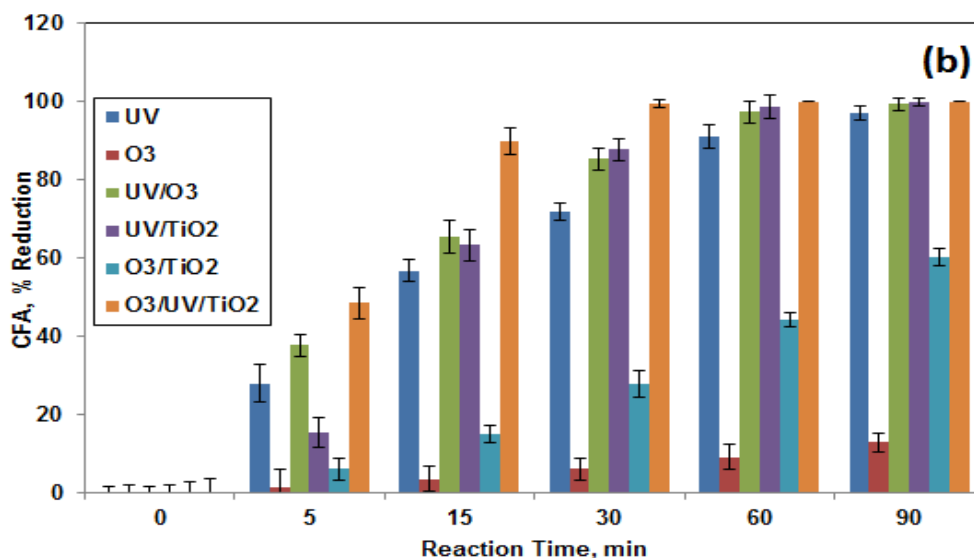
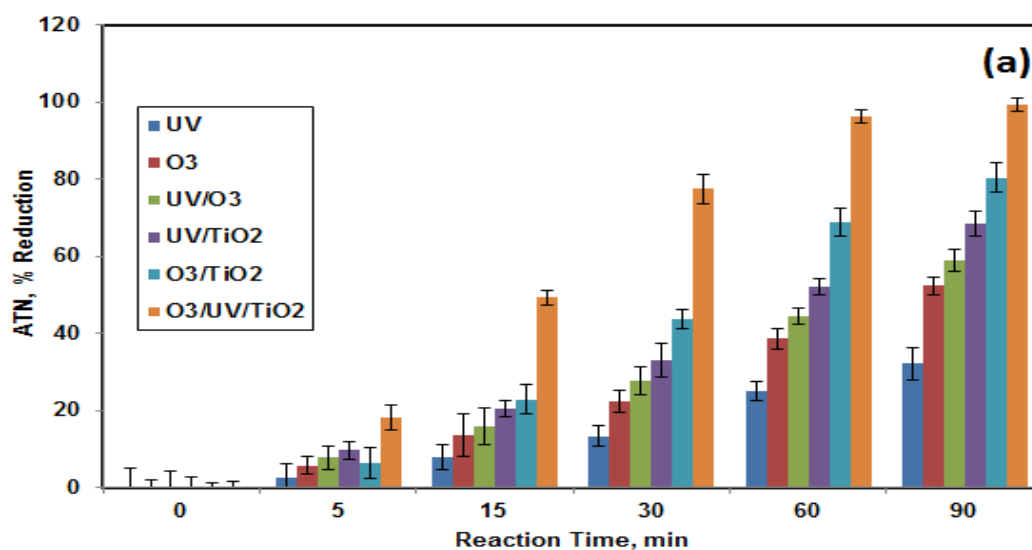
Figure 3.10. Effect of different oxidation process on relative concentration profiles (a) ATN (b) CFA and (c) DCF [ $C_0 = 10\text{mg/L}$ ,  $\text{TiO}_2 = 1\text{g/m}^2$ ,  $\text{pH} = 7.0$ ,  $T = 23 \pm 1^\circ\text{C}$ ]

The relative concentration profiles for ATN follows the order as  $\text{O}_3/\text{UV}/\text{TiO}_2 > \text{O}_3/\text{TiO}_2 > \text{UV}/\text{TiO}_2 > \text{UV}/\text{O}_3 > \text{O}_3 > \text{UV}$  as shown in Figure 3.10a whereas for CFA and DCF are  $\text{O}_3/\text{UV}/\text{TiO}_2 > \text{UV}/\text{TiO}_2 > \text{UV}/\text{O}_3 > \text{UV} > \text{O}_3/\text{TiO}_2 > \text{O}_3$  and  $\text{O}_3/\text{UV}/\text{TiO}_2 > \text{O}_3 > \text{UV} > \text{UV}/\text{TiO}_2 > \text{O}_3/\text{TiO}_2 > \text{UV}/\text{O}_3$  as observed in Figures 3.10b and 3.10c. From the above data it is observed that by ozonation alone the removal efficiency is less effective for removal of CFA and ATN because of its selective reactions with organic contaminants (Brillas, et al., 2003; Agustina, et al., 2005; Li, et al., 2005). Therefore at elevated pH, ozone decomposition leads to the generation of free radicals (Munter, 2001). Some further batch studies were conducted on ATN to study the effect of pH elevation on various AOPs.

It was observed that the percent removal by ozone was around 52.3% and 13% for ATN and CFA (Figure 3.11) due to its slow photolysis process in the beginning. Several mechanisms were proposed in the generation of  $\cdot\text{OH}$ . The generation of large number of



$\cdot\text{OH}$  from ozone photolysis is considered an important mechanism after few minutes due to its high extinction coefficient value ( $\epsilon = 3300/\text{M}/\text{cm}$ ) at 254 nm wavelength (Munter, 2001). Adsorbed source of  $\cdot\text{OH}$  production is ozonide ion radical ( $\text{O}_3^-$ ) formed due to the reaction between titanium and ozone. Upon UV irradiation, dissolved ozone produces large number of  $\cdot\text{OH}$  and hydrogen peroxide (Beltran, et al., 2005). Therefore in addition to ozonation and direct photolysis, several pathways as mentioned above were responsible for generation of  $\cdot\text{OH}$ . Due to synergistic effects between ozonation and photocatalysis, mineralization of organics is enhanced in the  $\text{O}_3/\text{UV}/\text{TiO}_2$  (Giri et al., 2008).



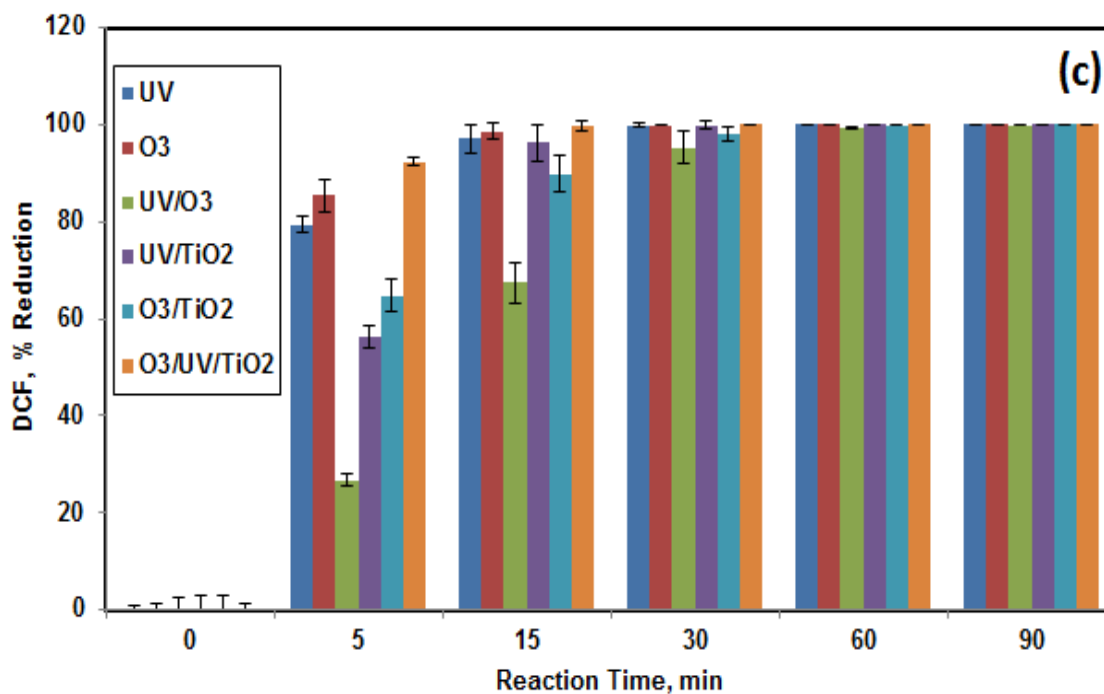
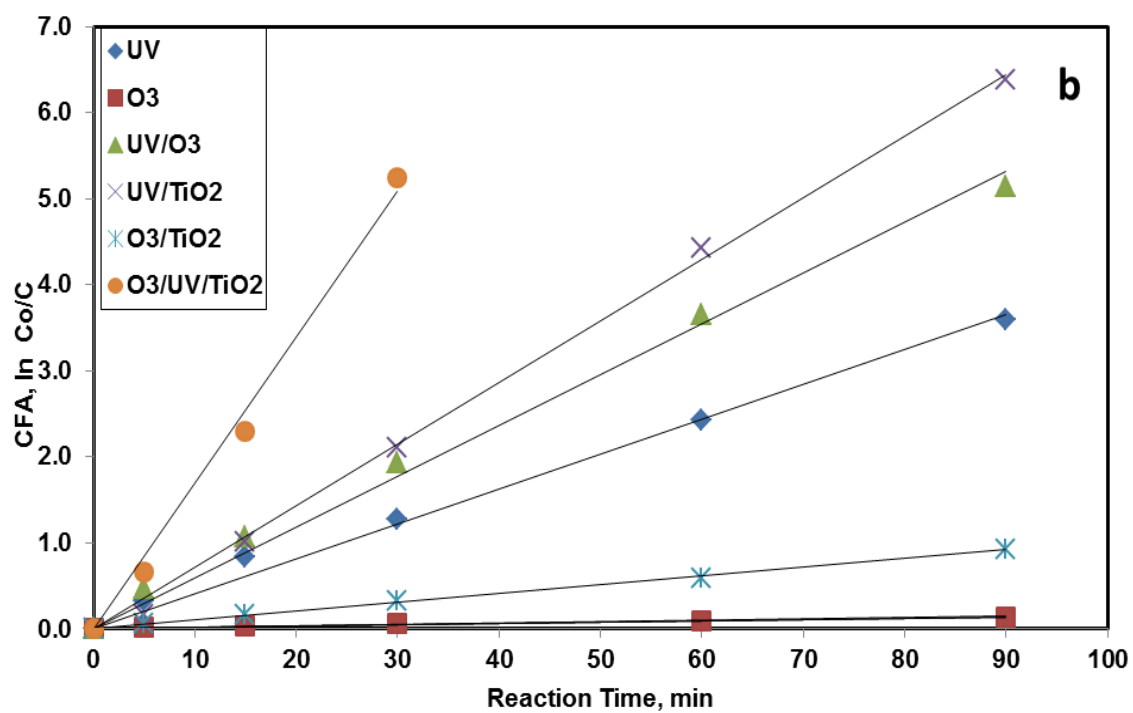
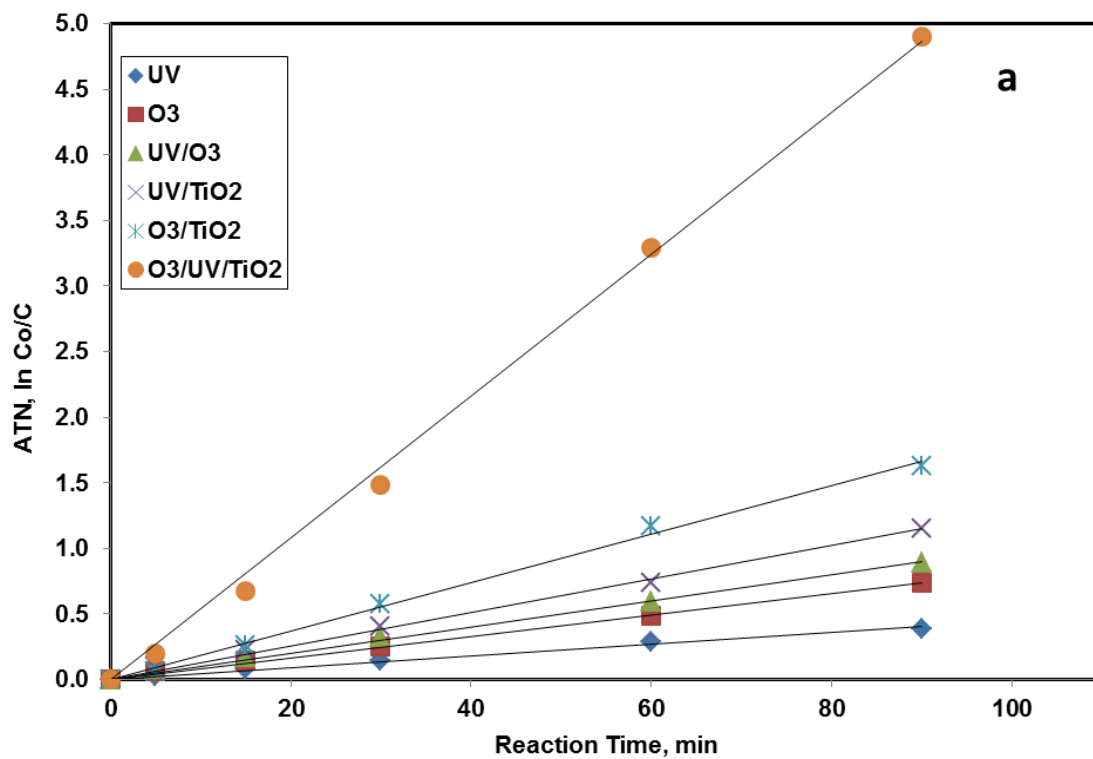


Figure 3.11. Percent Reduction under influence of various AOPs a) ATN, b) CFA and c) DCF [ $C_{Co} = 10\text{mg/L}$ ,  $O_3 = 2\text{mg/L}$ ,  $UV = 13\text{W}$ ,  $TiO_2 = 1\text{g/m}^2$ ,  $pH = 7.0$ ,  $T = 23 \pm 1^\circ\text{C}$ ]

For ATN, the reactor subjected to only UV showed 32.2% reduction, only ozone showed 52.3% reduction, whereas a combination of UV/O<sub>3</sub>, UV/TiO<sub>2</sub>, O<sub>3</sub>/TiO<sub>2</sub> and O<sub>3</sub>/UV/TiO<sub>2</sub> showed 59%, 68.5%, 80.4% and 99.9 % reduction in 90min. For CFA, the percent removal for UV, O<sub>3</sub>, UV/O<sub>3</sub>, UV/TiO<sub>2</sub> and O<sub>3</sub>/TiO<sub>2</sub> were 97.3%, 13.0%, 99.4%, 99.8% and 60.4% in 90min while O<sub>3</sub>/UV/TiO<sub>2</sub> showed a 99.5% reduction in 30min. The percent removal for DCF was observed to be 99%, 99.8% and 100% in 30min for UV, UV/TiO<sub>2</sub> and O<sub>3</sub> whereas 99.4% and 100% in 60 min UV/O<sub>3</sub> and O<sub>3</sub>/TiO<sub>2</sub> and 99.9% in 15min by O<sub>3</sub>/UV/TiO<sub>2</sub>.



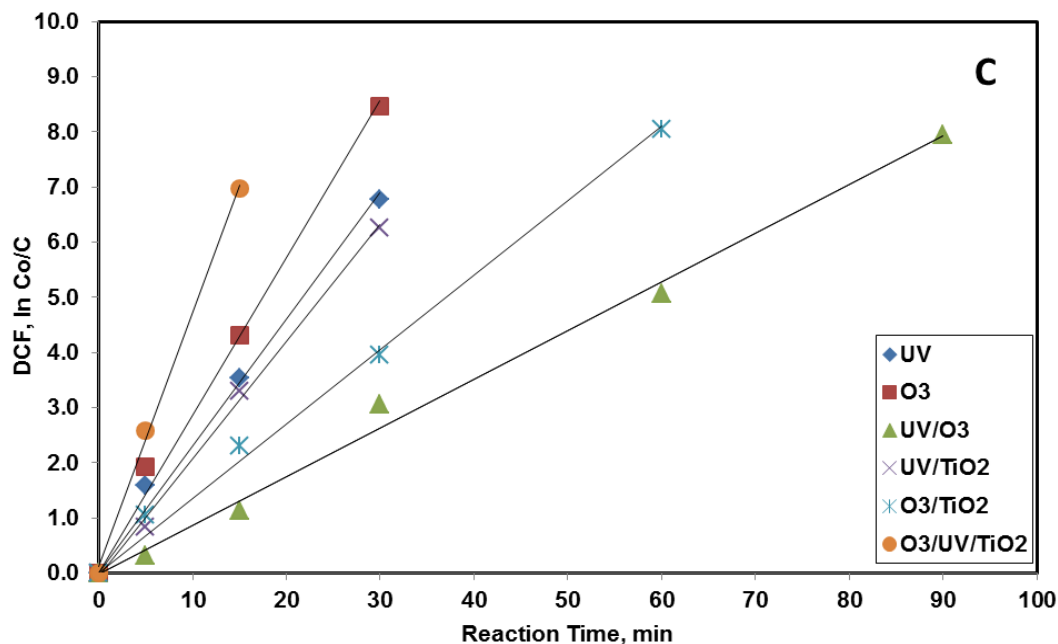


Figure 3.12. Relative concentration profiles with various AOPs a) ATN, b) CFA and c) DCF [ $Co = 10\text{mg/L}$ ,  $O_3 = 2\text{mg/L}$ ,  $UV = 13\text{W}$ ,  $TiO_2 = 1\text{g/m}^2$ ,  $pH = 7.0$ ,  $T = 23 \pm 1^\circ\text{C}$ ]

Table 3.9: Comparison of various AOPs with their degradation parameters (rate constant  $k$  and correlation coefficient  $R^2$ ) of ATN, CFA and DCF in SE [ $Co = 10\text{mg/L}$ ,  $TiO_2 = 1\text{g/m}^2$ ,  $UV = 13\text{W}$ ,  $O_3 = 2\text{mg/L}$ ,  $pH = 7.0$ ,  $T = 23 \pm 1^\circ\text{C}$ ]

| PPCPs →                             | ATN                      |        | CFA                      |        | DCF                      |        |
|-------------------------------------|--------------------------|--------|--------------------------|--------|--------------------------|--------|
|                                     | $k$ in $\text{min}^{-1}$ | $R^2$  | $k$ in $\text{min}^{-1}$ | $R^2$  | $k$ in $\text{min}^{-1}$ | $R^2$  |
| UV                                  | 0.0045                   | 0.9921 | 0.0405                   | 0.9917 | 0.2298                   | 0.992  |
| O <sub>3</sub>                      | 0.0082                   | 0.9977 | 0.0016                   | 0.958  | 0.2855                   | 0.9934 |
| UV/O <sub>3</sub>                   | 0.0100                   | 0.996  | 0.0590                   | 0.9934 | 0.0883                   | 0.9944 |
| UV/TiO <sub>2</sub>                 | 0.0128                   | 0.9953 | 0.0715                   | 0.9981 | 0.2127                   | 0.9974 |
| O <sub>3</sub> /TiO <sub>2</sub>    | 0.0185                   | 0.9973 | 0.0102                   | 0.9978 | 0.1386                   | 0.9950 |
| O <sub>3</sub> /UV/TiO <sub>2</sub> | 0.0541                   | 0.9977 | 0.1695                   | 0.9927 | 0.4616                   | 0.9983 |

A pseudo-first-order degradation kinetic model was used to calculate  $k$  values of ATN, CFA and DCF as given in Table 3.9 with rate constant  $k$  and the coefficient of determination  $R^2$  values obtained for various AOPs.

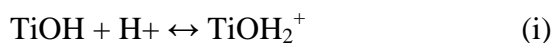
Equation (3.1) was used to plot the first-order rate constants for various AOPs.

$$\ln (C_0/C) = kt \quad \text{Eq. (3.1)}$$

where,  $k$  is the first-order degradation rate constant ( $\text{min}^{-1}$ ),  $C_0$  and  $C$  are the concentrations of ATN, CFA and DCF at time zero and at time  $t$  (min). All the AOPs showed pseudo-first order kinetics with linear plots of  $\ln(C_0/C)$  against  $t$ .

### 3.5.3 Effect of pH

The efficiency of the photocatalytic activity is governed by solution pH as it can influence both the charge state of the photocatalyst and/or the cationic or anionic organic compounds. As per Hapeshi et al., 2010, it is known that there exists an electrostatic repulsion between  $\text{TiOH}_2^+$  and protonated ATN (i and iii) that hinders photocatalysis at pH 3.0 because the  $\text{pK}_a$  of ATN is 9.6 whereas it is 6.25 of Degussa P25  $\text{TiO}_2$  as the zero point charge ( $\text{pH}_{zpc}$ ). At  $\text{pH} < 6.7$ , an electrostatic repulsion takes place as both ATN and catalyst are positively charged. Based on this factor, pH studies at 7, 8 and 9 were conducted on ATN to observe the degradation efficiency as at neutral pH the electrostatic attraction was less as ATN exists in neutral molecular form.



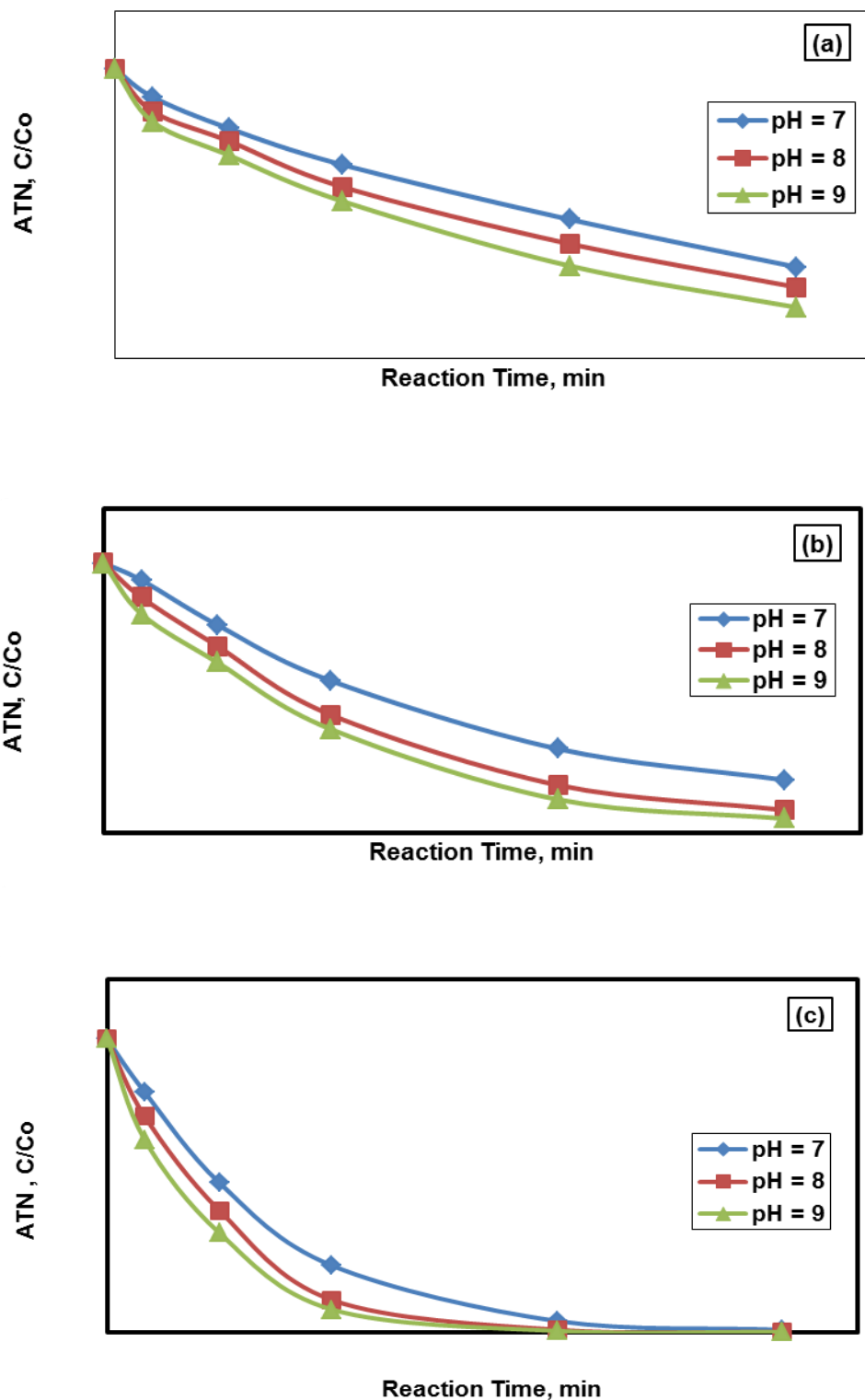
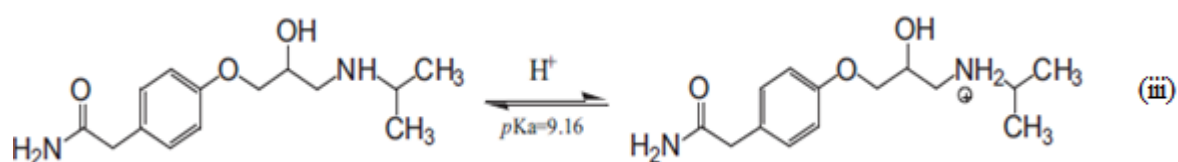
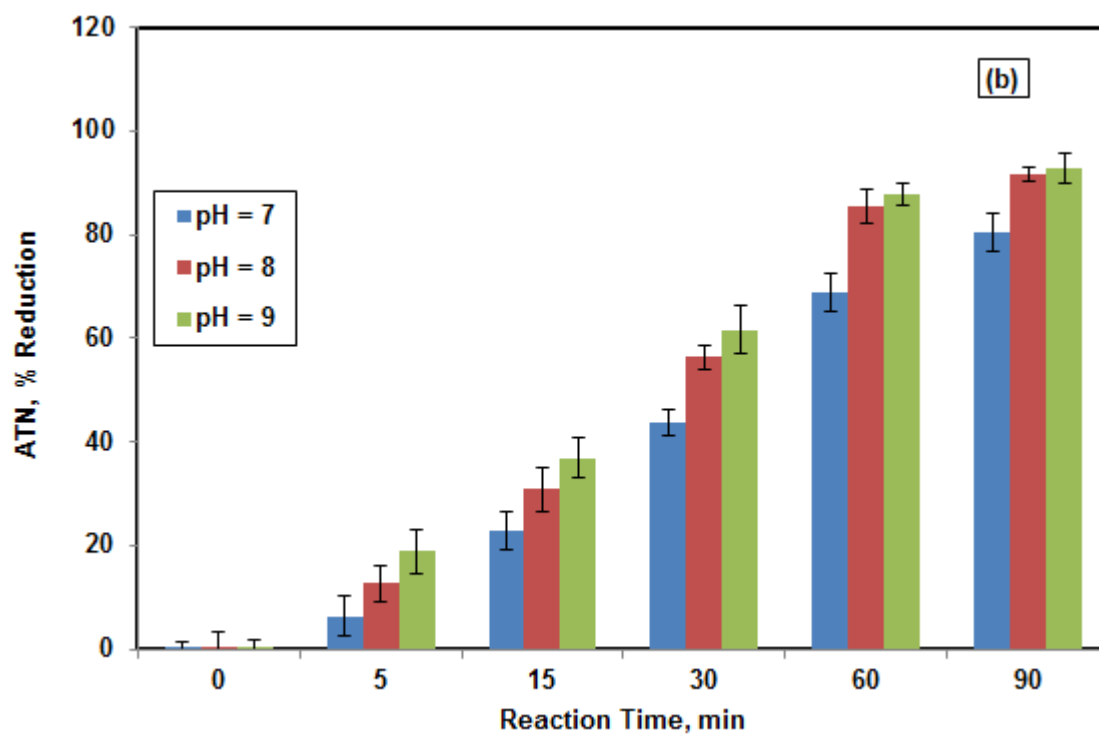
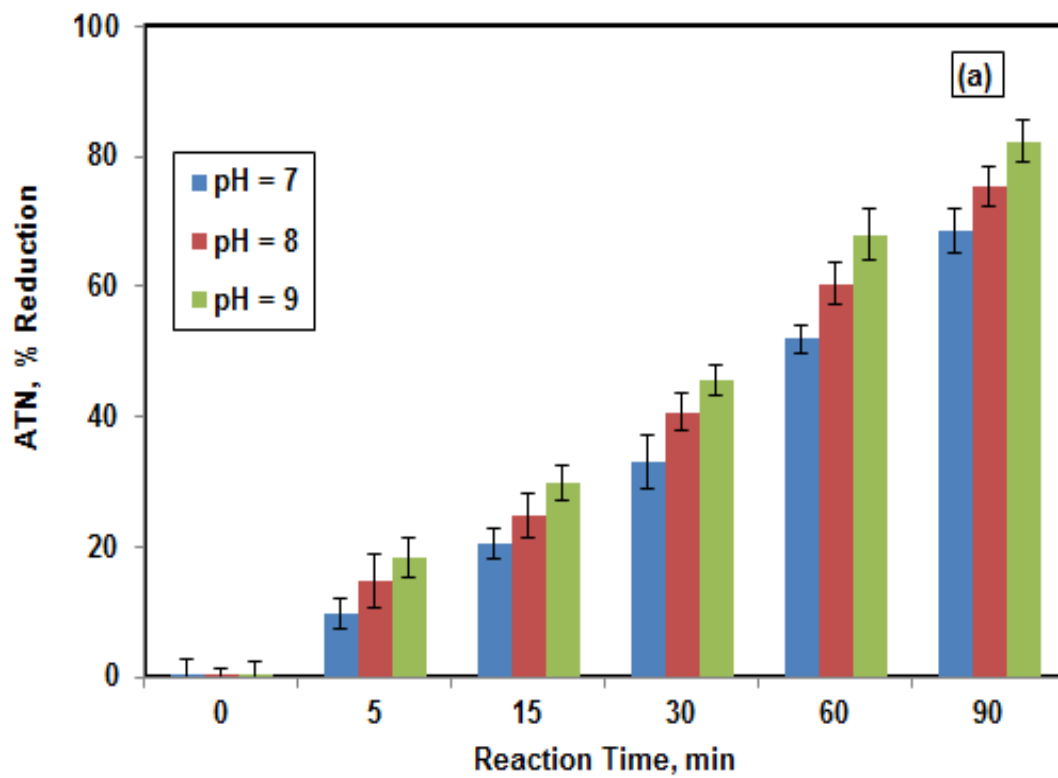


Figure 3.13. Relative concentration profiles of pH on ATN (a) UV/TiO<sub>2</sub> (b) O<sub>3</sub>/TiO<sub>2</sub> and (c) O<sub>3</sub>/UV/TiO<sub>2</sub> [ $C_0 = 10\text{mg/L}$ ,  $\text{TiO}_2 = 1\text{g/m}^2$ ,  $\text{O}_3 = 2\text{mg/L}$ ,  $\text{UV} = 13\text{W}$ ,  $T = 23 \pm 1^\circ\text{C}$ ]

Figure 3.13, 3.14 and 3.15 showed higher removal rates at pH 9 compared to pH 7 which followed the order  $O_3/UV/TiO_2 > O_3/TiO_2 > UV/TiO_2$ . A removal efficiency of 99% at pH 7 was observed using  $O_3/UV/TiO_2$  whereas increasing the pH to above 8 accelerated the degradation for  $O_3/TiO_2$  and  $UV/TiO_2$  as electrostatic attraction takes place between  $TiO^-$  and protonated ATN (ii and iii).



At  $9.6 (pK_a) > pH > 6.7$  (Degussa P25), a higher removal efficiency was observed at near neutral conditions due to the electrostatic attractions between protonated ATN and negatively charged  $TiO_2$  surface. Increasing solution pH from 7 to 9 lead to more efficient  $HO^\bullet$  formation from  $OH^-$  than water that favored  $TiO_2$  photocatalysis (Khodja et al., 2002) and there is a possibility that under alkaline conditions, the structural orientation of ATN favors the attack of the reactive species for better degradation (Haque et al., 2006). The effect of pH also depends on other reactive species present in the sample matrix as well as on the rate of formation of radicals. The ATN compound contains amine-moieties and thus this amino group gets protonated at  $pH < pK_a = 9.6$  as shown (iii).





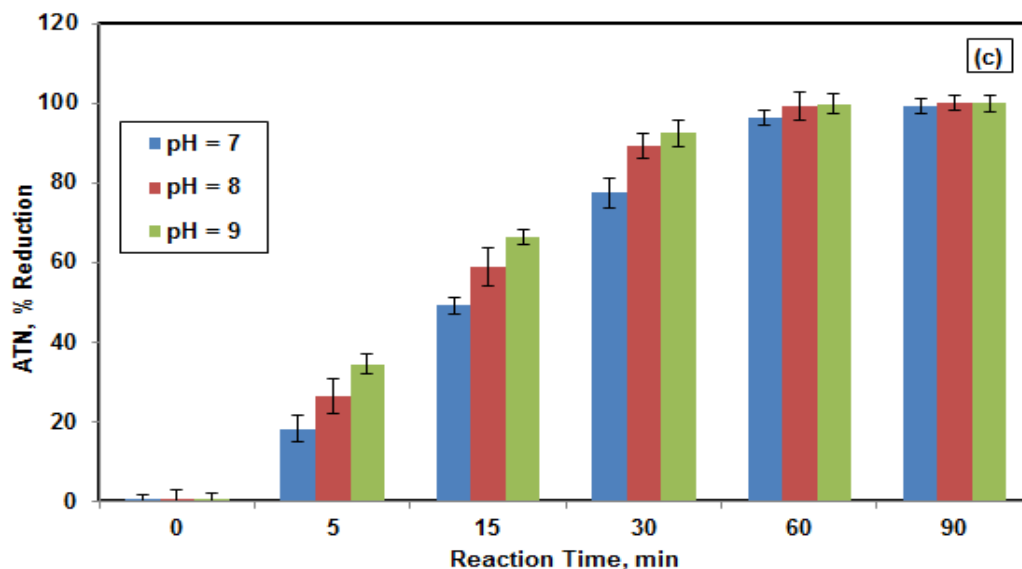
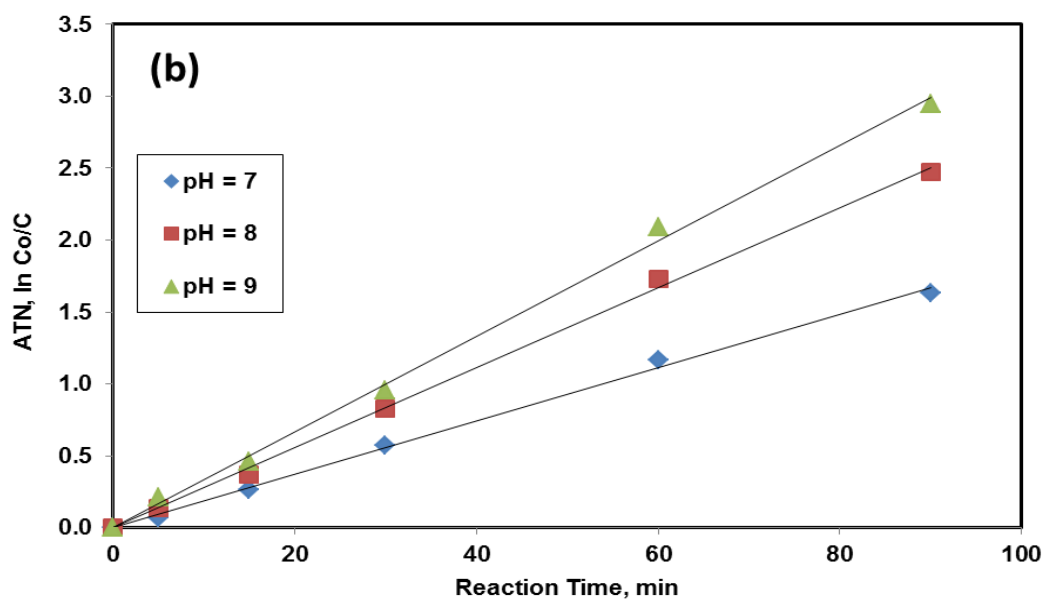
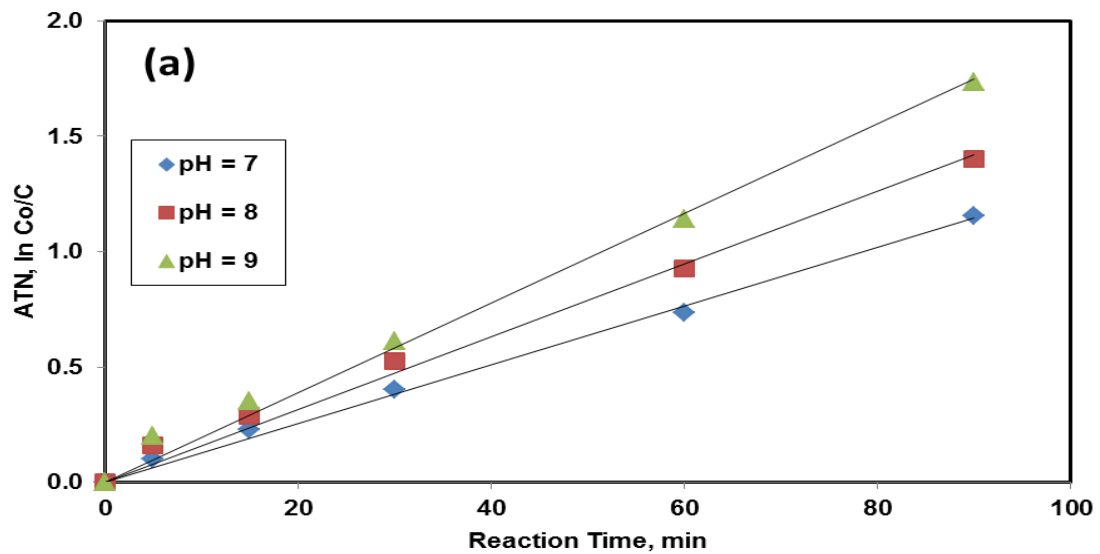


Figure 3.14. Percent removal of ATN at varying pH (a) UV/TiO<sub>2</sub> (b) O<sub>3</sub>/TiO<sub>2</sub> and (c) O<sub>3</sub>/UV/TiO<sub>2</sub> [Co = 10mg/L, TiO<sub>2</sub> = 1g/m<sup>2</sup>, O<sub>3</sub> = 2mg/L, UV = 13W, T = 23 ± 1°C]

It was also observed that light absorption of ATN was strengthened as the pH increased (Liu et al., 2013). The effect of pH not only influences charge state of ATN and TiO<sub>2</sub>, but also affects equilibrium of water dissociation in terms of generation of hydroxyl radical levels and oxidation of photogenerated holes (Ioannou et al., 2011).

Table 3.10: Comparison of various AOPs with pH (rate constant  $k$  and correlation coefficient  $R^2$ ) of ATN in SE [Co = 10 mg/L, TiO<sub>2</sub> = 1 g/m<sup>2</sup>, UV = 13W, O<sub>3</sub> = 2 mg/L, T = 23 ± 1°C]

| pH                                  | 7                      |                | 8                      |                | 9                      |                |
|-------------------------------------|------------------------|----------------|------------------------|----------------|------------------------|----------------|
|                                     | k in min <sup>-1</sup> | R <sup>2</sup> | k in min <sup>-1</sup> | R <sup>2</sup> | k in min <sup>-1</sup> | R <sup>2</sup> |
| UV/TiO <sub>2</sub>                 | 0.0128                 | 0.9953         | 0.0158                 | 0.9912         | 0.0194                 | 0.9921         |
| O <sub>3</sub> /TiO <sub>2</sub>    | 0.0185                 | 0.9973         | 0.0278                 | 0.9985         | 0.0333                 | 0.9976         |
| O <sub>3</sub> /UV/TiO <sub>2</sub> | 0.0541                 | 0.9977         | 0.079                  | 0.991          | 0.0922                 | 0.9928         |



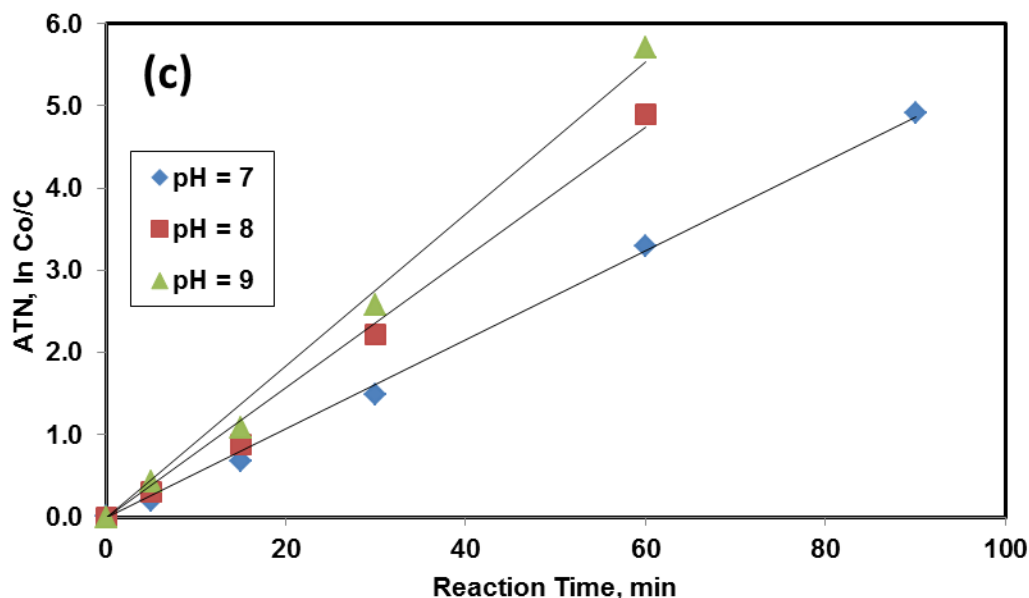


Figure 3.15. Relative concentration of ATN at varying pH (a) UV/TiO<sub>2</sub> (b) O<sub>3</sub>/TiO<sub>2</sub> and c) O<sub>3</sub>/UV/TiO<sub>2</sub> [Co = 10mg/L, TiO<sub>2</sub> = 1g/m<sup>2</sup>, O<sub>3</sub> = 2mg/L, UV = 13W, T = 23 ± 1°C]

The first-order kinetic values for ATN increase in pH from 7 to 9 were compared with UV/TiO<sub>2</sub>, O<sub>3</sub>/TiO<sub>2</sub> and UV/O<sub>3</sub>/TiO<sub>2</sub> as shown in Table 3.10. It can be seen from Figure 3.15 that the rate constant was the least for ATN at pH 9 compared to UV/O<sub>3</sub>/TiO<sub>2</sub> which showed a value of 0.0922. Similarly at pH 7 and 8, the rate constants were 0.0128 and 0.0158 for UV/TiO<sub>2</sub> followed by O<sub>3</sub>/TiO<sub>2</sub> and maximum by UV/O<sub>3</sub>/TiO<sub>2</sub>.

### 3.5.4 Effect of Natural Organic Matter and Bromine

In wastewater the dissolved organic matter (DOM) acts as chromophoric and shows recalcitrance to biological degradation especially to UV radiation. Several studies have reported the degradation of contaminants is mostly favored by the presence of these photoactive DOMs as they generate not only reactive oxygen species (ROS) but also solvated electrons, superoxide anion, singlet oxygen, organic peroxy and alkoxy radicals, hydroxyl radical and natural organic matter containing reactive triplet states (Heberer et al., 1998; Canonica and Freiburghaus, 2001; Chin et al., 2004). Another

study found that during the oxidation reactions, the degradation in two natural waters was faster when compared to Milli-Q water for octylphenol which were triggered by photo processes that involved excited state of DOM generating hydroxyl radicals and singlet oxygen reactive species (Neamtu et al., 2009).

The photodegradation rates were observed to be lower in secondary effluent for ATN compared to CFA and DCF which is due to the presence of inorganic species such as chloride ( $\text{Cl}^-$ ), carbonates ( $\text{CO}_3^{2-}$ ), bicarbonates ( $\text{HCO}_3^-$ ) and dissolved organic matter (DOM). The efficiency of photocatalysis process is directly affected by the presence of these species that act as hydroxyl radical scavengers. Presence of high content of chloride ( $\text{Cl}^-$ ) species form dichloride anion radical ( $\text{Cl}_2^{\cdot-}$ ) and chlorine radical ( $\text{Cl}^\cdot$ ) that are less reactive than  $\cdot\text{OH}$  radical (De Laat and Truong, 2006 and Ji et al., 2013). Similarly the presence of carbonates are 40 times more kinetically effective than bicarbonate ions and thus the degradation of ATN and CFA are significantly decreased as these  $\text{CO}_3^{2-}$  compete with organic contaminants scavenging hydroxyl radical reactions (Klamerth et al., 2009).

The secondary effluent contains several major ions and other dissolved organics that can either enhance or inhibit the degradation rates. For example in the present study, the secondary effluent contains nitrates in an appreciable amount that can increase or decrease the efficiency of degradation of PPCPs. For example, in the presence of HA and nitrates in different water matrices, the degradation efficiency increased while undergoing photochemical transformation of sulfamethoxazole because these constituents under solar irradiation generated strong singlet oxygen and  $\cdot\text{OH}$  radicals (Trovo et al., 2009).

Presence of bromate anions in water resources is highly toxic for humans especially in drinking water where the maximum concentration permitted is 25  $\mu\text{g/L}$  as per World Health Organization (WHO, 1996). These bromate anions are generated from water treatment plants when bromide anions react with oxidant agents (von Gunten, 2003). Various studies have shown that the removal efficiency was not effective to remove these halide anions from drinking water on large scale (Sánchez-Polo et al., 2006). In

the present study 100ppm each of stock NOM and Bromine were prepared and stored at 4°C. An aliquot was taken from the stock solutions and introduced into the reactor containing secondary effluent and subjected to various AOPs. The kinetics of degradation with varying concentrations of NOM and Br are shown in Table 3.11.

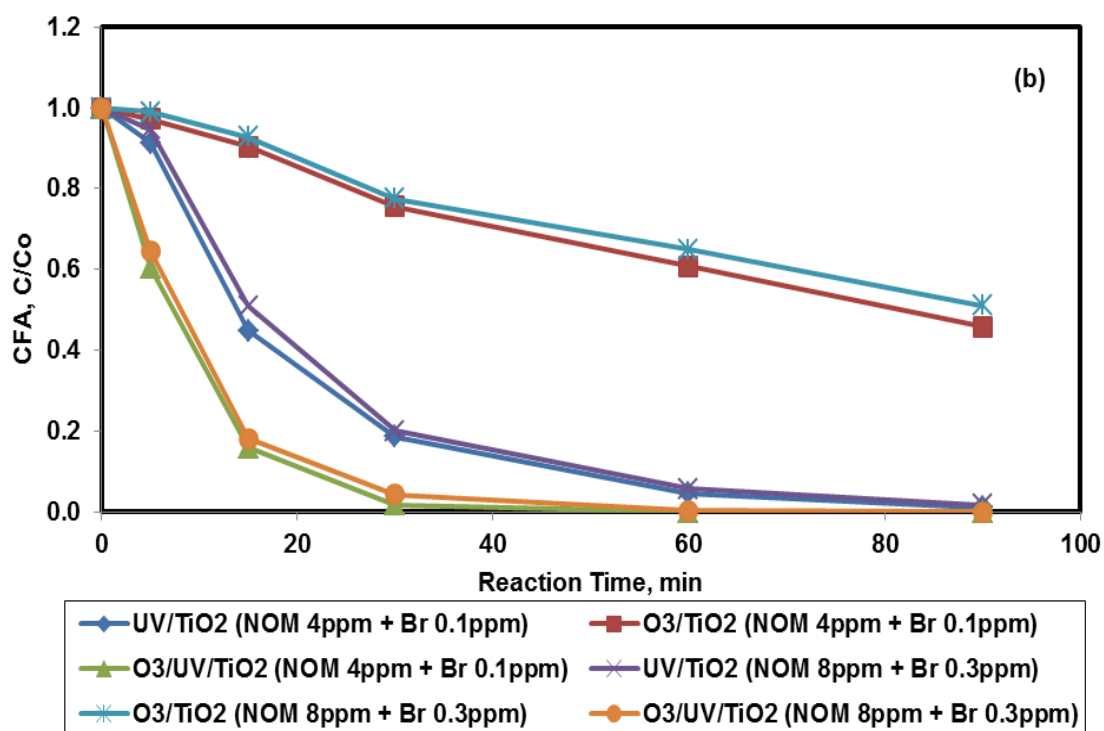
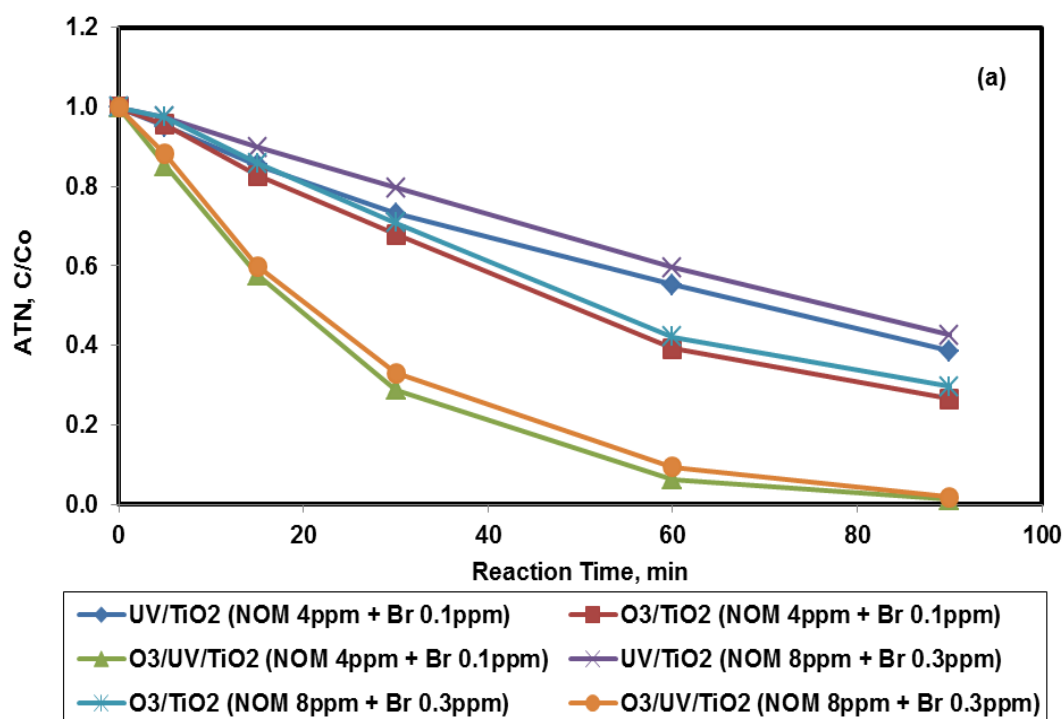
Table 3.11: Comparison of various AOPs on degradation of PPCPs in presence of varying concentrations of NOM and Br with their k and R<sup>2</sup> values

| PPCPs                                   | ATN                                   |                                       | CFA                                   |                                       | DCF                                   |                                       |
|---|---------------------------------------|---------------------------------------|---------------------------------------|---------------------------------------|---------------------------------------|---------------------------------------|
|   | NOM 4ppm<br>+ Br 0.1ppm               | NOM 8ppm<br>+ Br 0.3ppm               | NOM 4ppm<br>+ Br 0.1ppm               | NOM 8ppm<br>+ Br 0.3ppm               | NOM 4ppm<br>+ Br 0.1ppm               | NOM 8ppm<br>+ Br 0.3ppm               |
| <b>UV/TiO<sub>2</sub></b>               | k = 0.0104<br>R <sup>2</sup> = 0.9984 | k = 0.0091<br>R <sup>2</sup> = 0.9906 | k = 0.051<br>R <sup>2</sup> = 0.9966  | k = 0.0468<br>R <sup>2</sup> = 0.9934 | k = 0.1798<br>R <sup>2</sup> = 0.9989 | k = 0.136<br>R <sup>2</sup> = 0.9930  |
| <b>O<sub>3</sub>/TiO<sub>2</sub></b>    | k = 0.0148<br>R <sup>2</sup> = 0.9948 | k = 0.0136<br>R <sup>2</sup> = 0.9913 | k = 0.0086<br>R <sup>2</sup> = 0.9961 | k = 0.0074<br>R <sup>2</sup> = 0.9910 | k = 0.1124<br>R <sup>2</sup> = 0.9964 | k = 0.0994<br>R <sup>2</sup> = 0.9917 |
| <b>O<sub>3</sub>/UV/TiO<sub>2</sub></b> | k = 0.0477<br>R <sup>2</sup> = 0.9932 | k = 0.0422<br>R <sup>2</sup> = 0.9907 | k = 0.1338<br>R <sup>2</sup> = 0.9936 | k = 0.0984<br>R <sup>2</sup> = 0.9943 | k = 0.3945<br>R <sup>2</sup> = 0.9968 | k = 0.36<br>R <sup>2</sup> = 0.9963   |

It can be seen that the removal rate k value was highest for CFA with 2.24 and 1.81 folds by O<sub>3</sub>/UV/TiO<sub>2</sub> (NOM 4ppm + Br 0.1ppm and NOM 8ppm + Br 0.3ppm) than the summation of k values for UV/TiO<sub>2</sub> and O<sub>3</sub>/TiO<sub>2</sub> put together. Similarly k values of 1.89 and 1.86 fold for ATN and 1.35 and 1.52 folds for DCF were observed for O<sub>3</sub>/UV/TiO<sub>2</sub> than the summation of k values for other two processes of UV/TiO<sub>2</sub> and O<sub>3</sub>/TiO<sub>2</sub> put together.

The relative concentration profiles for ATN, CFA and DCF were studied in presence of NOM and Br at varying concentrations. It was observed that the initial concentration

decreased slightly as the NOM and Br concentration increased for all the target PPCP compounds chosen as shown in Figures 3.16 and 3.17.



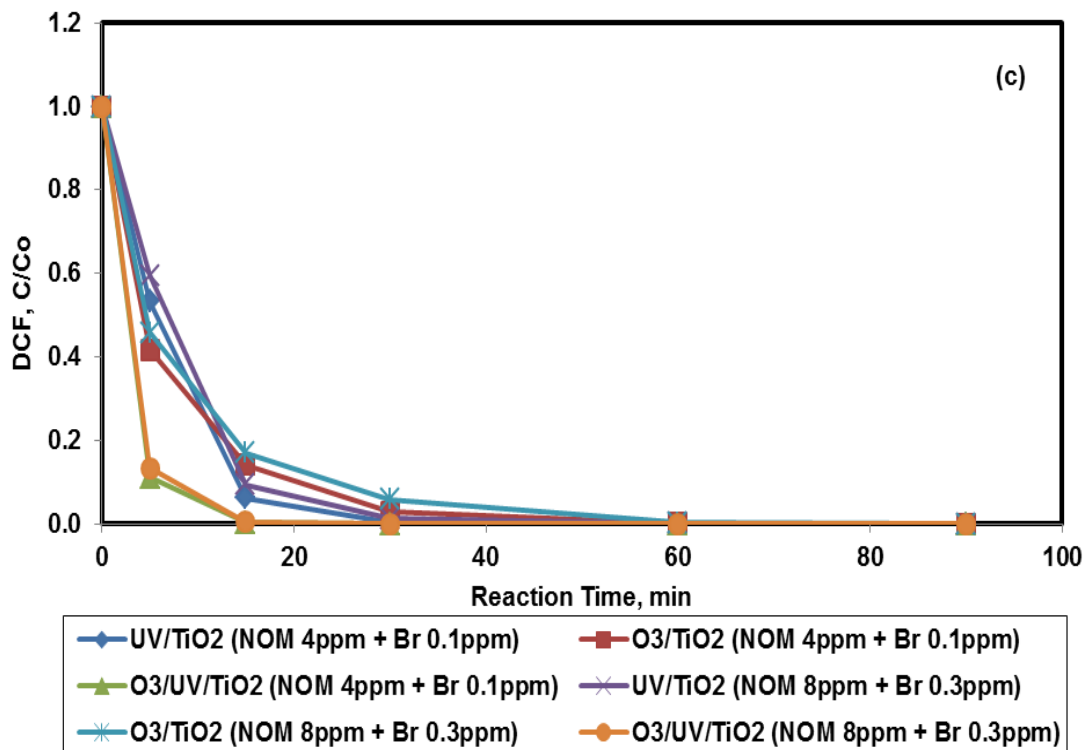


Figure 3.16. Effect of varying concentrations of NOM and Br on ATN, CFA and DCF a) UV/TiO<sub>2</sub> (b) O<sub>3</sub>/TiO<sub>2</sub> and (c) O<sub>3</sub>/UV/TiO<sub>2</sub> [Co = 10mg/L, TiO<sub>2</sub> = 1g/m<sup>2</sup>, O<sub>3</sub> = 2 mg/L, UV = 13W, T = 23 ± 1°C]

It was observed that removal efficiency of CFA in solar/ZnO process showed an inhibitory effect due to the presence of 20mg/L HA thus decreasing the efficiency of degradation rate in winter. Usually with increase in HA concentration, the light attenuation decreases the interaction of ATN, CFA and DCF with reduced number of available photons. The steady state concentration of ROS decreases effectively due to the reaction with HA and compete with ATN, CFA and DCF rather than ROS. Thus a decrease in photodegradation rate is mainly attributed to increase in HA concentration that mainly acts as inner filter (Gao and Zepp et al., 1998). Studies have shown that in solar/TiO<sub>2</sub> process, nitrate and bicarbonates showed a slight inhibitive effect on CFA degradation. Thus nitrate can also act as inner filter for the UV light as it absorbs light in the UV range (Zepp et al., 1987).

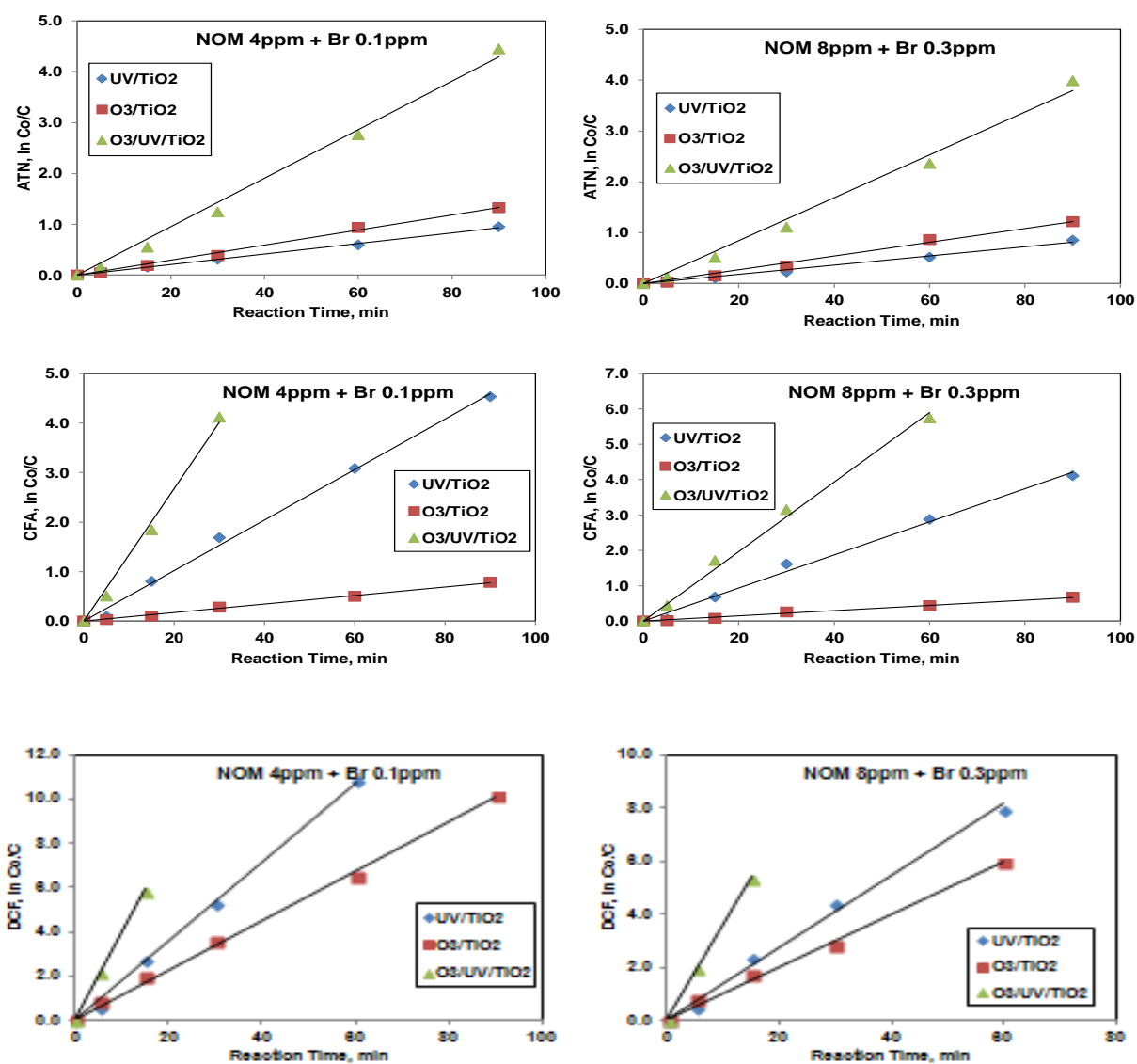


Figure 3.17. Determination of rate constant  $k$ ,  $\text{min}^{-1}$  at varying concentrations of NOM and Br on ATN, CFA and DCF using UV/TiO<sub>2</sub> (b) O<sub>3</sub>/TiO<sub>2</sub> and (c) O<sub>3</sub>/UV/TiO<sub>2</sub> [ $C_0 = 10\text{mg/L}$ ,  $\text{TiO}_2 = 1\text{g/m}^2$ ,  $\text{O}_3 = 2\text{mg/L}$ ,  $\text{UV} = 13\text{W}$ ,  $T = 23 \pm 1^\circ\text{C}$ ].

The photodecomposition of DCF also gets affected due to the presence of humic acids that act as inner filters (Andreozzi et al., 2003). Finally, the content of humic substances in different surface waters plays an important role in absorption or transmission of light (Huovinen et al., 2003).



### 3.5.5 Identification of UV-transformation products

Quantification of ATN, CFA and DCF and identification of the transformation products were performed by using Agilent 1290 (HPLC) coupled with 6460 Triple Quadrupole Mass Spectrometer. Higher sensitivity and structural information was obtained for CFA and DCF using a fragmentor voltage of 60 V while 100 V was used for ATN to study the formation of ion fragments other than deprotonized molecular ion  $[M-H]^-$ , Santos et al., 2000.

#### 3.5.5.1 Degradation products of Atenolol

The spectrometric data obtained from ozonation, UV, and UV/O<sub>3</sub> analysis were compared with initial ATN control sample by taking a known aliquot at different intervals of time. Figure 3.18, 3.19 and 3.20 presents the MS/MS spectrum in ATN, CFA and DCF and fragmentation of transformation products. At pH 7, 8 and 9, a total of 12 transformation products were formed for ATN when subjected to ozonation. As the pH was increased from 7 to 9 for ATN, the amount of hydroxide ions produced also increased and thus the basicity of the solution acting as an initiator and more number of transformation products were detected. Fragmentation of protonated ATN by LC-MS/MS is shown in Figure 3.18a with their molecular ion,  $[M+H]^+$  of  $m/z$  267.1710.

When ozonation was applied to ATN, transformation products obtained were aromatic ring opening reaction between both  $\bullet OH$  and ozone, oxidation and cleavage of 2-hydroxy-3-(isopropylamino) propoxy group and mono-, di and tri-hydroxylation reactions and their derivatives. ATN was also mainly degraded by reaction of  $\bullet OH$  with aliphatic chain.

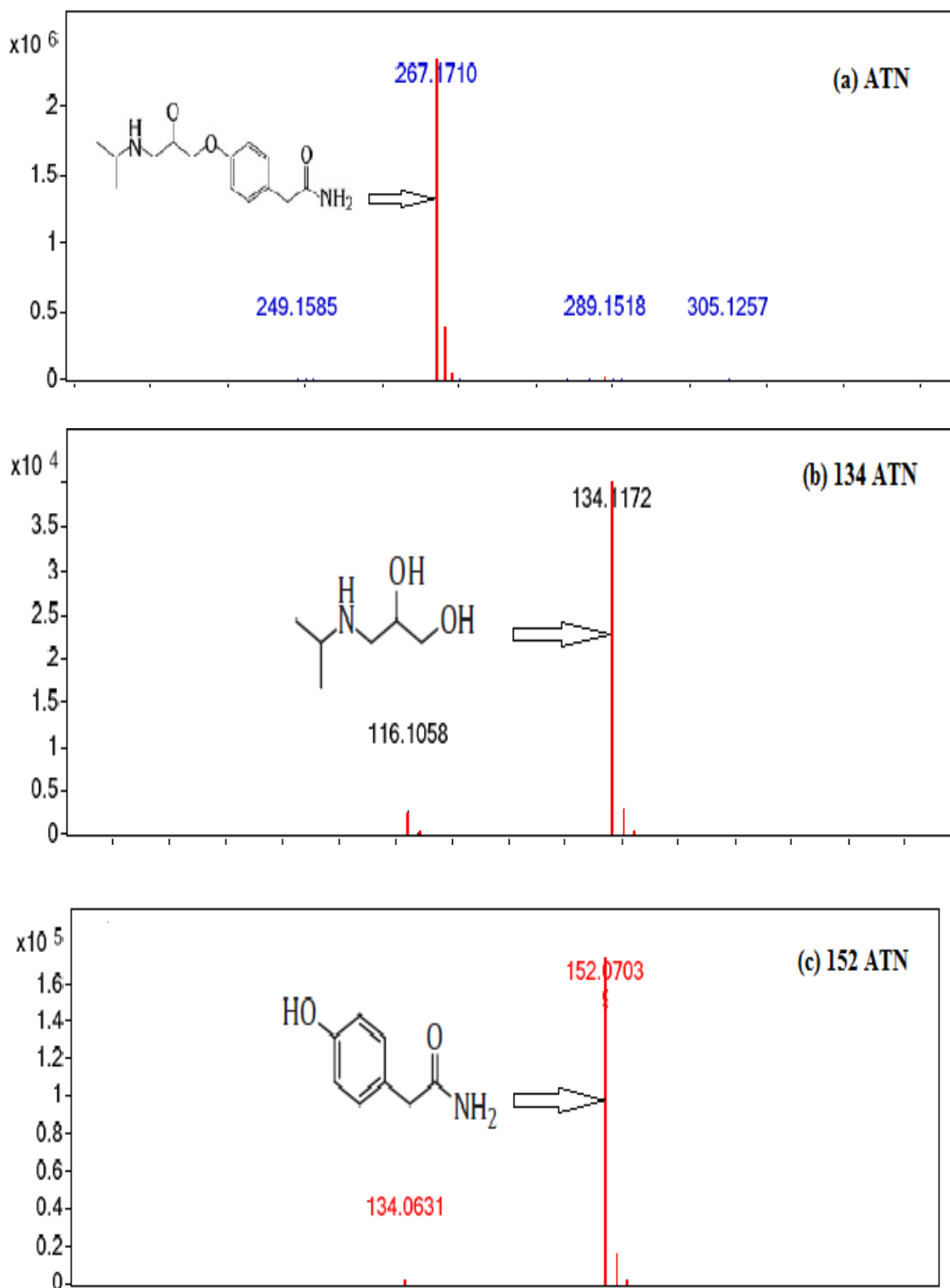


Figure 3.18b shows insertion of OH groups into the aromatic ring by  $m/z$  299.1926 dihydroxylated forming 2-hydroxy-3-(isopropylamino)propoxy chain of atenolol of  $m/z$

134 ion. Breakdown of C<sub>10</sub>-O bond of atenolol leads to formation of m/z 134 and m/z 152 as other atenolol breakdown products. By the loss of one water molecule each in Figure 3.18b and Figure 3.18c from molecular ions, a prominent product ion is formed at m/z 116.1058 and m/z 134.0631. Figure 3.18d shows the aromatic ring breakdown product of atenolol at m/z 206.0809 and loss of one water molecule shows a prominent peak at 188.0703.

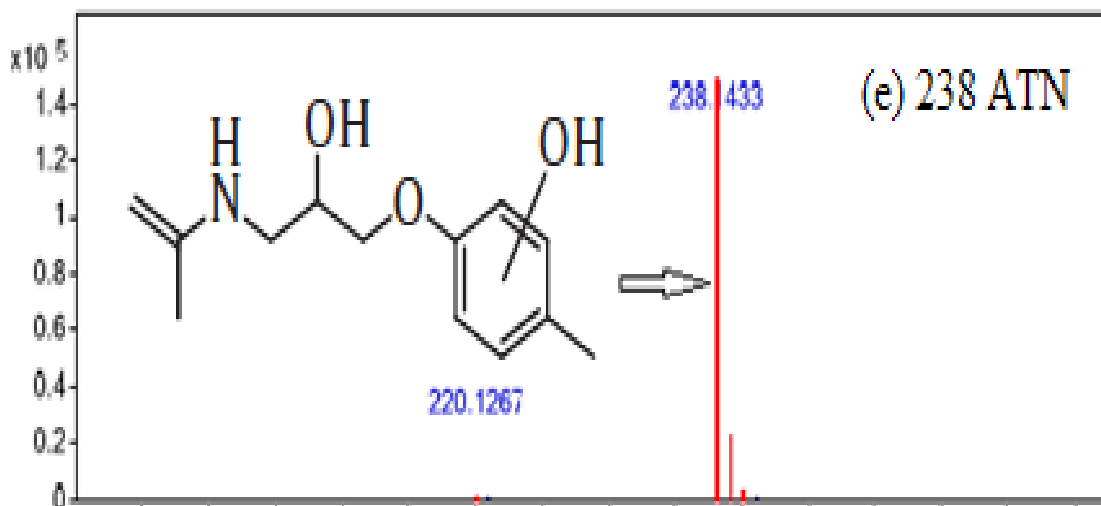
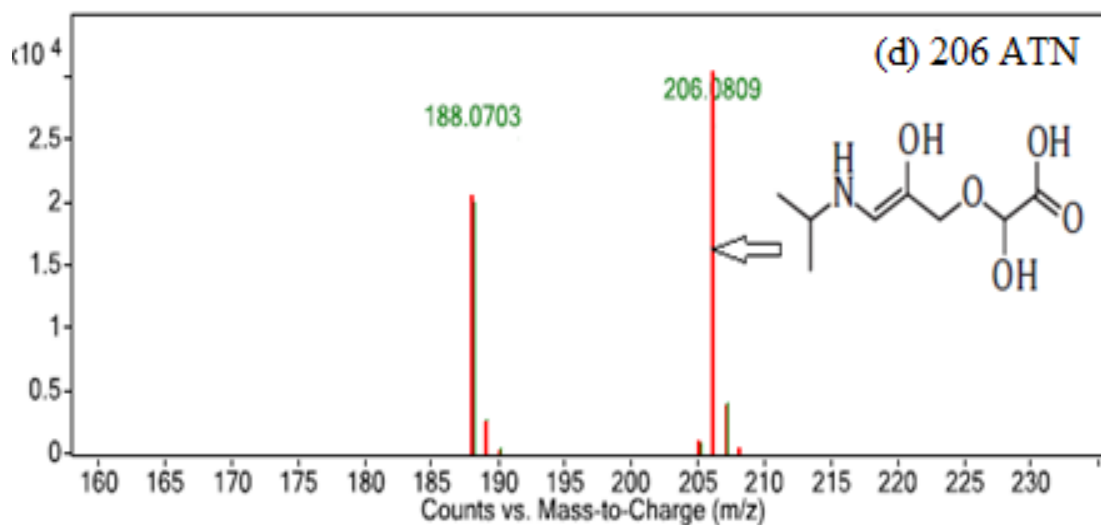
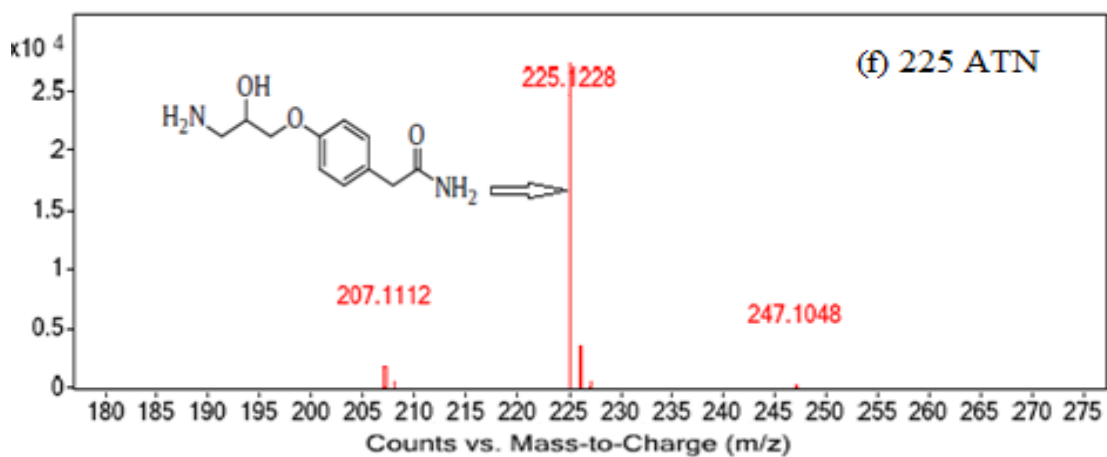
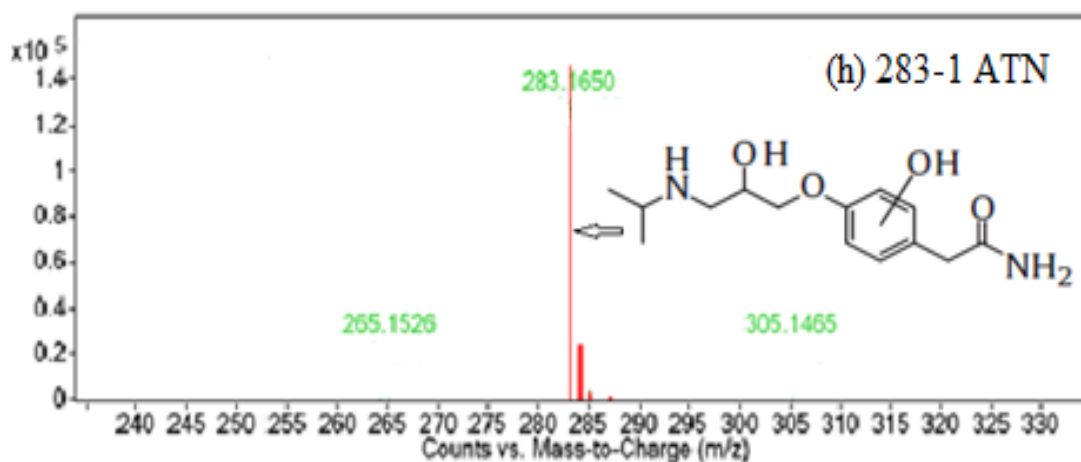
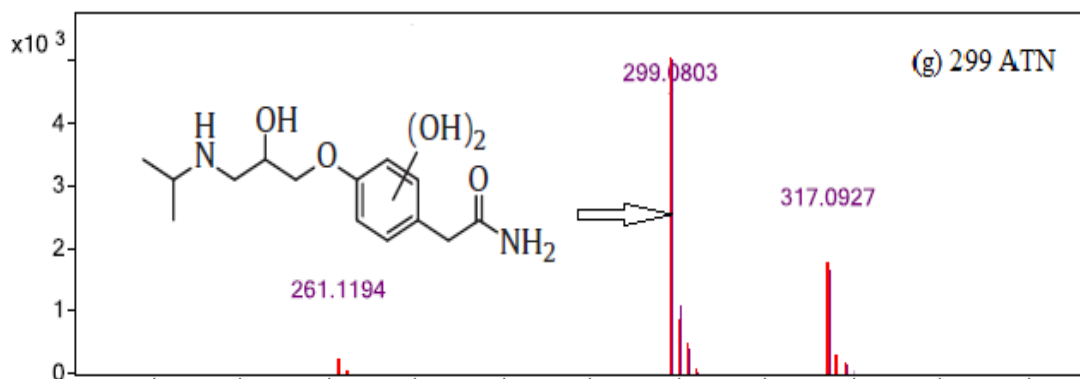
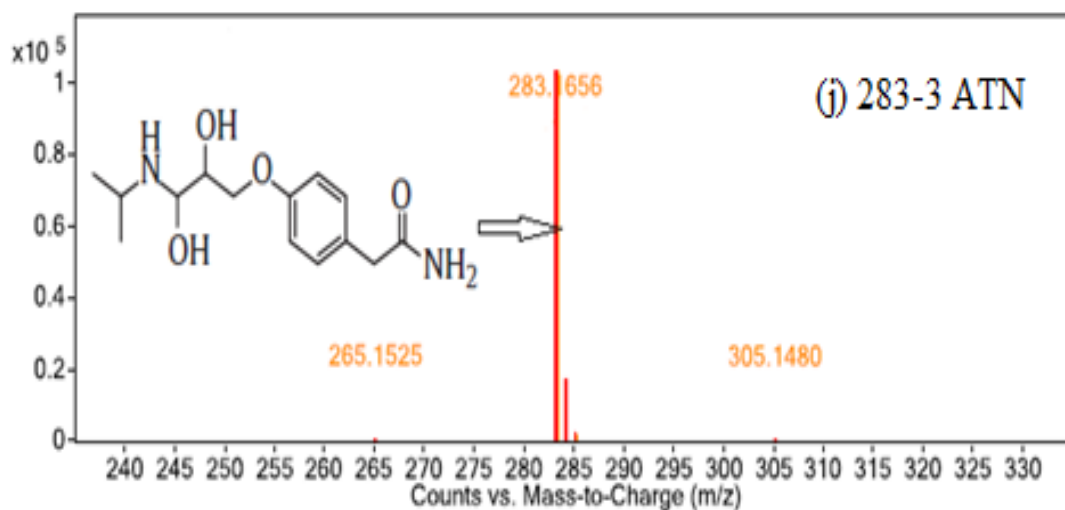
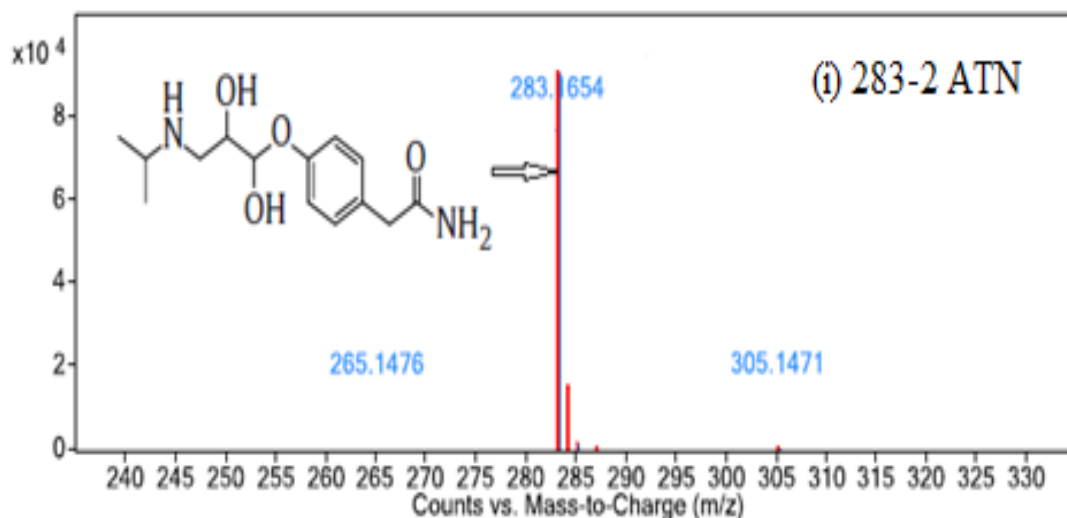


Figure 3.18e illustrates m/z 238.1433 formed by the degradation of atenolol at 2-hydroxy-3-(isopropylamino)propoxy group by the loss of formamide from isopropyl group.



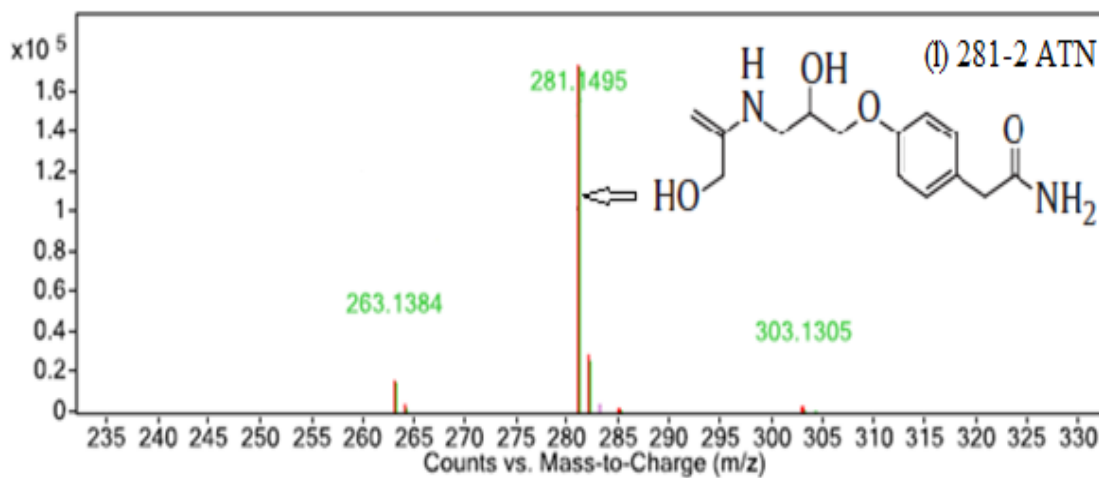
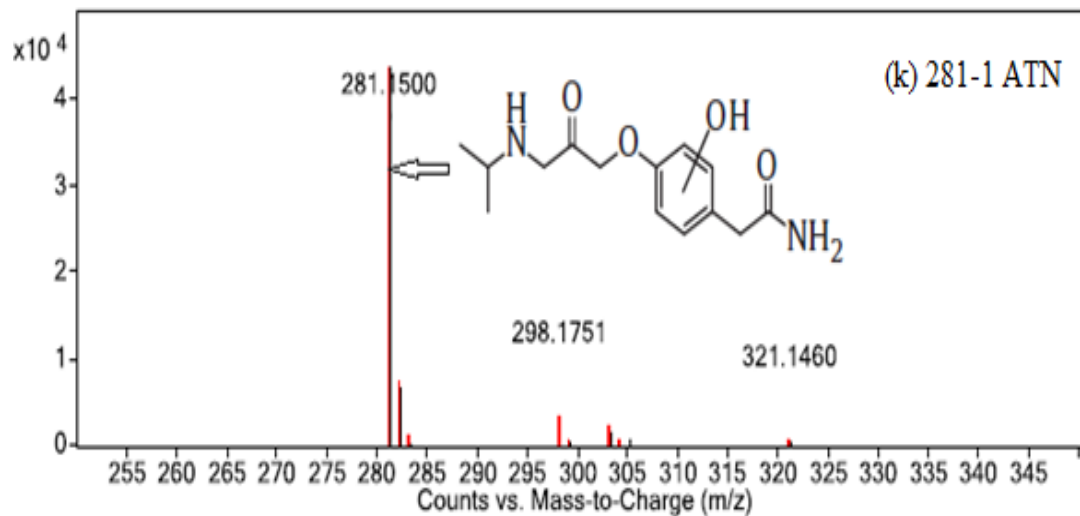
The ion peak observed at m/z 225.1228 is formed through the loss of isopropyl from the molecular ion as illustrated in Figure 3.18f.





Compounds with m/z 283 mono-hydroxylated and m/z 299 di-hydroxylated Figure 3.18g were detected as the transformation products with  $[M+H]^+$  ion. From  $[M+H]^+$  ion of atenolol, addition of 16 and 32 amu forms mono- and di-hydroxylated atenolol which indicates the addition of one and two hydroxyl groups to the atenolol. Figures 3.18h, i and j represents atenolol with  $[M+H]^+$  ion of m/z 283 with three species of monohydroxylated labeled as 283-1, 283-2 and 283-3. By the loss of one water molecule from 283-1 which is more polar than atenolol, elutes earlier forming another most dominant product at m/z 265.1526 in the MS/MS spectrum. 283-2 and 283-2 are less polar compared to atenolol and hence elutes at longer retention time. As an electron withdrawing group, when hydroxyl group is added close to secondary amine to the carbon atoms, the electron density of nitrogen group is reduced thus decreasing the

polarity of that compound. Further,  $m/z$  206.0809 is formed due to the loss of hydroxyl and isopropylamine group from fragmentation of  $m/z$  265.1526 as illustrated in Figure 3.18d.



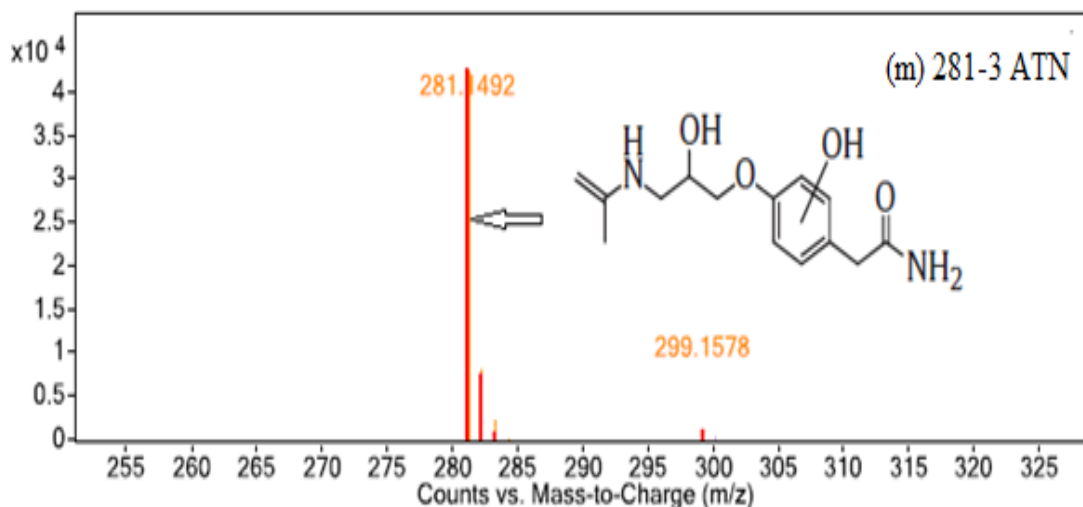


Figure 3.18. (a) to (m) Spectrum of ATN and its transformation products by MS/MS with its proposed structure and molecular ion  $[M+H]^+$

Figures 3.18k,l and m illustrates the degradation by-products of monohydroxylated atenolol labeled as 281-1, 281-2 and 281-3 with molecular ion peak at 281.1500. Most of these transformation products agree well with the literature as per Tay et al., 2011.

The reactive species is  $\cdot\text{OH}$  at basic pH during ozonation. An unselective behavior of  $\cdot\text{OH}$  at different reaction sites in reacting to ATN increased the aromatic ring oxidation and aliphatic chain by-products. Hydroxylation is the main reaction mechanism in the ozonation of ATN under various pH conditions based on identified transformation products.

### 3.5.5.2 Degradation products of Clofibric acid

For CFA, various aliphatic and aromatic photocatalytic degradation products were identified and quantified by multi-step degradation steps. The main transformation pathways for CFA are interconnected pathways and multi-step involving various oxidative and reductive degradation routes. 2-(4-hydroxyphenoxy)-isobutyric acid, Isobutyric acid, hydroxyisobutyric acid, hydroquinone, 4-chlorophenol and 4-

chlorocatechol are some of the photocatalytic degradation products of CFA as per literature (Doll et al., 2004). Some of degradation products were characterized by the use of mass spectra interpretation.

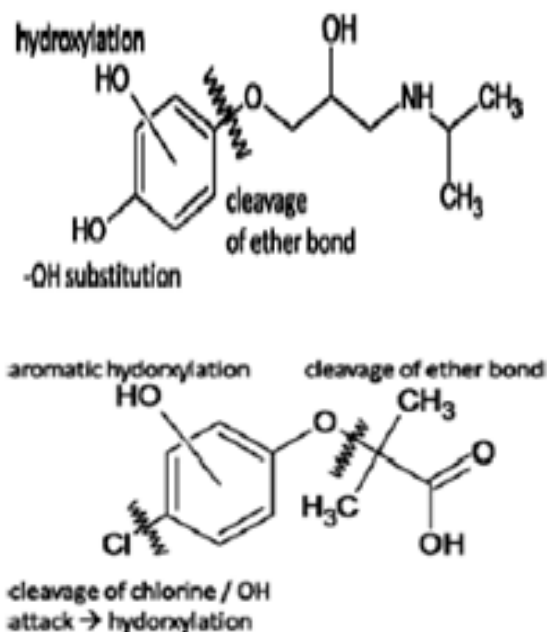


Figure 3.19. Various oxidative and reductive pathways for degradation of CFA

Therefore it indicates that photocatalysis is a powerful tool to mineralize CFA. Another promising technology to degrade CFA is the use of semiconductor photocatalysis. Transformation, deactivation and minimization of persistent compounds are of the goals of the usage of photocatalysis and should enhance biodegradability of pollutants as a treatment step but not complete mineralization. The formation of pharmaceutical by-products at the water treatment is unavoidable and cost-effective treatment is not practicable. In order to optimize each treatment process, by-product evaluation is the key to identify these highly toxic compounds at low levels for assessment of treated water. A combination of O<sub>3</sub>/UV/TiO<sub>2</sub> will be a promising advanced water treatment technique.



### 3.5.5.3 Degradation products of Diclofenac

In diclofenac an initial photocyclization step leads to formation of 1-(8-chlorocarbazolyl) acetic acid. Other carbazole products (Moore et al., 1990; Encinas et al., 1998) are produced subsequently by photodechlorination.

Andreozzi et al., (2003) and Packer et al., (2003) reported photolysis of diclofenac by hydroxyl radical-mediated although singlet oxygen also takes place in some. Both singlet oxygen and hydroxyl radicals act as strong oxidant species that enhances indirect photolysis apart from direct photolysis reported for diclofenac in various studies (Tixier et al., 2003; Andreozzi et al., 2003; Agüera et al., 2005). The log  $K_{OW}$  values calculated for carbazole and diphenyl derivatives and diclofenac are 1.35 to 3.19 ( $\pm 0.47$ ), 3.61 and 5.10 ( $\pm 0.47$ ) and  $4.12 \pm 0.47$  respectively. It was presumed that diphenylamine derivatives are the main reason for enhanced phytotoxicity. The phototransformation products of diclofenac indicated an increase in enhanced toxicity of 5-6 times compared to the parent substance. It was observed that in reversed-phase chromatography, the phototransformation products eluted earlier and were more polar than DCF. Agüera et al., 2005, showed 11 of 13 products as being more hydrophilic than diclofenac based on calculation of log  $K_{OW}$  values for all the decomposition products. In humans, the cyclooxygenase enzyme(s) (COX1/2) were inhibited by diclofenac.

It was observed that formation of photosensitive photolysis products, stable and metastable is linked to decomposition of DCF as 2, 6-dichloroaniline, 2,6-dichlorophenol and 2-chloroaniline, were identified as three new UV-decomposition products of DCF. In the present study, only two photolysis products namely, 2-chloroaniline and 2, 6-dichloroaniline were observed as shown in Figure 3.20a and b.

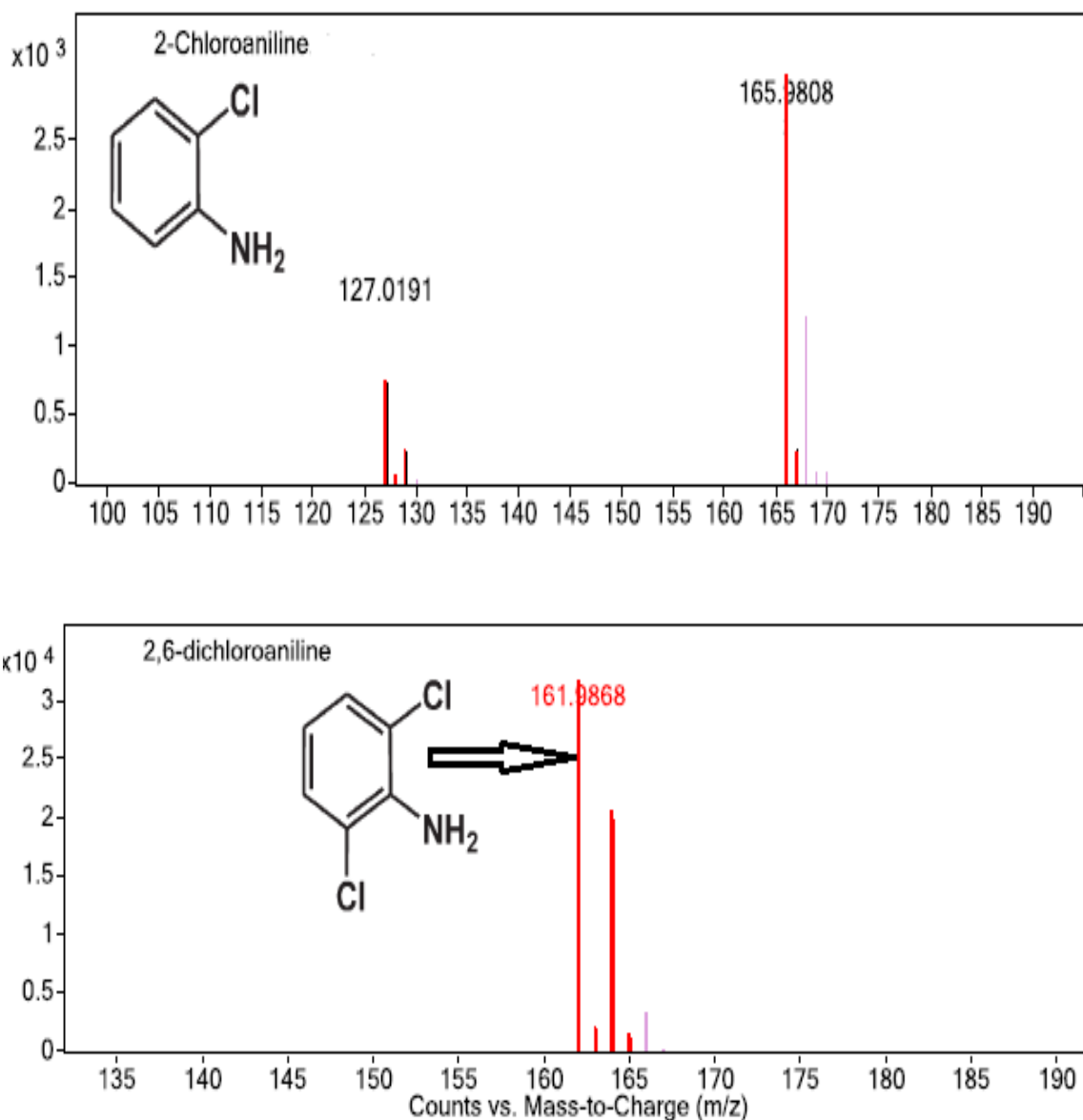


Figure 3.20. (a) and (b) Spectrum of DCF and its transformation products by MS/MS with its proposed structure and molecular ion  $[\text{M}+\text{H}]^+$

The 8-Hydroxy- and 8-Chlorocarbazole derivatives and 2-Chloro- and 2,6-Dichlorodiphenylamine derivatives are the two main substructures among several photochemical decomposition products reported (Moore et al., 1990; Agüera et al., 2005). A rapid  $6\pi$  electrocyclization lead to formation of 8-Hydroxy- and 8-Chlorocarbazole derivatives followed by dehydrohalogenation (Encinas et al., 1998).

## 3.6 Conclusions

Some of the conclusions and future recommendations are

- The kinetics of degradation and optimum reactor conditions will provide useful information for scaling up of AOP for the removal of PPCPs.
- Photodegradation rates will provide an insight to the environmental life time of such chemicals in natural water
- Provide comprehensive information useful for predicting the fate and transport of environmental pollutants.
- Increasing the concentration of HA, Nitrates and Chlorides can be studied further to gather more information on the efficiency of  $O_3/UV/TiO_2$ .
- Immobilization of Degussa P25 catalyst was achieved successfully as a uniform thickness layer of coating could be obtained with 2%, 4% and 20%.
- All the optimized conditions were fed into the reactor for degradation of PPCP compounds [ $O_3=2ppm$ ,  $TiO_2 = 1g/m^2$ ,  $UV = 13W$ ] in secondary effluent.
- A comparison of various AOPs conducted on secondary effluent revealed that  $O_3/UV/TiO_2$  was able to remove 99.9% of ATN in 90 min, 99.5% of CFA in 30min and 99.9% of DCF in 15min respectively. Hence  $O_3/UV/TiO_2$  is considered as the best treatment option for the removal of these PPCP compounds from secondary effluent.
- 100% ATN removal could be achieved in 60 min by increasing the pH from 7 to 9.
- The concentration of organic matter and various ions in secondary effluent had negligible effect in percent removal of ATN, CFA and DCF.

- Increasing the catalyst loadings to 40 – 50% would reduce the number of dip-coating and drying cycles.
- Other PPCP compounds that show very low degradation rates can also be studied for their kinetics.
- Photocatalytic efficiency of O<sub>3</sub>/UV/TiO<sub>2</sub> can be studied further by increasing the NOM concentration to 25, 50, 100 and 250ppm.
- Cost-benefit analysis of preparation of immobilized catalyst and use of O<sub>3</sub>/UV/TiO<sub>2</sub> at an industrial scale is really a challenging task and should be considered.

### 3.7 References

Agüera, A., Pérez Estrada L.A., Ferrer, I., Thurman, E.M., Malato, S., Fernández-Alba, A.R., 2005. Application of time-of-flight mass spectrometry to the analysis of phototransformation products of diclofenac in water under natural sunlight. *J Mass Spectrom.* 40:908–15.

Agustina, T. E., Ang, H. M., Vareek, V. K., 2005. A review of synergistic effect of photocatalysis and ozonation on wastewater treatment. *J. Photoch. Photobio. C.*, 6, 264-273.

American Public Health Association, American Water Works Association, and Water Environment Federation (APHA), 1998. *Standard Methods for the Examination of Water and Wastewater*, 20th ed. American Public Health Association, Washington, DC.

Andreozzi, R., Raffaele, M., and Nicklas, P., 2003. Pharmaceuticals in STP effluents and their solar photodegradation in aquatic environment. *Chemosphere.* 50 (10), 1319–1330.

Bartels, P., Tümpling Jr. v. W., 2007. Solar radiation influence on the decomposition process of diclofenac in surface waters. *Science of the Total Environment*, 374, 143–155.

Beltran, F. J., Rivas, F. J., Gimeno, O., 2005. Comparison between photocatalytic ozonation and other oxidation processes for the removal of phenols from water. *J. Chem. Tech. Biotech.*, 80, 973-984.

Benner, J., Ternes, T.A., Scholz, J., 2009. Ozonation of beta-blockers: kinetic studies, identification of oxidation products and pathways. *Environ. Sci. Technol.* 42, 10–18.

Bickley, R.I., Carreno, T.G., Lees, J.S., Palmisano, L., Tilley, R.J.D., 1991. A structural investigation of titanium dioxide photocatalysts. *J. Solid State Chem.* 92, 178–190.

Brillas, E., Calpe, J. C., Cabot, P., 2003. Degradation of the herbicide 2,4-dichlorophenoxy acetic acid by ozonation catalyzed with  $\text{Fe}^{2+}$  and UVA light. *Appl. Catal. B.*, 46, 381-391.

Canonica, S., Freiburghaus, M., 2001. Electron-rich Phenols for Probing the Photochemical Reactivity of Freshwaters. *Environ. Sci. Technol.* 35, 690.

Castiglioni, S., Bagnati, R., Calamari, D., Fanelli, R., Zuccato, E., 2005. A multiresidue analytical method using solid-phase extraction and high-pressure liquid chromatography tandem mass spectrometry to measure pharmaceuticals of different therapeutic classes in urban wastewaters. *Journal of Chromatography A.* v 1092, n 2, p 206-215.

Chatzisyneon, E., Stypas, E., Bousios, S., Xekoukoulotakis, N.P., Mantzavinos, D., 2008. Photocatalytic treatment of black table olive processing wastewater. *J. Hazard. Mater.* 154, 1090–1097.

ChemIDplus 2014. <http://chem.sis.nlm.nih.gov/chemidplus/> (Date Retrieved: 2014/02/16).

Chin, Y. P., Miller, P. L., Zeng, L., Cawley, K., Weavers, L. K., 2004. Photosensitized Degradation of Bisphenol A by Dissolved Organic Matter. *Environ. Sci. Technol.* 38, 5888.

Christian D., 26 October 2005. "Introduction to Pharmaceuticals and Personal Care Products (PPCPs)," Pollutants of Emerging Concern Panel Series, sponsored by U.S. EPA Region 2, New York, NY.

Crescenzi, C., Corcia, D. A., Marchese, S., Samperi, R., 1995. Determination of acidic pesticides in water by a benchtop LC–ESI-MS. *Anal. Chem.* 67, 1968.

Daughton, C.G., October 2001. Emerging pollutants, and communicating the science of environmental chemistry and mass spectrometry: Pharmaceuticals in the environment. *Journal of the American Society for Mass Spectrometry.* v 12, n 10, p 1067-1076.

Daughton, C., 26 October 2005. "Introduction to Pharmaceuticals and Personal Care Products (PPCPs)," Pollutants of Emerging Concern Panel Series, sponsored by U.S. EPA Region 2, New York, NY.

De Laat, J., Truong, L. G., 2006. Effects of Chloride Ions on the Iron (III) - Catalyzed Decomposition of Hydrogen Peroxide and on the Efficiency of the Fenton-like Oxidation Process. *Appl. Catal., B*, 66, 137.

Doll, E. T., Frimmel, H. F., 2004. Kinetic study of photocatalytic degradation of carbamazepine, clofibrac acid, iomeprol and iopromide assisted by different TiO<sub>2</sub> materials—determination of intermediates and reaction pathways. *Water Research* 38, 955–964.

Emilio, C.A., Litter, M.I., Marinus, K., Bouchard, M., Justin, C.C., 2006. Phenol degradation on platinized-TiO<sub>2</sub> photocatalysts related to charge-carrier dynamics. *Langmuir*. 22, 3606–3613.

Encinas, S., Boscá, F., Miranda, M.A., 1998. Photochemistry of 2,6-dichlorodiphenylamine and 1-chlorocarbazole, the photoactive chromophores of diclofenac, meclofenamic acid and their major photoproducts. *Photochem Photobiol.* 68:640–645.

Farre, M. J., Franch, M. I., Malato, S., Ayllon, J. A., Peral, J., Domenech, X., 2005. Degradation of some biorecalcitrant pesticides by homogeneous and heterogeneous photocatalytic ozonation. *Chemosphere*. 58, 1127-1133.

Gao, H., Zepp, R. G., 1998. Factors Influencing Photoreaction of Dissolved Organic Matter in a Coastal River of the Southeastern United States. *Environ. Sci. Technol.* 32, 2940.

Giri, R. R., Ozaki, H., Taniguchi, S., Takanami, R., 2008. Photocatalytic ozonation of 2, 4-dichlorophenoxyacetic acid in water with a new TiO<sub>2</sub> fiber. *Int. J. Environ. Sci. Tech.*, 5 (1), 17-26.

Halling-Sorensen, B., Nielsen, S.N., Lanzky, P.F., Ingerslev, F., Lutzhoft, H.C.H., and Jorgensen, S.E., Occurrence, fate and effects of pharmaceutical substances in the environment — A review, *Chemosphere* 36 (2), 357–394, 1998.

Hapeshi, E., Achilleos, A., Vasquez, M.I., 2010. Drugs degrading photocatalytically: kinetics and mechanisms of ofloxacin and atenolol removal on titania suspensions. *Water Research* 44 (2010) 1737–1746.

Haque, M.M., Muneer, M., Bahnemann, D.W., 2006. Semiconductor-mediated photocatalyzed degradation of a herbicide derivative, chlorotoluron, in aqueous suspensions. *Environmental Science and Technology*. 40, 4765–4770.

Heberer, T., Schmidt-Baumler, K., Stan, H. J., 1998. Occurrence and Distribution of Organic Contaminants in Aquatic Systems in Berlin. Part I. Drug Residues and Other Polar Contaminants in Berlin Surface and Groundwater. *Acta Hydrochim. Hydrobiol.* 26, 272.

<http://www.epa.gov/nerlesd1/chemistry/pharma> (Date Retrieved: 2015/05/24).

Huovinen, P.S., Penttilä, H., Soimasuo, M.R., 2003. Spectral attenuation of solar ultraviolet radiation in humic lakes in Central Finland. *Chemosphere*. 51:205–14.

Ioannou, L.A., Hapeshi, E., Vasquez, M.I., Mantzavinos, D., Fatta-Kassinos, D., 2011. Solar/TiO<sub>2</sub> photocatalytic decomposition of  $\beta$ -blockers atenolol and propranolol in water and wastewater. *Solar Energy*. 85, 1915–1926.

IMS Health MIDAS, 2014. (Date retrieved: 4<sup>th</sup>, December, 2014).

Ji Y., Zhou, L., Ferronato, C., Yang, X., Salvador, A., Zeng, C., Chovelon, M. J., 2013. Photocatalytic degradation of atenolol in aqueous titanium dioxide suspensions: Kinetics, intermediates and degradation pathways. *Journal of Photochemistry and Photobiology A: Chemistry* 254, 35–44.

Joseph P.D., and Mannervik, B., 2006. *Molecular Toxicology*, New York: Oxford University Press.

Kaneko, M., Okura, I., 2002. *Photocatalysis: Science and Technology*, second ed. Springer, Japan.

Klammerth, N., Miranada, N., Malato, S., Aguera, A., Alba, A. R.F, Maldonado, M. I., Coronado, J. M., 2009. Degradation of Emerging Contaminants at Low Concentrations in MWTPs Effluents with Mild Solar Photo-Fenton and TiO<sub>2</sub>. *Catal. Today*, 144, 124.

Khodja, A.A., Lavedrine, B., Richard, C., Sehili, T., 2002. Photocatalytic degradation of metoxuron in aqueous suspensions of TiO<sub>2</sub>. analytical and kinetic studies. *International Journal of Photoenergy*. 4, 147–151.

Koutsouba, V., Heberer, T., Fuhrmann, B., Baumler, K.S., Tsipi, D., Hiskia, A., 2003. Determination of polar pharmaceuticals in sewage water of Greece by gas chromatography-mass spectrometry. *Chemosphere*. v 51, p69-75.

Li, L., Zhu, W., Chen, L., Zhang, P., Chen, Z., 2005. Photocatalytic ozonation of dibutyl phthalate over TiO<sub>2</sub> film. *J. Photoch. Photobiol. A*. 175, 172-177.

Liu, X., Zhang, T., Zhou, Y., Fang, L., Shao, Y., 2013. *Chemosphere* 93. 2717–2724.

Martin, S.T., Herrmann, H., Choi, W., Hoffmann, M.R., 1994. Timeresolved microwave conductivity. Part 1. TiO<sub>2</sub> photoreactivity and size quantization. *J. Chem. Soc., Faraday Trans. 21*, 3315–3322.

Mohamad, A., 2010. Environmental chemical analysis related to drug industries: Fate monitoring of diclofenac in water/sediment systems. Thesis dated: 08.12.2010.

Moore, D. E., Roberts -Thomson, S., Zhen, D., Duke C. C., 1990. Photochemical studies on the anti-inflammatory drug diclofenac. *Photochem. Photobiol.* 52, 685-690.

- Munter, R., 2001. Advanced oxidation processes: current status and prospects. *Proc. Estonian Acad. Sci., Chem.*, 50(2), 59-80.
- Neamtu, M., Popa, D. M., Frimmel, F. H., 2009. Simulated Solar UV irradiation of Endocrine Disrupting Chemical Octyl phenol. *J. Hazard. Mater.* 2009, 164, 1561.
- Otsuka, K., Smith, C.J., Grainger, J., Barr, J.R., Patterson Jr., D.G., Tanaka, N., Terabe, S., 1998. *J. Chromatogr. A.* 817, 75.
- Ryu, J., Choi, W., 2008. Substrate-specific photocatalytic activities of TiO<sub>2</sub> and multiactivity test for water treatment application. *Environmental Science and Technology.* 42, 294–300.
- Packer, J. L., Werner, J. J., Latch, D. E., McNeill, K., Arnold, W. A., 2003. Photochemical Fate of Pharmaceuticals in the Environment: Naproxen, Diclofenac, Clofibric Acid, and Ibuprofen. *Aquat. Sci.* 65, 342-351.
- Polo, M.S., Utrilla, J. R., Salhi, E., Gunten, v. U., 2006. Removal of bromide and iodide anions from drinking water by silver-activated carbon aerogels. *Journal of Colloid and Interface Science.* 300, 437–441.
- Puig, D., Silgoner, I., Grasserbauer, M., Barcelo', D., 1997. *Anal. Chem.* 69 (14), 2756-2761.
- Quinata, J., Reemtsma, T., 2004. Sensitive determination of acidic drugs and triclosan in surface and wastewater by ion-pair reverse-phase liquid chromatography/tandem mass spectrometry. *Rapid Communications in Mass Spectrometry*, v 18, p 765-774.
- Sánchez-Polo, M., Rivera-Utrilla, J., Salhi, E., von Gunten, U., 2006. Removal of bromide and iodide anions from drinking water by silver-activated carbon aerogels. *Journal of Colloid and Interface Science* 300 (2006) 437–441.
- Santos, J.L., Aparicio, I., Callejon, M., Alonso, E., 2009. Occurrence of pharmaceutically active compounds during 1-year period in wastewaters from four wastewater treatment plants in Seville (Spain). *J. Hazard. Mater.* 164, 1509–1519.
- Santos, T. C. R., Rocha, C. J., Barcelo, D., 2000. Determination of rice herbicides, their transformation products and clofibric acid using on-line solid-phase extraction followed by liquid chromatography with diode array and atmospheric pressure chemical ionization mass spectrometric detection. *Journal of Chromatography A*, 879, 3–12.
- Schmitt-Jansen, M., Bartels, P., Adler, N., Altenburger, R., 2007. Phytotoxicity assessment of diclofenac and its phototransformation products. *Anal Bioanal Chem.* 387:1389–1396 DOI 10.1007/s00216-006-0825-3.
- Sclafani, A., Herrmann, J.M., 1996. Comparison of the photoelectronic and photocatalytic activities of various anatase and rutile forms of titania in pure liquid organic phases and in aqueous solutions. *J. Phys. Chem.* 100, 13655–13661.



- Tay, S. K., Rahman, A. N., Abas, B.R.M., 2011. Characterization of atenolol transformation products in ozonation by using rapid resolution high-performance liquid chromatography/quadrupole-time-of-flight mass spectrometry. *Microchemical Journal*. 99, 312–326.
- Ternes, T., Bonerz, M., Schmidt, T. 2001. Determination of neutral pharmaceuticals in wastewater and rivers by liquid chromatography-electrospray tandem mass spectrometry.
- Tixier, C., Singer, H.P., Oellers, S., Muller, S.R., 2003. Occurrence and fate of carbamazepine, clofibric acid, diclofenac, ibuprofen, ketoprofen, and naproxen in surface waters. *Environmental Science & Technology* 37, 1061-1068.
- Trovo, A. G., Nogueira, R. F. P., Aguera, A., Sirtori, C., Fernandez-Alba, A. R., 2009. Photodegradation of Sulfamethoxazole in Various Aqueous Media: Persistence, Toxicity and Photoproducts Assessment. *Chemosphere*. 77, 1292.
- Turchi, C.S., Ollis, D.F., 1990. Photocatalytic degradation of organic water containments: mechanisms involving hydroxyl radical attack. *J. Catal.* 122, 178–192.
- von Gunten, U., 2003. Review: Ozonation of drinking water: Part II. Disinfection and by-product formation in presence of bromide, iodide or chlorine. *Water Research* 37, 1469–1487.
- Li, W., Lu, S., Qiu, Z, Lin, K., 2011. Photocatalysis of Clofibric Acid under Solar Light in Summer and Winter Seasons. *Ind. Eng. Chem. Res.*, 50, 5384–5393.
- WHO. Guidelines for drinking water quality, 2 ed. Geneva: World Health Organisation, 1996.
- Winkler, M., Lawrence, J. R., Neu, T. R., 2001. Selective Degradation of Ibuprofen and Clofibric Acid in Two Model River Biofilm Systems. *Water Res.* 35, 3197.
- Zeng, C., Ji, Y., Zhou, L., Zhang, Y., Yang, X., 2012. The role of dissolved organic matters in the aquatic photodegradation of atenolol. *J. Hazard. Mater.* 239–240, 340–347.
- Zepp, R.G., Hoigne, J., Bader, H., 1987. Nitrate-induced Photooxidation of Trace Organic Chemicals in Water. *Environ. Sci. Technol.* 21, 443.

## Chapter 4

### 4 Preparation of Indium Oxide nanocubes, porous microspheres, nanoplates and nanocrystals, its characterization and application in degradation of PPCPs from wastewater

#### 4.1 Introduction

In the last century, society, through either industry, agriculture or in households, used more than 100,000 chemicals that entered the environment without a proper assessment of the direct or indirect consequences and health effects on humans. Even though environmental risk assessment (ERA) has been catching up with these chemicals since the mid-1980s, it is now known that drugs were not included in these studies. Hence there is a need to know the occurrence, the fate and the effect of approximately 4000 medical compounds that are being used in drugs today and their ERA. These drugs are not readily biodegradable, are biologically active and have high water solubility.

For the present study, Atenolol, Clofibric acid and Diclofenac are the three pharmaceutical and personal care products (PPCPs) studied in detail for assessment of their degradation and its kinetics in the environment. According to the rankings of active pharmaceutical ingredients (APIs) present in sewage in Germany in 2005 based on a threshold of 6 t, Diclofenac ranks 15<sup>th</sup> with input of 16.2 t, while Atenolol ranks 31<sup>st</sup> with input of 8.3 t. It was also observed that according to the consumption of selected pharmaceuticals in Germany on a nation-wide (Kummerer et al., 2008, excretion rate not included) atenolol ranked 12<sup>th</sup> with 8.7 t consumption for the population and with 0.11 g per capita and 0.7 % yearly share. In comparison, a local catchment, AZV Breisgauer Bucht, shows atenolol at 5<sup>th</sup> ranking with 145.5 t consumption and 0.43 g per capita and 2.2 % yearly share. In a study conducted by Heberer and Feldmann (2005), it was found that in total, 2.0 kg per week of the anti-epileptic drug carbamazepine (105 kg per year) and 4.4 kg per week of the nonsteroidal

anti-inflammatory drug diclofenac (226 kg per year) were discharged into Berlin's surface water.

Most of the pharmaceuticals and personal care products (PPCPs) are resistant to conventional treatment processes. These compounds are discharged into the environment and are subjected to the same potential transport and degradation processes as other organics such as herbicides, (poly) aromatic compounds, solvents, polychlorinated biphenyls and insecticides. In general, most of these PPCPs enter the aquatic environment after passing through the human and animal digestive systems and are modified by a biochemical metabolism and if they are resistant to acid- and enzyme-promoted hydrolysis reactions, then they are released into the environment unaltered (Arnold and McNeill, 2003).

Two most important metabolic enzymes oxidize drugs that are present in the bodies, but differ in their substrate scope and product distribution namely, Cytochrome P450 located in the liver hydroxylates C-H bonds and widely distributed monoamine oxidase (MAO) deaminate primary and secondary amines oxidatively. For example, pharmaceuticals such as misoprostol and aspirin are not released into the environment in their parent form as these compounds are rapidly hydrolyzed in the stomach. Metabolic enzyme-mediated oxidation processes has been observed in tolbutamide, a drug used to treat diabetes, and epinephrine, which lead to additional pharmaceutical species being released into the environment (Thomas and Ikeda, 1966; Blashko, 1954). Cytochrome P450 has been estimated to metabolize over half of all drugs (Guengerich, 2006).

Several semiconductor materials, such as  $\text{Ga}_2\text{O}_3$ ,  $\text{ZnS}$  and  $\text{NiO}$  have been screened previously. It has been found that Indium oxide ( $\text{In}_2\text{O}_3$ ) is more effective in the decomposition of perfluorooctanoic acid (PFOA) under UV irradiation than titanium dioxide ( $\text{TiO}_2$ ).  $\text{In}_2\text{O}_3$  has a direct bandgap of 3.55-3.75 eV (Liang et. al., 2001) at room temperature, which is close to that of  $\text{GaN}$  and is an n-type semiconductor. In recent years  $\text{In}_2\text{O}_3$  has garnered much attention due to its wide bandgap and has attracted many applications in photocatalysis (Li et. al., 2006), nanoscale biosensors (Curreli et.

al. 2005), holographic recorders (Maillis et. al., 1996), field-emission and flat panel displays, thin film transistors (Lavareda et. al., 2006), electro-optic modulators, optoelectronics, lithium ion battery (Kim et al., 2007), gas sensor (Bianchi et al., 2006), as window heater in the electronic field, nanoelectronic building blocks, electrochromic mirrors (Gurlo et. al, 1997, Soulantica et. al., 2003 and Zhang et. al., 2003) and solar cells (Manifacier et. al., 1979).

Table 4.1. Comparison of various types of  $\text{In}_2\text{O}_3$  nanostructures produced by different methods comprising of all three phases, namely, the solution, solid and vapor phase and their properties

| <b>Type</b>                            | <b>Method</b>                   | <b>Properties</b>   | <b>References</b>     |
|--|---------------------------------|---|-----------------------|
| Nanospheres                            | Titania / Indium Oxide          | photo catalytically active, degrades 2-chlorophenol effectively | Shchukin et al., 2004 |
| 1-D nanostructures                     | vapor-solid mechanism           | optoelectronic properties                                       | Zhang et al., 2003    |
| Nanowires                              | carbothermal reduction reaction | photo luminescent   | Wu et al., 2003       |
| Nanofibers                             | electro-spinning                | optical   | Zhang et al., 2007    |
| Nanocubes                              | precipitation                   | NA  | Maqueda et al., 1998  |
| Whiskers and bi-pyramidal nanocrystals | carbothermal                    | $\text{H}_2\text{S}$ gas sensors                                | Kaur et al., 2008     |
| Nanobelts                              | physical vapor deposition       | NA  | Jeong et al., 2004    |

|   |                                |  |                      |
|---|--------------------------------|--|----------------------|
| Oxide films                                       | electrochemical deposition     | NA   | Ho et al., 2006      |
| Porous oxide thin films                           | electrostatic spray deposition | NA   | Ghimbeu et al., 2008 |
| Nanocrystals                                      | simple solution routes         | NA   | Chu et al., 2007     |
| Single crystalline nano pyramids and nano columns | Direct                         | photoluminescence                            | Guha et al., 2004    |
| Porous microsphere, nanocubes and nanoplates      | solvothermal process           | degrades perfluoro-octanoic acid effectively | Li et al., 2013      |
| Nanometer-sized particles                         | reverse micro emulsion         | NA   | Zhan et al., 2004    |

NA = Not Available

$\text{In}_2\text{O}_3$  nanostructures have been created by various methods to date, such as hollow spheres, lotus-root-like nanostructures, hierarchical microspheres and flower-like microstructures. Various synthesis methods that were utilized include using plant extract solution of aloe vera and indium acetylacetonate, and a novel synthesis of  $\text{In}_2\text{O}_3$  nanoparticles with particle sizes of 5-50 nm by Maensiri et al., (2008). Similarly, RAPET (reaction under the autogenic pressure at elevated temperature) method was employed by George et al., (2008) for preparing  $\text{In}_2\text{O}_3$  nanocrystals of average thickness 48 nm and average length 60 nm. Though various methods were utilized in the preparation of  $\text{In}_2\text{O}_3$  as shown in the Table 4.1 there is still a requirement to produce small particle sizes of high purity, homogeneity, non-toxicity, simplicity and cost effectiveness at low temperatures. In addition, there is the need to synthesize the nanostructured materials in such a way that the characteristics of the synthesis depends on the size, shape and size distribution of small units.

Due to its high electrical conductivity and high transparency in the visible region, the current motivation is to use indium oxide nanoparticles to investigate the removal of selected PPCPs from wastewater by the transparent conducting oxides (TCOs) approach.

## 4.2 Materials and Methods

### 4.2.1 Reagents and chemicals

Indium (III) nitrate hydrate, 99.99%, 1, 2-Diaminopropane, 98% and 1, 3-Diaminopropane, 98% were purchased from Alfa Aesar. Atenolol (ATN), Clofibric Acid (CFA), Diclofenac Sodium (DCF), Titanium Dioxide Degussa P25 and nitrocellulose membrane filters (pore size 0.22 $\mu$ m and diameter 47mm) were purchased from Sigma Aldrich. Ethanol was purchased from chemistry stores at the University of Western Ontario. 100mL PTFE liner was purchased from Parr Instruments, USA.

Exactly 10,000mg/L of individual stock solutions of ATN and CFA and 1,000mg/L of DCF were prepared in high purity water by weighing on the Mettler balance to 0.0001g and made up to the desired volume and stored at -20<sup>0</sup>C. A 10mg/L working solution was obtained by spiking a known aliquot of stock solution to 1L of secondary effluent. All aqueous solutions including 1M hydrochloric acid (HCl) and 1M sodium hydroxide (NaOH) were prepared with high purity water produced with a Thermo Barnstead Nanopure System (Thermo Fischer Scientific, Whaltman, MA, USA).

### 4.2.2 Experimental Methodology

Two different methods were employed to prepare In<sub>2</sub>O<sub>3</sub> nanostructures from In(NO<sub>3</sub>)<sub>3</sub>·4.5H<sub>2</sub>O and a comparison is performed on their removal efficiencies of PPCPs from wastewater.

#### 4.2.2.1 Synthesis of $\text{In}_2\text{O}_3$ from $\text{In}(\text{NO}_3)_3 \cdot 4.5\text{H}_2\text{O}$ via $\text{In}(\text{OH})_3$ by Solvothermal process

A solvothermal process as per Li et al., 2013 has been used in the synthesis of various  $\text{In}(\text{OH})_3$  nanostructures. In the synthesis of  $\text{In}(\text{OH})_3$  nanocubes, 34 mL of water was added to dissolve 1.77mmol of  $\text{In}(\text{NO}_3)_3 \cdot 4.5\text{H}_2\text{O}$ . While continuously stirring on a magnetic stirrer, 34mL of 1, 2-propanediamine was added to the above solution.



Figure 4.1. Stainless steel autoclave used to synthesize nanocubes, nanoplates and porous microspheres in Parr reactor at  $180^\circ\text{C} \pm 2^\circ\text{C}$  for 16h

The mixture was then transferred to a 100mL teflon lined stainless steel autoclave after stirring for 15 min. The Parr instrument (Parr 4848 reactor controller) was set at  $180^\circ\text{C} \pm 2^\circ\text{C}$  for  $16\text{ h} \pm 1\text{ h}$  after sealing the autoclave as shown in Figure 4.1. Once the reaction was complete, the autoclave was naturally allowed to cool to room temperature and after centrifugation, the white precipitate of  $\text{In}(\text{OH})_3$  was collected, washed several times with high purity deionized water and ethanol. Similarly,  $\text{In}(\text{OH})_3$  porous

microsphere was synthesized using the same procedure as above except the solvent was changed to ethanol and 1, 2-propanediamine whereas  $\text{In}_2\text{O}_3$  nanoplates was synthesized similarly except the solvents used were water and 1,3-propanediamine (Li et al., 2013).

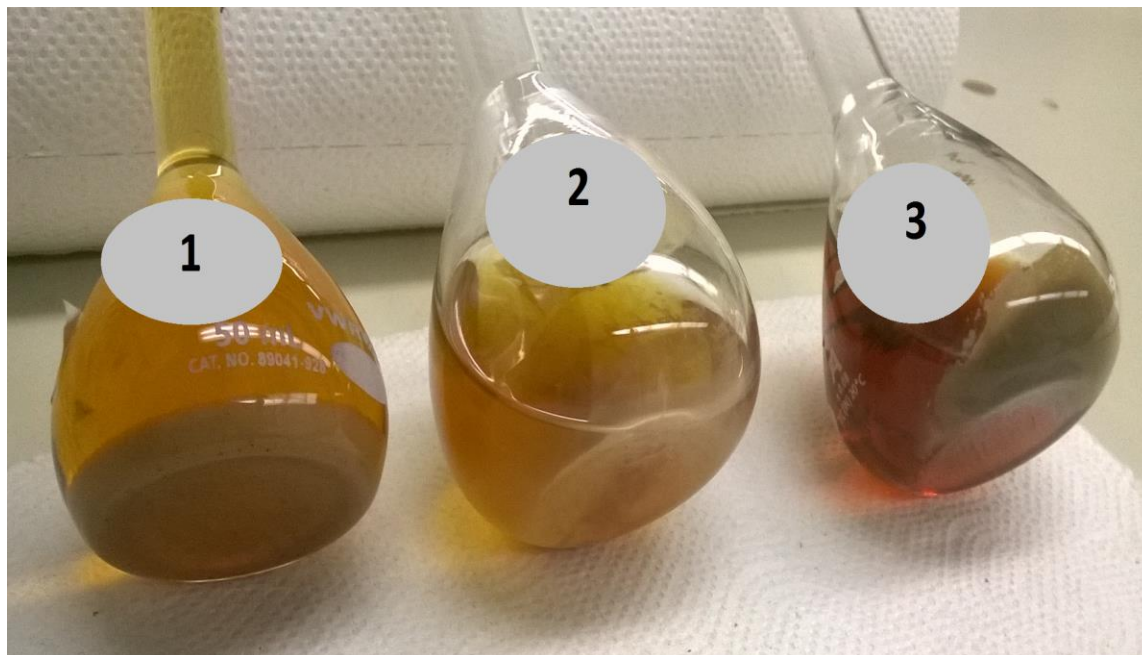


Figure 4.2. Precipitates of 1) porous microspheres (MS) 2) nanocubes (NC) and 3) nanoplates (NP), obtained after autoclaving in Parr reactor at  $180^\circ\text{C} \pm 1^\circ\text{C}$ .

Precipitates of  $\text{In}(\text{OH})_3$  nanocubes (NC), nanoplates (NP) and porous microspheres (MS) obtained as shown in Figure 4.2 were dried at  $60^\circ\text{C}$  for 2 h. After complete drying, the particles were ground to a powder with mortar and pestle and calcined.

#### 4.2.2.2 Formation of $\text{In}_2\text{O}_3$ nanocubes, nanoplates and porous microspheres

$\text{In}(\text{OH})_3$  synthesized from the above procedure were later calcined by loading it onto small quartz boats and placed in a muffle furnace. The furnace temperature was raised to  $500^\circ\text{C}$  at a rate of  $1^\circ\text{C}/\text{min}$  and the temperature was maintained at  $500^\circ\text{C}$  for 2 h in air. The furnace was later cooled to room temperature and the resulting light yellow color



of  $\text{In}_2\text{O}_3$  was formed as shown in Figure 4.3. During calcination, the hydroxyl group was removed from indium hydroxide in the form of water vapor leading to the formation of oxygen vacancy as given in Eq. 4.1.

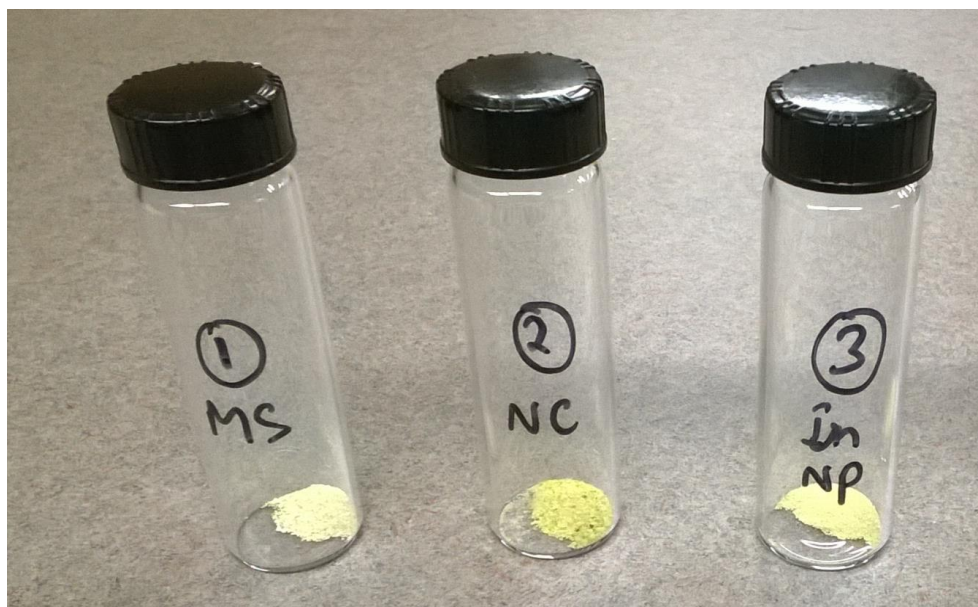
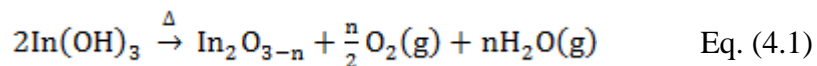
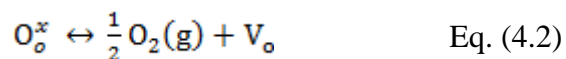


Figure 4.3. Formation of  $\text{In}_2\text{O}_3$  after calcination at  $500^\circ\text{C}$  for 2h producing 1) MS, 2) NC and 3) NP

The formation of oxygen vacancies is depicted in Eq. 4.2 as a result of some of the lattice oxygen released in the form of oxygen gas.



The formed neutral oxygen vacancies can be either ionized singly ( $\text{V}_\text{o}^\cdot$ ) Eq. 4.3 or doubly ( $\text{V}_\text{o}^{\cdot\cdot}$ ) Eq. 4.4 according to notation by Kröger-Vink (Cao et al., 2003 and Harvey et al., 2006), where  $e^-$  represents an electron in the conduction band,  $\text{O}_\text{o}^\times$  is an oxide anion in a regular lattice site and  $\text{V}_\text{o}$  is the neutral oxygen vacancy.



Electron Paramagnetic Resonance (EPR) analysis can be used to reveal the nature of oxygen vacancy in the synthesized  $\text{In}_2\text{O}_3$  nano-particles (Seetha et al., 2009).

#### 4.2.2.3 Preparation of $\text{In}_2\text{O}_3$ nanocrystals from $\text{In}(\text{NO}_3)_3 \cdot 4.5\text{H}_2\text{O}$ by a simple co-precipitation method

A 0.025 mol ratios of  $\text{In}(\text{NO}_3)_3 \cdot 4.5\text{H}_2\text{O}$  was prepared as per Chandradass et al., 2011 by dissolving it in 50 mL distilled water while continuously stirring on a magnetic plate at room temperature for half an hour. To this solution, ammonium hydroxide was added slowly until the pH was 9. Figure 4.4 shows the white precipitate obtained after washing several times with ethanol and dried in the oven for 24h at  $80^\circ\text{C}$ . The dried powder was then transferred to an alumina crucible and calcined at  $400^\circ\text{C}$  by raising the temperature at the rate of  $1^\circ\text{C}/\text{min}$  in an air temperature (Chandradass et al., 2011) and maintained it at that temperature for 2 hrs before cooling down to room temperature.



Figure 4.4. White precipitate of  $\text{In}(\text{NO}_3)_3 \cdot 4.5\text{H}_2\text{O}$  after co-precipitation followed by drying at  $80^\circ\text{C}$  for 24h.

The yellow nanoparticles as shown in Figure 4.5 thus obtained are further characterized for their activity.



Figure 4.5. Yellow  $\text{In}_2\text{O}_3$  nanocrystals obtained after calcination at  $400^\circ\text{C}$  for 2h.

#### 4.2.2.4 Characterization

The obtained  $\text{In}_2\text{O}_3$  nanocubes, nanoplates, porous microspheres and nanocrystals were characterized as per Table 4.2 shown.

Table 4.2. Characterization of various types of  $\text{In}_2\text{O}_3$  using various equipment types

| Equipment  | Characterization                    |
|--|-------------------------------------|
| High resolution-scanning electron microscopy (Leo-Zeiss, 1540XB FIB/HR-SEM)                          | Surface morphology                  |
| Energy-dispersive X-ray spectroscopy (EDX)   | Elemental composition               |
| Fourier transform infrared spectrometer (FTIR) Bruker Tensor II system with Hyperion 2000 microscope | Identification of functional groups |

The surface morphology was characterized using Leo (Zeiss) 1540XB FIB/SEM. The samples were prepared for micromachining using Focused Ion Beam (FIB) by sputter milling which can be monitored with the help of electron column at high resolution in real time where sub-100nm resolution can be achieved by selective etching or material deposition with appropriate gas precursor. FIB was used for sectioning of samples in-situ and the prepared milled samples were imaged by SEM.

The samples were analyzed directly by FTIR spectroscopy in the range from 500 – 4000  $\text{cm}^{-1}$  using platinum-attenuated total reflectance accessory equipped with a diamond crystal in the Bruker Tensor II main box. This experimental setup allows one to analyze an area of approximately 2mm x 2mm to a depth of 0.6-5 microns.

#### 4.2.2.5 Photocatalytic procedures

Approximately 20 L of secondary effluent (SE) from Adelaide Pollution Control Plant, London, ON, Canada was collected by grab method, filtered through 0.22 $\mu\text{m}$  filter paper and stored in 1 L amber colored bottles. Approximately 5-8 drops of 25% (w/v) sodium thiosulphate were added to each bottle, shaken well and preserved at 4°C for further analysis. All the experiments with secondary effluent were performed with and without the addition of PPCPs by adjusting the pH to 7.0 with 1M HCl, and the temperature was maintained at  $23 \pm 1^\circ\text{C}$ . In another set of experiments, the effect of pH at 3 was also investigated following the same steps as above with both secondary effluent and distilled water.

To 1000mL of sample, 0.1 g of  $\text{In}_2\text{O}_3$  catalyst was suspended at a pH adjusted to 7 and was stirred continuously to ensure adsorption–desorption equilibrium by complete mixing in the dark for 1h before irradiation. In the meantime, a 13 W low-pressure mercury lamp with UV light emitting at 254 nm was kept for warm-up to stabilize the lamp for 15 min. The suspension was then transferred into a tubular quartz reactor vessel and a known aliquot from the individual stock solution was spiked to obtain a known concentration of the mixed PPCP compounds while stirring continuously. A

cooling water jacket was kept around the reactor to maintain a constant temperature. During the whole reaction, oxygen was purged continuously at the flow rate of 60mL/min into the reactor. After stabilization, the lamp was kept in the center of the reactor with a protection of two-layer quartz tubes. Immediately 5mL of sample was withdrawn at regular intervals of 0, 5, 15, 30, 60 and 90 minutes respectively into amber glass vials after UV irradiation. The vials were spiked with 2-3 drops of sodium thiosulfate, mixed and stored under -20°C for further LC-MS/MS analysis. Under the same experimental conditions, another set of experiments were conducted with TiO<sub>2</sub> (Degussa P25) as reference. The photocatalytic activity of In<sub>2</sub>O<sub>3</sub> nanoparticles was compared with the photocatalytic activity of TiO<sub>2</sub> under the same experimental conditions. The effect of pH was also investigated by altering the solution pH to 3 with 1 M hydrochloric acid and followed the same experimental procedure under the same conditions as above. Another set of experiments were conducted for NCY following the same procedure as above and a comparison was made between secondary effluent and distilled water.

#### 4.2.2.6 Quantification of PPCPs by LC-MS/MS

The concentrations of various PPCPs in secondary effluent were determined by Agilent 1290 (HPLC), 6460 LC-MS/MS. An auto sampler injector with an injection volume of 5 µL was passed through a Poroshell 120 EC- C18 2.7µm (3.0 x 150mm) column for separation of various analytes. Mobile phase A (10mM ammonium formate and 0.1% formic acid in water) and mobile phase B (0.1% formic acid in acetonitrile) were used for the analysis with a flow rate of 0.35 mL/min. A positive and negative ion electrospray interface (ESI) mode with Agilent 6460 LC-MS/MS was used in the PPCP analysis. A computer based software Mass Hunter, version B.05.01 was used to process the data by peak area method for the acquired chromatograms.

By using linear regression, a six-point calibration curve was developed for each compound ranging from 0 to 200ng/mL as shown in Appendix 13 for ATN, Appendix 14 for CFA and Appendix 15 for DCF. R<sup>2</sup> values has a linearity range between 0.99 –

0.999 for all the compounds with RSD values lower than 10%. Percent recoveries ranged from 90 to 100 % for the effluent matrix. The concentration of the unknown is calculated by using regression analysis of calibration standard.

## 4.3 Results and discussion

### 4.3.1 Morphology and crystal structure of calcined $\text{In}_2\text{O}_3$ samples

The synthesized particles were analyzed by Leo (Zeiss) 1540XB FIB/SEM for surface morphology. The images for microspheres as shown in Figure 4.6 confirm to the formation of hollow spheres with diameters in the range from ~50nm to ~250nm composed of several nanoparticles with diameters between ~10-20nm.

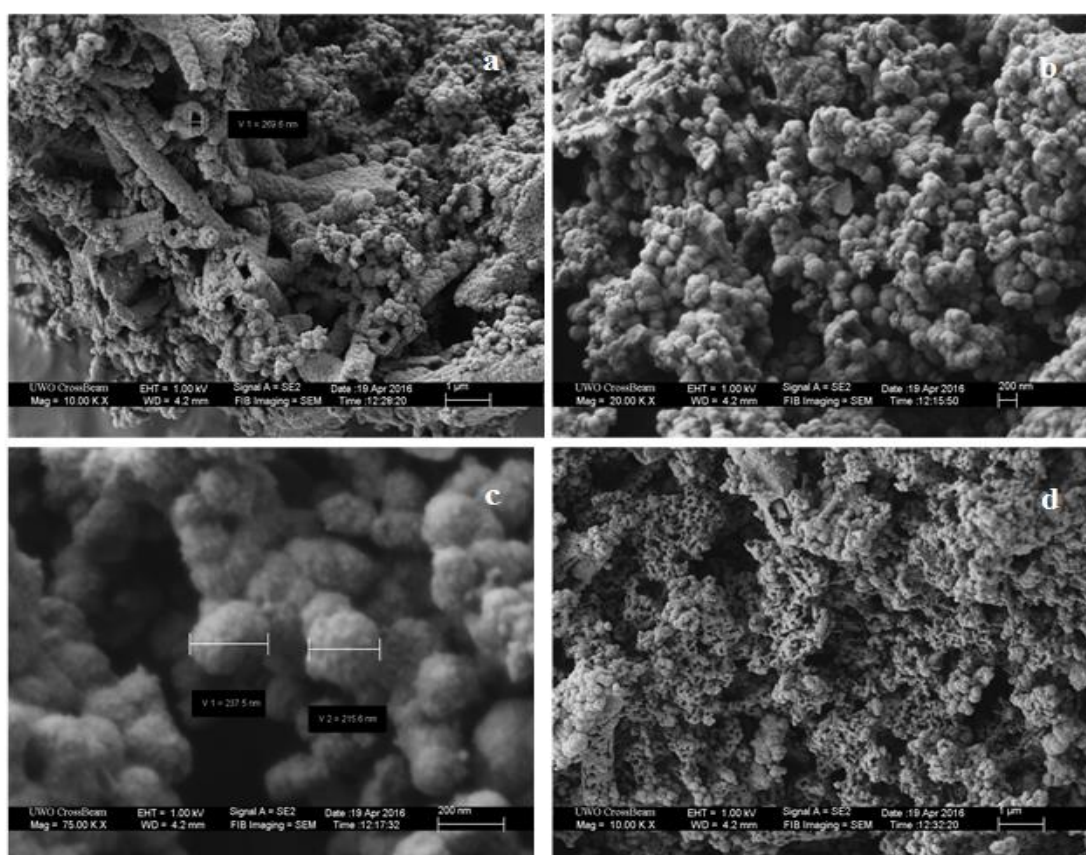


Figure 4.6. (a, b, c and d). Leo (Zeiss) 1540XB FIB/SEM images of microspheres

The formed spheres look rugged as they are arranged randomly to form porous structures and nano particles aggregated and became larger during calcination. Figure 4.7 shows formation of nanocube-like aggregates with ~50 to ~100nm with several oriented cube-like shapes and some interstices due to self-assembly process. During calcination, the interstices in  $\text{In}(\text{OH})_3$  nanocubes collapse due to loss of water into small fractures that become agglomerated and as a result the morphology distorts. In spite of its distortion, most of these particles exhibited cube-like shapes with each cube containing several nanoplates.

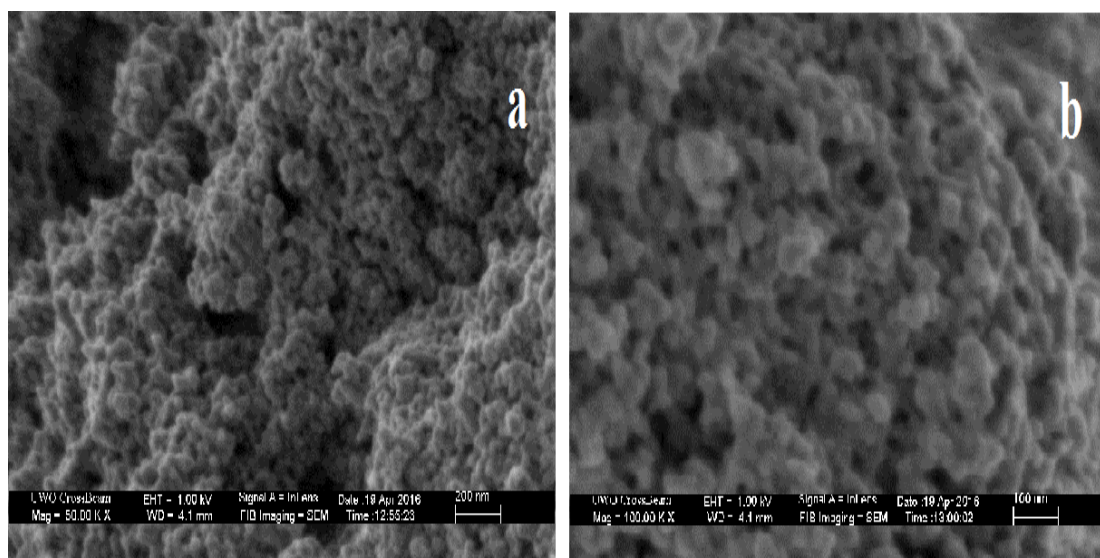


Figure 4.7. (a and b). Leo (Zeiss) 1540XB FIB/SEM images of nano cubes at 1kV

Figure 4.8 shows several nano plates with some interstices in between them due to loss of water during calcination with each nano plate composed of several smaller sizes of nano crystals. These nano plates have a side length of ~ 10-25nm with an edge length of ~ 25-50nm.

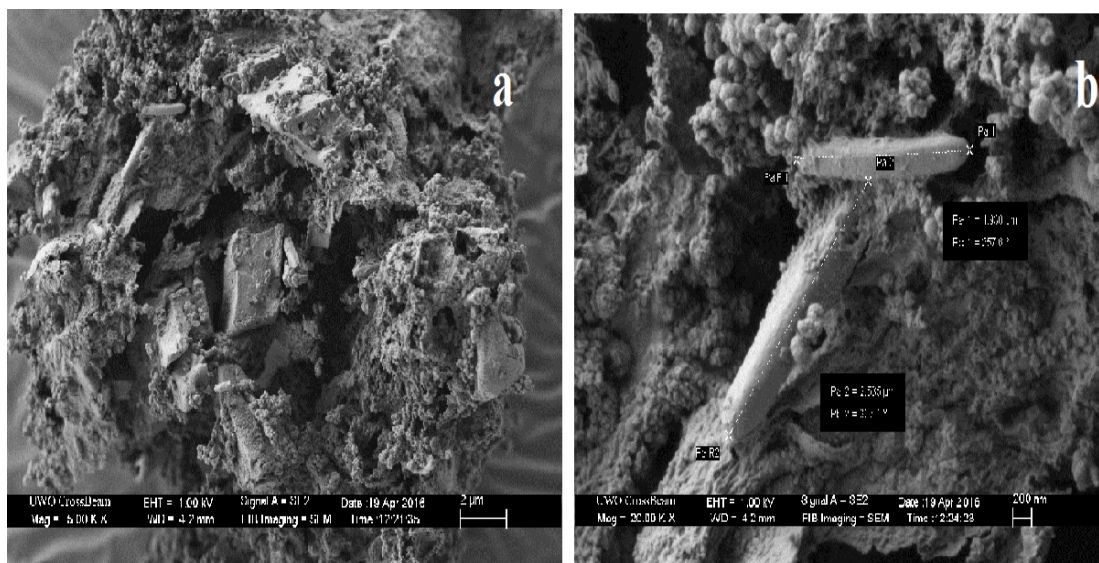


Figure 4.8. (a and b). Leo (Zeiss) 1540XB FIB/SEM images of nano plates

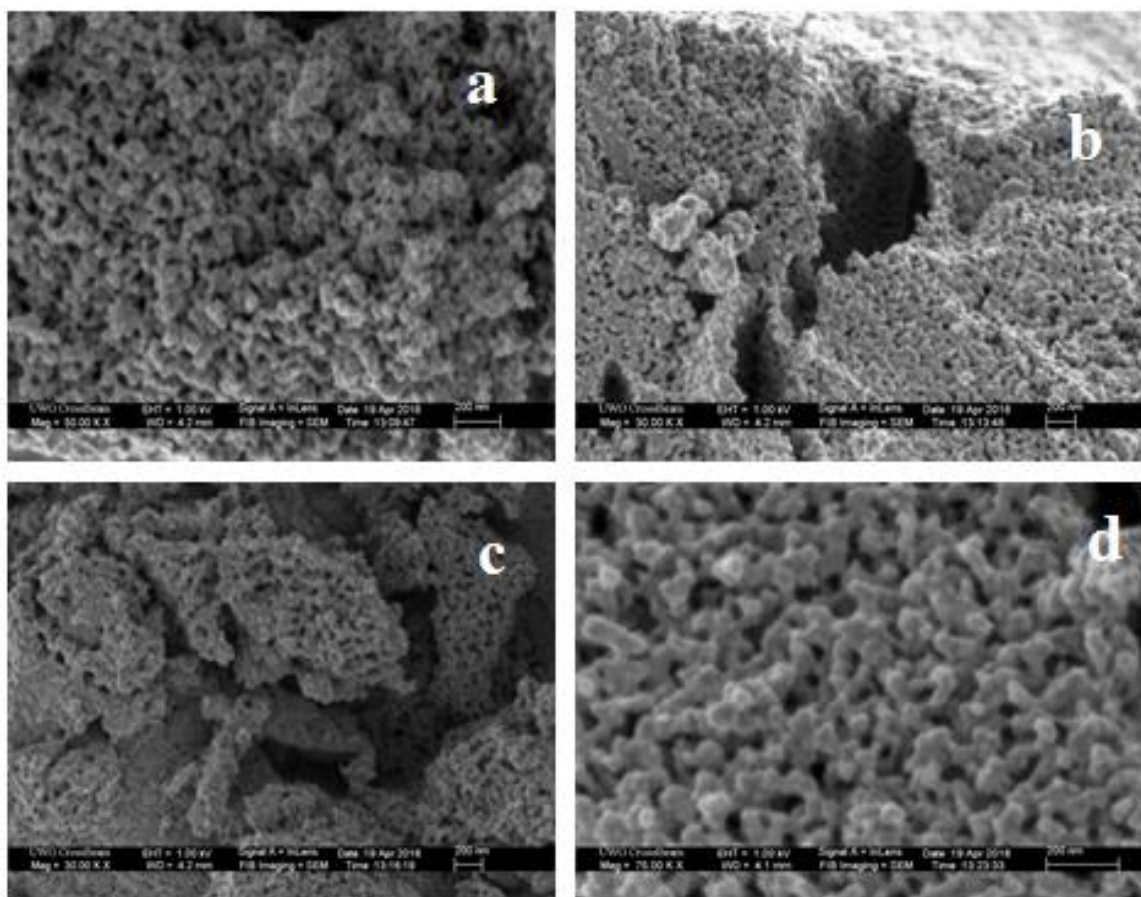


Figure 4.9. (a, b, c and d) Leo (Zeiss) 1540XB FIB/SEM images of nano crystals



Figure 4.9 shows the nano crystals containing definite shapes of some nano rods formed with around side length of 30 to 50nm after calcination with some interstices in between them. Initially small spherical nano crystals are formed as a result of nucleation and finally large crystalline nanorods are formed as the particles size grows and due to adhesion of the neighbouring nanoparticles at some point of time (Sarkar et al., 2009). Some of the shapes are not spherical but they are hexagonal in shape.

### 4.3.2 FTIR spectra of calcined and AOP treated samples

The FTIR spectra provide the chemical composition for the change in shifts and acts as a powerful tool for identifying and analyzing organic compounds. FTIR spectra for the four different nano particles obtained after calcination was carried out in the spectral range from  $4000\text{-}500\text{cm}^{-1}$  and is compared against the spectra of Advanced Oxidation Process (AOP) treated with PPCP compounds of ATN, CFA and DCF after photolysis.

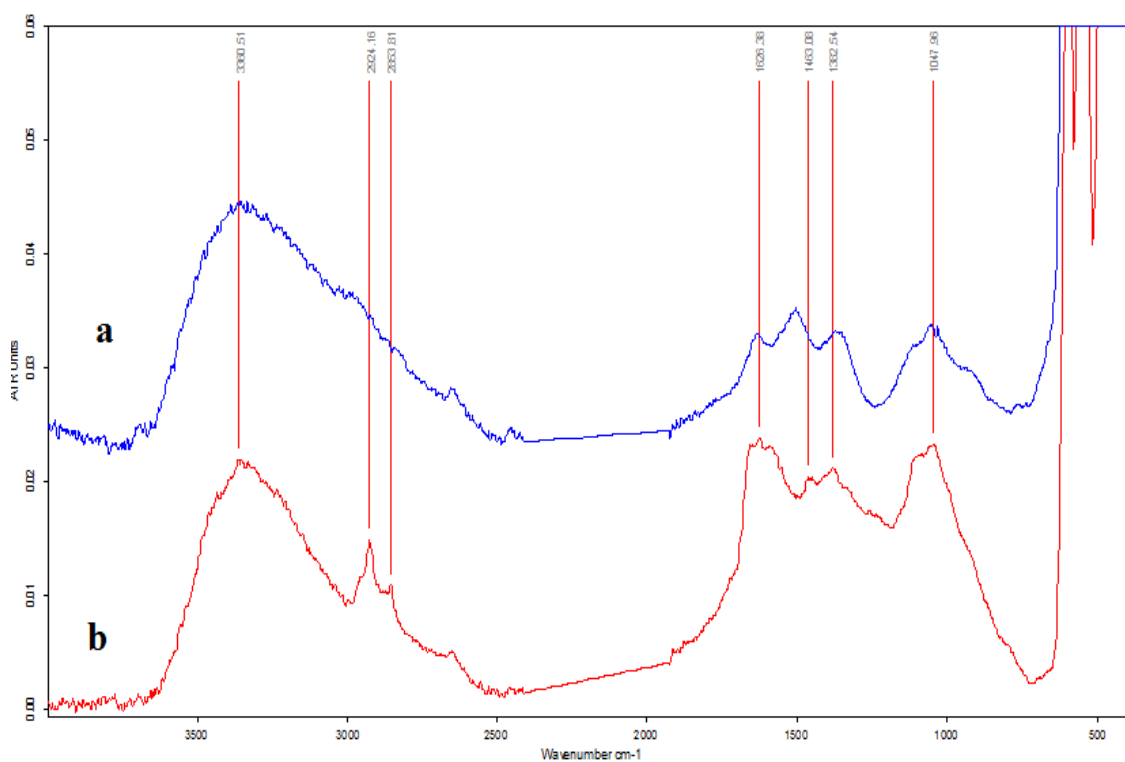


Figure 4.10. FTIR spectra of  $\text{In}_2\text{O}_3$  microspheres calcined at  $500^\circ\text{C}$  for 2h (a) before AOP treatment and (b) after AOP treatment of PPCPs.

Figure 4.10 shows the IR spectra of before and after AOP treatment of  $\text{In}_2\text{O}_3$  microspheres calcined at  $500^\circ\text{C}$ . Table 4.3 lists the microsphere peaks obtained after AOP treatment of ATN, CFA and DCF with UV. These peaks are interpreted with standard peaks with their surface groups of FTIR. It was found that at  $3360\text{cm}^{-1}$ , a large absorption band was observed at that wavenumber which is characteristics of hydrogen bonds (H-bonded O–H stretching vibrations) occurring among hydroxyl groups or water molecules adsorbed on nano particles surface. The nitrate group shows an absorption band at  $1382\text{cm}^{-1}$  (Singh et al., 2003) and  $\text{NH}_2$  in-plane bending and/or asymmetric  $\text{CO}_2$  stretch at  $1626\text{cm}^{-1}$ .

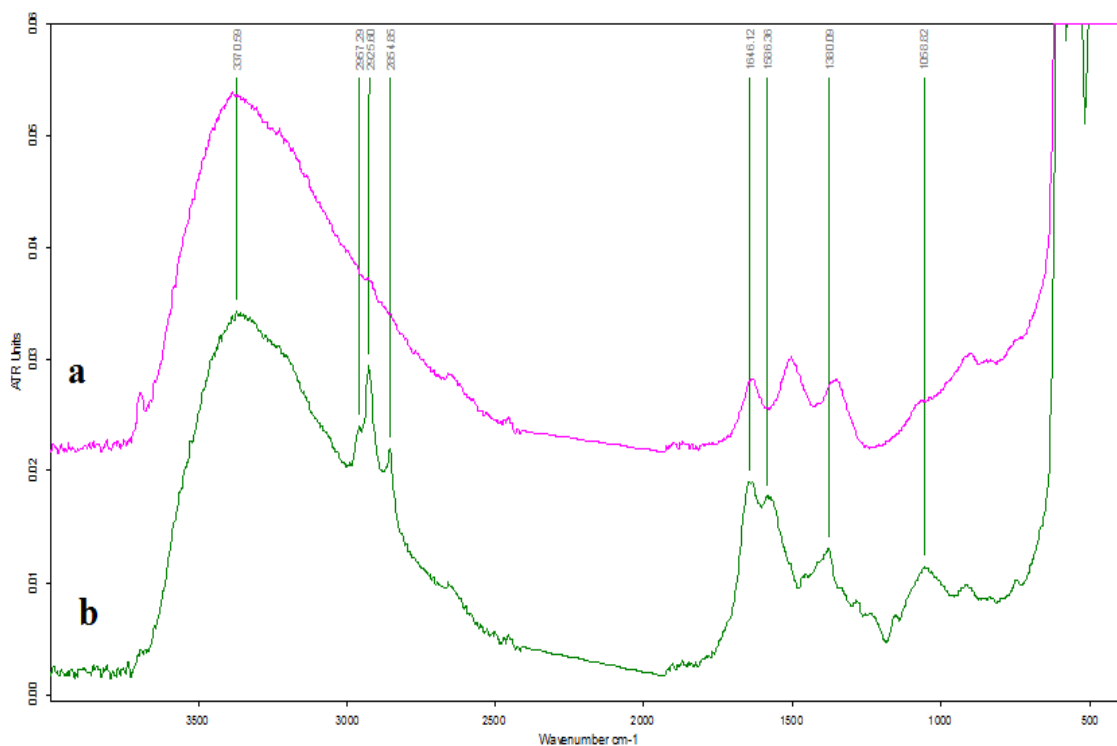


Figure 4.11. FTIR spectra of  $\text{In}_2\text{O}_3$  nano cubes calcined at  $500^\circ\text{C}$  for 2h (a) before AOP treatment and (b) after AOP treatment of PPCPs.

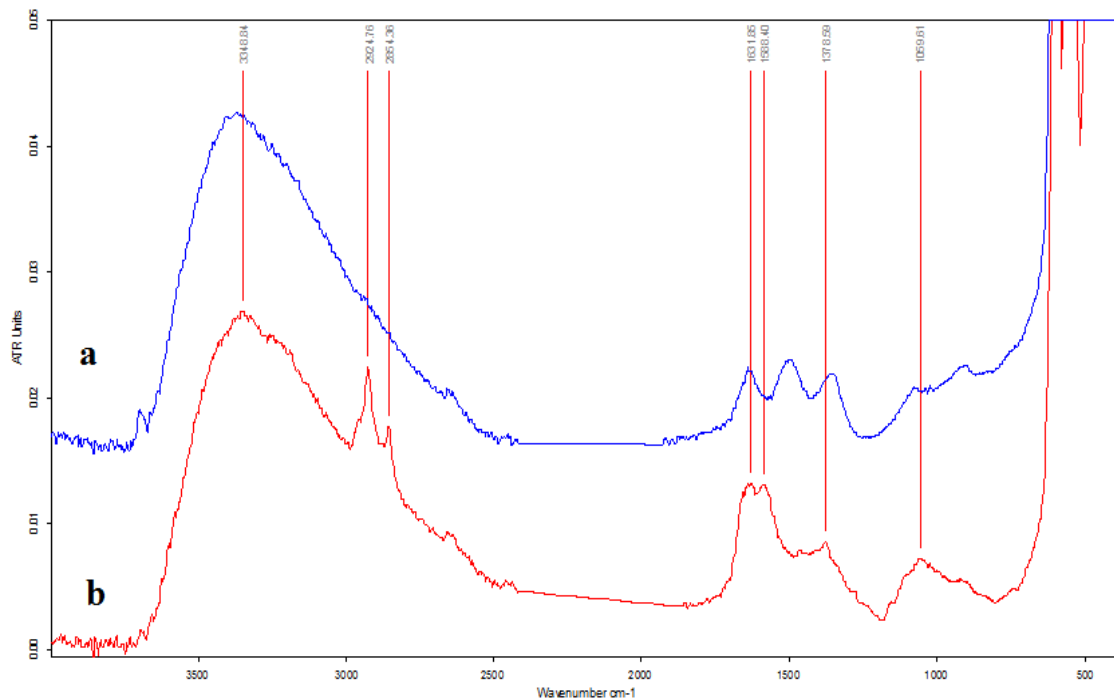


Figure 4.12. FTIR spectra of  $\text{In}_2\text{O}_3$  nano plates calcined at  $500^\circ\text{C}$  for 2h (a) before AOP treatment and (b) after AOP treatment of PPCPs.

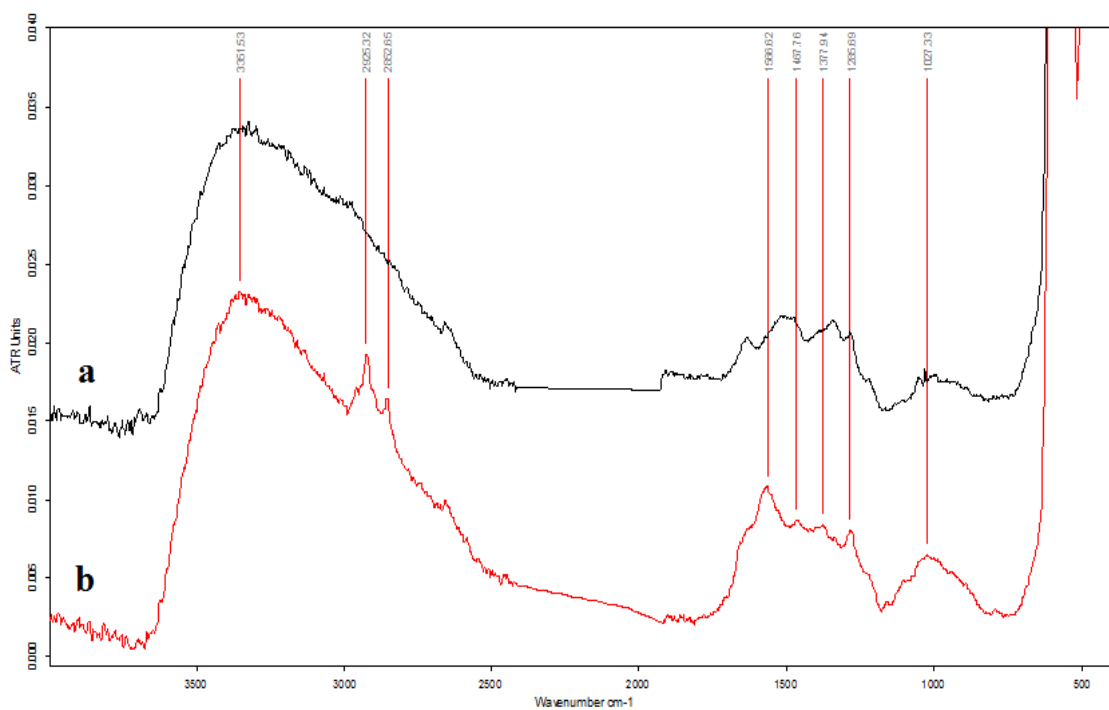


Figure 4.13. FTIR spectra of  $\text{In}_2\text{O}_3$  nano crystals calcined at  $400^\circ\text{C}$  for 2h (a) before AOP treatment and (b) after AOP treatment of PPCPs.

Figure 4.11, 4.12 and 4.13 shows the presence of CO<sub>2</sub> and OH vibrations due to the absorption of moisture from atmosphere after calcination. Aliphatic C-H stretching at increased temperature results in aliphatic loss as represented by FTIR bands at 2850-2950 cm<sup>-1</sup>. It was also observed that C-O, C-C and C=C stretching takes place. Thus it can be seen that as the temperature is increased to 400 or 500°C for calcining the samples, the functional groups also changes (Lee et al., 2010). Finally a summary of all the synthesized nano materials are listed in Tables 4.4, 4.5 and 4.6 for nano cubes, nano plates and nano crystals with FTIR spectra peaks obtained after AOP treatment.

Table 4.3. Comparison of FTIR spectra of microsphere peaks with literature values (Tom Tague).

| <b>Microsphere<br/>Peak, cm<sup>-1</sup></b> | <b>Surface Group</b>   | <b>Peak Range,<br/>± 10 cm<sup>-1</sup></b> |
|--|--|---|
| 3360   | OH stretching, one N-H stretching<br>OH stretching (carboxylic acid)       | 3200 – 3400<br>2500 – 3500                  |
| 2924   | CH <sub>2</sub> (C–H asymmetric stretching of alkyl group)                 | 2926  |
| 2853   | CH <sub>2</sub> (C–H symmetric stretching of alkyl structures)             | 2855  |
| 1626   | NH <sub>2</sub> in-plane bending, asymmetric -COO <sup>-</sup> stretch     | 1580-1650                                   |
| 1463   | CH <sub>2</sub> (Scissors bending) and symmetric -COO <sup>-</sup> stretch | 1455  |
| 1382   | CH-N-CH bending, OH bend   | 1390  |
| 1047   | C-O-C ether groups, primary alcohol, -CN stretching                        | 1000-1075                                   |

Table 4.4. Comparison of FTIR spectra of nano cube peaks with literature values (Tom Tague).

| <b>Nanocubes<br/>Peak, cm<sup>-1</sup></b> | <b>Surface Group</b>  | <b>Peak Range,<br/>± 10 cm<sup>-1</sup></b> |
|--|---|---|
| 3370                                       | OH stretching, one N-H stretching<br>OH stretching (carboxylic acid)  | 3200 – 3400<br>2500 – 3500                  |
| 2957                                       | C–H stretching of alkyl structures  | 2850 to 2950                                |
| 2925                                       | CH <sub>2</sub> (C–H asymmetric stretching of alkyl group)  | 2926  |
| 2854                                       | CH <sub>2</sub> (C–H symmetric stretching of alkyl structures)  | 2855  |
| 1646                                       | aromatic and olefinic C=C vibrations, C=O in amide (I),<br>ketone, quinone groups; bend deformation of water, -NH<br>vibrations, asymmetric -COO <sup>-</sup> stretch | 1400-1620<br>1580-1650                      |
| 1586                                       | NH <sub>2</sub> in-plane bending  | 1580-1650                                   |
| 1380                                       | CH-N-CH bending, OH bend  | 1390  |
| 1058                                       | C-O-C ether groups, primary alcohol, -CN stretching   | 1000-1075                                   |

An asymmetric and symmetric mode at around 3300 – 3400 cm<sup>-1</sup> is mainly attributed due to water molecules while –CH<sub>2</sub> groups are assigned due to strong peaks at 1455, 2855 and 2926 cm<sup>-1</sup>. At ~1650cm<sup>-1</sup>, the peaks are assigned to asymmetric stretching modes of –COO group. –NH vibrations is mainly attributed due to strong peaks at around 1646 cm<sup>-1</sup> and peaks at around 1058 is due to –CN stretching vibration bands.

Table 4.5. Comparison of FTIR spectra of nano plate peaks with literature values (Tom Tague).

| <b>Nanoplates<br/>Peak, cm<sup>-1</sup></b> | <b>Surface Group</b>  | <b>Peak Range,<br/>± 10 cm<sup>-1</sup></b> |
|---|---|---|
| 3348  | OH stretching, one N-H stretching<br>OH stretching (carboxylic acid)  | 3200 – 3400<br>2500 – 3500                  |
| 2924  | CH <sub>2</sub> (C–H asymmetric stretching of alkyl group)  | 2926  |
| 2854  | CH <sub>2</sub> (C–H symmetric stretching of alkyl structures)  | 2855  |
| 1631  | aromatic and olefinic C=C vibrations, C=O in amide (I), ketone, quinone groups; bend deformation of water, -NH vibrations, asymmetric -COO <sup>-</sup> stretch | 1400-1620<br>1580-1650                      |
| 1588  | NH <sub>2</sub> in-plane bending  | 1580-1650                                   |
| 1378  | CH-N-CH bending, OH bend  | 1390  |
| 1059  | C-O-C ether groups, primary alcohol, -CN stretching   | 1000-1075                                   |

CH<sub>2</sub> (scissors bending) at ~ 1463 cm<sup>-1</sup> was observed for microspheres (Table 4.3), while NH<sub>2</sub> in-plane bending was observed at 1586 cm<sup>-1</sup> and C–H stretching of alkyl structures at 2957 cm<sup>-1</sup> for nano cubes (Table 4.4), O–H stretching of phenolic compounds at 1285 cm<sup>-1</sup> and C-H deformation of CH<sub>3</sub> group at 1467 cm<sup>-1</sup> for nano crystals (Table 4.6) were observed for some but not for other nano structures.

Table 4.6. Comparison of FTIR spectra of nano crystal peaks with literature values (Tom Tague).

| <b>Nano Crystals<br/>Peak, cm<sup>-1</sup></b> | <b>Surface Group</b>   | <b>Peak Range,<br/>± 10 cm<sup>-1</sup></b> |
|--|--|---|
| 3351   | OH stretching, one N-H stretching<br>OH stretching (carboxylic acid)   | 3200 – 3400<br>2500 – 3500                  |
| 2925   | CH <sub>2</sub> (C–H asymmetric stretching of alkyl group)   | 2926  |
| 2852   | CH <sub>2</sub> (C–H symmetric stretching of alkyl structures)   | 2855  |
| 1631   | aromatic and olefinic C=C vibrations, C=O in amide (I), ketone, quinone groups; bend deformation of water, NH vibrations, asymmetric -COO <sup>-</sup> stretch | 1400-1620<br>1580-1650                      |
| 1566   | asymmetric CO <sub>2</sub> stretch   | 1540-1650                                   |
| 1467   | C–H deformation of CH <sub>3</sub> group, symmetric -COO <sup>-</sup> stretch  | 1460  |
| 1377   | CH-N-CH bending, OH bend   | 1390  |
| 1285   | O–H stretching of phenolic compounds   | 1280–1270                                   |
| 1027   | C-O-C ether groups, primary alcohol, -CN stretching  | 1000-1075                                   |

### 4.3.3 Energy Dispersive X-ray (EDX) Spectroscopy

An EDX spectra measurement for each nano structures was performed for all elements normalized with three iterations each. Figure 4.14 to 4.17 shows the spot EDX spectra for various nano structures that were prepared for SEM. Similarly Table 4.7 to 4.10 shows semi-quantitative results in weight percent and atomic percent.

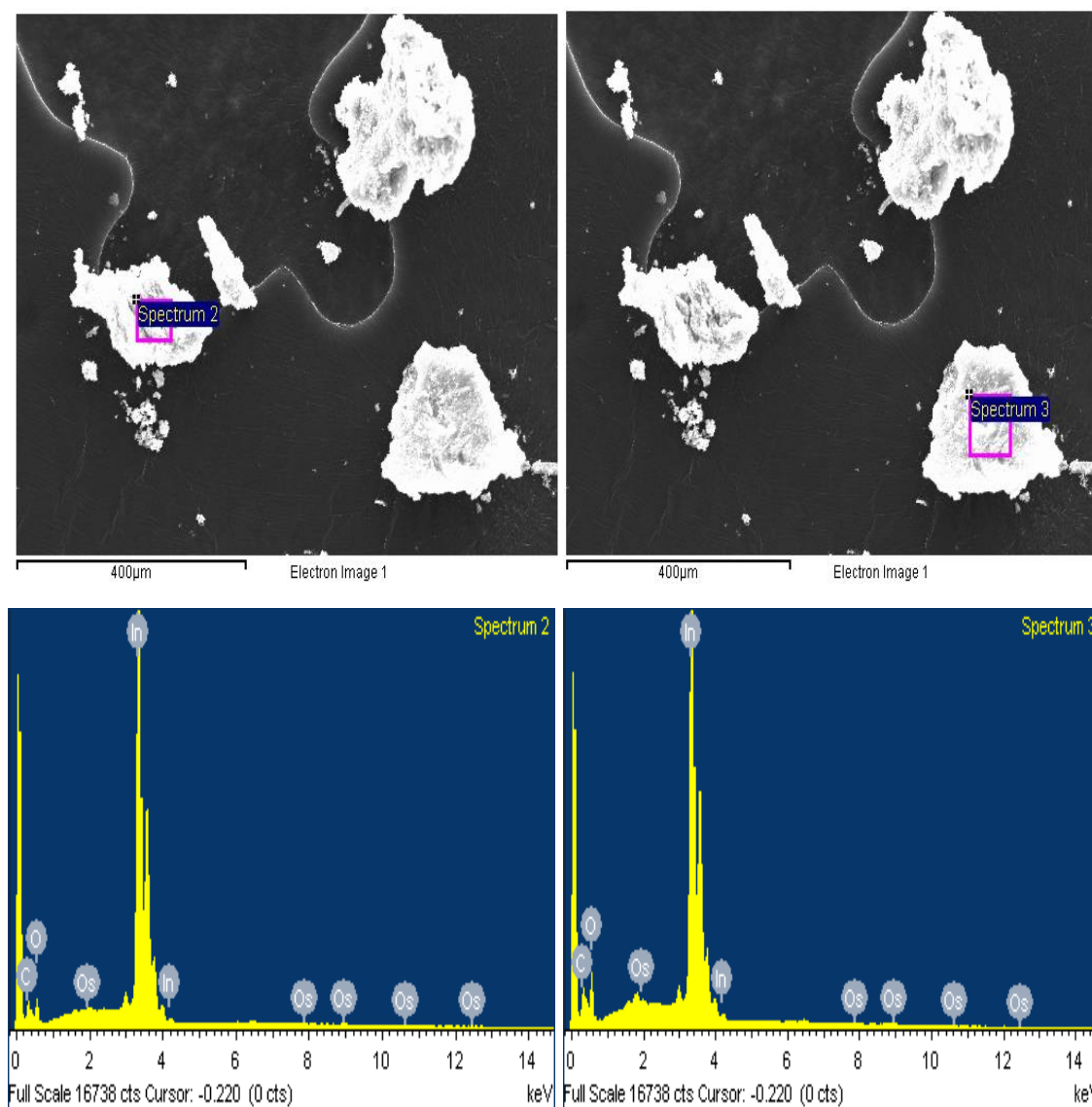


Figure 4.14. Spot EDX spectra of  $\text{In}_2\text{O}_3$  microspheres calcined at 500°C for 2h



From the spectra, it was observed that different samples showed slight variation in the concentration of  $\text{In}^+$  ion in the solution. At higher  $\text{In}^+$  concentration, the measured intensity of the film increases for In spectral lines. From scientific literature, it is known that the element abundance is directly proportional to the spectral lines intensities on EDX. The line EDX analysis also provides important information on chemical homogeneity of In films. The results on nano-films shows only an increase in concentration of In mainly attributed due to increased content of In and cannot distinguish between In atoms and elemental In. Highest average weight % of Indium was observed for nano crystals as seen in Table 4.10, while lowest was observed for nano plates in Table 4.8.

Table 4.7. EDX results in duplicate for  $\text{In}_2\text{O}_3$  microspheres after calcination.

| Element     | MS-1     |          | MS-2     |          |
|-------------|----------|----------|----------|----------|
|             | Weight % | Atomic % | Weight % | Atomic % |
| <b>C K</b>  | 3.80     | 16.14    | 4.16     | 14.96    |
| <b>O K</b>  | 15.03    | 47.90    | 21.12    | 56.97    |
| <b>In L</b> | 80.71    | 35.84    | 74.65    | 28.05    |
| <b>Os M</b> | 0.46     | 0.12     | 0.07     | 0.02     |

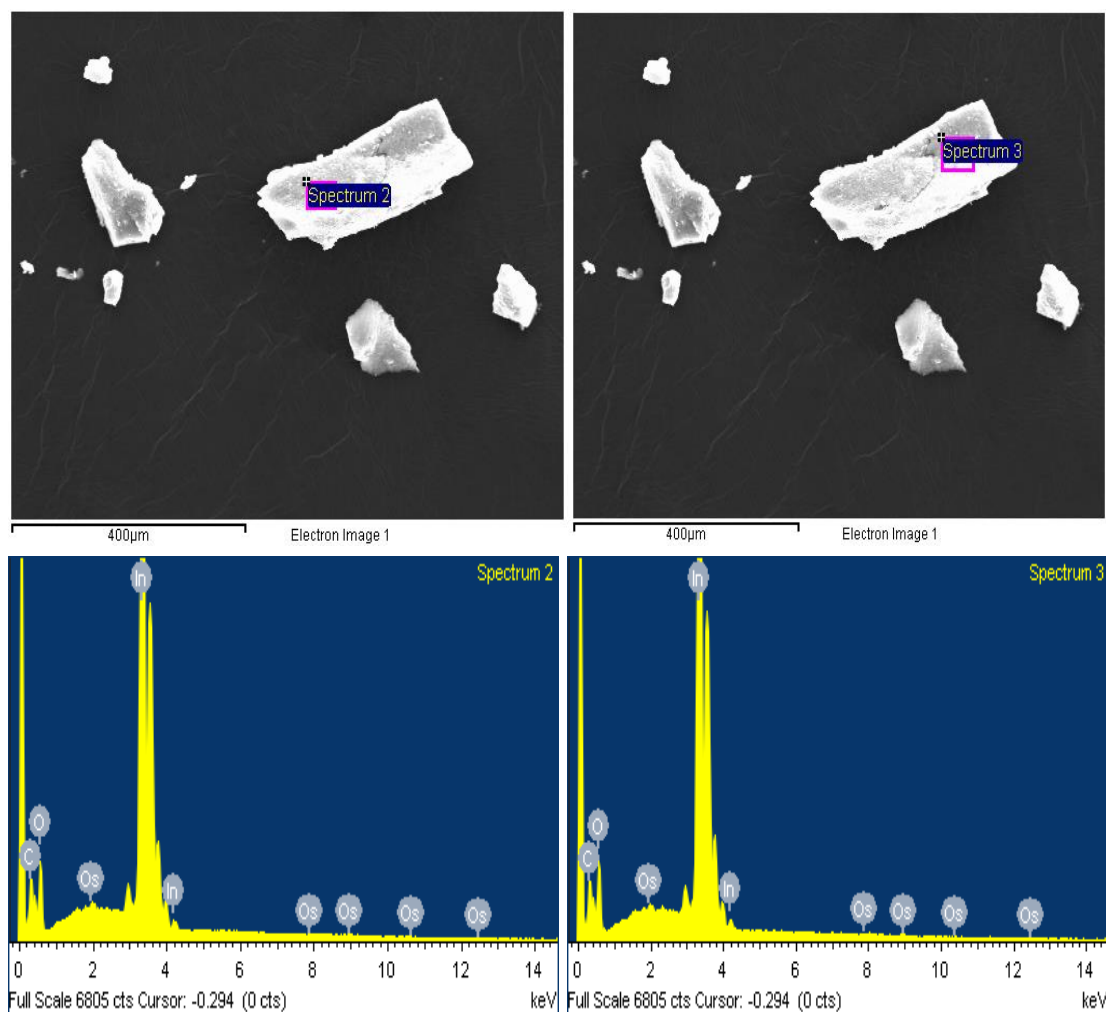


Figure 4.15. Spot EDX spectra of  $\text{In}_2\text{O}_3$  nano plates calcined at  $500^\circ\text{C}$  for 2h

Table 4.8. EDX results in duplicate for  $\text{In}_2\text{O}_3$  nano plates after calcination

| Element     | NP-1     |          | NP-2     |          |
|-------------|----------|----------|----------|----------|
|             | Weight % | Atomic % | Weight % | Atomic % |
| <b>C K</b>  | 3.31     | 11.73    | 3.44     | 12.00    |
| <b>O K</b>  | 22.98    | 61.08    | 23.50    | 61.46    |
| <b>In L</b> | 72.97    | 27.02    | 72.45    | 26.41    |
| <b>Os M</b> | 0.73     | 0.16     | 0.61     | 0.13     |

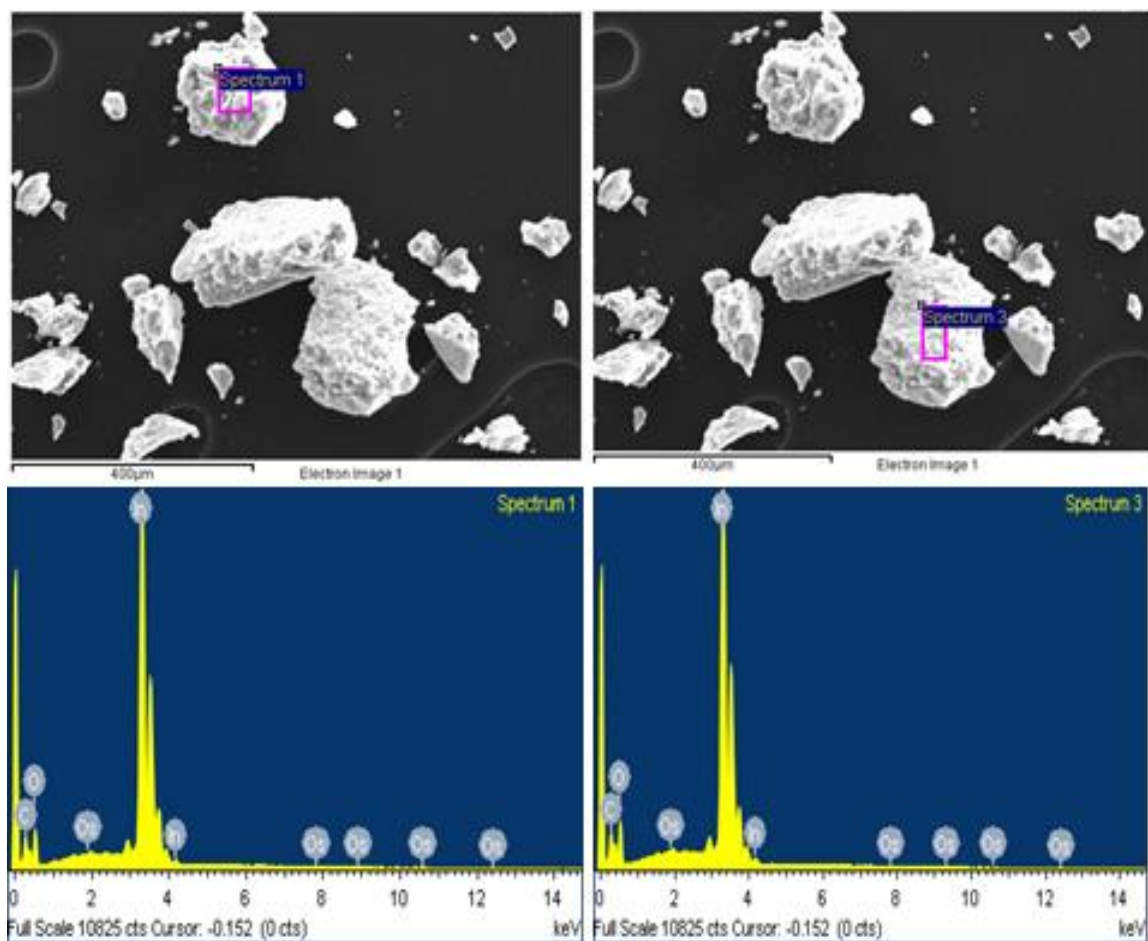


Figure 4.16. Spot EDX spectra of  $\text{In}_2\text{O}_3$  nano cubes calcined at  $500^\circ\text{C}$  for 2h

Table 4.9. EDX results in duplicate for  $\text{In}_2\text{O}_3$  nano cubes after calcination

| Element     | NC-1     |          | NC-2     |          |
|-------------|----------|----------|----------|----------|
|             | Weight % | Atomic % | Weight % | Atomic % |
| <b>C K</b>  | 3.52     | 12.76    | 3.27     | 11.44    |
| <b>O K</b>  | 21.67    | 58.95    | 23.53    | 61.84    |
| <b>In L</b> | 74.34    | 28.18    | 72.64    | 26.60    |
| <b>Os M</b> | 0.46     | 0.11     | 0.56     | 0.12     |

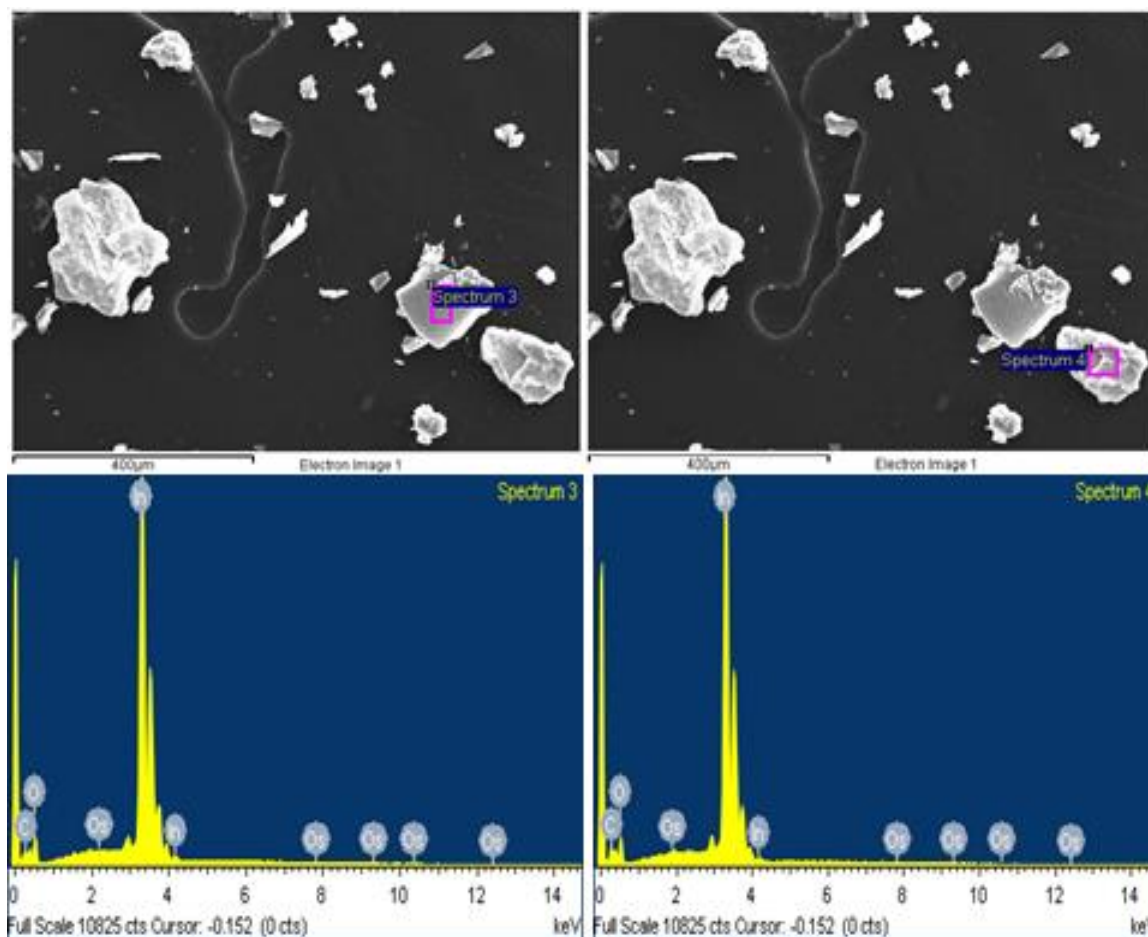


Figure 4.17. Spot EDX spectra of  $\text{In}_2\text{O}_3$  nano crystals calcined at  $400^\circ\text{C}$  for 2h

Table 4.10. EDX results in duplicate for  $\text{In}_2\text{O}_3$  nano crystals after calcination

| Element     | NCY-1    |          | NCY-2    |          |
|-------------|----------|----------|----------|----------|
|             | Weight % | Atomic % | Weight % | Atomic % |
| <b>C K</b>  | 0.93     | 4.19     | 1.72     | 7.36     |
| <b>O K</b>  | 16.95    | 57.25    | 17.62    | 56.62    |
| <b>In L</b> | 81.70    | 38.44    | 80.17    | 35.89    |
| <b>Os M</b> | 0.42     | 0.12     | 0.49     | 0.13     |

#### 4.3.4 Decomposition of PPCPs using various photocatalytic $\text{In}_2\text{O}_3$ nano particles

Several experiments were conducted to study the decomposition of selected compounds of PPCPs from secondary effluent (SE) at an adjusted pH 7 and the photocatalytic activity was performed on various  $\text{In}_2\text{O}_3$  structures for decomposition of PPCPs and to calculate its kinetics. The photocatalytic decomposition, percent reduction and apparent rate constants were determined for each type of nanoparticles for a reaction period of 90min. A pseudo-first-order kinetics was observed for the photocatalytic decomposition of selected PPCPs by various nano particles.

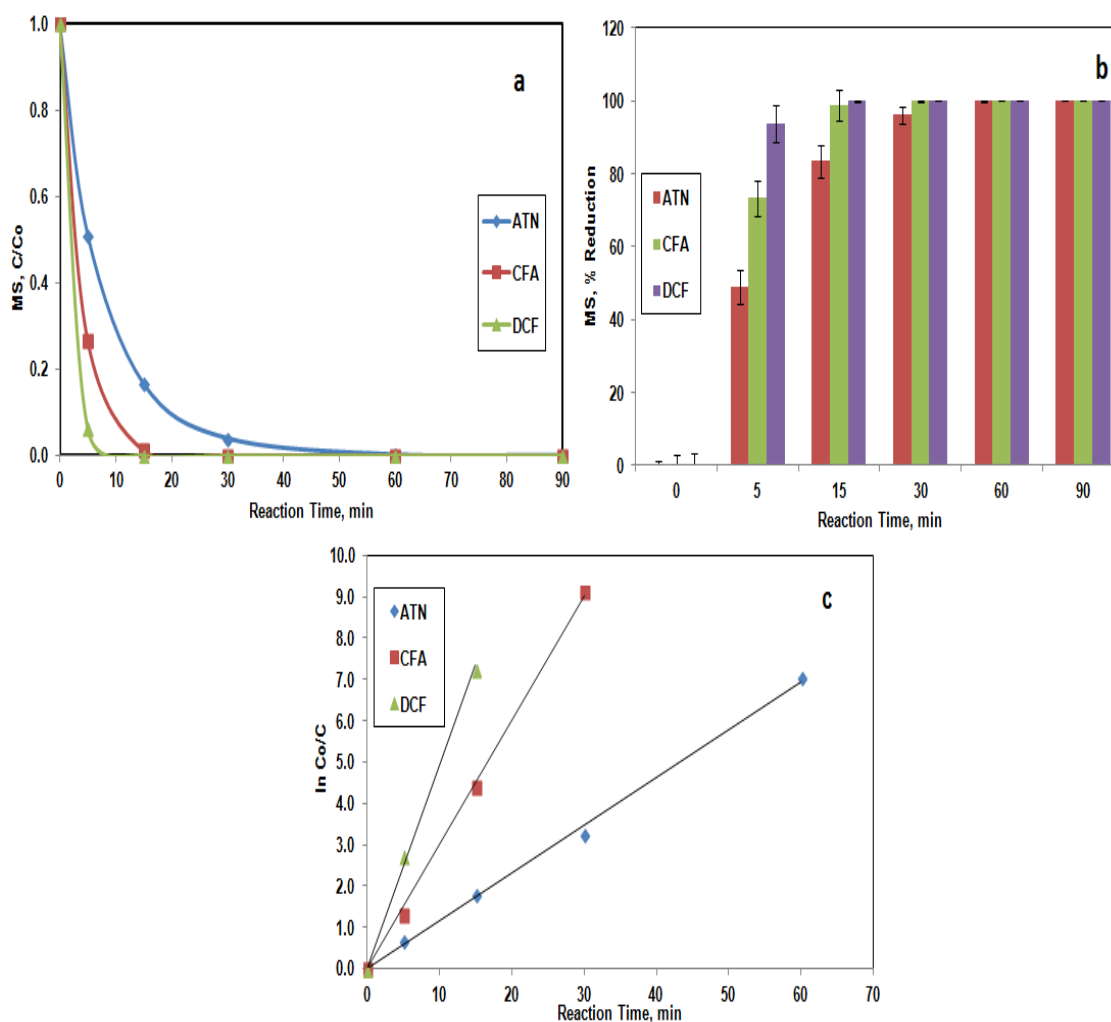


Figure 4.18. Photocatalytic decomposition of ATN, CFA and DCF by  $\text{In}_2\text{O}_3$  microsphere at pH 7 for SE at  $23 \pm 1^\circ\text{C}$  (a)  $C/C_0$  (b) % Reduction and (c)  $\ln C_0/C$

Figure 4.18, shows photocatalytic activity of microspheres with fastest degradation rates for DCF and slowest for ATN. Almost 99.9% reduction was observed for DCF within 15 min whereas CFA showed 100% in 30min followed by ATN with 99.9% reduction in 60min. The rate constant for ATN, CFA and DCF photocatalyzed in presence of microspheres were  $0.1156 \text{ min}^{-1}$ ,  $0.3009 \text{ min}^{-1}$  and  $0.4894 \text{ min}^{-1}$  and follows the order  $\text{DCF} > \text{CFA} > \text{ATN}$ . The rate constant for DCF was almost 4.2 times higher compared to ATN for mesospheres.

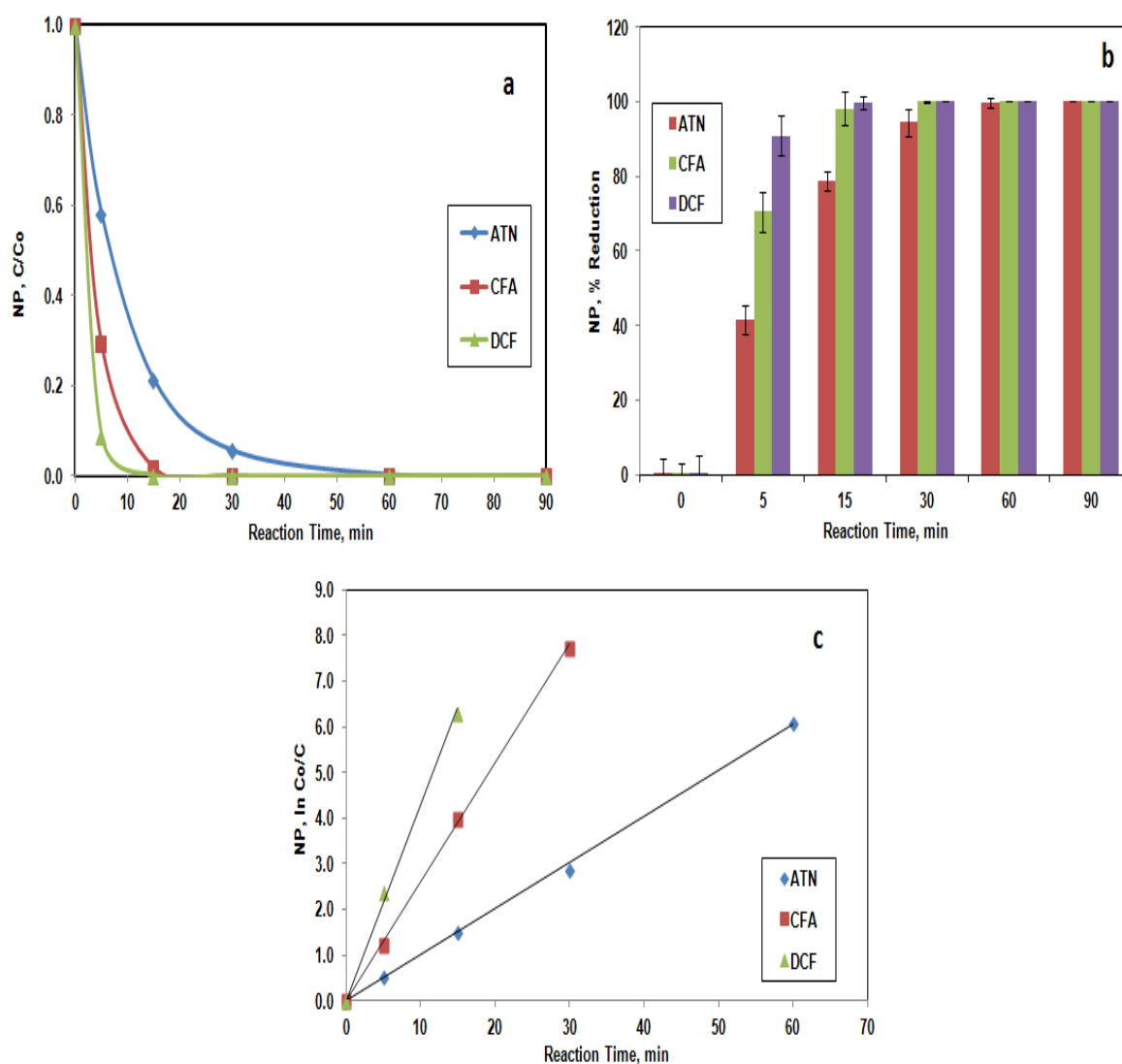


Figure 4.19. Photocatalytic decomposition of ATN, CFA and DCF by  $\text{In}_2\text{O}_3$  nano plates at pH 7 for SE at  $23 \pm 1^\circ\text{C}$  (a) C/Co (b) % Reduction and (c) ln Co/C

Similarly the photocatalytic decomposition of ATN, CFA and DCF was conducted using nano plates (Figure 4.19) for secondary effluent at pH 7 and the rate constants were observed to be  $0.101 \text{ min}^{-1}$ ,  $0.2597 \text{ min}^{-1}$  and  $0.427 \text{ min}^{-1}$ . The percent reduction of DCF was observed to be far greater compared to ATN.

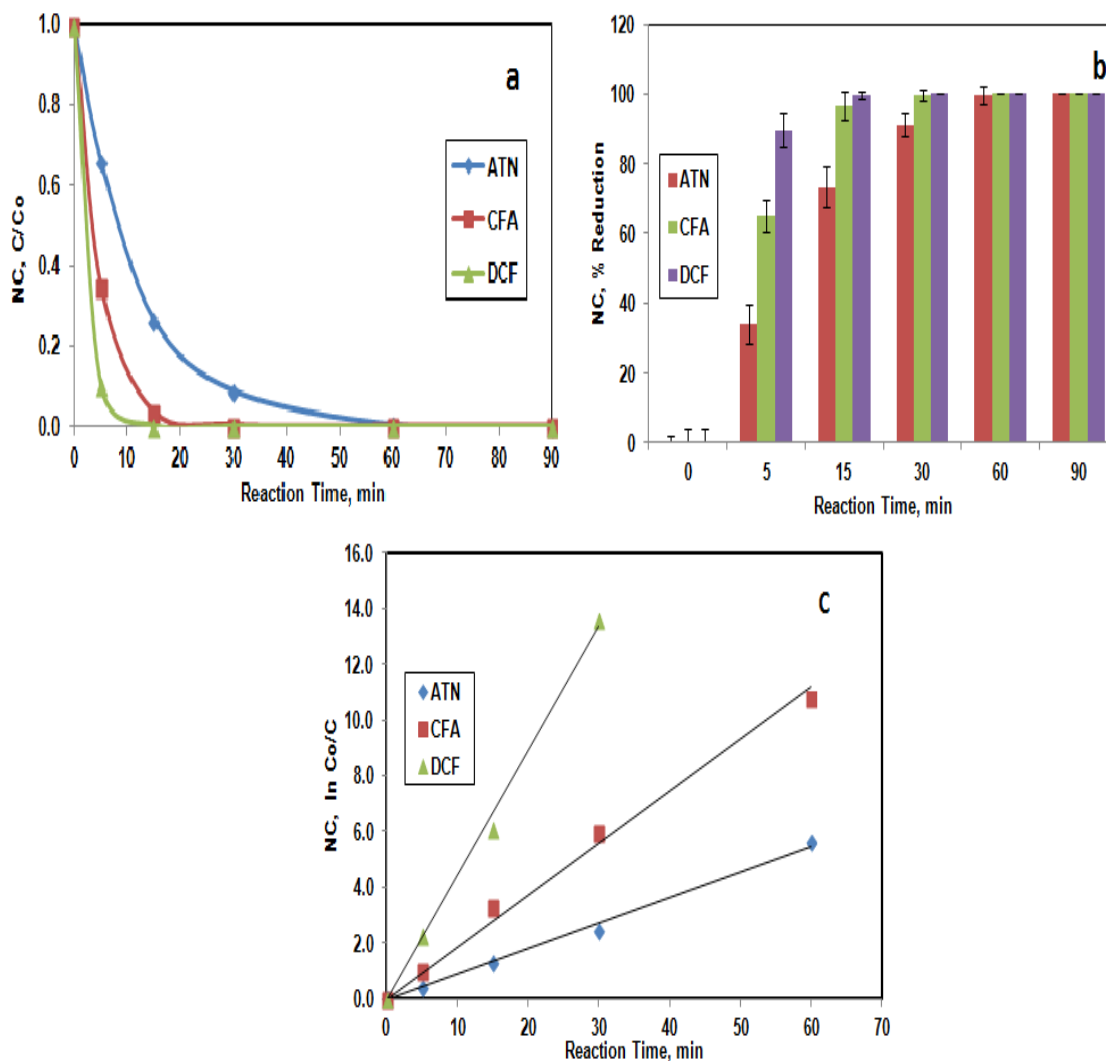


Figure 4.20. Photocatalytic decomposition of ATN, CFA and DCF by  $\text{In}_2\text{O}_3$  nano cubes at pH 7 for SE at  $23 \pm 1^\circ\text{C}$  (a) C/Co (b) % Reduction and (c)  $\ln \text{Co}/\text{C}$

Figure 4.20 and Figure 4.21 shows the photocatalytic decomposition of ATN, CFA and DCF by nano cubes and nano crystals, respectively and their rate constants were observed to be  $0.0906 \text{ min}^{-1}$ ,  $0.186 \text{ min}^{-1}$  and  $0.4437 \text{ min}^{-1}$  for nano cubes where as

$0.0824 \text{ min}^{-1}$ ,  $0.1476 \text{ min}^{-1}$  and  $0.2796 \text{ min}^{-1}$  for nano crystals as shown in Table 4.11 for secondary effluent.

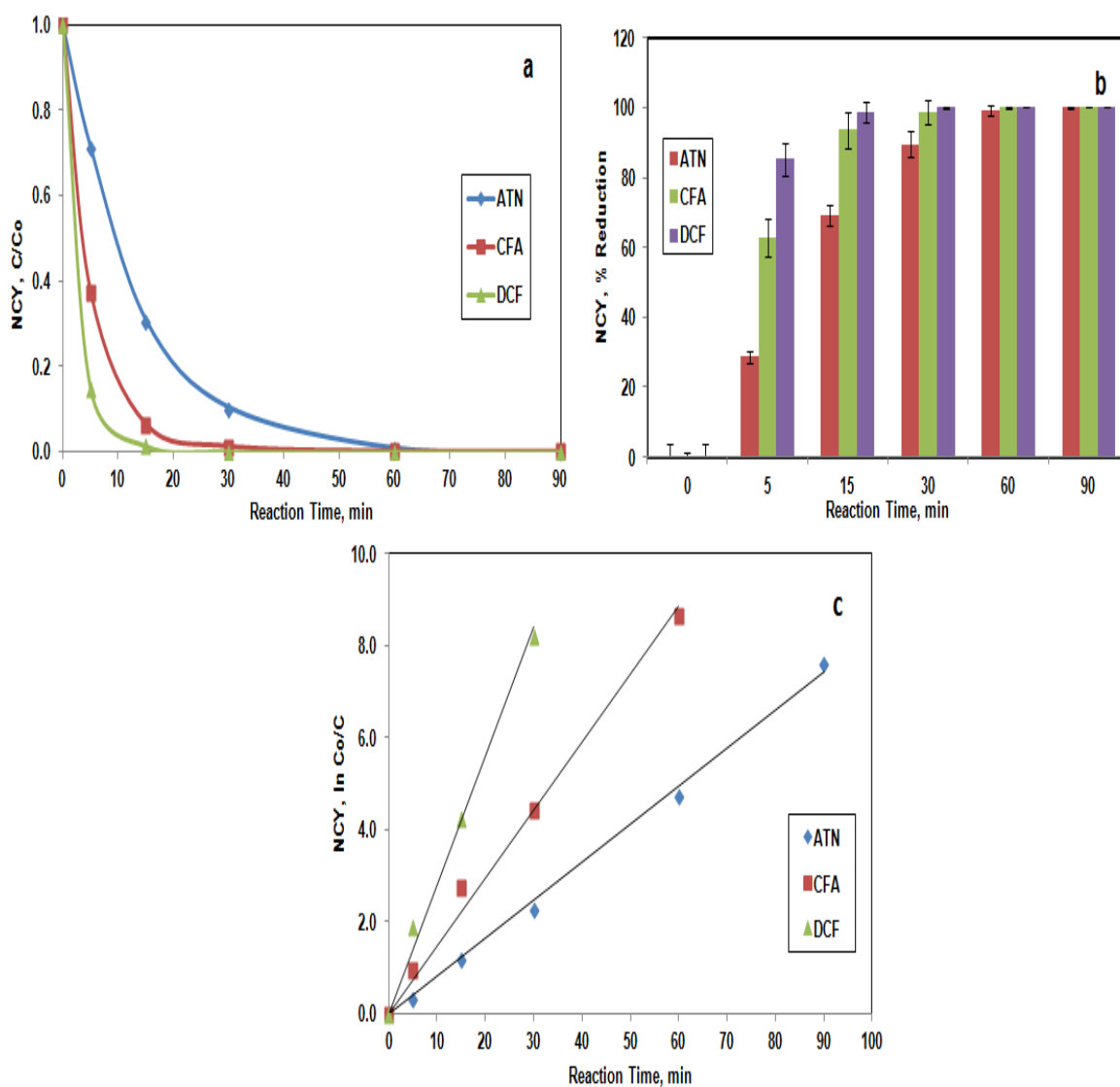


Figure 4.21. Photocatalytic decomposition of ATN, CFA and DCF by  $\text{In}_2\text{O}_3$  nano crystals at pH 7 for SE at  $23 \pm 1^\circ\text{C}$  (a) C/Co (b) % Reduction and (c)  $\ln \text{Co}/\text{C}$

The rate constants was the highest for microspheres followed by nano plates, nano cubes and nano crystals and follows the order as  $\text{MS} > \text{NP} > \text{NC} > \text{NCY}$  (Table 4.11). It was observed that the rate constant for DCF was 4.2, 4.9 and 3.4 times greater compared to ATN for NP, NC and NCY. The highest activity for DCF is because of its



Lewis acid–base character that acts as proton acceptor or proton donor due to the presence of secondary amino group and carboxylic group (Zilnik et al., 2007). A slightly lower rate constant was observed for NP whereas almost half for NCY compared to MS.

Table 4.11. Rate constants ( $k$ ,  $\text{min}^{-1}$ ) of various nano particles with their correlation coefficient ( $R^2$ ) values for ATN, CFA and DCF for SE

|            | MS                      |        | NP                      |        | NC                      |        | NCY                     |        |
|------------|-------------------------|--------|-------------------------|--------|-------------------------|--------|-------------------------|--------|
|            | $k$ , $\text{min}^{-1}$ | $R^2$  | $k$ , $\text{min}^{-1}$ | $R^2$  | $k$ , $\text{min}^{-1}$ | $R^2$  | $k$ , $\text{min}^{-1}$ | $R^2$  |
| <b>ATN</b> | 0.1156                  | 0.9978 | 0.101                   | 0.9988 | 0.0906                  | 0.9942 | 0.0824                  | 0.9966 |
| <b>CFA</b> | 0.3009                  | 0.9989 | 0.2597                  | 0.9995 | 0.186                   | 0.9915 | 0.1476                  | 0.9919 |
| <b>DCF</b> | 0.4894                  | 0.9959 | 0.427                   | 0.9962 | 0.4437                  | 0.9965 | 0.2796                  | 0.9925 |

These results follow the same order as that was observed for photocatalytic degradation of perfluorooctanoic acid (PFOA) where similar nanoparticles were used such as MS, NC and NP except NCY (Li et al., 2013) with highest photocatalytic activity observed for MS.

#### 4.3.5 Comparison of photocatalytic decomposition between distilled water and secondary effluent at pH 7

A comparison of photocatalytic decomposition between pure distilled water (DW) and secondary effluent (SE) was performed at pH 7. Figure 4.22 showed a faster decomposition rate with distilled water compared to Figure 4.23 with secondary effluent. Within the first 5 min, the percent reduction for ATN, CFA and DCF in case of distilled water was observed at 39.5%, 75.9% and 94.9% and that of secondary

effluent was 28.7%, 62.6% and 85.2% respectively. The complete percent reduction for DW could be achieved in 60min, 30min and 15min for ATN, CFA and DCF while SE showed slightly longer reaction time for complete removal.

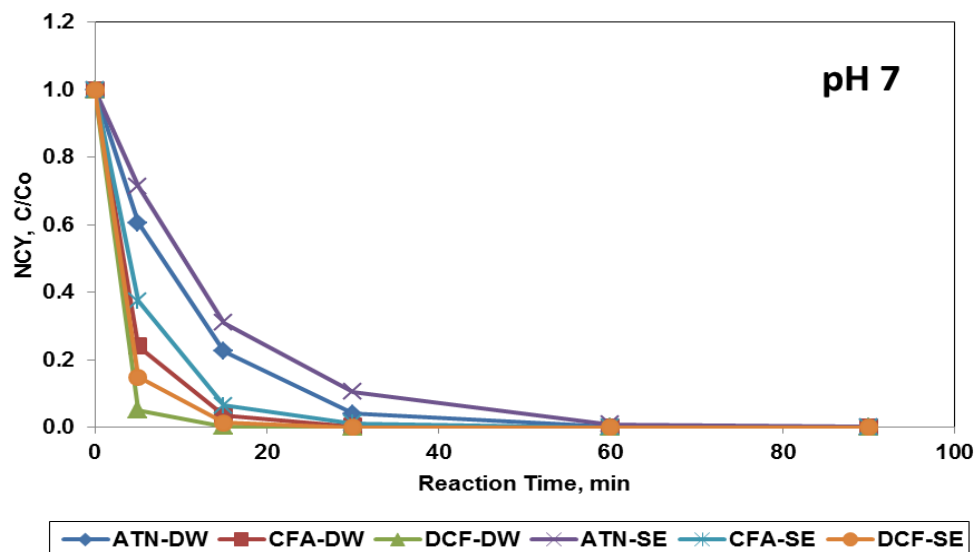


Figure 4.22. A comparison of photocatalytic decomposition of ATN, CFA and DCF by  $\text{In}_2\text{O}_3$  NCY at pH 7,  $23 \pm 1^\circ\text{C}$  between DW and SE

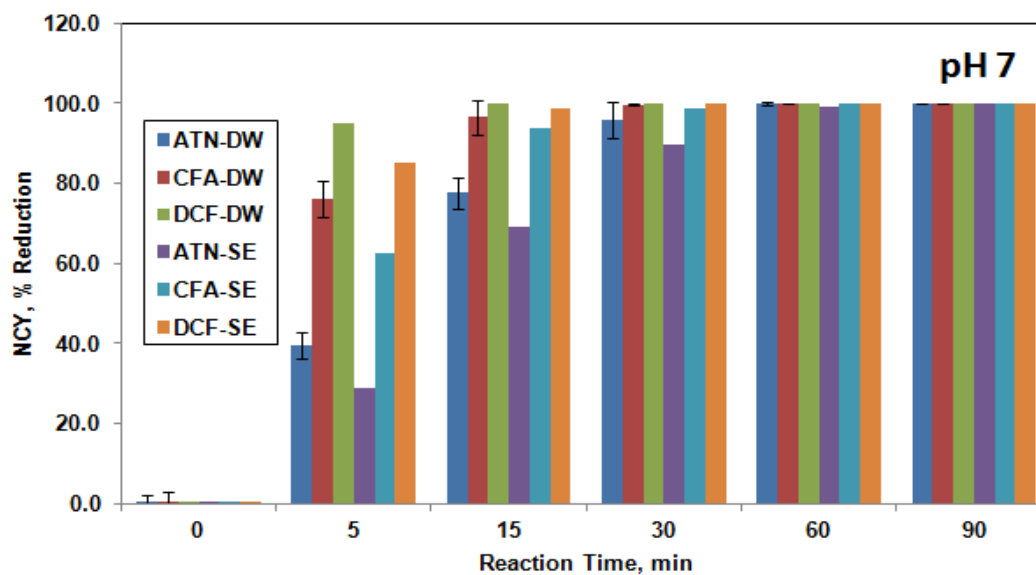


Figure 4.23. Percent reduction of ATN, CFA and DCF by  $\text{In}_2\text{O}_3$  NCY at pH 7,  $23 \pm 1^\circ\text{C}$  between DW and SE

The rate constant at pH 7 for distilled water was  $0.1089 \text{ min}^{-1}$ ,  $0.1964 \text{ min}^{-1}$  and  $0.4268 \text{ min}^{-1}$  for ATN, CFA, and DCF whereas it was  $0.0824 \text{ min}^{-1}$ ,  $0.1476 \text{ min}^{-1}$  and  $0.2796 \text{ min}^{-1}$  which shows that distilled water has a higher rate constant and hence higher removal efficiency compared to secondary effluent as shown in Figures 4.22 and Figure 4.23. The slightly lower decomposition activity of secondary effluent over distilled water is due to the presence of various ions such as nitrates, chlorides, bicarbonates and natural organic matter that inhibits the photocatalytic decomposition efficiency and hence delays the decomposition although complete removal was observed within 90min of reaction time.

#### 4.3.6 Effect of pH

The photocatalytic decomposition of ATN, CFA and DCF was also conducted using nano crystals (NCY) by varying the pH and studying the removal efficiency at 3, 5 and 7.

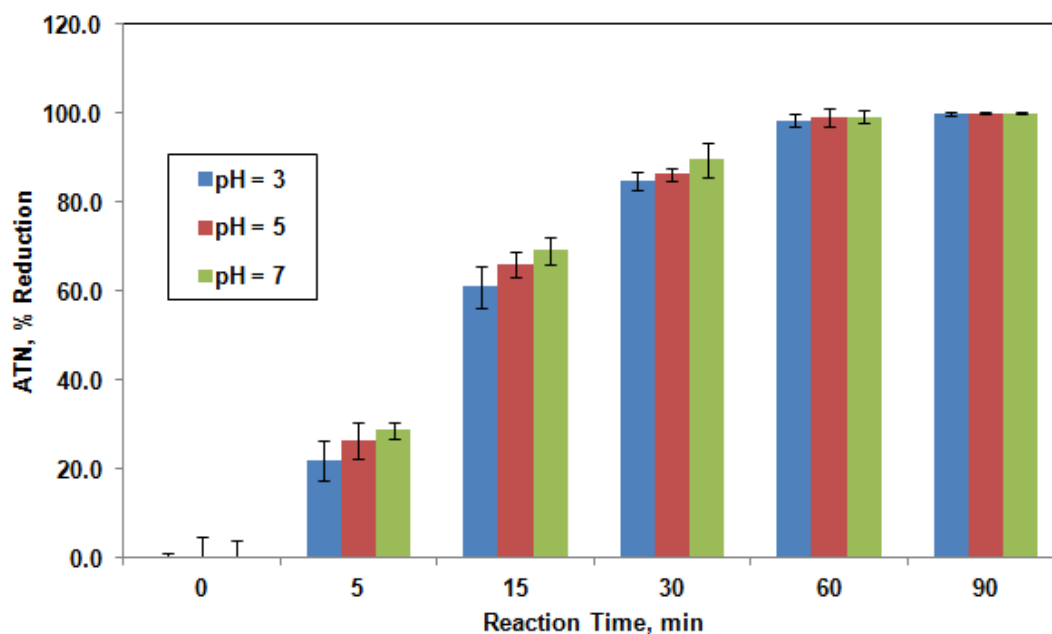


Figure 4.24. Percent reduction of ATN by NCY on SE at pH 3, 5 and 7

Figure 4.24 shows increase in the percent reduction for ATN at 99.9% in 90 min at pH 3 to 99.1% in 60 min when pH was increased to 7. This increase for ATN is due to its high pKa value of 9.16.

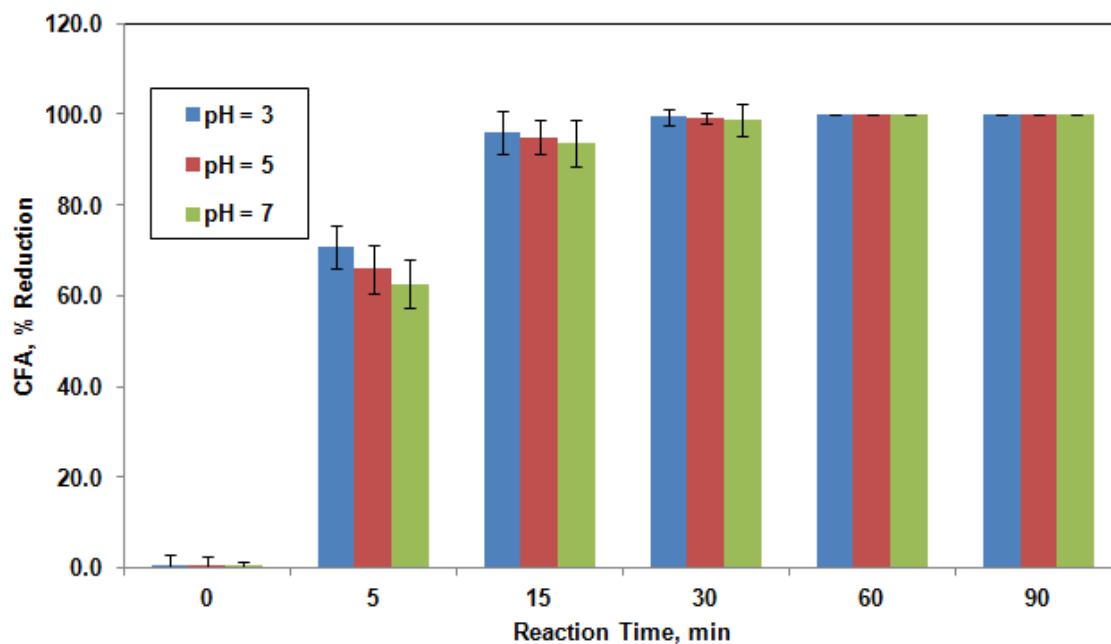


Figure 4.25. Percent reduction of CFA by NCY on SE at pH 3, 5 and 7

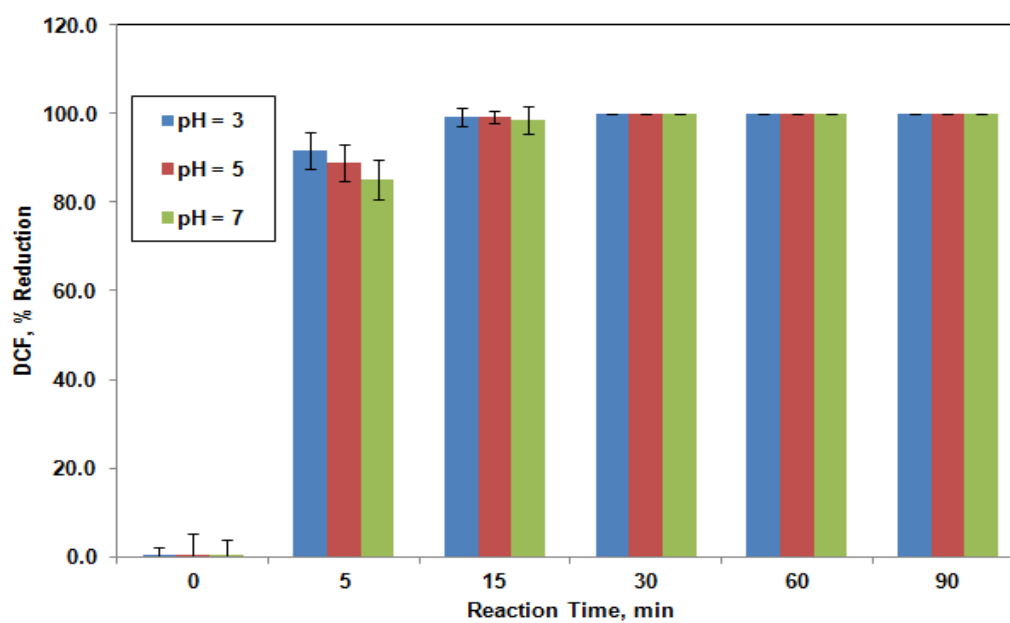


Figure 4.26. Percent reduction of DCF by NCY on SE at pH 3, 5 and 7

Figure 4.25 shows decrease for CFA from 99.5% in 30 min at pH 3 to 100% in 60 min at pH 7 and from 99.4% in 15 min at pH 3 to 100% in 30 min at pH 7 for DCF when the pH was increased from 3 to 7 as shown in Figure 4.26. On the contrary, when the pH was decreased from 7 to 3, the percent reduction increased for DCF and CFA and decreased for ATN.

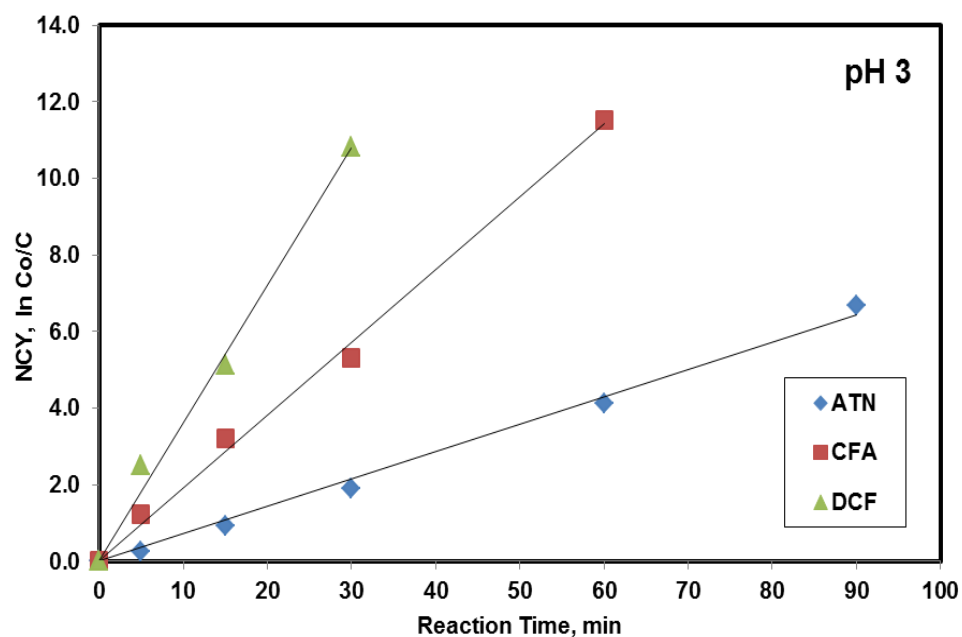


Figure 4.27. Rate constants of ATN, CFA and DCF by NCY on SE at pH 3

The rate constants for NCY were obtained for secondary effluent at pH 3, 5 and 7 by plotting reaction time in min vs.  $\ln C_0/C$  for ATN, CFA and DCF. The total reaction time was conducted for 90min.

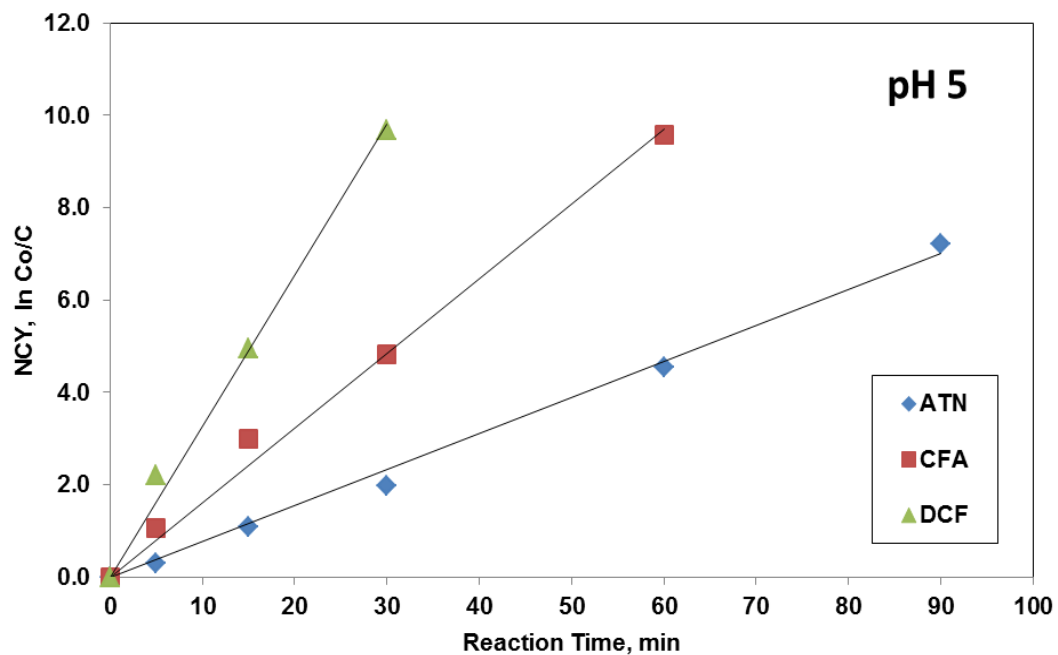


Figure 4.28. Rate constants of ATN, CFA and DCF by NCY on SE at pH 5

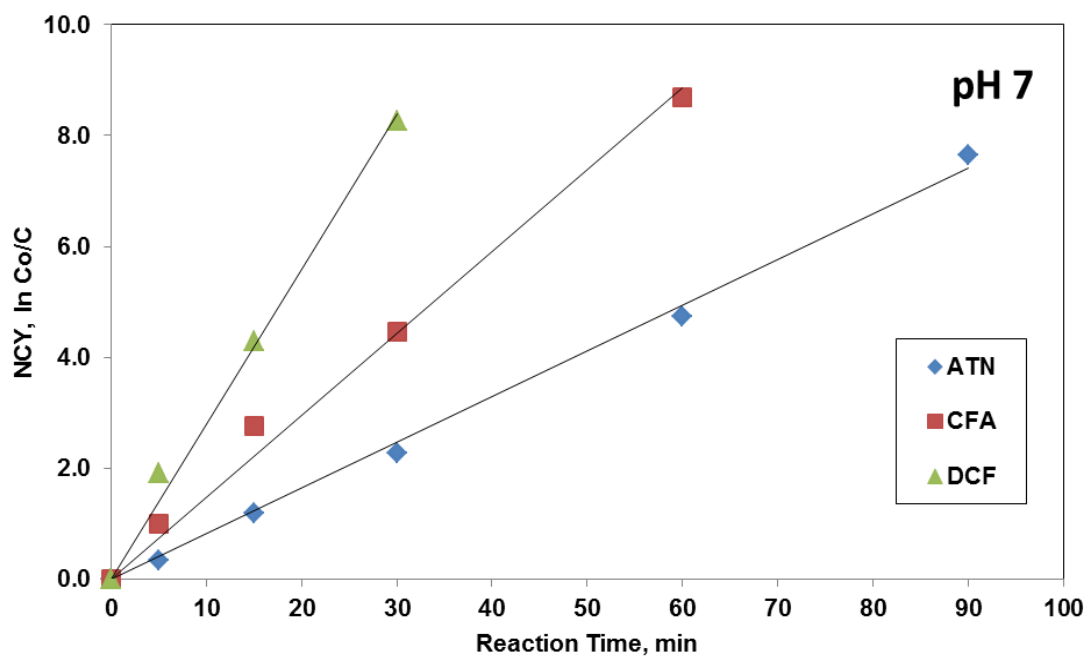
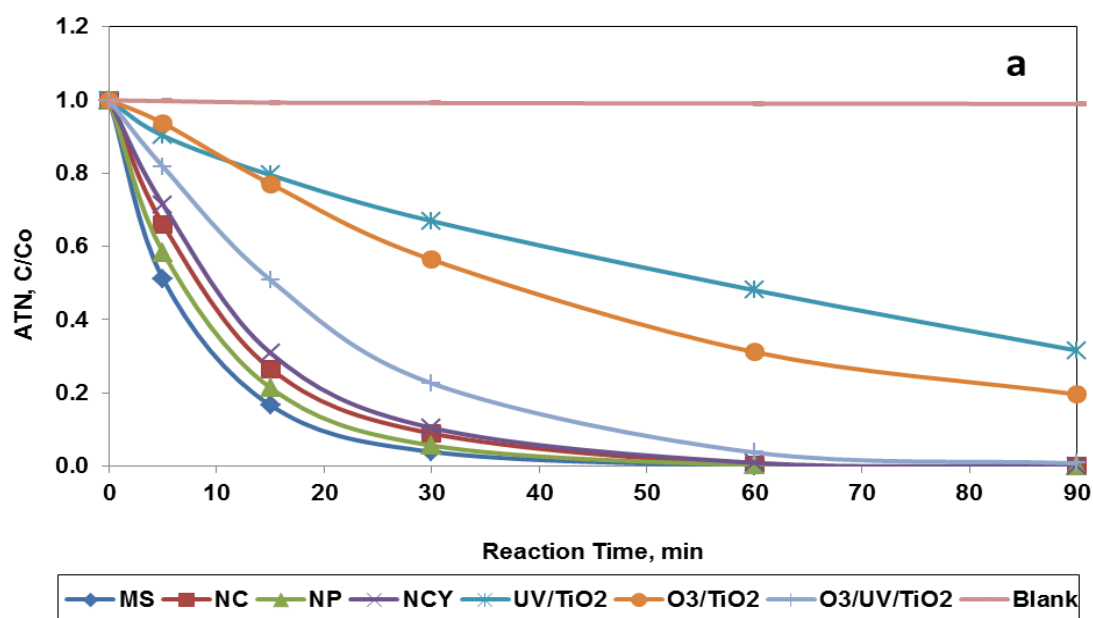


Figure 4.29. Rate constants of ATN, CFA and DCF by NCY on SE at pH 7

The rate constants for ATN, CFA and DCF at pH 3 for Figure 4.27 were observed to be  $0.0716 \text{ min}^{-1}$ ,  $0.1904 \text{ min}^{-1}$  and  $0.3601 \text{ min}^{-1}$ . Similarly, Figure 4.28 and Figure 4.29 showed the rate constants for ATN, CFA and DCF at pH 5 to be  $0.0778 \text{ min}^{-1}$ ,  $0.1619 \text{ min}^{-1}$ ,  $0.3264 \text{ min}^{-1}$  and at pH 7 to be  $0.0824 \text{ min}^{-1}$ ,  $0.1476 \text{ min}^{-1}$  and  $0.2796 \text{ min}^{-1}$  respectively. These results show that the highest rate constants were observed to be for DCF followed by CFA and ATN.

#### 4.3.7 Comparison of various $\text{In}_2\text{O}_3$ nano structures with AOPs

The photocatalytic decomposition of ATN, CFA and DCF was investigated using various nano structures obtained by various synthesis processes of MS, NP, NC and NCY and compared versus UV/ $\text{TiO}_2$ ,  $\text{O}_3/\text{TiO}_2$  and  $\text{O}_3/\text{UV}/\text{TiO}_2$  for secondary effluent and the results are plotted. From Figure 4.30 and Figure 4.31, it shows that the photocatalytic decomposition and removal efficiency for ATN was highest for microsphere and the least for UV/ $\text{TiO}_2$ , whereas the photocatalytic activity and removal efficiency was least for CFA with  $\text{O}_3/\text{TiO}_2$  and for DCF, the least degradation was observed to be with UV/ $\text{TiO}_2$  and  $\text{O}_3/\text{TiO}_2$ .



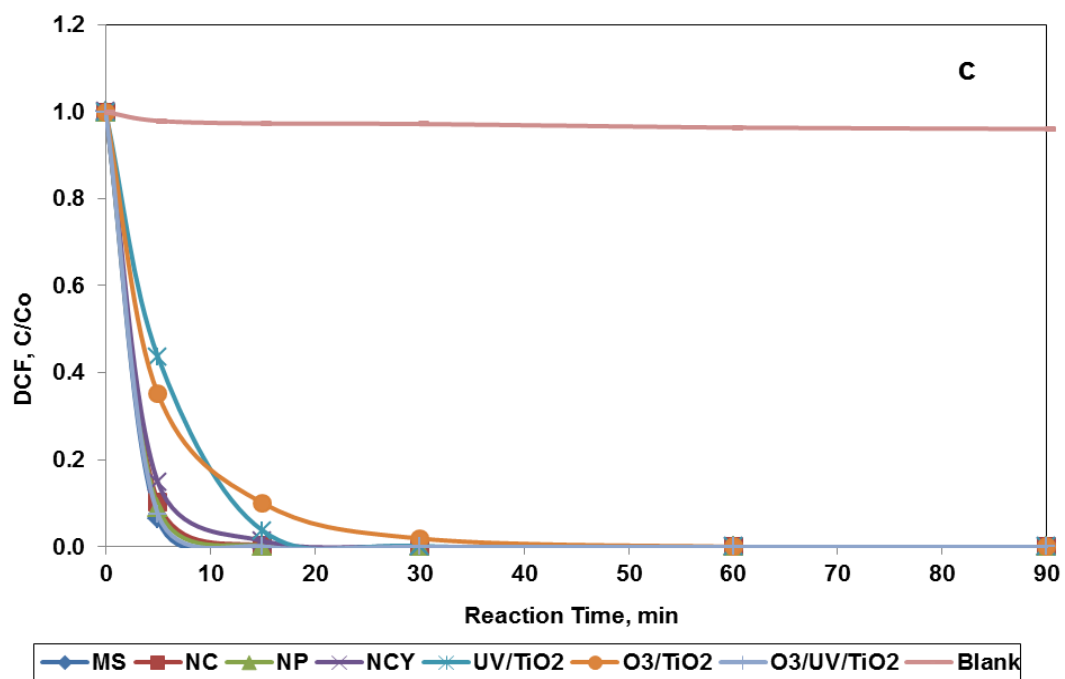
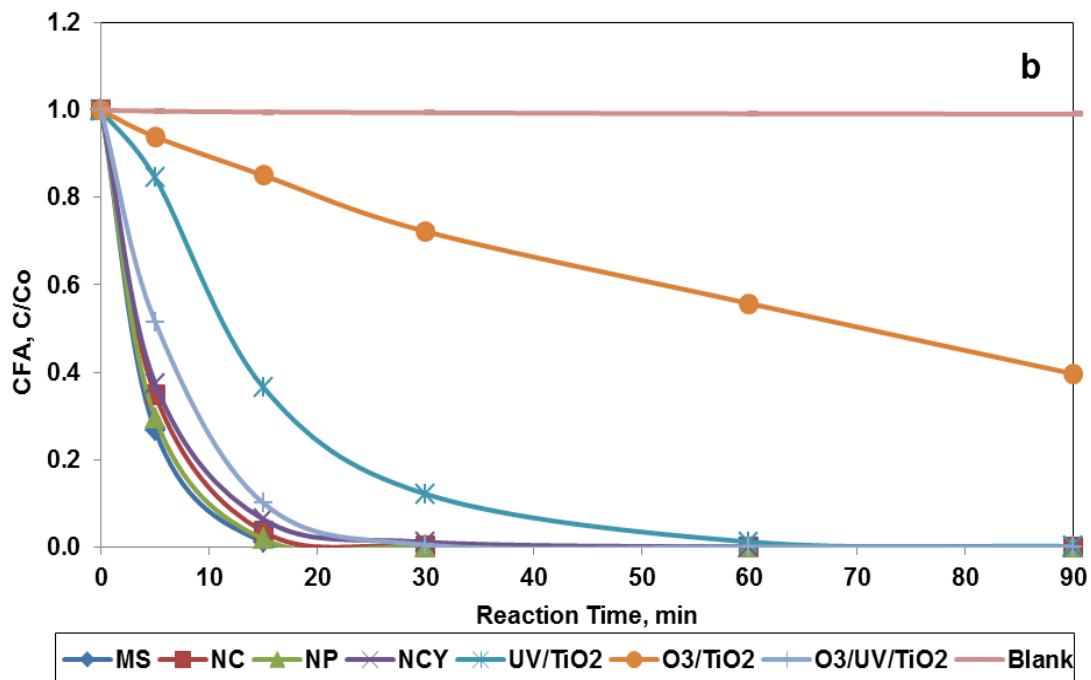
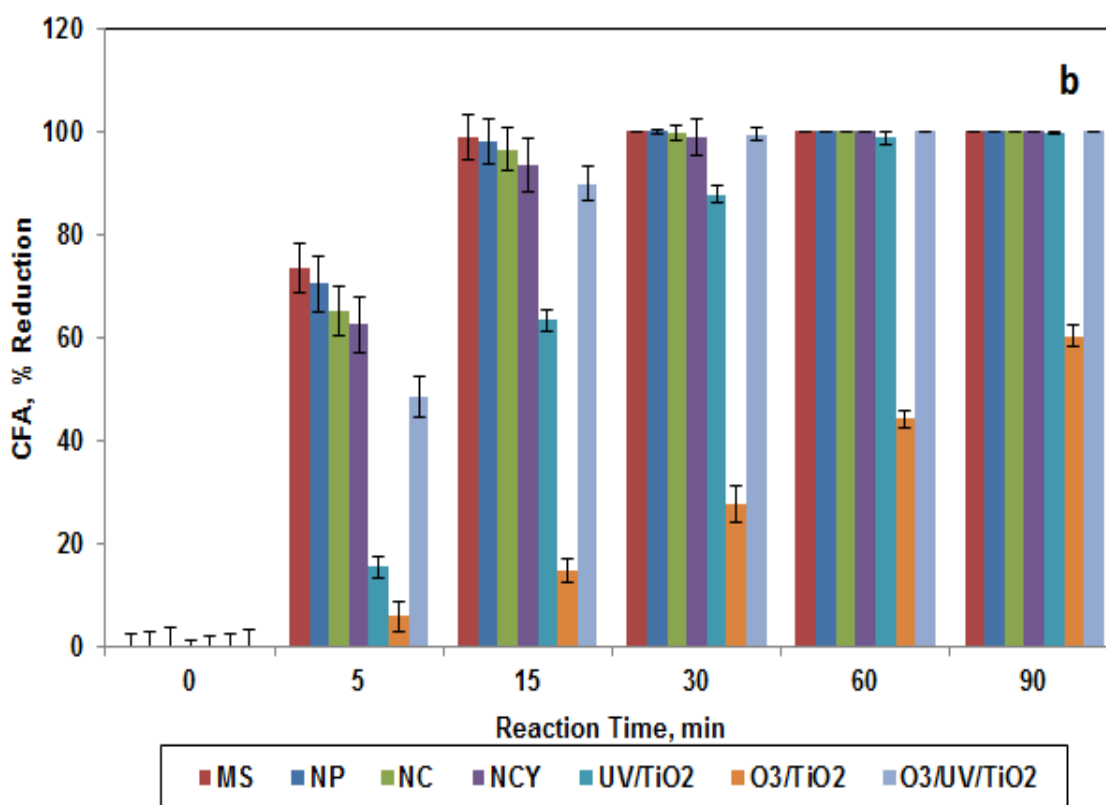
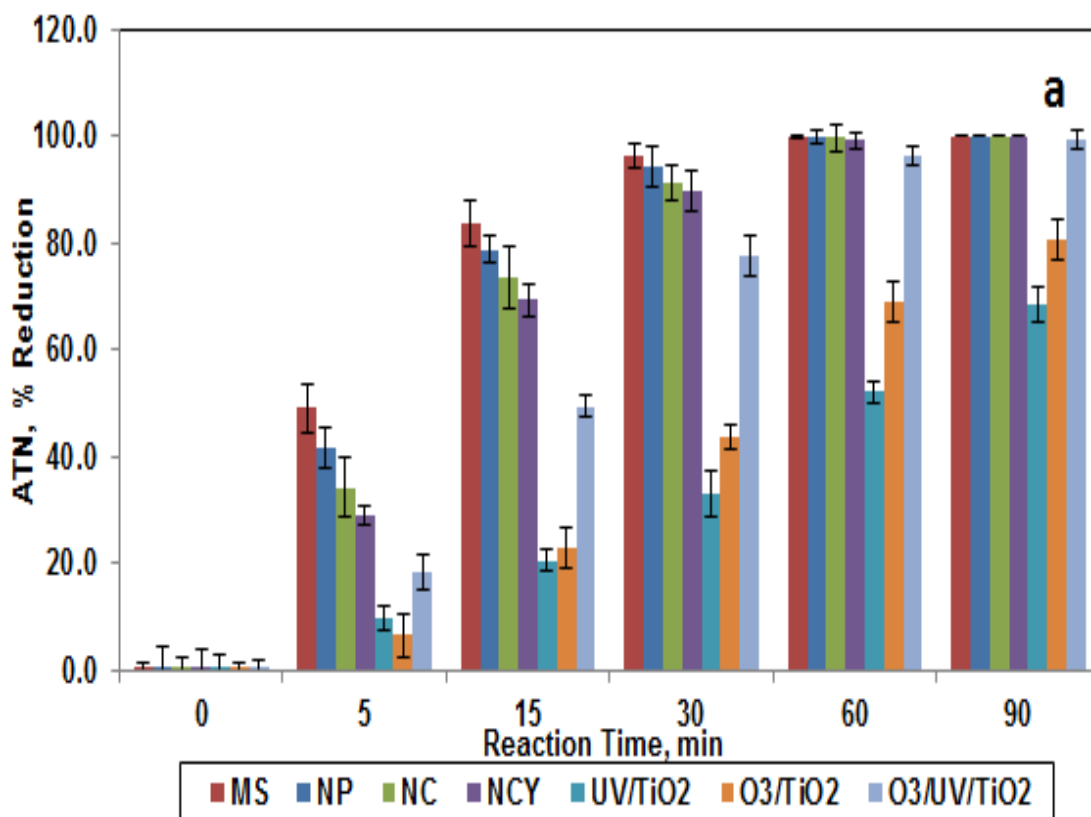


Figure 4.30. Comparison of photocatalytic decomposition of MS, NP, NC and NCY  $\text{In}_2\text{O}_3$  versus UV/TiO<sub>2</sub>, O<sub>3</sub>/TiO<sub>2</sub> and O<sub>3</sub>/UV/TiO<sub>2</sub> for SE at pH = 7, T = 23 ± 1°C (a) ATN (b) CFA and (c) DCF





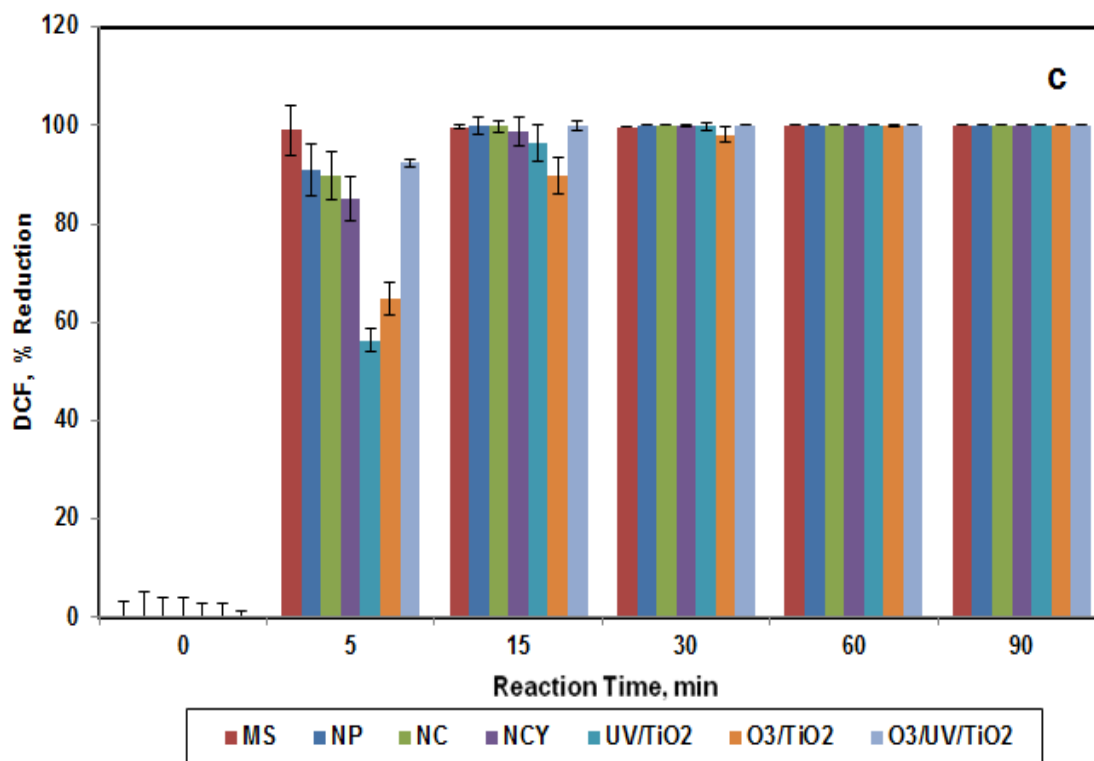


Figure 4.31. Comparison of removal efficiency of MS, NP, NC and NCY  $\text{In}_2\text{O}_3$  versus UV/TiO<sub>2</sub>, O<sub>3</sub>/TiO<sub>2</sub> and O<sub>3</sub>/UV/TiO<sub>2</sub> for SE at pH = 7, T = 23 ± 1°C (a) ATN (b) CFA and (c) DCF

Table 4.12. Rate constants ( $k$ , min<sup>-1</sup>) of various AOPs with their correlation coefficient ( $R^2$ ) values for ATN, CFA and DCF for SE (Chapter 3. V.R. Kandlakuti).

| PPCPs                               | ATN                     |        | CFA                     |        | DCF                     |        |
|-------------------------------------|-------------------------|--------|-------------------------|--------|-------------------------|--------|
|                                     | $k$ , min <sup>-1</sup> | $R^2$  | $k$ , min <sup>-1</sup> | $R^2$  | $k$ , min <sup>-1</sup> | $R^2$  |
| UV/TiO <sub>2</sub>                 | 0.0128                  | 0.9953 | 0.0715                  | 0.9981 | 0.2127                  | 0.9974 |
| O <sub>3</sub> /TiO <sub>2</sub>    | 0.0185                  | 0.9973 | 0.0102                  | 0.9978 | 0.1386                  | 0.995  |
| O <sub>3</sub> /UV/TiO <sub>2</sub> | 0.0541                  | 0.9977 | 0.1695                  | 0.9927 | 0.4616                  | 0.9983 |

A comparison of rate constant for UV/TiO<sub>2</sub>, O<sub>3</sub>/TiO<sub>2</sub> and O<sub>3</sub>/UV/TiO<sub>2</sub> are shown in Table 4.12. It can be seen that for DCF, MS showed an increased rate constant of 0.4894 min<sup>-1</sup> compared to 0.4616 min<sup>-1</sup> of O<sub>3</sub>/UV/TiO<sub>2</sub>. For CFA and ATN, the rate constant of MS was almost double compared to O<sub>3</sub>/UV/TiO<sub>2</sub>. It can also be seen that NP and NC has higher k values for CFA and ATN but slightly lower k values for DCF compared to O<sub>3</sub>/UV/TiO<sub>2</sub>. The k values for ATN with NCY were higher compared to O<sub>3</sub>/UV/TiO<sub>2</sub>.

As per FTIR spectral results, it can be seen that due to presence of hydroxyl groups, the surface of nano particles is highly active which produces several types of defects. Other point defects and oxygen vacancies originate in these defects due to high active surface on indium oxide nano particles. On the hydrophilic surface of the oxide several In<sup>3+</sup> ions may be found due to high specific surface area of indium oxide nano particles (Taguchi and Saito, 1999). Water molecules or hydroxyl groups produce hydrogen bonds that may adsorb on the surface of nano particles. From literature (Ohhata and Shinoki, 1979) it was observed that nanostructures and thin films emit photoluminescence compared to conventional micron sized In<sub>2</sub>O<sub>3</sub> which at room temperature does not emit light (Murali et al., 2001; Seo et al., 2003; Zhao et al., 2004; Zhou et al., 1999; Peng et al., 2002 and Guha et al., 2004). According to Li et al., (2013) the surface area of microspheres determined by BET was far greater compared to other nano particles offering greater reaction centers for active adsorption and higher activity which closely agrees to the microspheres prepared in the present study showing greater number of porous microspheres for increased activity.

Based on the above observations, it is seen that microspheres, nanoplates and nanocubes acts as a very good substitute for O<sub>3</sub>/UV/TiO<sub>2</sub> in the degradation of ATN, CFA and DCF from secondary effluents. Indirect ·OH radicals for TiO<sub>2</sub> or direct hole oxidation for In<sub>2</sub>O<sub>3</sub> are the two types of mechanisms proposed by Li et al., 2012 for PFOA decomposition. Similar assumptions can be made in the present study, as it was observed that the rate constants were higher for PPCPs decomposition by In<sub>2</sub>O<sub>3</sub> nano particles compared to indirect ·OH radicals for TiO<sub>2</sub>. Although indirect ·OH radicals showed effective removal of PPCPs from SE, but a tight coordination between In<sub>2</sub>O<sub>3</sub>

and PPCPs may be due to bridging or bidentate mode which may provide a higher activity of  $\text{In}_2\text{O}_3$  to photo generate holes under UV irradiation thus directly aiding in the decomposition of PPCPs. The high specific surface area on the surface of a photocatalyst will enable the photocatalytic reaction to take place and depends on the various nano structures and their preparation that leads to different oxygen vacancies and surface area on the catalyst (Li et al., 2013). The chemical states of surface O and In elements may undergo direct charge transfer between functional groups of ATN, CFA and DCF and  $\text{In}_2\text{O}_3$  leading to the adsorption and decomposition of PPCPs.

#### 4.4 Conclusion

- A solvothermal and co-precipitation method followed by calcination was used to synthesize four nanostructures of porous microspheres, nanoplates, nanocubes and nano crystals.
- The photocatalytic decomposition of ATN, CFA and DCF by MS was greater due to higher oxygen vacancies and surface area compared to NP, NC and NCY and follows the order  $\text{MS} > \text{NP} > \text{NC} > \text{NCY}$ .
- Photocatalytic activity of DW was higher compared to SE for NCY.
- The photocatalytic activity of porous microspheres, nanoplates, nanocubes and nanocrystals exhibited superior catalytic performance compared to  $\text{O}_3/\text{UV}$ ,  $\text{UV}/\text{TiO}_2$  and  $\text{O}_3/\text{UV}/\text{TiO}_2$  in the degradation of ATN, CFA and DCF from secondary effluents.
- Complete photocatalytic decomposition could be achieved at a faster rate compared to  $\text{O}_3/\text{UV}/\text{TiO}_2$ .

## 4.5 References

- Blaschko, H., 1954. Metabolism of epinephrine and norepinephrine. *Pharmacol. Rev.* 6, 23-28.
- Bianchi, S., Comini, E., Ferroni, M., Faglia, G., Vomiero, A., Sberveglieri, G., 2006. Indium oxide quasi-monodimensional low temperature gas sensor, *Sens. Actuators, B* 118, 204–207.
- Cao, H., Qiu, X., Ciang, Y., Zhu, Q., 2003. Room-temperature ultraviolet-emitting  $\text{In}_2\text{O}_3$  nanowires. *Appl Phys Lett.* 83:761–3.
- Chandradass, J., Bae D.S., Kim K.H., 2011. A simple method to prepare indium oxide nanoparticles: Structural, microstructural and magnetic properties. *Advanced Powder Technology.* 22, 370–374.
- Chandradass, J., Kyong, S.H., Dong, S.B., 2008. Synthesis and characterization of zirconia and silica doped zirconia nanopowders by oxalate processing. *J. Mater. Sci. Technol.* 206, 315–321.
- Chu, D., Zhung, Y., Jiang, D., Xu, J., 2007. Tuning the phase and morphology of  $\text{In}_2\text{O}_3$  nanocrystals via simple solution routes. *Nanotech.* 18:435605.
- Curreli, M., Li, C., Sun, Y., Lei, B., Gundersen, M.A., Thompson, M.E., Zhou, C., 2005. Selective functionalization of  $\text{In}_2\text{O}_3$  nanowire mat devices for biosensing applications. *J. Am. Chem. Soc.* 127, 6922–6923.
- George, P.P., Gedanken, A., 2008. Synthesis, characterization and photoluminescence properties of  $\text{In}_2\text{O}_3$  nanocrystals encapsulated by carbon vesicles and neat  $\text{In}_2\text{O}_3$  nanocrystals generated by the RAPET technique. *Eur. J. Inorg. Chem.* 919–924.
- Ghimbeu, C.M., Schoonman, J., Lumberras, M., 2008. Porous indium oxide thin films deposited by electrostatic spray deposition technique. *Ceram Int.*34:95.
- Guengerich, P.F., 2006. Cytochrome P450s and other enzymes in drug metabolism and toxicity. *The AAPS Journal.* 8 (1). Article 12. (<http://www.aapsj.org>).
- Guha, P., Kar, S., Chaudhun, S., 2004. Direct synthesis of single crystalline  $\text{In}_2\text{O}_3$  nanopyramids and nanocolumns and their photoluminescence properties. *Appl. Phys. Lett.* 85, 3851–3853.
- Gurlo, A., Ivanovskaya, M., Barsan, N., Schweizer-Berberich, M., Weimar, U., Gopel, W., Die´guez, A., 1997. Grain size control in nanocrystalline  $\text{In}_2\text{O}_3$  semiconductor gas sensors. *Sens. Actuators. B* 44, 327–333.
- Harvey, S.P., Mason, T.O., Gassenbauer, Y., Schafranek, R., Klein, A., 2006. Surface versus bulk electronic/ defect structures of transparent conducting oxides: I. Indium oxide and ITO. *J Phys D, Appl Phys.* 39:3959–68.

- Heberer, T., Feldmann, D., 2005. Contribution of effluents from hospitals and private households to the total loads of diclofenac and carbamazepine in municipal sewage effluents-modeling versus measurements. *J Hazard Mater.* 122:211–218. Erratum in: *J Hazard Mater* 127:249.
- Ho, W.H., Yen, S.K., 2006. Preparation and characterization of indium oxide film by electrochemical deposition. *Thin Solid Films.* 498:80–4.
- Jeong, J.S., Lee, J.Y., Lee, C.J., An, S.J., Yi, G.C., 2004. Synthesis and characterization of high quality  $\text{In}_2\text{O}_3$  nanobelts via catalyst-free growth using a simple physical vapour deposition at low temperature. *Chem Phys Lett.* 384:246–50.
- Kaur, M., Jain, N., Sharma, K., Bhattacharya, S., Roy, M., Tyagi, A.K., 2008. Room temperature  $\text{H}_2\text{S}$  gas sensing at ppb level by single crystal  $\text{In}_2\text{O}_3$  whiskers. *Sens Actuators, B.* 133:456–60.
- Kim, D.W., Hwang, I.S., Kwon, S.J., Kang, H.Y., Park, K.S., Choi, Y.J., Choi, K., Park, J.G., 2007. Highly conductive coaxial  $\text{SnO}_2$ - $\text{In}_2\text{O}_3$  heterostructured nanowires for Li ion battery electrodes. *Nano Lett.* 7, 3041–3045.
- Kumar, M., Singh, V.N., Singh, F., Lakshmi, K.V., Mehta, B.R., Singh, J.P., 2008. On the origin of photoluminescence in indium oxide octahedron structures. *Appl. Phys. Lett.* 92, 171907–171911.
- Kümmerer, K., Längin, A., Hädrich, C., Schuster, A., 2008. Flows of active pharmaceutical ingredients due to health care-on a local, regional, and nationwide level in Germany – is hospital effluent treatment an effective approach for risk reduction? Submitted.
- Lavareda, G., Nunes D.C.C., Fortunato, E., Ramos, A.R., Alves, E., Conde, O., 2006. Transparent thin film transistors based on indium oxide semiconductor. *J. Non-cryst Solids.* 352:2311–4.
- Lee, J. W., Kidder, M., Evans, B. R., Paik, S., Buchanan, A. C., Garten, C. T., and Brown, R. C., 2010. Characterization of of biochars produced from cornstovers for soil amendment, *Environ. Sci. Technol.*, 44, 7970–7974.
- Li, B., Xie, Y., Jing, M., Rong, G., Tang, Y., Zhang, G., 2006.  $\text{In}_2\text{O}_3$  hollow microspheres: synthesis from designed  $\text{In}(\text{OH})_3$  precursors and applications in gas sensors and photocatalysis. *Langmuir.* 22, 9380–9385.
- Li, Z., Zhang, P., Shao, T., Wang, J., Jin, L., Li, X., 2013. Different nanostructured  $\text{In}_2\text{O}_3$  for photocatalytic decomposition of perfluorooctanoic acid (PFOA). *Journal of Hazardous Materials.* 260 (2013) 40– 46.
- Liang, C., Meng, G., Lei, Y., 2001. Catalytic growth of semiconducting  $\text{In}_2\text{O}_3$  nanofibers. *Adv Mater.* 13:1330–3.

- Maensiri, S., Laokul, P., Klinkaewnarong, J., Phokha, S., Promarak, V., Seraphin, S., 2008. Indium oxide ( $\text{In}_2\text{O}_3$ ) nanoparticles using Aloe vera plant extract: synthesis and optical properties. *J. Opt. Adv. Mater.* 10, 161–165.
- Maillis, S., Boutsikaris, L., Vainos, N.A., Xirouhaki, C., Vasiliou, G., Garawal, N., 1996. Holographic recording in indium-oxide ( $\text{In}_2\text{O}_3$ ) and indium–tin-oxide ( $\text{In}_2\text{O}_3:\text{Sn}$ ) thin films. *Appl Phys Lett.* 69:2459–61.
- Manificier, J.C., Szepersy, L., Bresse, J.F., Perotin, M., 1979.  $\text{In}_2\text{O}_3:(\text{Sn})$  and  $\text{SnO}_2:(\text{F})$  films – application to solar energy conversion Part II – electrical and optical properties. *Mater Res Bull.* 14:163–75.
- Maqueda, L.A., Wang, L., Matijevic, E., 1998. Nanosize indium hydroxide by peptization of colloidal precipitates. *Langmuir.* 14:4397–401.
- Murali, A., Barve, A., Leppert, V.J., Risbud, S.H., 2001. Synthesis and characterization of indium oxide nanoparticles. *Nano Lett.* 1. 287–289.
- Ohhata, Y., Shinoki, F., Yoshida S., 1979. Optical properties of R.F. reactive sputtered tin-doped  $\text{In}_2\text{O}_3$  films. *Thin Solid Films.* 59, 255–261.
- Packer, J.L., Werner, J.J., Latch, D, E., Arnold, W.A., and McNeill, K., 2003. Photochemical fate of pharmaceuticals in the environment: naproxen, diclofenac, clofibric acid, and ibuprofen. *Aquatic Sciences*, v. 65(4), pp. 342-351.
- Peng, X.S., Meng, G.W., Zhang, J., Wang, X.F., Wang, Y.W., Wang, C.Z., 2002. Synthesis and photoluminescence of single crystalline  $\text{In}_2\text{O}_3$  nanowires. *J. Mater. Chem.* 12, 1602–1605.
- Sarkar, A., Kapoor, S., Mukherjee, T., 2009. Effective chemical route for the synthesis of silver nanostructures in formamide. *Res. Chem. Intermed.* 35, 71–78.
- Seetha, M., Bharathi, S., Dhayal, R.A., Mangalaraj, D., Nataraj, D., 2009. Optical investigations on indium oxide nano-particles prepared through precipitation method. *Materials Characterization.* 60, 1578 – 1582.
- Seo, W.S., Jo, H.H., Lee, K., Park, J.T., 2003. Preparation and optical properties of highly crystalline, colloidal and size controlled indium oxide nanoparticles. *Adv. Mater.* 15, 795–797.
- Shchukin, D.G., Caruso, R.A., 2004. Template synthesis and photocatalytic properties of porous metal oxide spheres formed by nanoparticle infiltration. *Chem Mater.* 16:2287–92.
- Singh, V.N., Mehta, B.R., 2003. A two-step synthesis procedure for  $\text{In}_2\text{O}_3$  nanoparticle films having well-defined particle size, *Jpn. J. Appl. Phys* 42, 4226–4232.

Soulantica, K., Erades, L., Sauvan, M., Senooq, F., Maisonnat, A., Chandret, B., 2003. Synthesis of indium and indium oxide nanoparticles from indium cyclopentadienyl precursor and their application for gas sensing. *Adv. Funct. Mater.* 13, 553–557.

Souza, E.C.C., Rey, J.F.Q., Muccillo, E.N.S., 2009. Synthesis and characterization of spherical and narrow size distribution of indium oxide nanoparticles. *Applied Surface Science* 255, 3779–3783.

Taguchi, Y., Saito, N., 1999. Preparation of fine composite particles composed of inorganic solid powders and organic polymers by utilizing liquid-liquid dispersion. *Colloids Surf. A* 153, 401–404.

Thomas, R.C., and Ikeda, C.J., 1966. *J. Med. Chem.* 9: 507.

Tom Tague, Bruker Optics Inc., Infrared Spectral Interpretation ([www.bruker.com](http://www.bruker.com)). Date retrieved: 2016/02/11.

Wu, X.C., Hong, J.M., Han, Z.J., Tao, Y.R., 2003. Fabrication and photoluminescence characteristics of single crystalline  $\text{In}_2\text{O}_3$  nanowires. *Chem Phys Lett.* 373:28–32.

Zhan, Z., Song, W., Jiang, D., 2004. Preparation of nanometer-sized  $\text{In}_2\text{O}_3$  particles by a reverse micro emulsion method. *J. Colloid Interf. Sci.* 271, 366–371.

Zhang, D., Li, C., Han, S., Liu, X., Tang, T., Jin, W., 2003. Ultraviolet photodetection properties of indium oxide nanowires. *Appl Phys A, Mater Sci Process.* 77:163–6.

Zhang, D.H., Li, C., Han, S., Liu, X.L., Tang, T., Jin, W., Zhou, C.W., 2003. Electronic transport studies of single-crystalline  $\text{In}_2\text{O}_3$  nanowires. *Appl. Phys. Lett.* 82, 112–114.

Zhang, Y., Li, J., Li, Q., Zhu, L., Liu, X., Zhang, X., 2007. Preparation of  $\text{In}_2\text{O}_3$  ceramic nanofibers by electrospinning and their optical properties. *Scripta Materialia.* 56:409–12.

Zhao, Y., Zhang, A., Wu, Z., Dang, H., 2004. Synthesis and characterization of single-crystalline  $\text{In}_2\text{O}_3$  nanocrystals via solution dispersion. *Langmuir* 20, 27–29.

Zhenmin, Li., Pengyi, Z., Tian, S., Jinlong, W., Ling, J., Xiaoyun, L., 2013. Different nanostructured  $\text{In}_2\text{O}_3$  for photocatalytic decomposition of perfluorooctanoic acid (PFOA). *Journal of Hazardous Materials* 260, 40– 46.

Zhou, H., Cai, W., Zhang, L., 1999. Synthesis and structure of indium oxide nanoparticles dispersed within pores of mesoporous silica. *Mater. Res. Bull.* 34, 845–849.

Zilnik, L. F., Jazbinsek, A., Hvala, A., Vrecer, F., Klamt, A., 2007. Solubility of sodium diclofenac in different solvents. *Fluid Phase Equilibria* 261, 140-145.



## Chapter 5

### 5 Preparation and characterization of Biochar and its application in the removal of PPCPs from wastewater and comparison to removals by natural zeolites

#### 5.1 Introduction

For the past 30 years pharmaceuticals and personal care products (PPCPs) have fuelled the interest to research beyond surface-water bodies to examine issues in other matrices such as groundwater (Mozaz et al., 2004; Kreuzinger et al., 2004; Scheytt et al., 2004; Heberer et al., 2004; Bruchet et al., 2005; Verstraeten et al., 2005), landfill leachates (Barnes et al., 2004; Bound et al., 2005; Slack et al., 2005), sediments (Aguera et al., 2003 and Morales et al., 2005) and biosolids (Harrison et al., 2006 and Kimney et al., 2006) and their fate and transport in surface water (Ashton et al., 2004; Glassmeyer et al., 2005; Batt et al., 2006 and Gros et al., 2006), groundwater (Drewes et al., 2003; Kreuzinger et al., 2004; Heberer et al., 2004; Masters et al., 2004; Asano et al., 2004; Cordy et al., 2004; Zuehlke et al., 2004; Snyder et al., 2004 and Matamoros et al., 2005) and soils amended with reclaimed water (Kinney et al., 2006 and Pedersen et al., 2005) or biosolids (Buyuksonmez et al., 2005, Overcash et al., 2005 and Xia et al., 2005).

Studies on source elucidation of PPCPs in wastewater treatment plant (WWTP) effluents (Gross et al., 2004; Glassmeyer et al., 2005; Zuccato et al., 2005; Lindqvist et al., 2005; Gros et al., 2006; Verenitch et al., 2006 and Brun et al., 2006), confined animal feeding operations (CAFOs) (Batt et al., 2006 and Brown et al., 2006) and aquaculture (Dietze et al., 2005 and Cabello et al., 2006), their removal during wastewater (Gros et al., 2006, Lee et al., 2005, Quintana et al., 2004 and 2005, Clara et al., 2005; Bendz et al., 2005; Santos et al., 2005; Miao et al., 2005 and Roberts et al., 2006) and drinking-water (Bruchet et al., 2005; Stackelberg et al., 2004; Westerhoff et al., 2005; Jones et al., 2005; Snyder et al., 2003; Hernando et al., 2006; Rule et al.,

2005; Dodd et al., 2004 and Seitz et al., 2006) treatment and their effects on aquatic ecosystems (Cunningham et al., 2006; Sanderson et al., 2004; Fent et al., 2006; Richards et al., 2004 and Mimeault et al., 2005), terrestrial ecosystems (Swan et al., 2006 and Meteyer et al., 2005) and human health (Pomati et al., 2006 and Jones et al., 2004) have also been conducted. Studies have shown toxicological effects of diclofenac in kidney, intestine, liver and gills of rainbow trout (*Oncorhynchus mykiss*) as the lowest observed effect concentration (LOEC) was 1µg/L for cytological alterations (Triebkorn et al., 2004). Similarly surface waters showed around 500ng/L of Atenolol as the initial predicted environmental concentration (PEC) which exceeded the 10ng/L of action limit in Phase I of risk assessment as per European guidelines. Thus, further risk assessment of Phase II was conducted to show acceptable risks for aquatic microorganisms, ground water and surface water. Atenolol showed low lipophilicity and low affinity for sorption to sediment (Anette Kuster et al., 2009). Clofibric acid has been detected in Berlin tap water samples between 10 and 165 ng/L as well as 0.5 to 7.8 ng/L concentration in North sea due to its large consumption in thousands of tons annually as it is used to treat high blood pressure, cardiac function failure, coronary heart disease, arrhythmia etc. Several literature studies have shown limited biodegradation of clofibric acid in wastewater treatment plant (Wenzhen Li et al., 2011).

PPCPs are bioactive chemicals of growing concern throughout the world due to high usage of drugs, their partial metabolism after ingestion and improper disposal in the aquatic environment. These issues raise concerns for immediate action to be taken to further understand the factors that contribute to the combined load of these chemicals in the environment. Most drug manufacturing industries dispose waste (by-products, solvents, catalysts, intermediates and salts) per unit of actual product that is produced from the pharmaceutical industry. These compounds show low concentrations in water from a few parts per billion to few parts per trillion. Every day the United States and Canada discharge 4.8 billion gallons of treated effluent from 1400 wastewater treatment plants into the Great Lakes which can pose a great threat to humans and aquatic organisms as some of these compounds are persistent in the environment and breakdown into intermediate products or form cocktail (mixture of different

compounds) that are more toxic than the parent compound. Sewage treatment plants are not able to remove these compounds as concentrations of 1-2 $\mu\text{g/L}$  of diclofenac for example are found in streams connected to these plants (Heberer et al., 1998; Ternes, 1998; Lehmann 2000; Ternes, 2001). Currently there are no federal regulations on pharmaceuticals in drinking water or waste water. Unwanted side effects of diclofenac have been reported to occur in the kidneys, livers and intestines of humans and other mammals (Bhogaraju et al., 1999; Revai and Harnos, 1999; Ramesh et al., 2002). It has been observed that the exposure of zebrafish embryos to diclofenac at concentrations over 10.13 $\mu\text{M}$  were lethal to all the embryos while it was teratogenic at 3.78 $\mu\text{M}$ . Various abnormalities were reported for the embryos such as smaller eye, body edema and pericardial, shorter body length, abnormal pigmentation, muscle degeneration, lack of circulation, intestine and liver and even altered genes expression to a certain extent (Bin et al., 2014). In the present study, atenolol, clofibrac acid and diclofenac are the selected PPCPs, as they are consumed widely around the world and often end up at wastewater treatment plants.

Biochar has a high organic C content and a long-term stability (mean residence time of C varies 90 to 1600 years based on intermediate and labile stable C components (Singh et al., 2012) that improve the biological and physicochemical properties of soil and serves as soil conditioner and increases the water retention capacity as organic carbon increases. The biochar is produced by thermochemical process when biomass (such as manure, leaves or wood) rich in carbon is heated in a closed container in the absence of oxygen (Lehmann and Joseph, 2009). The produced porous biochar has physicochemical properties that are suitable for safe and long-term storage of carbon in the environment (Shackley et al., 2012). In general, pyrolysis and gasification or dry carbonization produces biochar, whereas hydrothermal carbonization of biomass produced under pressure as a slurry in water is termed hydrochar. The hydrochar and biochar differ in physical and chemical properties widely (Bargmann et al., 2013). Waste management, energy production, climate change mitigation and soil improvement are the four major areas in environmental management where biochar is being used (Lehmann and Joseph, 2009).

Figure 5.1 shows the reaction that takes place in the carbonization of wood that leads to the formation of biocarbon, water, carbon dioxide, carbon monoxide and pyrolysis tars (<http://www.alternabiocarbon.com/carbonization/carbonization-of-wood>).

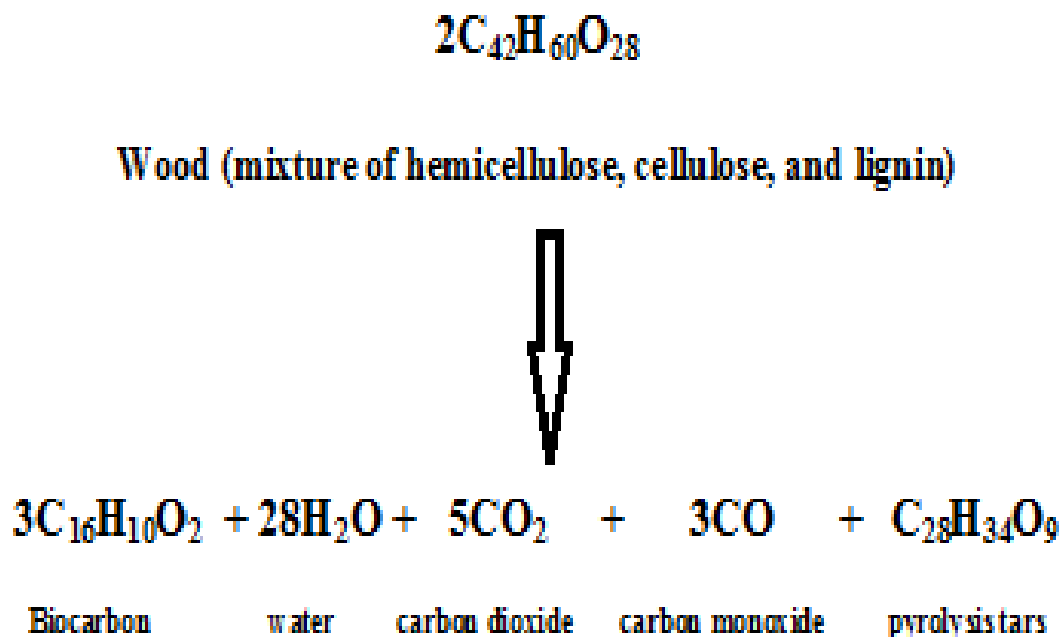


Figure 5.1. Carbonization of Wood

Most biochars have neutral to alkaline pH while acidic biochars have also been reported (Chen et al., 2007) and the pH mostly depends on the feedstock type and the thermochemical process of production. Biochar produced from waste biomass includes waste from forestry, food processing, municipal and paper mill, crop residues, sewage sludge and animal manure (Brick, 2010; Chen et al., 2011; Cantrell et al., 2012; Enders et al., 2012). Biochar provides five valuable benefits such as soil fertilization (increases nutrient retention, crop yields, mineral nutrition and mycorrhizal fungal activity), carbon sequestration, energy production, waste reduction and pollution prevention (reduces greenhouse gas emissions such as CH<sub>4</sub> and N<sub>2</sub>O) apart from adsorption of ammonium and phosphates chemical fertilizers, reducing irrigation requirement and

acidity and protection of water quality by preventing leaching and runoff of nutrients from the soil.

Application of biochar in environmental remediation has been studied recently and provides information on the effect of feedstock types, pyrolysis conditions, including temperature, residence time and heat transfer rate with water and soil contaminants. Biochar also known as black carbon or ‘supersorbent’ (Lohmann 2003; Koelmans et al., 2006; Bornemann et al., 2007) acts as a universal sorbent because of its ability to adsorb organic contaminants in soils and finds several applications in the remediation of inorganic and organic contaminants in water and soil (Saeed et al., 2005; Salih et al., 2011; Yang et al., 2011; Ahmad et al., 2012c) and improves microbial population which accelerates decomposition of soil native C (Kuzyakov et al., 2013). It was also observed that pesticides such as atrazine and simazine adsorption capacities are 1~2 orders of magnitude higher on biochar compared to compost or agricultural soils.



Figure 5.2. Probable mechanisms of the interactions of organic contaminants with biochar (Ahmad, M. et al., 2013)

Several mechanisms such as adsorption or electrostatic attraction/repulsion or partitioning between organic contaminants and biochar interactions had been summarized in Figure 5.2 and studies have been focused on herbicides, dyes, polycyclic aromatic hydrocarbons, antibiotics and pesticides (Qiu et al., 2009; Beesley et al., 2010; Zheng et al., 2010; Teixido et al., 2011; Xu et al., 2012). In Figure 5.2, partition or adsorption is shown in circles on biochar particle where I indicate the electrostatic interaction between organic contaminant and biochar, II shows interaction between polar organic contaminant and biochar due to electrostatic attraction, and III shows interactions between non-polar contaminants and biochar due to electrostatic attractions. Biochar produced at  $> 400^{\circ}\text{C}$  has high microporosity, surface area and aromaticity but low surface polarity and is mostly negatively charged.

In the present study biochar (BC) was synthesized at  $700^{\circ}\text{C}$  by a slow pyrolysis process and adsorption experiments were conducted to investigate the removal of selected PPCPs namely atenolol (ATN), clofibrac acid (CFA) and diclofenac (DCF) from municipal wastewater secondary effluent.

Zeolites have Aluminum (Al) and Silica (Si) covalent oxides that form interconnected cages or channels due to their porous structure. Due to the difference in oxidation states of Si (IV) and Al (III), the negative charge on zeolite framework is balanced by exchangeable cations. The general chemical formula of zeolite is  $\text{M}^{\text{k}+}_{\text{x/k}}[\text{Al}_x\text{Si}_y\text{O}_{2(\text{x}+\text{y})}] \text{ZH}_2\text{O}$  (where  $\text{M}^+$  is the exchangeable cation) and these zeolites show vast structural diversity with different pore opening, topologies and pore sizes. So for the present study Chabazite (Chb) was considered as one of the natural zeolites as it is porous and has crystalline aluminosilicates framework of 8-ring class with cation exchangeable sites as shown in Figure 5.3 (Barrer 1949, Barrer and Brook 1953). Chb is also selective as it occludes and based on their size separates the molecules. It was seen in previous studies that zeolites alone cannot remove PPCPs from water due to its selectivity. Hence the current purpose of choosing chabazite was to form a framework along with biochar

which will enhance the exchange capacity and adsorption of micropollutants based on their molecular size, porosity and surface area.

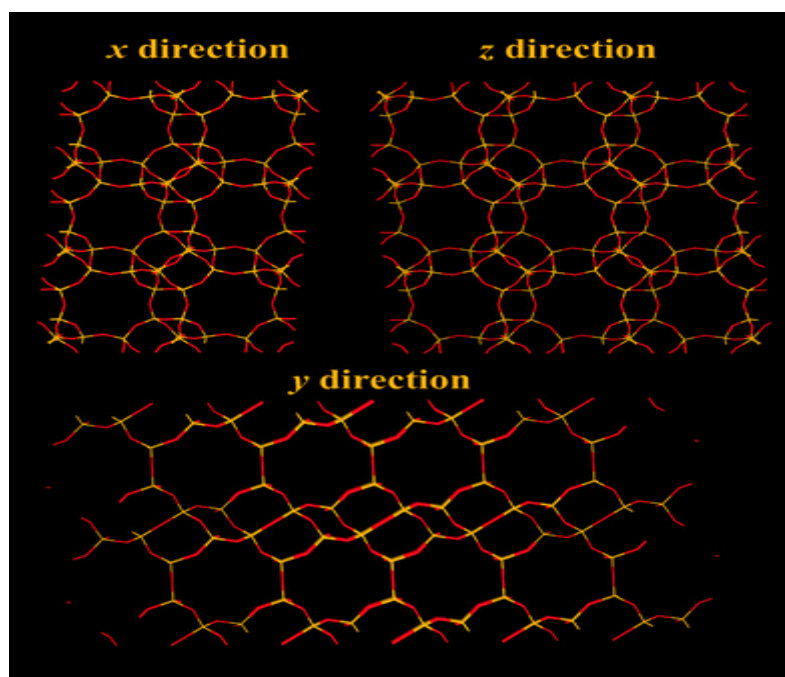


Figure 5.3. Representation of the Chabazite structure with O atoms represented by red lines and Si (or Al) bonds to O represented by yellow lines.

Activated Carbon (AC) is a black solid carbonaceous material with high porosity, surface area and adsorbing capacity produced by pyrolysis where a carbonaceous source material such as wood, coconut shell, lignite, coal, coir pith, paddy husk, etc is heated in the absence of air followed by decomposition and conversion to carbonized material (Yusof and Ismail, 2012). The obtained AC finds wide applications in the removal of metals and other organic contaminants from air, water and gases (Ding et al., 2014). Both physical and chemical oxidation methods are used to impregnate the surface oxygen functional groups into the carbon. The adsorption capacity is mainly attributed to pores ranging from micropores ( $r < 1\text{nm}$ ) and macropores ( $r > 25\text{nm}$ ) to its internal pore volume that are distributed throughout the solid as mesospheres ( $1 < r < 25\text{nm}$ ) shown in Figure 5.4 (Begg Cousland Envirotech Limited., 2015). The micropores are the main areas responsible for adsorption, the mesopores aid in

transportation while macropore acts as an entrance to the activated carbon. Adsorption process will be enhanced when the pore sizes of pollutants are of the same size as that of AC (Huang et al., 2014). Powdered Activated Carbon (PAC), Granular Activated Carbon (GAC) and Fiber Activated Carbon (FAC) are some of the commercially available ACs.

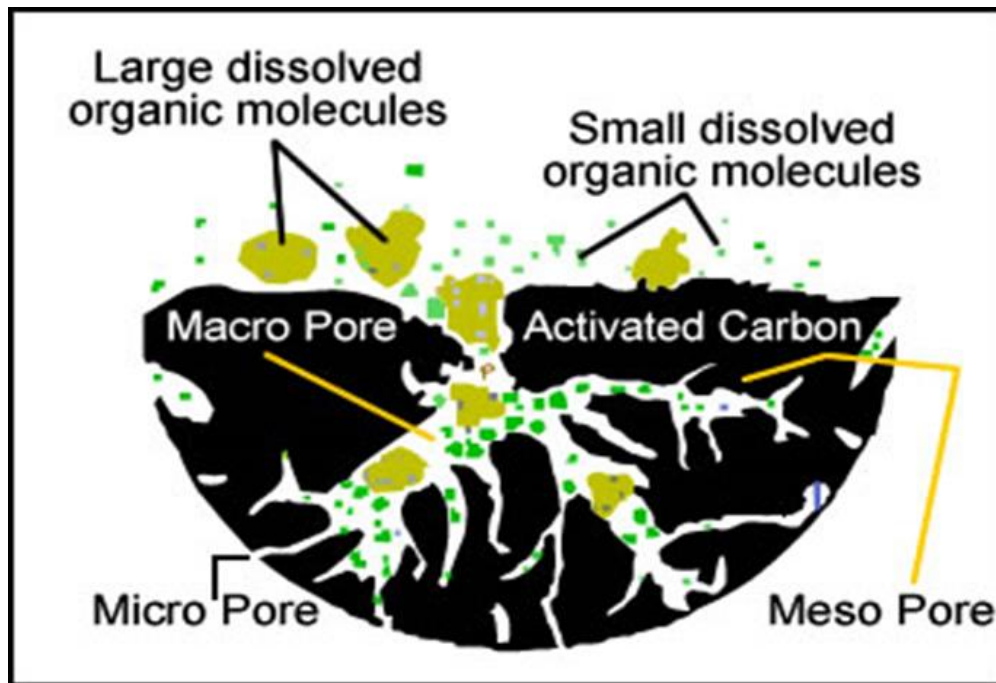


Figure 5.4. Distribution sizes of various pores and its adsorption phenomena in activated carbon.

ACs exhibits high surface areas ranging from 500 to 2000  $\text{m}^2/\text{g}$ , with their pore sizes in the range of 0.5 to  $2.5\text{m}^2/\text{g}$  (Marsh, 2001). AC finds several applications in metal extraction, gold purification, medicine, water purification, sewage treatment, gas purification, solvent recovery and other vapours, filters in compressed air and gas masks and respirators.



## 5.2 Experimental Methods

### 5.2.1 Materials and Reagents

Atenolol, Clofibric Acid, Diclofenac Sodium, activated carbon, potassium hydroxide (KOH), sodium chloride (NaCl), hydrochloric acid (HCl), sodium hydroxide (NaOH) and nitrocellulose membrane filters (pore size 0.22 $\mu$ m and diameter 47mm) were purchased from Sigma Aldrich. Natural zeolite as Chabazite (Chb), was obtained from AECL, Canada, and deciduous wood material (charcoal) from Ghana, West Africa.

Exactly 10,000mg/L of individual stock solutions of ATN and CFA and 1,000mg/L of DCF were prepared in Milli-Q water by weighing on the Mettler balance to 0.0001g and made up to the desired volume and stored at -20<sup>0</sup>C for further analysis. Several intermediate and mixed standard solutions of 10, 20 and 30ppm were prepared by taking a known aliquot from the stock standard solution. All aqueous solutions were prepared with high purity water produced with a Thermo Barnstead Nanopure System (Thermo Fischer Scientific, Whaltman, MA, USA).

### 5.2.2 Synthesis of biochar

A thermochemical decomposition of biomass at 700<sup>0</sup>C by a slow pyrolysis results in the production of biochar as shown in Figure 5.5. A waste biomass such as charcoal wood was taken in the present study and temperature of the muffle furnace was raised at a rate of 7<sup>0</sup>C/min to reach the desired temperature of 700<sup>0</sup>C in the absence of oxygen. The sample was kept at the set temperature for 1 hr and allowed to cool to room temperature. Immediately, the sample was transferred into an air tight sealed container as shown in Figure 5.6.

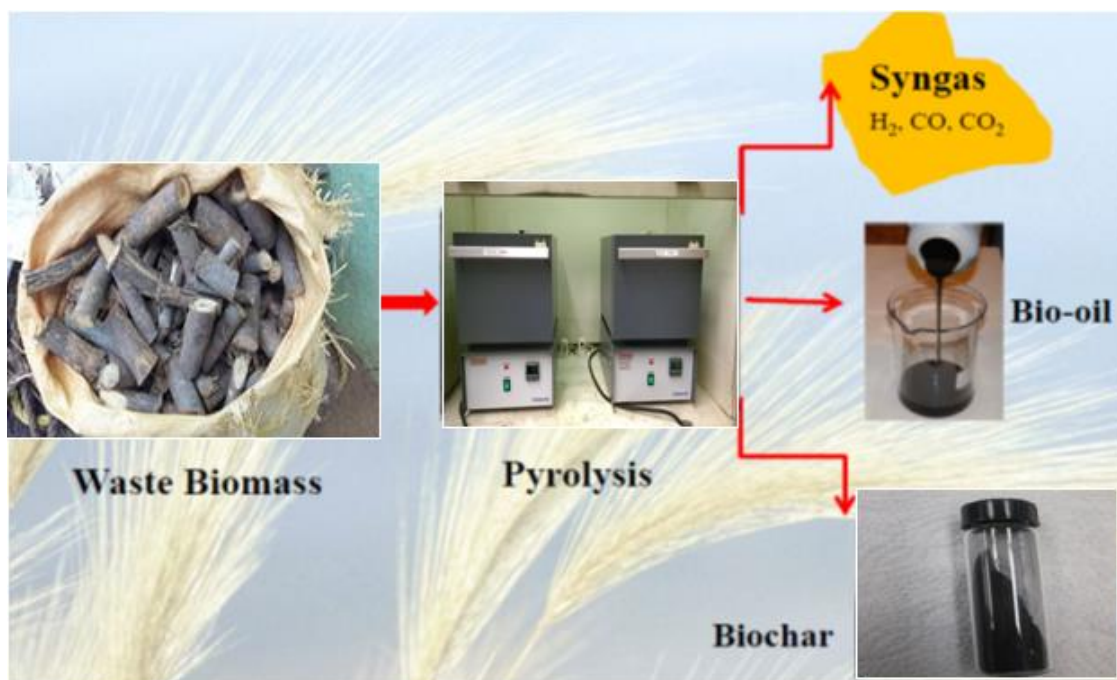


Figure 5.5. Production of biochar, biooil and syngas from thermochemical decomposition of waste biomass by a process of pyrolysis.

Hemicellulose, cellulose and lignin are the three main components produced at different pyrolysis temperatures (Yang et al., 2007). Hemicellulose decomposes between 220 and 315°C and the reaction is exothermic, while cellulose decomposes between 315 and 400°C in an endothermic reaction and lignin decomposes between 160 and 900°C and is exothermic. Various saccharides such as glucose, mannose, galactose and xylose are present in hemicellulose. A very high yield of CO<sub>2</sub> was generated for hemicellulose while higher CO yield was observed for cellulose, whereas lignin generated higher amounts of CH<sub>4</sub> and H<sub>2</sub>.



Figure 5.6. Biochar obtained after slow pyrolysis at 700°C with a ramp temperature of 7°C/min for 1h.

### 5.2.3 Characterization

Field Emission Scanning Electron Microscope (FE-SEM) using Hitachi S-4500 was used for the physical characterization of biochar such as surface structure, size and shape while Energy-dispersive X-ray spectroscopy (EDX) was used for elemental composition with a Quartz PCI XOne SSD X-ray Analyzer.

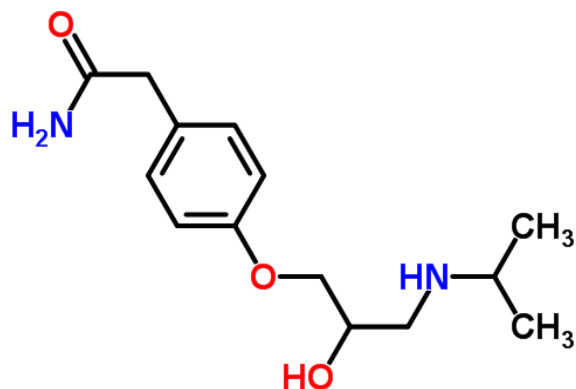
Quantitative structural analyses of the biochars were obtained by solid-state  $^{13}\text{C}$  nuclear magnetic resonance (NMR) spectra using a 4-mm MAS probe on a Varian Inova 500 spectrometer (Palo Alto, CA, USA). NMR was employed to understand the interaction of biochar with solute and elucidate the carbonaceous structure of the adsorbent. Fourier Transform Infra-Red (FTIR) spectroscopy was used to identify the functional groups present in the biochar by Bruker Tensor II system with Hyperion 2000 microscope whereas carbon, hydrogen, nitrogen and sulfur were analyzed by Thermo Scientific FlashEA 1112 series CHNS analyzer. The surface area was analyzed by Brunauer–Emmett–Teller (BET), whereas Agilent 1290 (HPLC), 6460 Liquid Chromatography Triple Quadrupole Mass Spectrometry (LC-MS/MS) was used for the determination of the selected PPCPs.

Table 5.1. Physico-chemical properties of the selected PPCPs

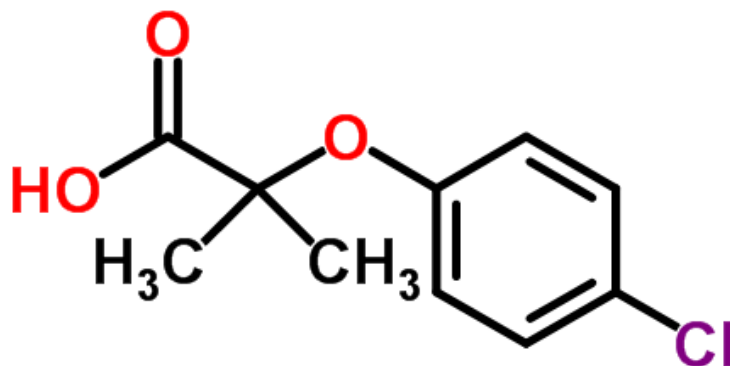
| <b>Compound</b>  | <b>Atenolol</b>  | <b>Clofibric<br/>Acid</b> | <b>Diclofenac<br/>Sodium</b> |
|--|------------------|---------------------------|------------------------------|
| <b>Molecular polarizability,<sup>a</sup> C·m<sup>2</sup>/V</b> | 29.09            | 20.80                     | 29.03                        |
| <b>Molecular refractivity, m<sup>3</sup>/mol</b>               | 73.505           | 52.618                    | 75.461                       |
| <b>pi energy<sup>a</sup></b>                                   | 25.78            | 23.11                     | 33.22                        |
| <b>logP</b>  | 0.43             | 2.90                      | 4.26                         |
| <b>Polar surface area, Å<sup>2</sup></b>                       | 84.58            | 46.53                     | 49.33                        |
| <b>Dreiding energy, kcal/mol</b>                               | 38.10            | 28.6                      | 44.86                        |
| <b>Volume<sup>a</sup>, Å<sup>3</sup></b>                       | 261.34           | 184.05                    | 236.81                       |
| <b>Molecular Weight, g/mol</b>                                 | 266.16           | 214.6                     | 318.13                       |
| <b>pH</b>  | Basic            | Acidic                    | Acidic                       |
| <b>pKa<sup>a</sup></b>   | 9.6              | 3.2                       | 4.15                         |
| <b>log Kow</b>   | 0.16             | 2.57                      | 4.51                         |
| <b>log D (pH 6)<sup>b</sup></b>                                | -1.84            | 0.56                      | 1.77 (pH 7)                  |
| <b>Stokes Diameter (Å)<sup>b</sup></b>                         | 4.9              | 4.1                       | Not Available                |
| <b>Molecular Dimension, (Å * Å * Å)<sup>b</sup></b>            | 3.8 * 6.7 * 14.4 | 3.8 * 5.7 * 9.8           | 4.8 * 7.2 * 10.1             |

<sup>a</sup> Chemicalize.org by ChemAxon (<http://www.chemicalize.org>)

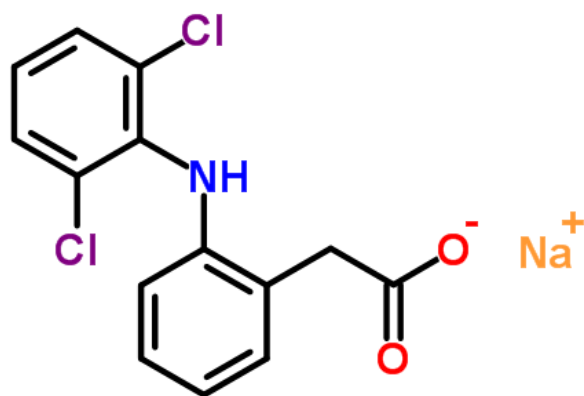
<sup>b</sup> Ridder et al., 2012



(a) Structure of Atenolol



(b) Structure of Clofibric acid



(c) Structure of Diclofenac Sodium

Figure 5.7. Chemical structures of targeted PPCPs compounds

Table 5.1 represents the physico-chemical properties of the selected PPCP compounds where two acidic drugs and one basic drug were chosen. Molecular polarizability, Polar surface area (PSA), Volume and pKa values of ATN are higher compared to CFA and DCF. Whereas Molecular refractivity, log Kow, log P, Volume, Drieding energy, Pi energy, and molecular weight of DCF are considered to be higher compared to CFA. Molecular polarizability provides information on the interactions between electric dipole moment induced by ions or polar molecules by an external electric field with that of nonpolar atoms and molecules. ATN has slightly higher molecular polarizability than DCF. ATN has high water solubility of 26.5 mg/mL at 37°C and a log octanol-water partition coefficient of 0.16 as it is relatively a polar hydrophilic compound. The total hydrogen bonding capacity is measured by a simple tool known as PSA. The PSA of a molecule is the van der Waals surface area of all the nitrogen and oxygen atoms attached to hydrogen atoms in them and shows higher values for ATN compared to CFA and DCF. Passage across human intestinal absorption (Palm et al. 1998 and Clark, D.E., 1999) blood-brain barrier (Kelder et al. 1999 and Clark, D.E., 1999) and flux across a Caco-2 monolayer (Camenisch et al., 1997) can be predicted by using PSA. Some of the physico-chemical properties are explained in more detail in Chapter 2 and Table 2.5 of this thesis (V.R. Kandlakuti). Molecular refractivity is dependent on refractive index, pressure and temperature and is a measure of total polarizability of a mole of a substance. The stability of the input molecule is determined by Drieding energy for the actual 3-D structure. In conjugated hydrocarbon systems, the values of Pi energy is determined by Pi electron energies of molecular orbitals and shows DCF having higher Molecular refractivity, Drieding energy and Pi energy compared to ATN and CFA.

Figure 5.7 represents the chemical structure of Atenolol, Clofibric Acid and Diclofenac. Figure 5.7c represents diclofenac structure as a hybrid between a class derivative of an acetic acid and fenamic acid. For a diclofenac molecule, between the two aromatic rings, a bridging is formed by a secondary amino group (N-H) and represents intramolecular H-bonds towards a carboxylic group of one and the chlorine atom of the other aromatic ring. Between the two different diclofenac molecules, there exist H-

bonds between the carboxylic groups which involve the hydrophilic groups as inter- and intra-molecularly facing together in a dimer (Fini et al., 2010).

Some of the physical properties of chabazite for the present study are represented in Table 5.2 with a BET surface area of  $495.2\text{m}^2/\text{g}$  and a mean particle size diameter of  $930\ \mu\text{m}$ .

Table 5.2. Physical properties of the tested Natural Zeolites (Gallant et al., 2009)

| Type             | Mean Particle Diameter ( $\mu\text{m}$ ) | Skeletal Density ( $\text{kg}/\text{m}^3$ ) | Particle Density ( $\text{kg}/\text{m}^3$ ) | BET Pore Volume ( $\text{mL}/\text{g}$ ) | BET Surface Area ( $\text{m}^2/\text{g}$ ) | Static Bed Voidage |
|------------------|--|---|---|--|--|--------------------|
| <b>Chabazite</b> | 930                                      | 2106  | 1630  | 0.359                                    | 495.2                                      | 0.35               |

\* Company no longer exists, further information can be obtained from L.E.W. Hogg of Arenito Minerals and Chemicals Corporation, Peachland, B.C.

#### 5.2.4 Wastewater collection

A grab method was used to collect 20L of secondary effluent from Adelaide Pollution Control Plant, London, ON, Canada. The sample was filtered through  $0.22\mu\text{m}$  filter paper and stored in 1 L amber colored bottle with approx. 5 drops of 25% (w/v) sodium thiosulphate added as a preservative to each bottle, shaken well and stored at  $4^\circ\text{C}$  for further analysis. All the experiments with secondary effluent free from selected PPCPs were performed by adjusting pH to 9.0 and the temperature was maintained at  $23 \pm 1^\circ\text{C}$ . In another set of experiments, the effect of pH at 3, 5 and 7 were also measured by adjusting the pH with 1N HCl or 1N NaOH.

### 5.2.5 Sorption studies on biochar

Batch experiments were conducted for adsorption of atenolol, clofibric acid and diclofenac in 125ml amber glass containers with different concentrations of PPCPs compounds at varying conditions such as effect of pH, change in concentration of PPCPs. The batch experiments were conducted for biochar by weighing exactly 0.1g, 0.2g, 0.5g, 1.0g and 2.0g each separately and adding 100mL of secondary effluent spiked with known concentration of intermediate standard solution. A blank experiment was also performed similar to the conditions as performed for samples by weighing the same amounts of biochar and mixing with 100mL high purity water and subjected to the same conditions as for the samples. By using a Max-Q 4000 orbital shaker, the bottles were shaken at 180rpm for 1hr at  $25 \pm 1^\circ\text{C}$  without any pH adjustment. After 1hr, initial sample pH was recorded at room temperature after calibration of the pH meter with 4.00, 7.00 and 10.00 pH buffers. The samples were again equilibrated for another 47hrs by keeping in the shaker and adjusted the pH to desired levels periodically. The final pH was measured after 48hrs duration. Another set of adsorption studies were conducted by taking 1:1 ratio of biochar : chabazite and followed the same steps as above. The samples were centrifuged and the supernatant filtered into the glass vials and stored further for LC-MS/MS analysis.

As per previous literature studies conducted on activated carbon and biochar using other organic compounds, the adsorption equilibrium for the present studies were conducted over 24, 48 and 72hr duration. Preliminary studies showed that adsorption equilibrium could be achieved within 48hr and so this period was selected for all the adsorption studies. After the initial batch adsorption experiments, batch desorption studies were conducted by decanting the supernatant and replacing it with high purity water and shaking it at 180rpm for 48hrs. The samples were filtered through 0.22 $\mu\text{m}$  filter and analyzed by LC-MS/MS.



### 5.2.6 Use of Natural Zeolite for adsorption studies

Another set of adsorption studies were conducted by using 1:1 ratio of biochar with zeolite and activated carbon with zeolite. The samples were prepared exactly in similar manner as described in section 5.2.5. After 48hrs, the samples were filtered and analyzed by LC-MS/MS.

### 5.2.7 Use of Activated Carbon for comparison studies

Similarly for every batch of adsorption studies, activated carbon was used as reference at 1.0g of AC / 100ml of SE to study and compare the removal efficiency and the adsorption capacity of the target PPCP compounds.

### 5.2.8 Pre-conditioning of Biochar with 0.1N NaCl

Biochar surface was conditioned by the addition of 0.1N NaCl as electrolyte solution to adsorbent dosages to provide a particular ionic strength. Initially 10g biochar was washed for five times with 100mL of high purity water each time to remove any impurities and then conditioned by the addition of 0.1N NaCl to enrich biochar with sodium ions. As per 5.2.5, adsorption studies were conducted further to the obtained pre-conditioned biochar.

### 5.2.9 Chemical Activation of Biochar using KOH

Various chemical activating agents such as zinc chloride, potassium hydroxide and phosphoric acid have been used in previous studies by few to impregnate these chemicals into highly porous activated biochar. During activation at higher temperature, due to their dehydrating properties these impregnated chemical agents influence pyrolytic decomposition by preventing the formation of volatile organic compounds

and tars thus leading to highly porous activated biochar. For the present study, KOH : BC ratios of 0.25, 0.94, 1.63, 2.31 and 3.0 were each mixed with 100ml of DI water and refluxed at 50°C for 2hrs to ensure access of KOH into the interior of BC. The solids were then dried at 120°C overnight. These dried samples were subjected to activation at 700°C at 3°C/min for 2hrs and then cooled down. Adsorption studies were conducted further to the obtained activated biochar as per 5.2.5.

### 5.2.10 Quantification of PPCPs by LC-MS/MS

The concentrations of various PPCP's in secondary effluent were determined by Agilent 1290 (HPLC), 6460 LC-MS/MS. An auto sampler injector with an injection volume of 5 µL was passed through a Poroshell 120 EC- C18 2.7µm (3.0 x 150mm) column for separation of various analytes. Mobile phase A (10mM ammonium formate and 0.1% formic acid in water) and mobile phase B (0.1% formic acid in acetonitrile) were used for the analysis with a flow rate of 0.35mL/min. A positive and negative ion electrospray interface (ESI) mode with Agilent 6460 LC-MS/MS was used in the PPCP analysis. A computer based software Mass Hunter, version B.05.01 was used to process the data by the peak area method for the acquired chromatograms.

By using linear regression, a six-point calibration curve was developed for each compound ranging from 0 to 200ng/mL.  $R^2$  values were 0.99 – 0.999 for all the compounds with RSD values lower than 10%. Percent recoveries ranged from 90 to 100% for the secondary effluent matrix. The concentration of the unknown is calculated by using regression analysis of calibration standard.

### 5.2.11 Adsorption models

Adsorption studies were conducted on BC using target PPCPs concentration which were calculated as a function of PPCP concentration that were left in solution at equilibrium by using equation (5.1) (Ok et al., 2007; Wei and Seo, 2010).

$$Q_e = (C_o - C_e) \times V/M \quad \text{Eq. (5.1)}$$

where  $Q_e$  is the equilibrium PPCP concentration in mg/g;  $C_o$  is the initial PPCP concentration in mg/L and  $C_e$  is the PPCP concentration in aqueous at equilibrium in mg/L;  $V$  is the volume of PPCP aqueous solution in L and  $M$  is the adsorbent mass in g. The percent removal of PPCPs by BC from aqueous solutions was calculated using equation (5.2) (Ahmad et al., 2012b).

$$\% \text{ Removal} = \frac{(C_o - C_e) \times 100}{C_o} \quad \text{Eq. (5.2)}$$

Isotherms such as Langmuir and Freundlich were fitted to study the adsorption capacity of BC (Jung et al., 2011). The Langmuir adsorption model is used to quantify the adsorption capacity as given by equation (5.3).

$$\frac{C_e}{q_e} = \frac{C_e}{q_{\max}} + \frac{1}{K_L q_{\max}} \quad \text{Eq. (5.3)}$$

where  $C_e$  is the solute equilibrium concentration (mg/L) in the aqueous phase;  $q$  is the mass of adsorbed solute on a unit mass of adsorbent (mg/g);  $q_{\max}$  is the maximum mass adsorbed corresponding to complete surface coverage (mg/g) (Wei and Seo, 2010); and  $K_L$  is the empirical Langmuir constant indicating binding energy (L/mg). Similarly the Freundlich isotherm is given by equation (5.4).

$$q_e = K_f \cdot C^{1/n} \quad \text{Eq. (5.4)}$$

where  $K_F$  ((mg/g) (L/mg)<sup>1/n</sup>) is Freundlich constant roughly an indicator of the adsorption capacity and  $(1/n)$  a constant of the adsorption intensity. Value of  $n > 1$  represents a favorable adsorption condition. The linear form of Eq. (5.5) is

$$\ln q_e = \ln K_f + \frac{1}{n} \ln C_e \quad \text{Eq. (5.5)}$$

## 5.3 Results and Discussion

### 5.3.1 Morphology and structure of BC samples by FE-SEM

A small portion of the BC sample was placed on a carbon adhesive disk, gold coated to alleviate any charging during the analysis, and analyzed by scanning electron microscopy coupled with energy dispersive X-ray (SEM/EDX) spectroscopy using the Hitachi S-4500 Field Emission SEM quipped with a Quartz PCI XOne SSD X-ray Analyzer at an accelerating voltage of 10kV as shown in Figures 5.8 and 5.9. The EDX analysis of the BC samples, were analyzed similarly as shown in Figures 5.10 and 5.11.

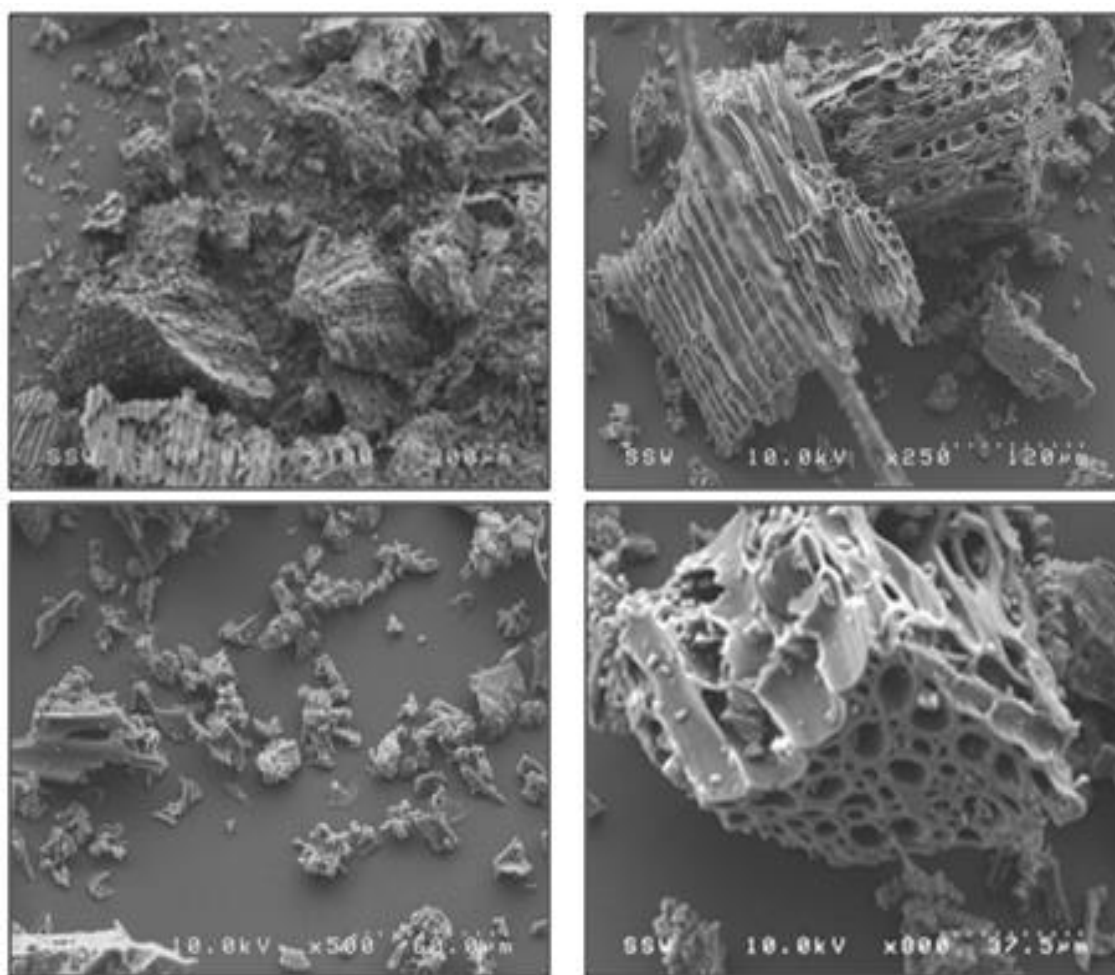


Figure 5.8. SEM images scanned at 200, 120, 60 and 37.5  $\mu\text{m}$  of biochar at 10 kV

It can be seen that the scanned images of Figure 5.8 at 200, 120, 60 and 37.5 $\mu\text{m}$  and Figure 5.9 at 20 and 30 $\mu\text{m}$  revealed the images of biochar pyrolyzed at 700 $^{\circ}\text{C}$  showing hollow pores with diameters in the range from  $<1\ \mu\text{m}$  to 20-30 $\mu\text{m}$ . These particles appear to be more rugged and arranged randomly forming longitudinal hollow tubes with honeycomb like structures.

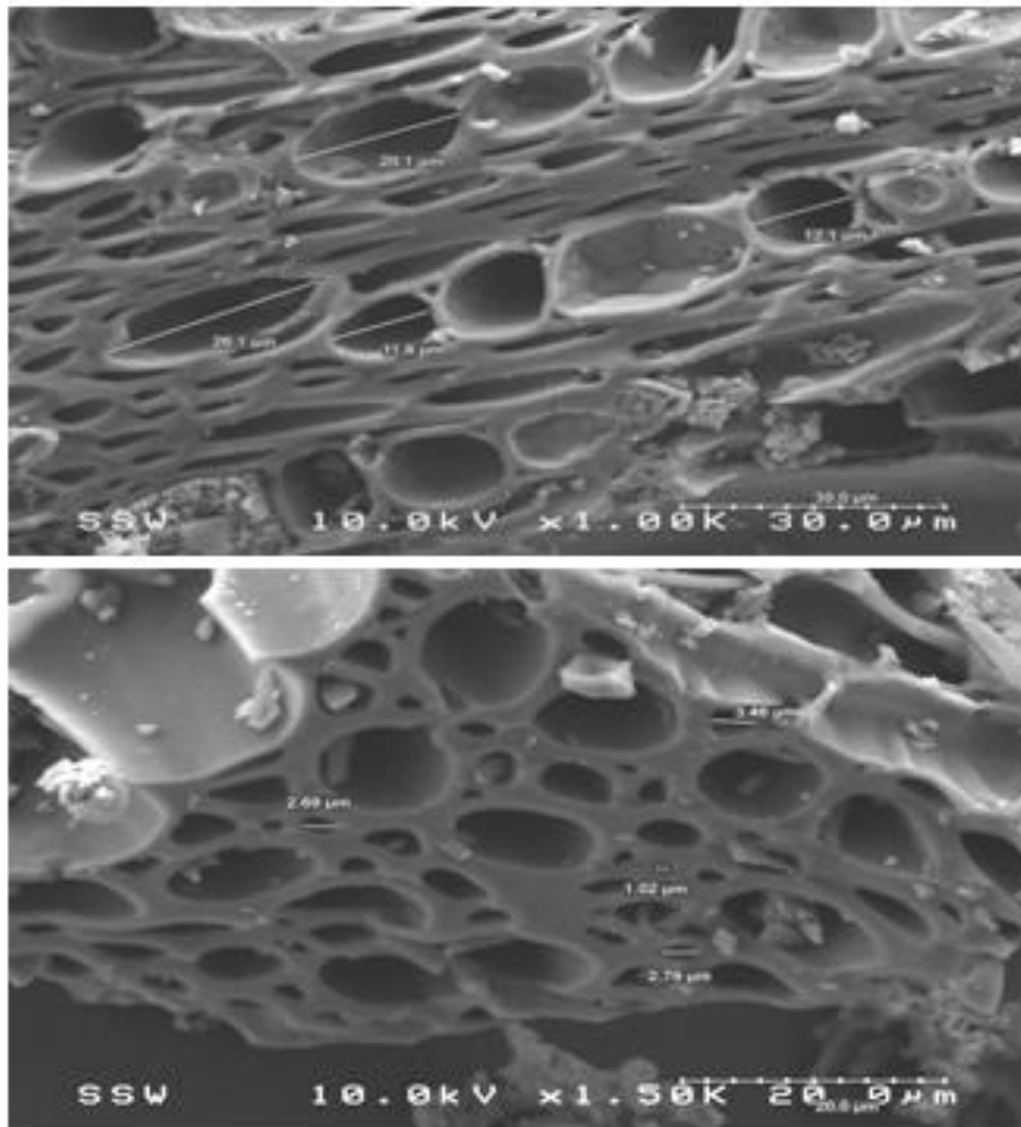


Figure 5.9. SEM images scanned at 30 and 20 $\mu\text{m}$  of biochar at 10kV

Some polygonal shapes can also be observed due to the lignin particles of woody plants with several conchoidal fracture surfaces while some of the fibrous structures get destroyed as their internal texture become sparse (cross-section image) and surface texture becomes coarse at high temperatures of 700 °C. These porous structures of varying diameter will aid in adsorption by size exclusion and separation of high molecular weight PPCP compounds from low molecular weight compounds and other organic matter present in secondary effluent.

### 5.3.2 Energy Dispersive X-ray (FE-SEM/EDX) Spectroscopy

Similarly three spots scanned at 300  $\mu\text{m}$  by FE-SEM were used to perform EDX analysis at 10kv as shown in Figure 5.10. The sample preparation was same as performed for SEM and the measurements for all the elements were normalized with three iterations each.

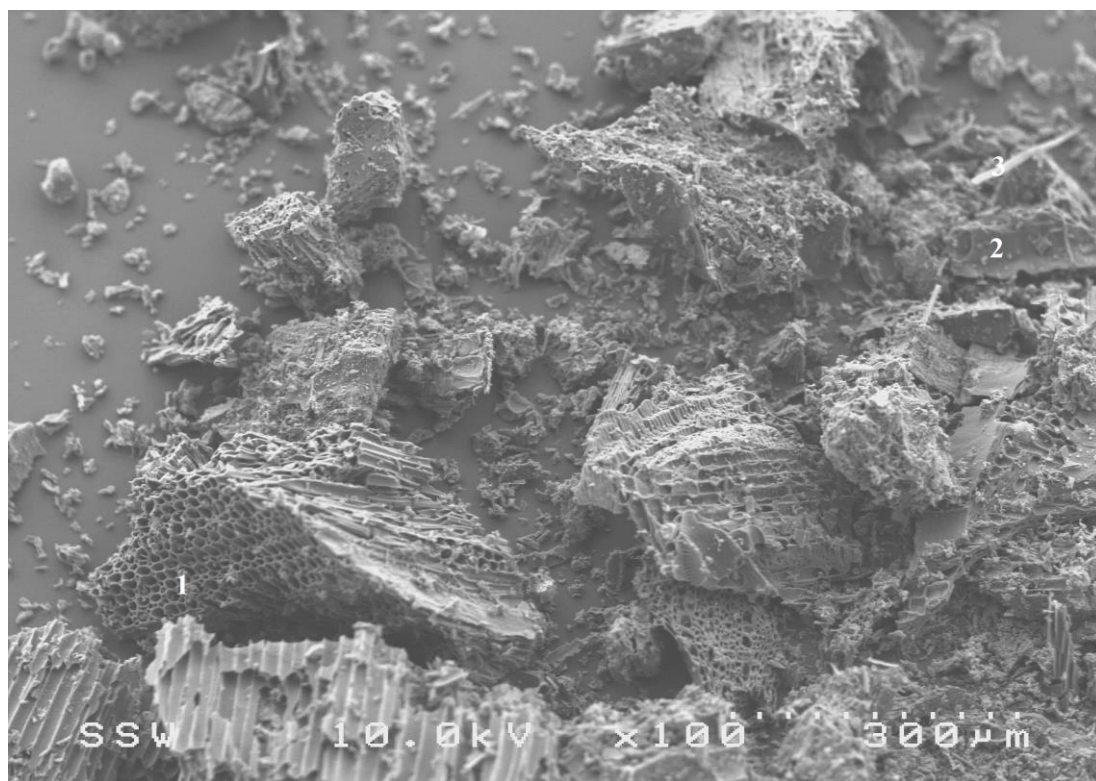


Figure 5.10. SEM images of three spots scanned at 300 $\mu\text{m}$  of biochar at 10kV

Spot EDX images for three areas were obtained as shown in Figure 5.11 scanned at 300 $\mu$ m of biochar at 10kv.

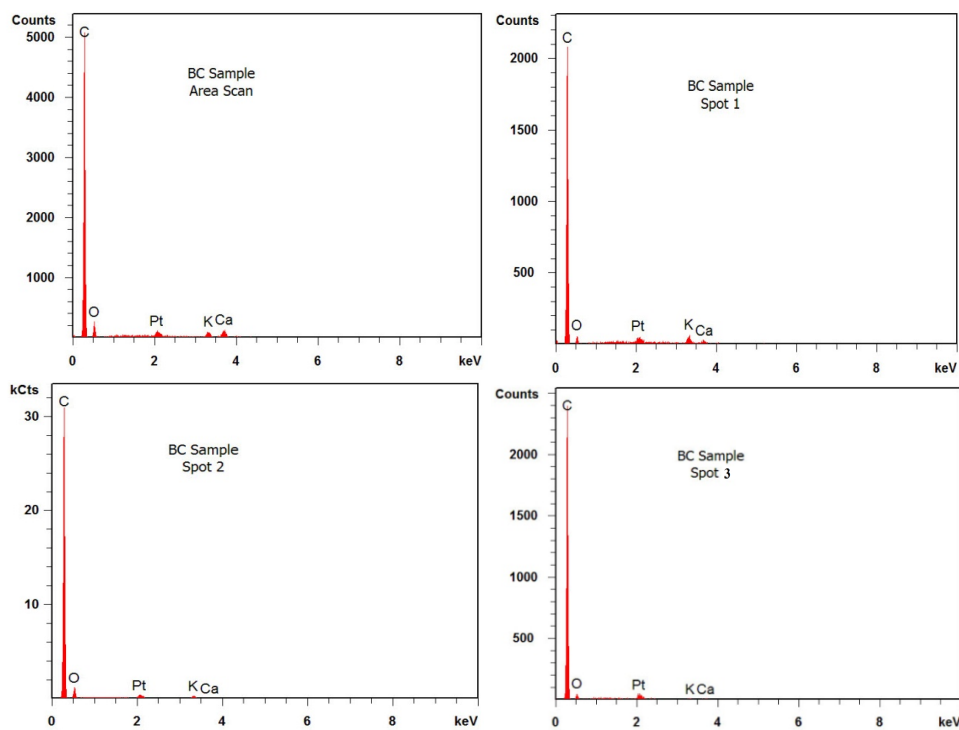


Figure 5.11. EDX images scanned at 300 $\mu$ m of biochar at 10kV

Table 5.3. EDX spectroscopy results of three spots scanned on the BC sample at 10kV

| <b>Semi-quantitative EDX Results, in weight %</b> | <b>C</b> | <b>O</b> | <b>Mg</b> | <b>K</b> | <b>Ca</b> |
|---|----------|----------|-----------|----------|-----------|
| <b>BC, Area Scan</b>                              | 81.8     | 10.1     | -         | 3.0      | 5.0       |
| <b>BC, Spot 1</b>                                 | 86.2     | 6.7      | -         | 4.8      | 2.2       |
| <b>BC, Spot 2</b>                                 | 89.2     | 9.1      | -         | 1.5      | 0.3       |
| <b>BC, Spot 3</b>                                 | 92.8     | 6.0      | -         | 0.6      | 0.7       |

Table 5.3 shows the semi-quantitative results for the three spots on biochar where it reveals that element C is present in abundance which is directly proportional to the intensities as shown by spectral lines on EDX. These spectral lines also show the chemical homogeneity on the biochar samples.

### 5.3.3 FTIR spectra of BC samples

FTIR acts as a powerful tool in identifying and analyzing organic compounds due to change in shifts as a result of chemical composition in BC samples. Figure 5.12 shows the IR spectra of BC sample after pyrolysis at 700°C. The samples were analyzed directly by FTIR spectroscopy in the range from 500 – 4000  $\text{cm}^{-1}$  using platinum-attenuated total reflectance accessory equipped with a diamond crystal in the Bruker Tensor II main box. This experimental setup was used to analyze an area of approximately 2mm x 2mm to a depth of 0.6-5 microns.

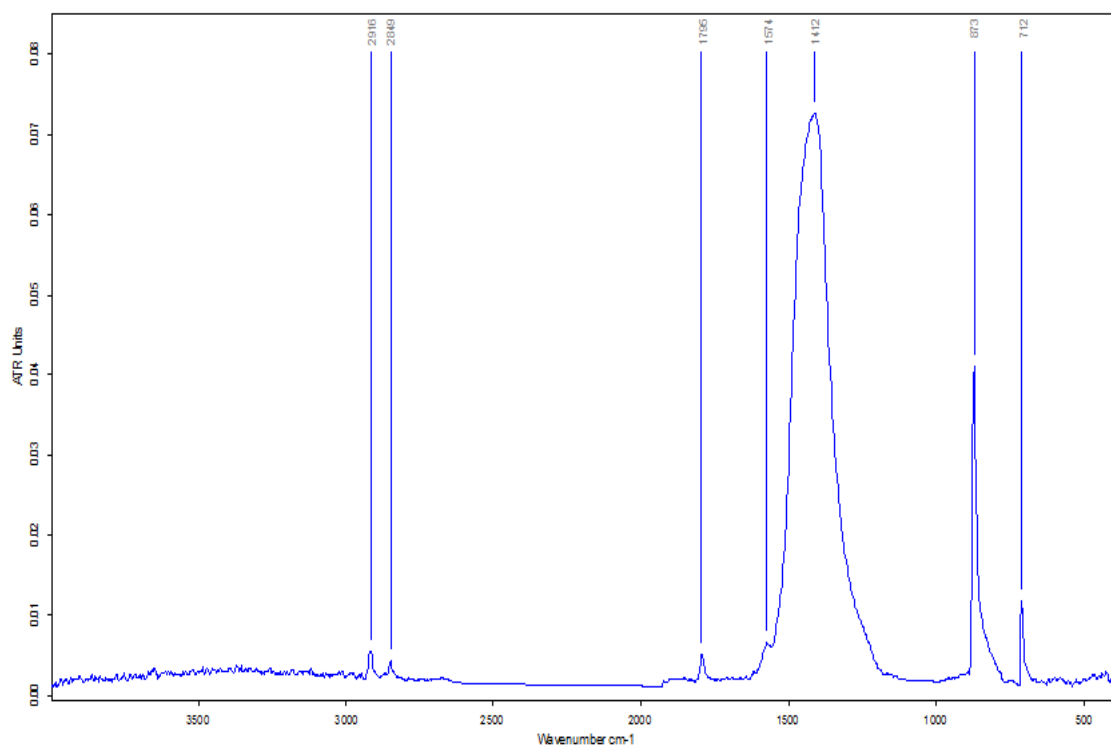


Figure 5.12. FTIR spectra of BC sample after pyrolysis at 700°C

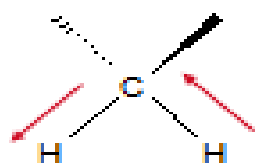


Table 5.4. FTIR spectra of BC peaks with literature values (Tom Tague)

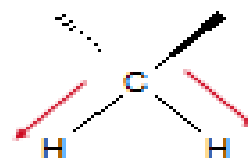
| <b>Biochar Peak, cm<sup>-1</sup></b> | <b>Surface Group</b>   | <b>Peak Range, ± 10 cm<sup>-1</sup></b>     |
|--------------------------------------|--|---|
| <b>2916</b>                          | CH <sub>2</sub> (asymmetric stretch)   | 2926  |
| <b>2849</b>                          | CH <sub>2</sub> (symmetric stretch)  | 2855  |
| <b>1795</b>                          | C=O (stronger asymmetric stretch)  | 1775-1800                                   |
| <b>1574</b>                          | aromatic and olefinic C=C vibrations, C=O in amide (I), ketone, and quinone groups; bend deformation of water          | 1400-1620<br>1580-1650                      |
| <b>1412</b>                          | Benzene ring modes<br><br>In-Plane OH bending broader than C-H bending (COOH group)<br><br>C-N stretching              | 1400-1620<br><br>1395-1440<br><br>1390-1430 |
| <b>873</b>                           | C-O-C symmetric stretch and C-H stretch  | 800-900                                     |
| <b>712</b>                           | CH <sub>2</sub> (rock bend), C-H (cis-alkenes, aromatic out-of-plane bend)<br><br>NH <sub>2</sub> out-of-plane bending | 720<br><br>600-750                          |

An aliphatic C-H stretching was observed at 2916 cm<sup>-1</sup> as seen in Figure 5.12 and Table 5.4 which is due to increase in temperature to 700°C and aliphatic loss process. Simultaneously C-H and C-O-C stretching was observed at 873 cm<sup>-1</sup>, while 1574 cm<sup>-1</sup> and 1795 cm<sup>-1</sup> were attributed to C=C vibrations and C=O asymmetric stretch whereas C-N stretching or in-plane OH bending was observed at 1412 cm<sup>-1</sup> due to aromatic carbon. The structure of straight chain alkanes with methylene group shows asymmetric

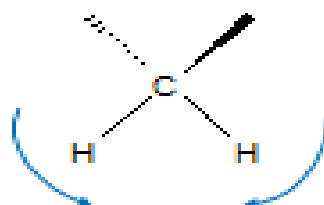
and symmetric stretch observed at  $2916\text{ cm}^{-1}$  and  $2849\text{ cm}^{-1}$  while out-of-plane bending can be observed at  $712\text{ cm}^{-1}$  as shown in Figure 5.13. C-O-C symmetric stretch was observed at  $873\text{ cm}^{-1}$  as shown in Figure 5.14 for some of the stretching and bending that occurs at various peaks. Further it may also be seen that silicon components in biochar subjected to  $700^{\circ}\text{C}$  got distanced physically from the carbon structure as confirmed by FTIR spectra (Figure 5.12). It was observed that during the charring process as the temperature increases, it modifies the functional groups thus increasing the aromatic carbon while decreasing the aliphatic carbon groups (Lee et al., 2010). The FTIR spectra show the presence of oxygen groups and absence of sulfur groups.



**Asymmetric stretch:**  
 $2926 \pm 10\text{cm}^{-1}$



**Symmetric stretch:**  
 $2855 \pm 10\text{cm}^{-1}$



**Rocking Bend**  
 (more than 4  $\text{CH}_2$  in a row):  
 $720 \pm 10\text{cm}^{-1}$

Figure 5.13. Structure of straight chain Alkanes with Methylene group ( $\text{CH}_2$ ) (Tom Tague)

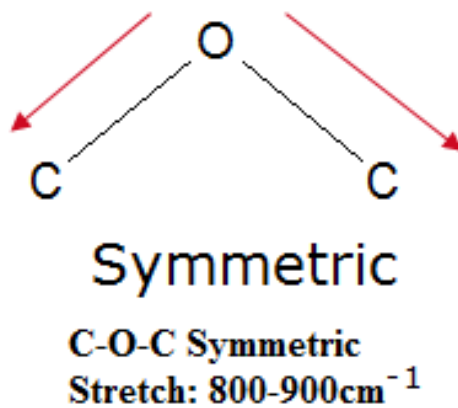


Figure 5.14. Structure of C-O-C symmetric stretch (Tom Tague)

### 5.3.4 $^{13}\text{C}$ NMR spectra of BC samples

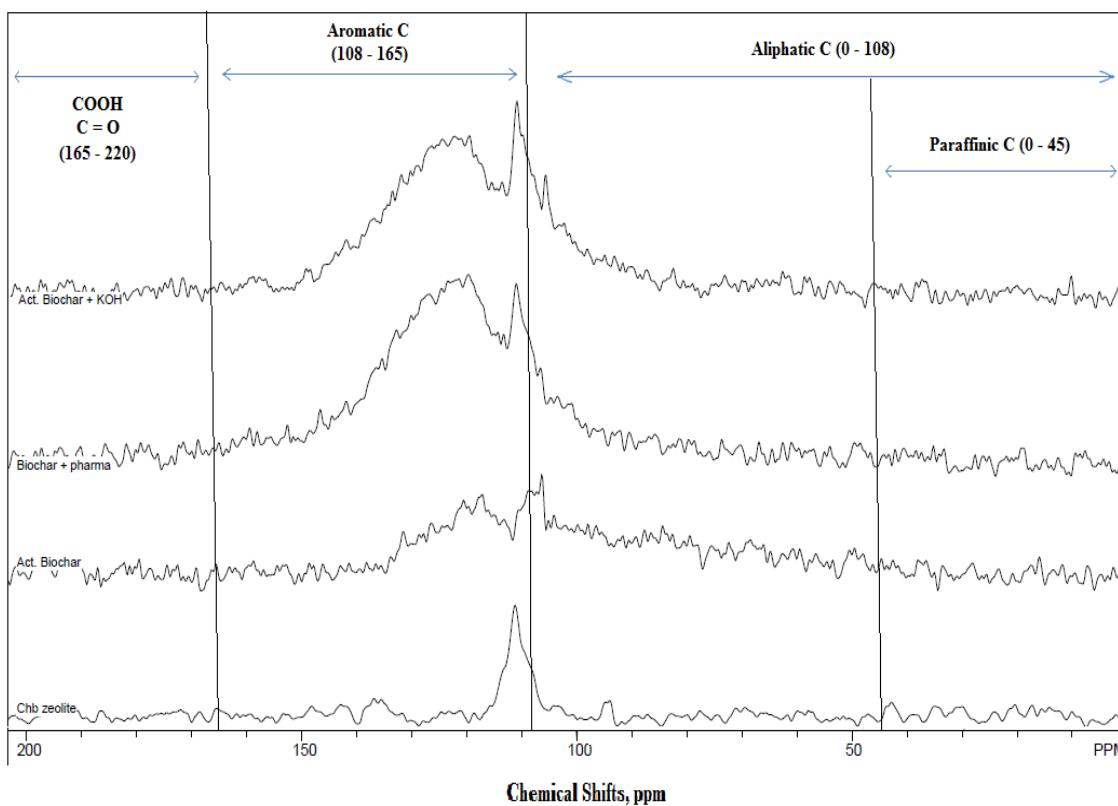


Figure 5.15. Comparison of various spectra using  $^{13}\text{C}$  NMR

A quantitative spectral analysis for biochar samples subjected to various treatments was conducted with  $^{13}\text{C}$  NMR as shown in Figure 5.15. The spectra shows a shift in the peak for biochar activated with KOH with maximum peak values at 122 and 110ppm which is composed of both aromatic and aryl carbon, while PPCPs adsorbed onto biochar showed peak shifts at 119, 111, and 106ppm whereas BC:chabazite showed maximum peak shift at 111ppm. All these revealed that the original biochar which showed a maximum peak shift at ~105ppm underwent some sort of changes due to its interaction with other adsorption/treatment processes. It showed that biochar activated with KOH showed more aromatic carbon with higher surface polarity and higher surface area.

### 5.3.5 CHNS analysis of BC samples

Carbon, hydrogen, nitrogen and sulfur elemental analysis was performed by using Thermo Scientific Flash EA 1112 series CHNS analyzer and the values are shown in Table 5.5.

Table 5.5. CHNS results of biochar analyzed by CHNS analyzer

| <b>Parameter</b> | <b>Percentage</b> |
|------------------|-------------------|
| <b>Carbon</b>    | 71.8              |
| <b>Hydrogen</b>  | 1.07              |
| <b>Nitrogen</b>  | 0.43              |
| <b>Oxygen</b>    | 22.4              |
| <b>Sulfur</b>    | <0.1              |
| <b>Ash</b>       | 4.3               |

The ash content was calculated after a known weight of the sample was heated in the muffle furnace at 700°C. From the values of carbon, hydrogen and nitrogen, the values of ash content is subtracted and the difference obtained was used to calculate the oxygen values. The character of biochar is represented by the hydrogen to carbon (H/C) ratio and oxygen to carbon (O/C) ratio which acts as useful indicator (Nguyen and Lehmann, 2009). The hydrogen to carbon (H/C) ratio was found to be 0.179 and oxygen to carbon (O/C) ratio was 0.23. The reduction in these ratios is due to decarboxylation and dehydration reactions taking place at higher temperature because of charring process. Change in recalcitrance of biochar is due to thermal induction leading to dehydrogenation of CH<sub>3</sub> group (Harvey et al., 2012).

### 5.3.6 BET analysis of BC samples

The wood material from Ghana, West Africa was used as the raw material to produce biochar after carbonization at 700°C. The adsorption capacity depends on the surface area of an adsorbent and greater the surface area greater will be the availability of sites to bind to the adsorbate (Magnan, J.-P., and Ghassem, Y., 1989). The BC sample obtained showed a surface area of  $301 \pm 7 \text{m}^2/\text{g}$  determined by using Brunauer–Emmett–Teller (BET) Gemini 2360 V5.01 and StarDriver V2.03 at 760 mm Hg as shown in Appendix 11. The surface area expanded as the temperature was increased to 700°C for these types of wood material unlike other biomass sources such as rice residues where its surface area diminishes at higher temperature due to blockage of micropores by the ash content (Mackay and Roberts, 1982; Song and Guo, 2011).

### 5.3.7 Adsorption of target PPCPs compounds

Biochar weights and the volume of standards spiked for each batch experiments were kept constant whereas pH and spiked solution concentrations were altered. Effect of pH, effect of adsorbent dosage, effect of PPCP concentration, effect of biochar : zeolite,

effect of pre-conditioning, effect of chemical activation of BC by KOH and isotherms were studied in detailed for atenolol, clofibric acid and diclofenac. With each batch of experiments, 1g/100ml of activated carbon was run (data not provided in this study).

### 5.3.7.1 Effect of pH on biochar

#### 5.3.7.1.1 Effect of pH at constant PPCP concentration of 10ppm

Four different batch experiments were conducted using 1N HCl or 1N NaOH to adjust the pH in the range 3 to 9 and were controlled to investigate the variation in adsorption of BC. A 0.1g, 0.2g, 0.5g, 1.0g and 2.0g of biochar were equilibrated for 48hrs at room temperature after spiking with an initial concentration ( $C_0$ ) of 10mg/L each of targeted PPCP compounds and the effect of pH was determined on the removal of ATN, CFA and DCF.

The adsorption capacity is greatly influenced by pH as it affects the solute solubility and the ionization degree (Noh and Schwarz 1989; Nandi et al., 2009).

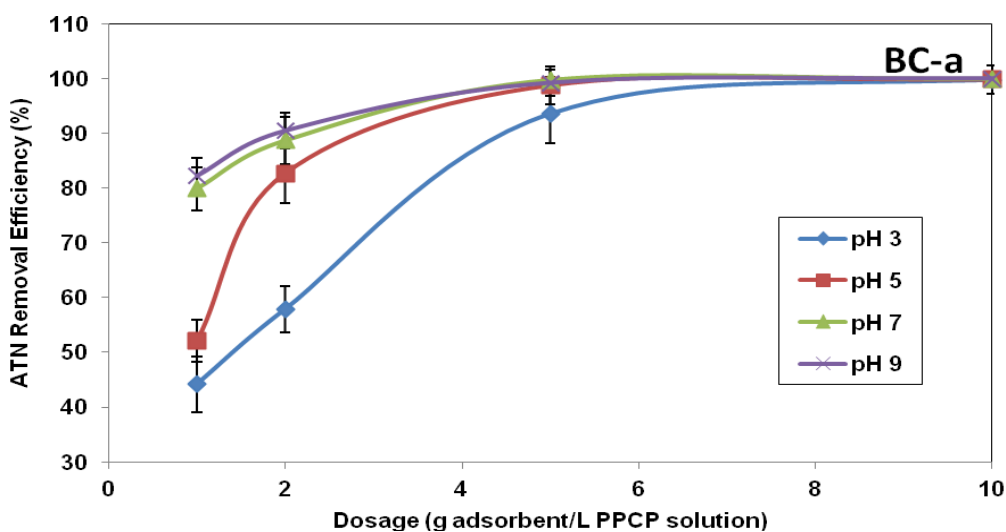
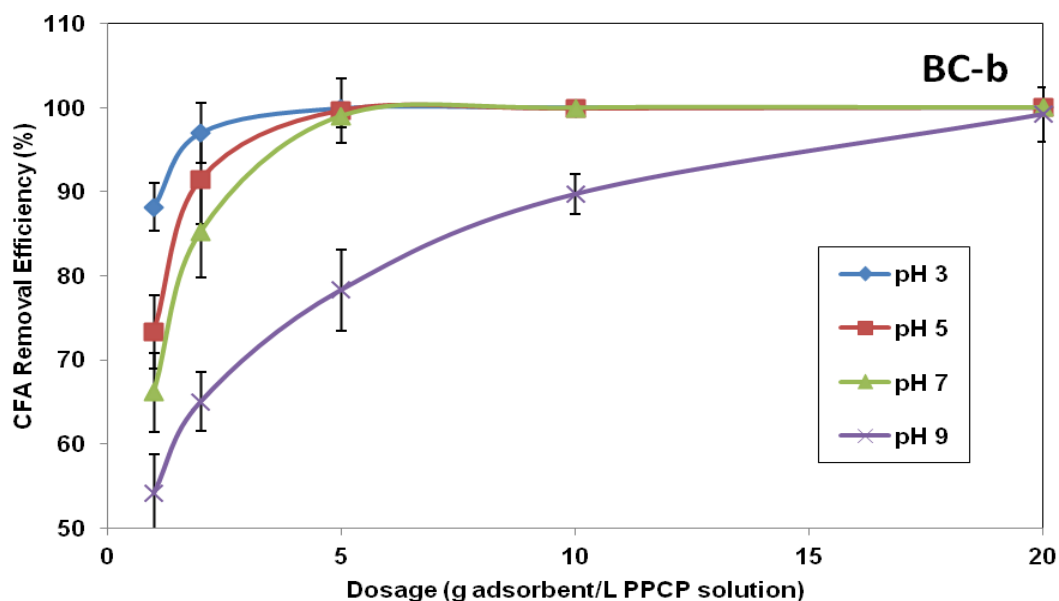


Figure 5.16a showed that at pH 3, the percent removal efficiency was the lowest for ATN at 44.1% and increased to 82.3% at pH 9 for the adsorbent dosage of 1 g/L. The

removal efficiency followed the order of pH 9 > 7 > 5 > 3. 100% removal was obtained at an adsorbent dosage of 10 g/L at pH 7 and 9.



While a reverse trend was observed for CFA and DCF as shown in Figure 5.16b and c, where percent removal efficiency was observed to be 54.1% and 73.9% at pH 9 and increased to 88.2% and 99.2% at pH 3 for adsorbent dosage of 1 g/L. The maximum removal efficiency was observed for DCF followed by CFA (99.9% removal at 5 g/L adsorbent dosage) and followed the order of pH 3 > 5 > 7 > 9. At fixed concentrations of 10ppm of CFA, DCF and ATN, the adsorption increased as the adsorbent dosage was increased from 1g/L to 20g/L thus increasing the PPCP removal by providing more available adsorption sites.

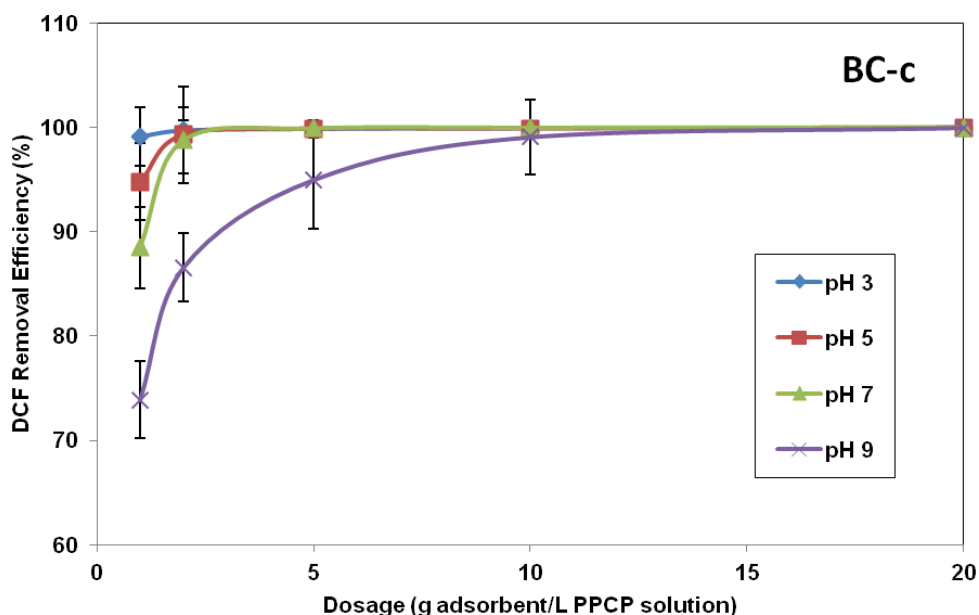


Figure 5.16. Effect of pH in percent removal onto BC (a) ATN, (b) CFA and (c) DCF [Co = 10 mg/L, adsorbent dosage = 1, 2, 5, 10 and 20 g/L]

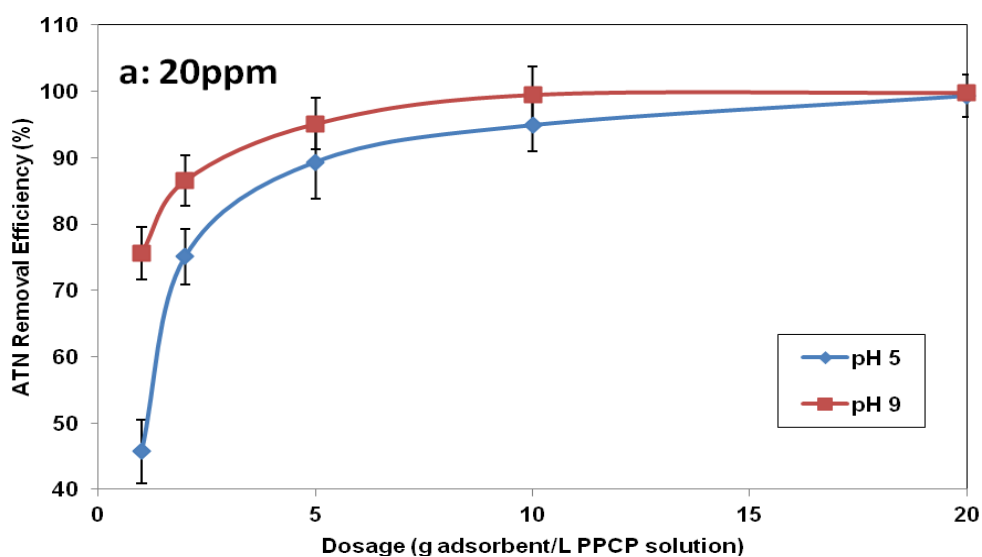
Overall, the removal efficiency was higher for DCF followed by CFA and ATN and follows the order DCF > CFA > ATN. Based on the results, it was observed that the optimum pH was 3 for the adsorption of DCF and CFA. The pKa values of DCF and CFA are 4.15 and 3.2 and are weak electrolytes and its ionization strongly depends on pH hence its solubility decreases in water as pH decreases. This results in increased Vander Waal interaction between adsorbent surface with DCF and CFA by a process of physical adsorption. Similarly the pKa value for ATN is 9.6 and the optimum pH was reached at 9 (Jodeh et al., 2015). This higher removal efficiency of DCF over other PPCP compounds may be based on an overall greater impact on adsorption capacity which may be due to its higher BET-N<sub>2</sub> surface area that is mainly responsible for the higher interaction strength of PPCPs onto biochar rather than fractions of aromatic carbon in the functional groups. The overall binding energy of a single DCF is -21.8 kcal/mol and its interaction strength decreases in the presence of other types and number of PPCP solutes competing on the available adsorption sites. The percentage of carbon in each functional group contributes a significant energy due to the presence of



carbohydrate and aryl functional groups, and its interaction energies in binding of BC onto PPCP compounds.

### 5.3.7.1.2 Effect of pH at constant PPCP concentration of 20ppm

To observe the effect of loading concentration on BC, the PPCP concentration was increased to 20ppm and its effect at pH 5 and 9 were studied. Figure 5.17a showed that the percent removal efficiency was 75.6% at pH 9 and decreased to 45.7% when the pH was decreased to pH 5 for ATN at an adsorbent dosage of 1 g/L. Almost 100% removal of ATN was observed at an adsorbent dosage of 10 g/L and 20g/L at pH 9 and 5.



When the concentration was increased to 20ppm, the adsorption phenomena decreased slightly than that of 10ppm which is due to slightly less available adsorption sites although complete removal was possible when the adsorbent dosage was increased from 1g/L to 20g/L.

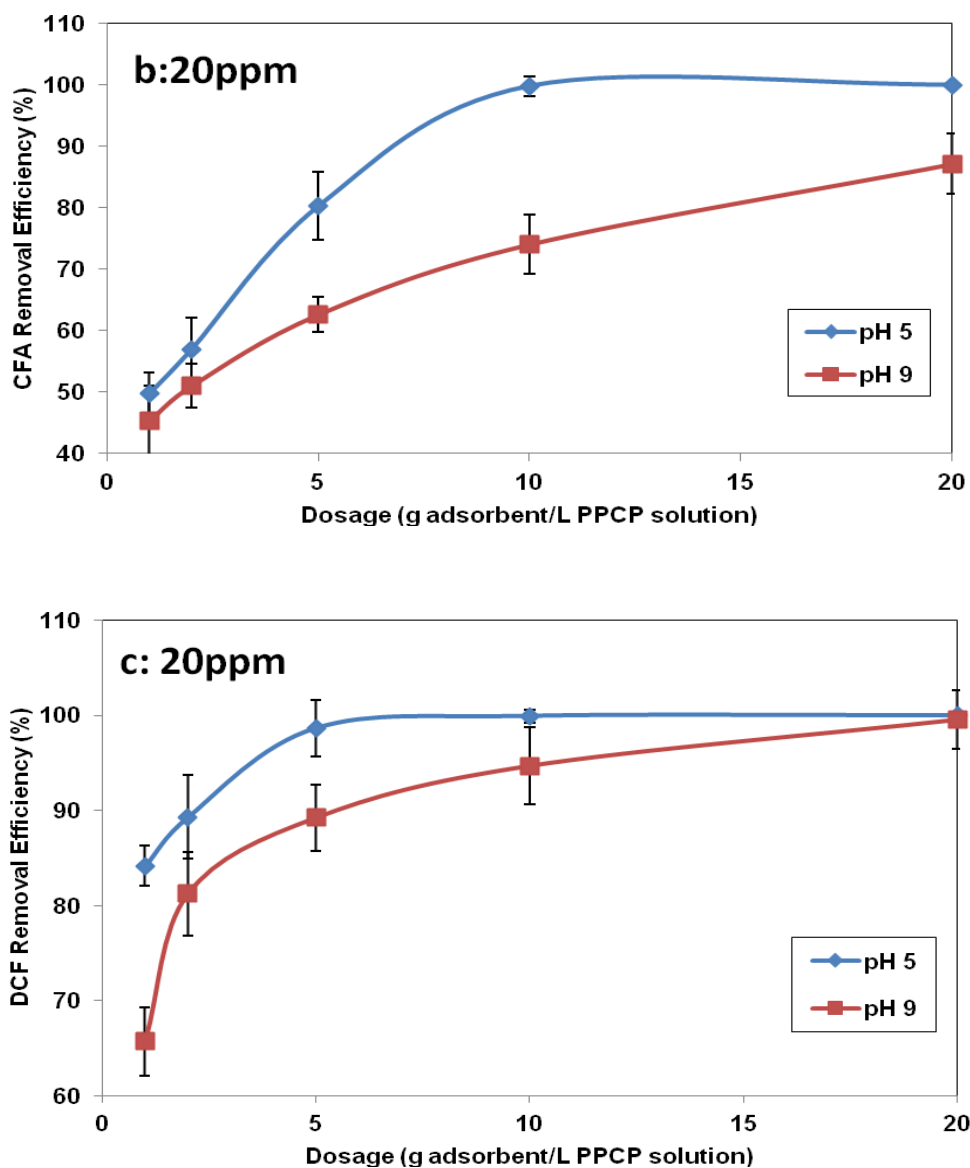


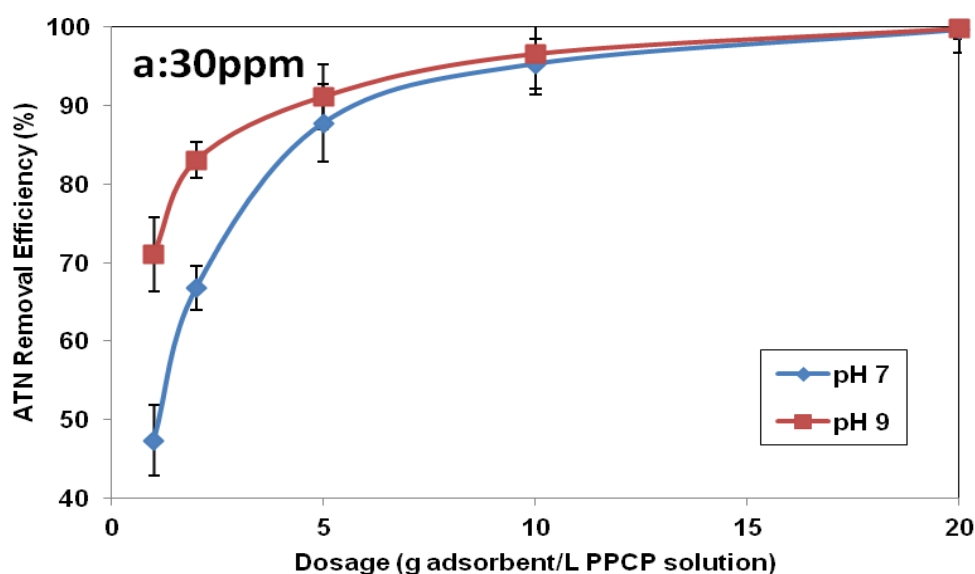
Figure 5.17. Effect of pH in percent removal onto BC a) ATN, (b) CFA and (c) DCF [Co = 20mg/L, adsorbent dosage = 1, 2, 5, 10 and 20 g/L]

Similarly, the percent removal was 45.4% and 65.7% for CFA and DCF at pH 9 and increased to 49.8% and 84.2% at pH 5 at an adsorbent dosage of 1 g/L as shown in Figure 5.17 b and c. From the experimental data, it may be observed that CFA and DCF may behave as neutral molecules and interact with BC via non-electrostatic interactions because of its pKa values of 3.2 and 4.15 and thus maximum removal could

be noticed at pH 3 for both CFA and DCF. Similarly when the pH was increased to 5, 7 and 9 which is above the pKa values of the molecules there exist an electrostatic repulsion between BC and PPCPs as BC also gradually tends to become negatively charged and thus the percent removal decreases. It was also observed that ATN was removed completely at pH 9 as its pKa is 9.6 and therefore a non-electrostatic interaction exists between BC and ATN.

### 5.3.7.1.3 Effect of pH at constant PPCP concentration of 30ppm

Similar loadings were conducted by increasing the PPCP concentration on BC to 30ppm and its effect at pH 7 and 9 were studied. Figure 5.18a showed that the percent removal efficiency was 71.1% at pH 9 compared to 47.4% at pH 7 for ATN at an adsorbent dosage of 1 g/L. Almost 100% removal of ATN was obtained at an adsorbent dosage of 20g/L for pH 9 and 7.



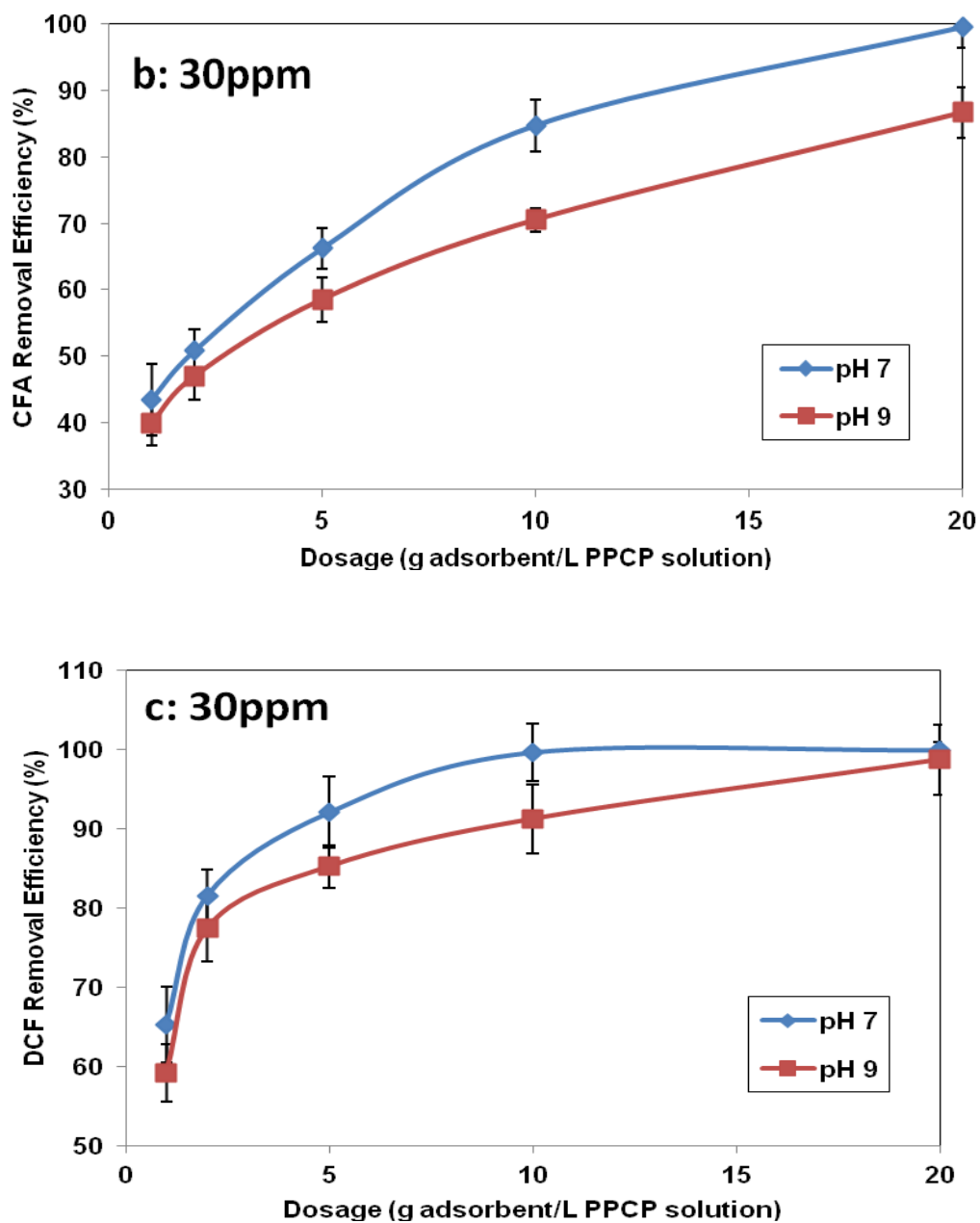


Figure 5.18. Effect of pH in percent removal onto BC (a) ATN, (b) CFA and (c) DCF [Co = 30mg/L, adsorbent dosage = 1, 2, 5, 10 and 20 g/L]

The percent removal was 39.8% and 59.2% for CFA and DCF at pH 9 and increased to 43.5% and 65.3% at pH 7 at an adsorbent dosage of 1 g/L as shown in Figure 5.18 b and c. It can be seen that from Figure 5.16, 5.17 and 5.18 that with increase in PPCPs

concentration from 10ppm to 30ppm, the removal efficiency slightly decreased. Based on the experimental data, the removal of selected PPCPs depends on the adsorption capacity of the adsorbent and its physico-chemical properties. There may be several mechanisms that can take place between BC and selected PPCPs. For example in a tri-solute, the adsorption behaviors are complicated and difficult to predict as they are controlled by the interaction between pH-dependent speciation or the behavior of specific functional groups which vary based on compound to compound (Kibbey et al., 2007). In addition, the acidic or basic drugs speciation in aqueous solutions is influenced by solution pH. It was observed that almost 100% ionization was possible when weak acids were more soluble in solution in the ionic form at pH at least two units above the pKa. But acidic drugs will form salts if the pH was very high and so the pH was maintained at a maximum of 9.

Other factors such as hydrophobicity, hydrophilicity, molecular size and surface charge are the main important physico-chemical properties that depend on the adsorption of PPCPs onto BC (Yoon et al., 2003; Carballa et al., 2005). These properties of biochar used in various applications are further governed by original feedstock used and the temperature and duration of pyrolysis conditions (Enders et al., 2012). It may also be observed as per  $^{13}\text{C}$  NMR Figure 5.15 that pyrolysis at higher temperatures lead to aromatic carbon content and large surface area on the surface of biochars thus increasing the recalcitrant and adsorption capacity (Lehmann, 2007). The water retention ability and adsorption capacity of PPCP properties may also be enhanced due to the physical properties of biochar such as surface area and porosity (Kalderis et al., 2008).

Studies conducted by Liu and Zhang, 2009; Spokas et al., 2010 and Joseph et al., 2013 observed that lignin was the main component in recalcitrant carbons derived from woody feed stocks. Higher saturated hydraulic conductivities may result when it was treated with woodchip biochar compared to manure-based (Lei and Zhang, 2013). The character of biochar depends on O=C and H=C ratios along with elements which acts as useful indicators (Nguyen and Lehmann, 2009) and these ratios gets reduced due to decarboxylation and dehydration reactions that takes place at charring process at higher

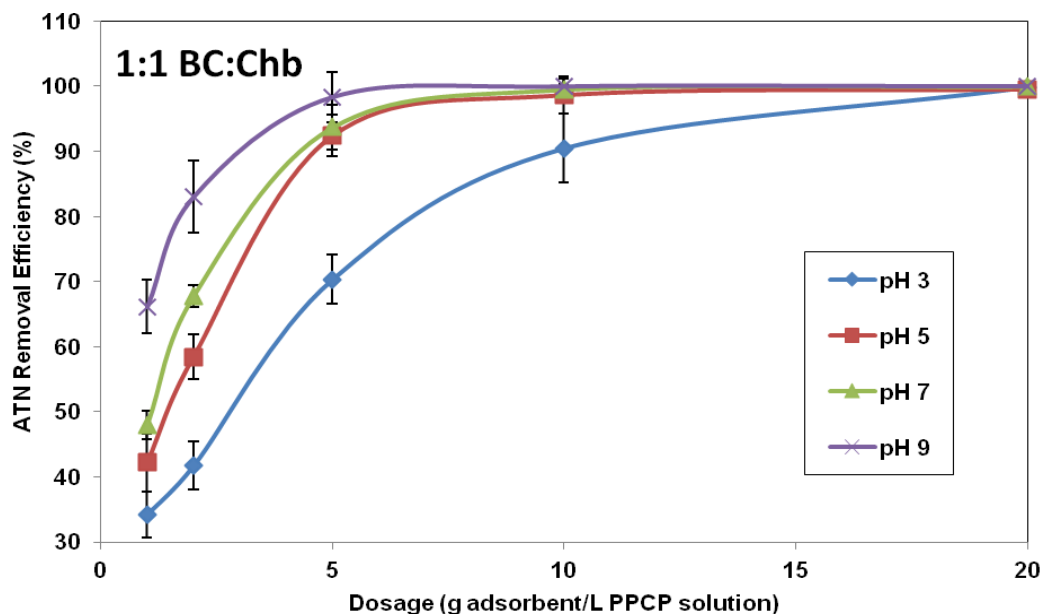
temperatures. As the temperature increases, the relative concentrations of non-pyrolyzed inorganic elements are responsible for increase in pH and depended on the original feedstocks (Novak et al., 2009).

The adsorption capacity may also be governed by log Kow (octanol-water partition coefficient) an important factor which also evaluates the sorption affinity on biochar. Generally a higher adsorption capacity will be observed for hydrophobic pollutants when log Kow is greater than 4.0 (Bertanza et al., 2009; Choi et al., 2005; Stackelberg et al., 2007) whereas if the compounds exhibited a log Kow between 2.5 and 4.0, then they are moderately removed by biochar. In the present study, the log Kow value for DCF is 4.51 and hence it shows higher adsorption capacity compared to other PPCP compounds. The log Kow values for CFA and ATN are 2.57 and 0.16 and so exhibit moderate sorption for CFA whereas very low sorption for ATN as its log Kow is less than 2.5.

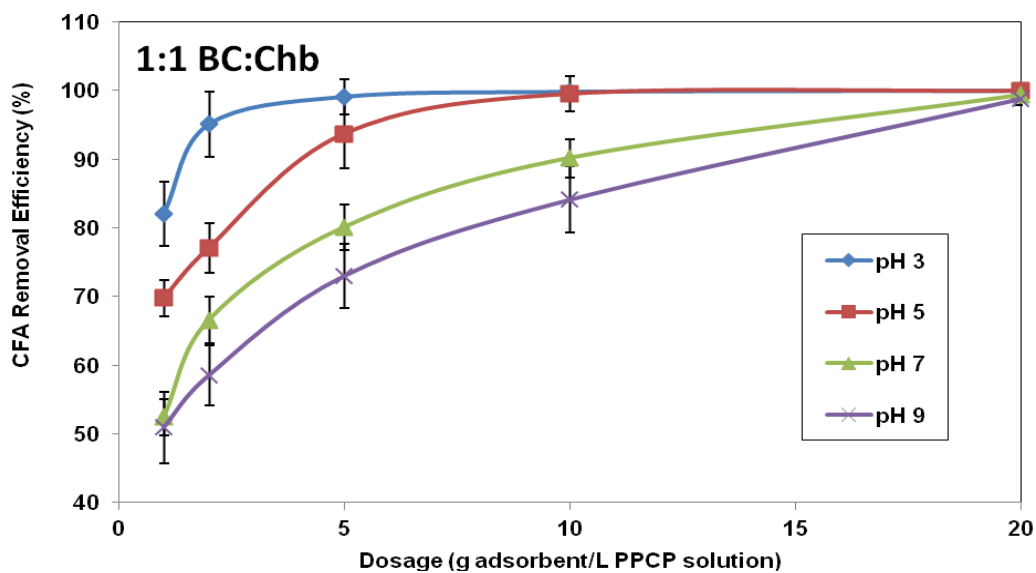
Hence we can conclude that ion exchange, complexation with functional groups, electrostatic interaction and chemical precipitation are some of the adsorption mechanisms that may take place on the surface of BC for complete removal of PPCP from secondary effluent.

### 5.3.7.2 Effect of pH on biochar : Chb

Similarly another batch of experiments were conducted with 1:1 ratio of biochar : chabazite at pH 3, 5, 7 and 9 at room temperature by adjusting the pH with 1N HCl or 1N NaOH. The initial concentration was maintained at 10ppm each of ATN, CFA and DCF. The percent removal studies were conducted after 48 hr to attain equilibrium concentration.



From Figure 5.19a, it may be concluded that the experimental data obtained shows remarkable effects in removal efficiency. Thus, the percent removal efficiency at pH 3 was observed to be the lowest for ATN at 34.3% and increased to 42.2%, 47.9% and 66.1% at pH 5, 7 and 9 for the dosage of 1 g/L. The removal efficiency followed the order of pH 9 > 7 > 5 > 3. 100% removal was obtained at a dosage of 10 g/L at pH 9.



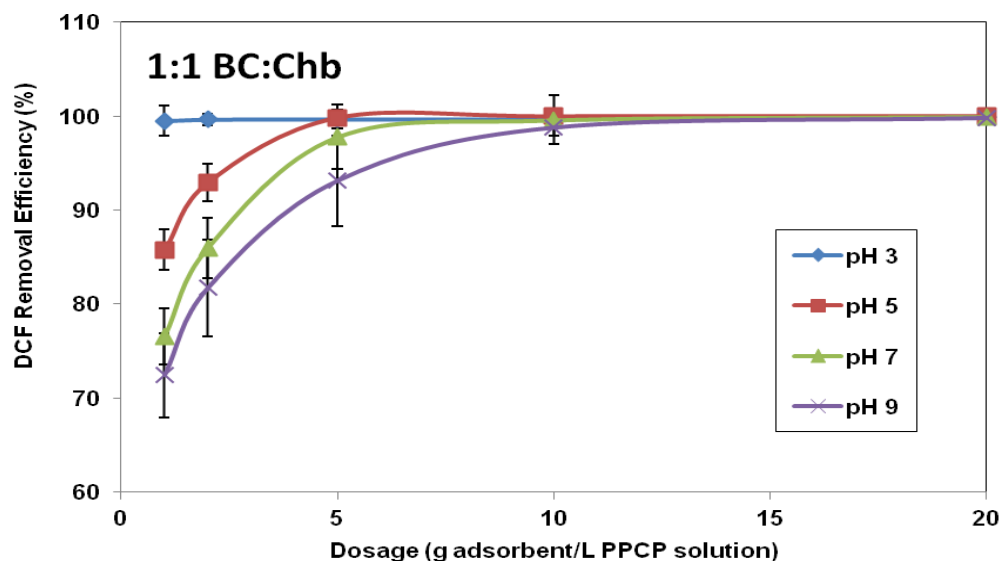


Figure 5.19. Percent removal efficiency of PPCPs from a mixture of BC:Chb (a) ATN, (b) CFA and (c) DCF [Co = 10 mg/L, dosage = 1, 2, 5, 10 and 20 g/L]

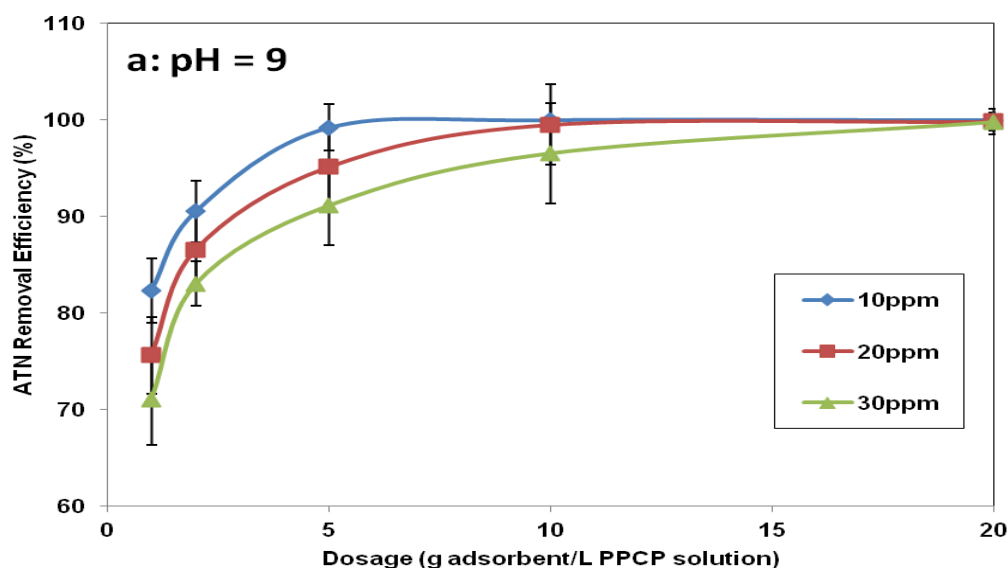
Although the removal efficiency trend was similar between biochar and biochar mixed with chabazite, but biochar showed 1.24 times greater removal rates compared to biochar mixed with chabazite for ATN. While a reverse trend was observed as shown in Figure 5.19b and c, for CFA and DCF, where percent removal efficiency was observed to be 50.9% and 72.4% at pH 9 and increased to 82.1% and 99.5% at pH 3. The removal efficiency followed the order of pH 3 > 5 > 7 > 9. 100% removal was obtained at a dosage of 10 g/L and 20 g/L at pH 3 and 5 for CFA whereas for DCF, 100% removal was obtained at adsorbent dosages of 2 and 5g/L at pH 3 and 5. When the pH was increased from acidic to basic conditions, a faster transport and sorption was observed for ATN in the beginning of adsorption which is due to its higher molecular polarizability, polar surface area and high water solubility compared to CFA and DCF while depending on the same sized pores there occurs, a competition between ATN, CFA and DCF molecules for the same adsorption sites (Matsui et al., 2002 and Jain and Snoeyink, 1973). A lower sorption was observed for DCF and CFA at basic pH conditions mainly attributing to the increase in hydroxyl ions that forms aqua-complexes thereby retarding the sorption (Venkata et al., 2007a, 2007b). Similarly



when the pH was decreased, the molecular dimensions and volume of ATN is higher than DCF, so the adsorption rate decreases as DCF overtakes ATN due to its smaller volume and has higher molecular refractivity, drying energy and pi energy compared to ATN and CFA. It may also be observed that diclofenac-Na possess O-H and N-H groups in them that is mainly responsible for its rapid and high adsorption and therefore adsorption equilibrium for DCF could be reached very fast.

### 5.3.7.3 Effect of PPCPs concentration at constant pH 9.0

Effect of PPCPs concentration was evaluated on the adsorption studies by varying PPCP concentrations of 10ppm, 20ppm and 30ppm at adsorbent dosages of 1, 2, 5, 10 and 20g/L for 48hrs.



It can be seen from Figure 5.20, that as the concentration of ATN, CFA and DCF was increased from 10ppm to 30ppm at pH 9, the percent removal decreased by a factor of 1.16, 1.36 and 1.25 times at a dosage of 1 g/L although complete removal could be achieved as the adsorbent dosage was increased from 1 g/L to 20g/L. It was observed that the highest decrease was observed for DCF followed by ATN and CFA this is because higher pH was unfavourable for DCF and CFA sorption onto BC.

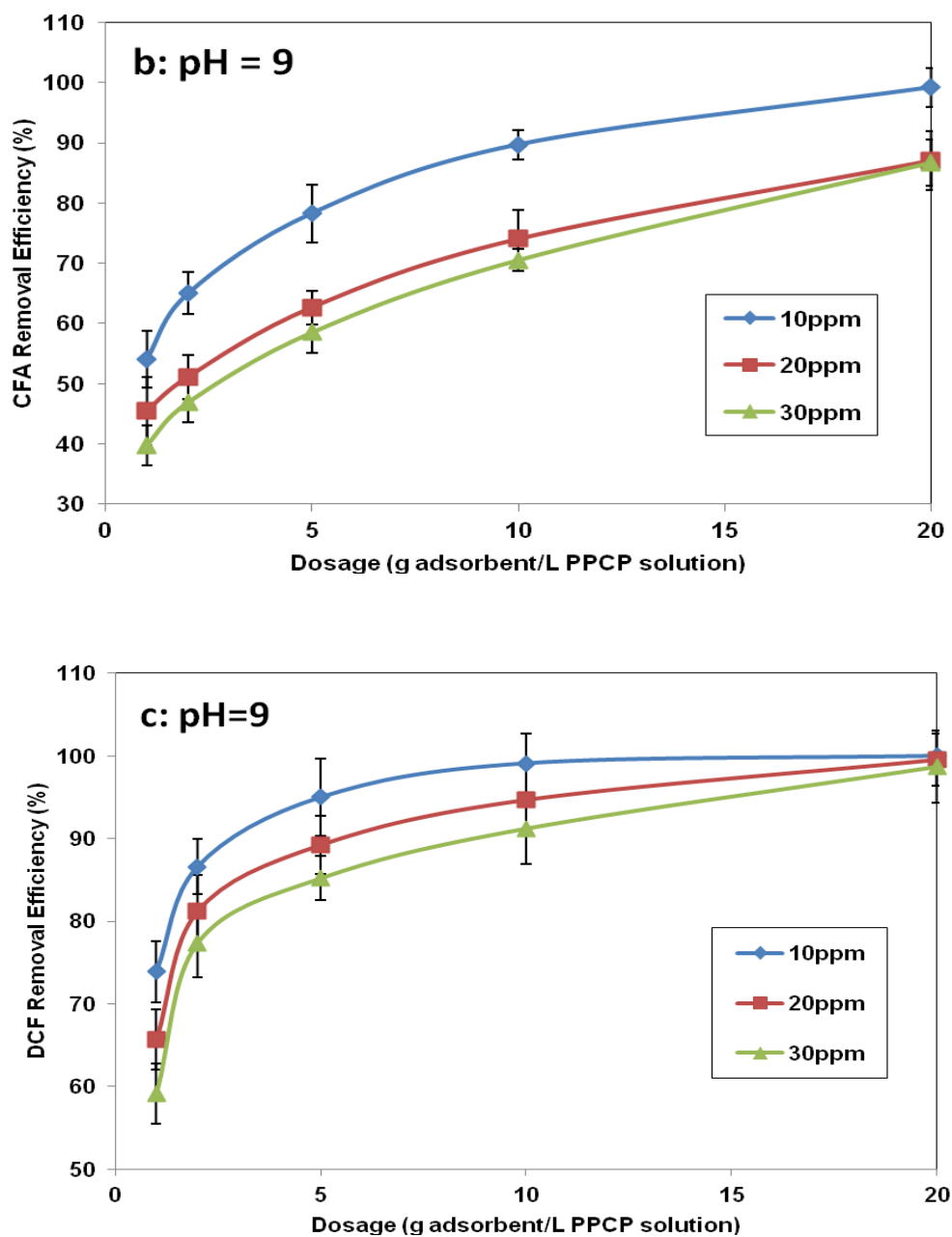


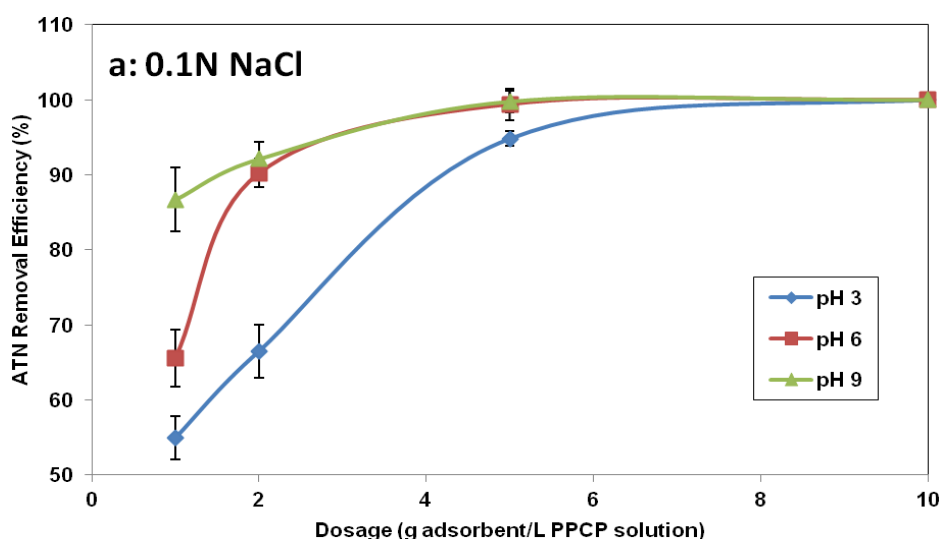
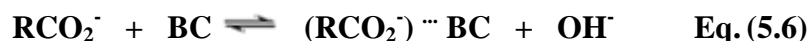
Figure 5.20. Effect of concentration onto BC and its removal efficiency (a) ATN, (b) CFA and (c) DCF [pH = 9, adsorbent dosage = 1, 2, 5, 10 and 20 g/L]

It was observed that at low concentration, higher sorption rates were achieved and when the concentration increased, the removal efficiency lowered which is due to electrostatic interactions between PPCPs and adsorbent surface and depended on the

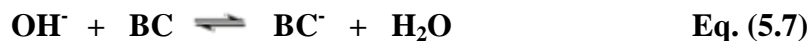
pollutant surface concentration (Muller et al., 1985) as there may be an effect by natural organic matter in the secondary effluent that blocks the pores on the surface of BC. Thus it may be assumed that there exist two simultaneous and coexisting processes that take place by hydrophobic PPCP compound adsorption into BC and absorbing into natural organic matter.

#### 5.3.7.4 Effect of Pre-conditioning on Sorbent Performance

Assuming sorption by anionic form, a cation bridge between negatively charged surface group (phenolate or carboxylate) and carboxylate group would enhance sorption. The anions may interact with metal either by solvent-separated ion pairing or by contact. An important mechanism that triggers in cation bridging is the aggregation of humic substances forming large natural organic matter in colloidal structures. As per Eq. 5.6, it can be seen that sorption of carboxylate group by biochar leads to release of hydroxide ion into solution causing progressive sorption suppression.



The buffering capacity of biochar should be taken into account to determine the extent of hydroxide release as per Eq. 5.7.



It can be seen from Figure 5.21a that percent removal improved with preconditioning of biochar with 0.1N NaCl and shows 1.24 times increase for ATN compared to biochar results without preconditioning at pH 3. Similarly Figure 5.21b and c shows slight increase for CFA and DCF showing 1.07 and 1.03 times by preconditioning at pH 9 compared to biochar.

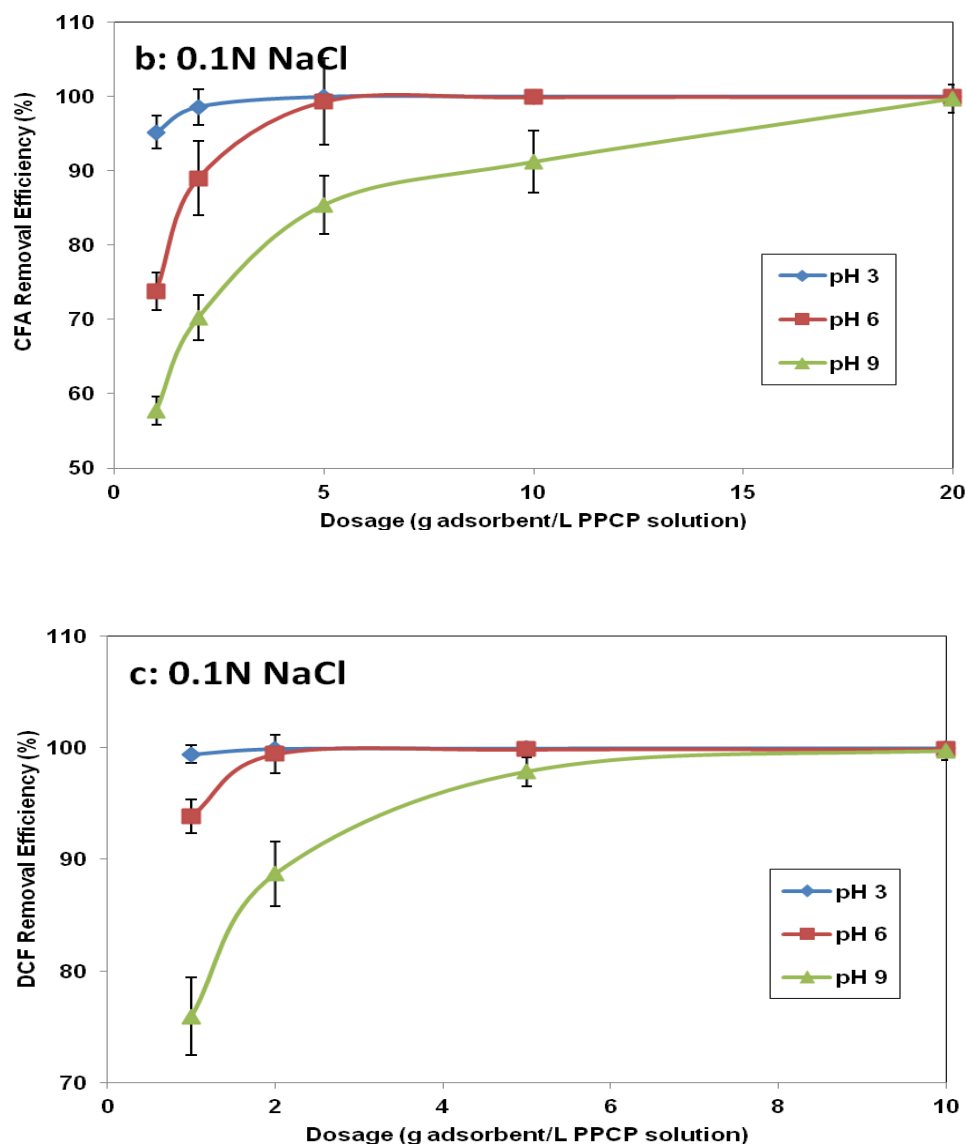


Figure 5.21. Effects of biochar pre-conditioning with 0.1N NaCl at pH 3, 6 and 9 (a) ATN (b) CFA and (c) DCF [Co = 10 mg/L]

### 5.3.7.5 Effect of Chemical conditioning

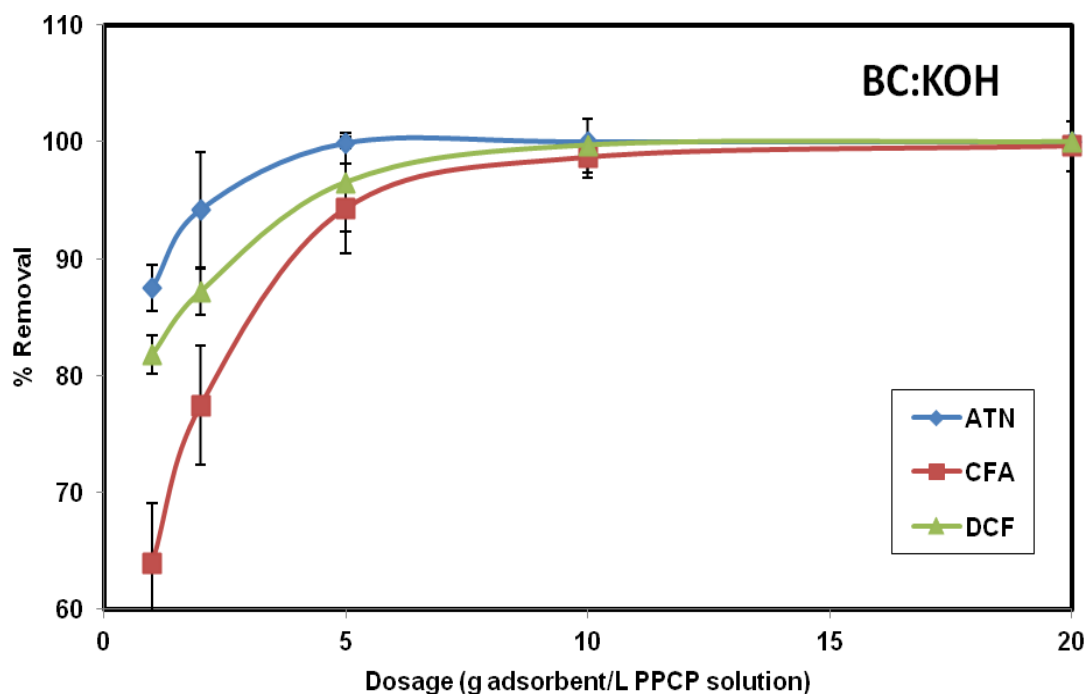


Figure 5.22. Effects of chemical activation of BC in removal efficiency at varying concentration of KOH [ $C_0 = 10\text{mg/L}$ ,  $\text{pH} = 9$ , adsorbent dosage = 1, 2, 5, 10, 20 g/L]

The biochar samples were activated by chemical conditioning and the obtained activated biochar was spiked with a 10 mg/L of all the three compounds at pH 9 and equilibrated for 48hrs. From the experimental data as shown in Figure 5.22, it can be concluded that a remarkable removal efficiency was observed at 87.5% ATN, 64% CFA and 81.8% DCF at an adsorbent dosage of 1g/L. 100% removal was reached at 5 g/L dosage for ATN compared to other PPCP compounds in solution. Depending on the same sized pores there occurs a competition between ATN, CFA and DCF molecules for the same adsorption sites (Matsui et al., 2002 and Jain and Snoeyink, 1973) and it was observed that ATN showed a faster transport at the beginning of adsorption studies due to its higher solubility in water and favourable pH conditions that sorbed ATN onto BC and may follow a process of pore-filling mechanism (Nguyen, et al., 2007) or ionic exchange interactions or complexation with functional groups on surface of BC. It can be seen that the sorption followed  $\text{ATN} > \text{DCF} > \text{CFA}$  and is in agreement with its  $\text{pK}_a$

values  $9.6 > 4.15 > 3.2$ . For DCF and CFA, there exists hydrophobic interaction mechanism for effective removal of non-polar organic compounds by activated biochar as these PPCP compounds possess  $\log K_{ow} > 2.5$ . Compared to other studies, the maximum removal efficiency was observed to be chemical activation of BC by KOH which leaves more empty spaces or pores on the carbon surface during carbonization process by evaporation of KOH (Jodeh et al., 2015).

### 5.3.8 Comparison of various adsorption methods with varying pH

The sorption process is influenced by pH of the solution which plays a significant role in determining the surface characteristics of BC and also chemical and stability forms of PPCP compounds.

From Figure 5.23 it can be concluded that biochar activated with KOH showed maximum percent removal followed by 0.1N NaCl which is followed by BC and the minimum percent removal was observed for BC:Chb. The removal efficiency follows the order  $\text{KOH} > 0.1 \text{ N NaCl} > \text{BC} > \text{BC:Chb}$  at  $\text{pH } 9 > 7 > 5 > 3$ . Presence of oxygenated functional groups on BC and ATN alters the electrostatic interaction between them when solution pH is varied affecting protonation or deprotonation of these functional groups. This shows that ATN has a pKa value of 9.16 and exists in deprotonated form at pH 11 and in the protonated form at  $\text{pH} \leq 9$  and is greatly influenced by pH. ATN consists of single aromatic ring and so there exists a weak  $\pi - \pi$  interaction between BC and ATN. In addition to electronic and  $\pi - \pi$  interaction, hydrogen bonding can also influence interactions between BC - ATN and adsorption (Yang and Xing 2009). ATN exists in neutral form at pH 7 whereas BC is negatively charged. Thus a hydrogen bond may be formed between  $-\text{O}^-$  group on BC and  $-\text{OH}$  group on ATN thus favouring ATN adsorption. At alkaline pH, the number of  $-\text{OH}$  groups decreased on ATN due to deprotonation and comparatively at acidic pH, the number of  $-\text{O}^-$  group on BC on BC decreases due to protonation. Thus both protonation and deprotonation mitigate hydrogen bonding between ATN and BC.

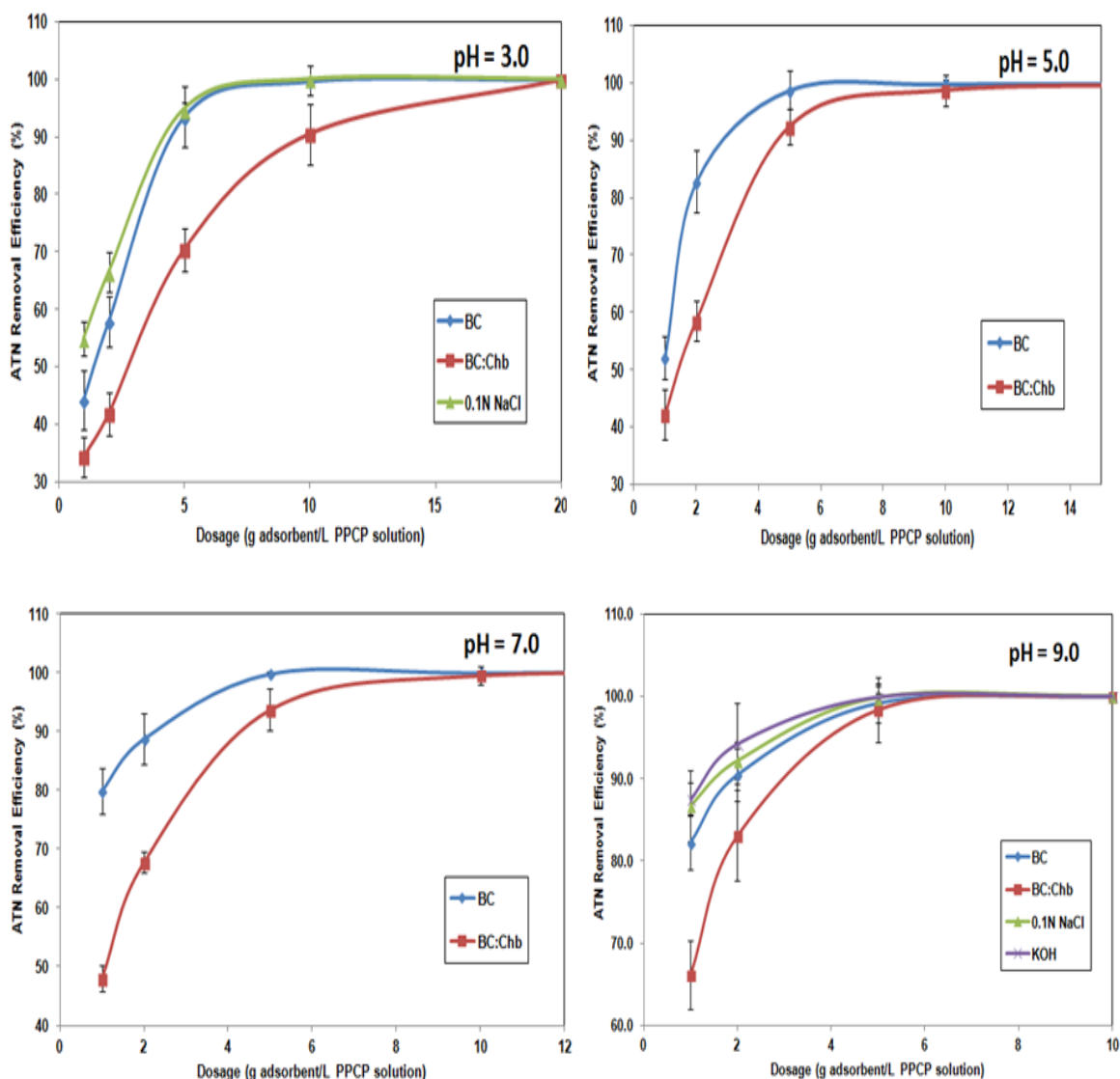


Figure 5.23. Comparison of various adsorption methods at varying pH onto BC and its removal efficiency for ATN [ $C_0 = 10\text{mg/L}$ , dosage = 1, 2, 5, 10, 20g/L]

Figure 5.24 shows the experimental data obtained by various adsorption process and found the maximum to minimum percent removal was obtained for  $\text{KOH} > 0.1\text{N NaCl} > \text{BC} > \text{BC} : \text{Chb}$ . Due to low  $\text{pK}_a$  value of 2.84 for clofibric acid (Xu et al., 2009a) it is found to dissociate highly in solution thus resulting in weak adsorption to organic matter. The adsorption also depends on pH especially when the biochar pH conditions are below their  $\text{pK}_a$ , then these organic acids will tend to be present in their undissociated or neutral form which in turn will have higher tendency to adsorb to

organic matter when compared to more polar dissociated forms. It is also not easy to predict the behavior of PPCPs adsorption in biochar due to its diverse structures whether ionic or polar. The lowest removal efficiency is due to the fact that at pH values between 7 and 11, the surface groups of the adsorbent as well as chemicals have high dissociation degree which leads to formation of negatively charged forms on the adsorbent and solutes that disfavors adsorption due to electrostatic repulsions.

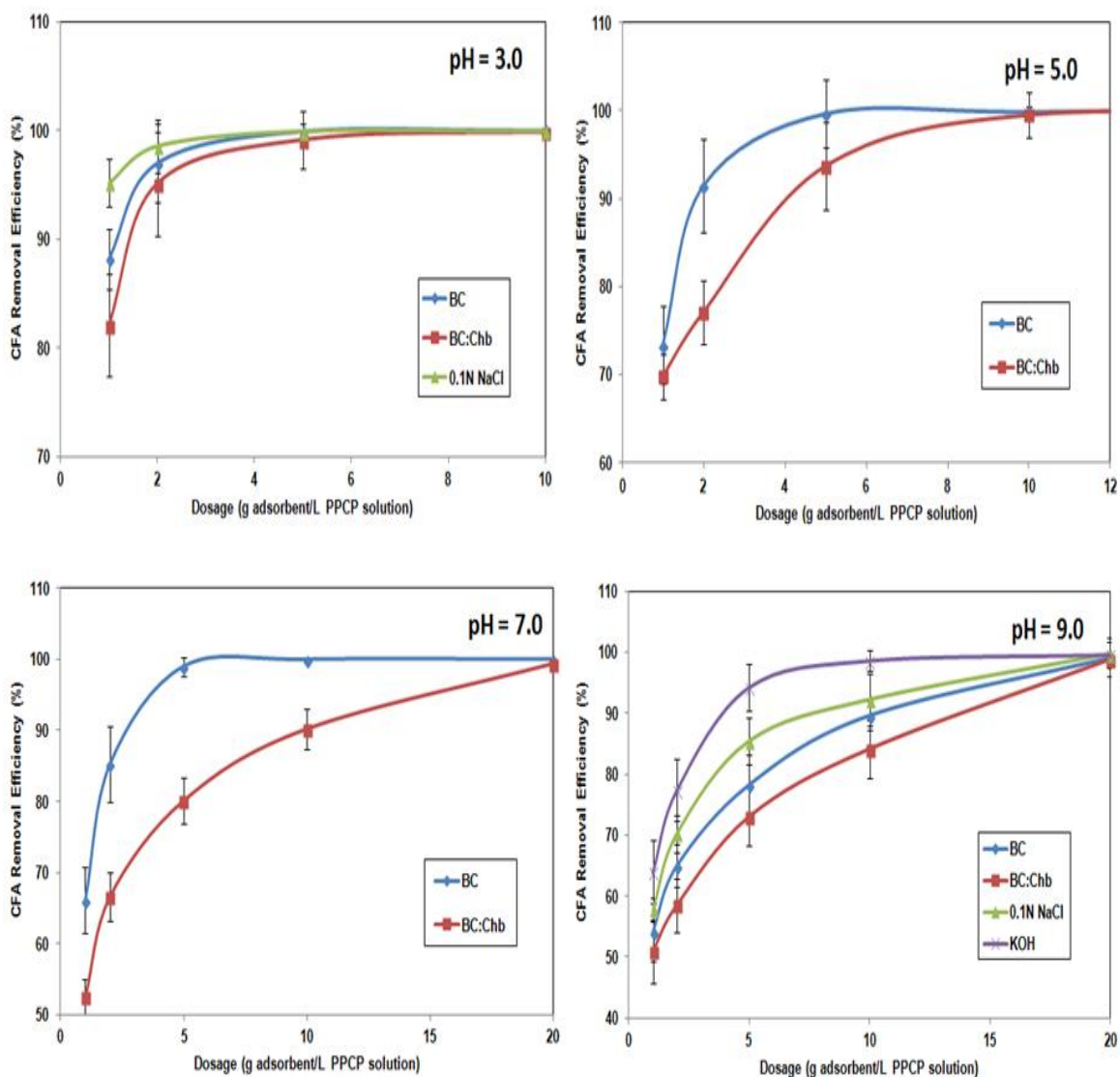


Figure 5.24. Comparison of various adsorption methods at varying pH onto BC and its removal efficiency for CFA [ $C_0 = 10\text{mg/L}$ , dosage = 1, 2, 5, 10, 20g/L]



Figure 5.25 shows that a strong interaction between electron donors on the polarisable biochars (aromatic carbon) and electron acceptors on the polar aromatic DCF which is dominant due to  $\pi - \pi$  EDA (electron donor acceptor) interaction between them (Chen et al., 2007).

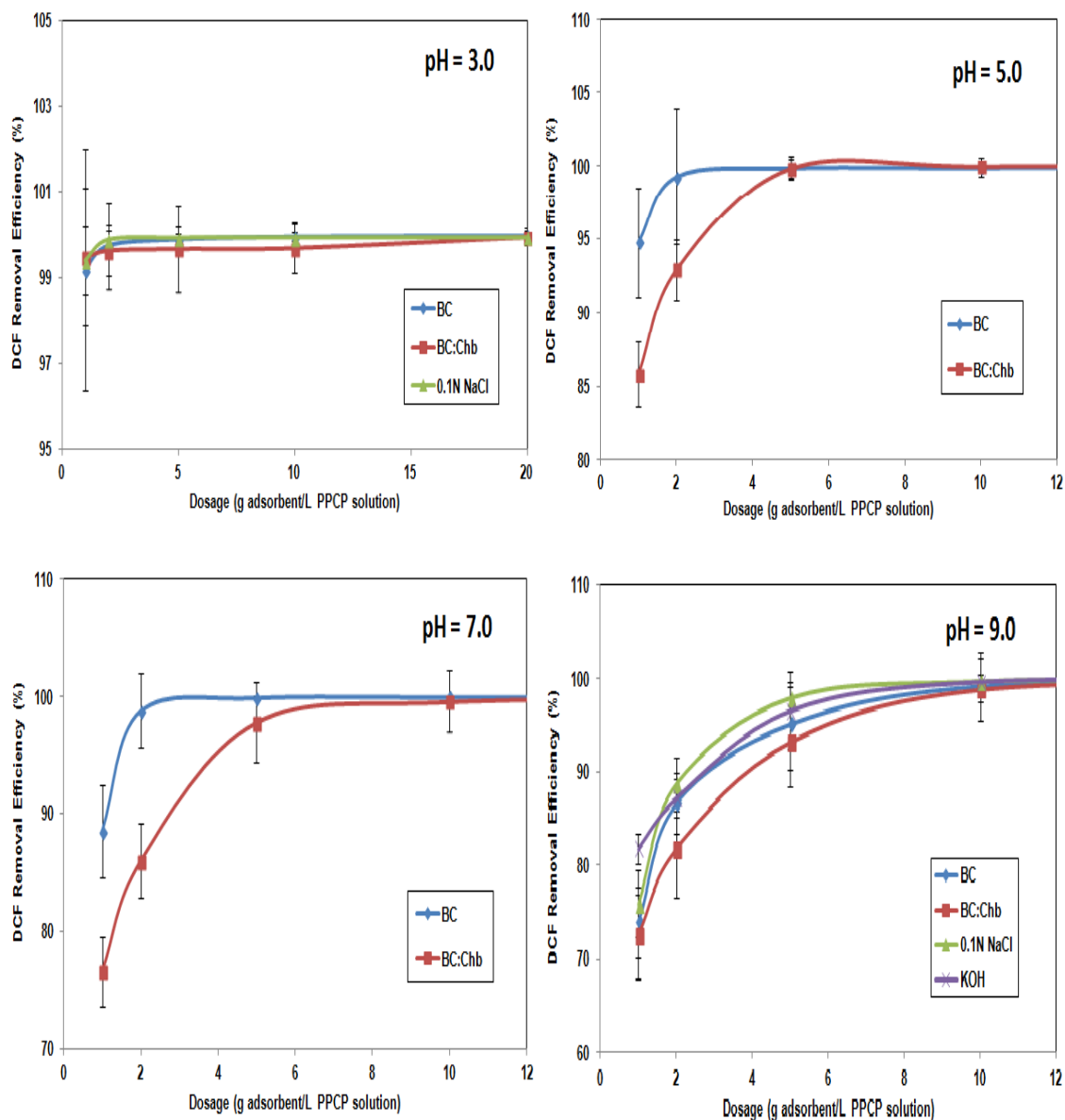


Figure 5.25. Comparison of various adsorption methods at varying pH onto BC and its removal efficiency for DCF [ $C_0 = 10\text{mg/L}$ , dosage = 1, 2, 5, 10, 20g/L]

The  $\pi$  -  $\pi$  interaction between BC and DCF is favoured due to the fact that DCF consists of two aromatic rings unlike ATN and CFA which consists of single aromatic ring. For DCF, a sieving effect is assumed to have occurred on the open sector of micro-sized pores with relatively large DCF molecular sizes that played an important role in DCF adsorption.

A better contact was observed between DCF and large pore sizes in greater number on biochar compared to other carbonaceous adsorbents with smaller pore-size leading to adsorption differences (Jung et al., 2013). The adsorption affinity of DCF on biochar increased due to its  $\pi$  energy values and high molecular polarizability compared to CFA and ATN despite its higher binding energy and aromaticity (Kusgens et al., 2009). As per literature, it was observed that the binding energy between DCF and each structure (groups of aliphatic, aryl, carbonyls and non-aromatic carbons) were greater than 18.8 kcal/mol regardless of carbonaceous structure ratios and elemental composition. Thus hydrophobic interaction was encouraged due to aromatic carbon due to component ratio.

The adsorption affinity of the three PPCPs on biochar was in the following order: DCF > CFA > ATN. Results suggest that ATN was most mobile, and DCF was the least mobile in biochar. The adsorption efficiency is strongly influenced by the physico-chemical properties of target adsorbates and biochar. A higher log Kow values shows stronger adsorption of microcontaminants onto biochars. Since DCF has higher adsorption energy, the electron density is decreased by the presence of chloride substituent and thus a higher chemical affinity for activated carbon surface is due to higher log Kow for DCF (Valladares et al., 2011).

More affined compounds are occupied preferentially with the highest adsorption potential at the active sites and the remaining available less favored molecules are adsorbed, by the remaining fewer adsorption sites that have higher adsorption potentials (suriyanon et al., 2013 and Pelekani et al., 1999). Thus a competition effect is caused by

the presence of one molecule which changes the energy field for another micropollutant in the active sites (Li et al., 2001). A lower log  $K_{ow}$ , higher water solubility and lower molecular weight are responsible for lower adsorption capacity for ATN compared to DCF. Since surface of biochar is non-polar, it generally favors compounds of non-polar adsorption rather than polar compounds although some adsorption of slightly polar compounds takes place due to the presence of some slightly polar carbon-oxygen groups present on activated carbon (Sulaymon and Ahmed, 2008). Some of the factors that influence the adsorption process are the biochar with pore size distribution that aids in adsorption of target compounds from water and molecular sizes of microcontaminants.

### 5.3.9 Isotherms

Adsorption isotherms of selected target PPCP compounds in BC were studied to find the relationship between ATN, CFA and DCF adsorbed ( $q_e$ ) and its equilibrium concentration ( $C_e$ ) as shown in Figures 5.26, 5.29 and 5.32. The Freundlich isotherms are shown in Figures 5.27, 5.30 and 5.33 where Freundlich linear isotherms were obtained by plotting  $q_e$  versus  $C_e$  to determine  $K_f$  and  $1/n$  values. For all tested PPCPs, the adsorption data best fits the Freundlich equation over the range of equilibrium concentrations and was quantified by the square of the correlation coefficient,  $R^2$  as given in Tables 5.6, 5.7 and 5.8. Freundlich isotherms will provide information on the adsorption characteristics of surface heterogeneity. The range of  $1/n$  values are from 0 to 1 and a more heterogeneity adsorbent surface dominates if the values are closer to zero. Langmuir isotherm model is based on few assumptions such as adsorption is restricted to monolayer and is independent of interactions between neighbouring sites of adjacent molecules on the surface and immobile adsorption. Thus Langmuir isotherm implies that all the sites are energetically equivalent and identical and are plotted between  $C_e/q_e$  versus  $C_e$  as shown in Figures 5.28, 5.31 and 5.34. Adsorption experiments were conducted in triplicate on tri-solutes where three solutes (ATN, CFA and DCF) were all combined in the experiments to produce competitive isotherms.

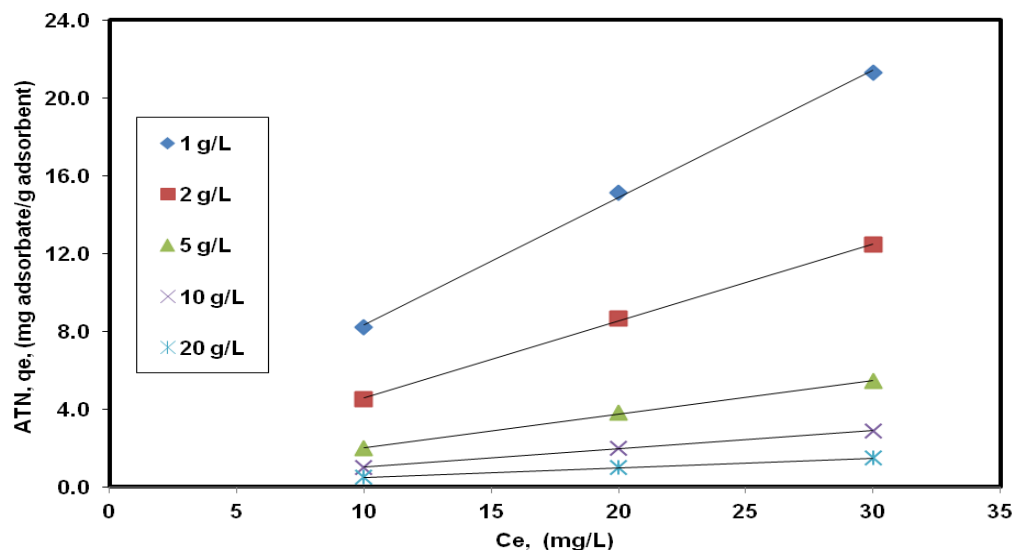


Figure 5.26. ATN equilibrium adsorption isotherm onto BC [pH = 9;  $C_o = 10, 20, 30$ mg/L; dosage = 1, 2, 5, 10, 20g/L]

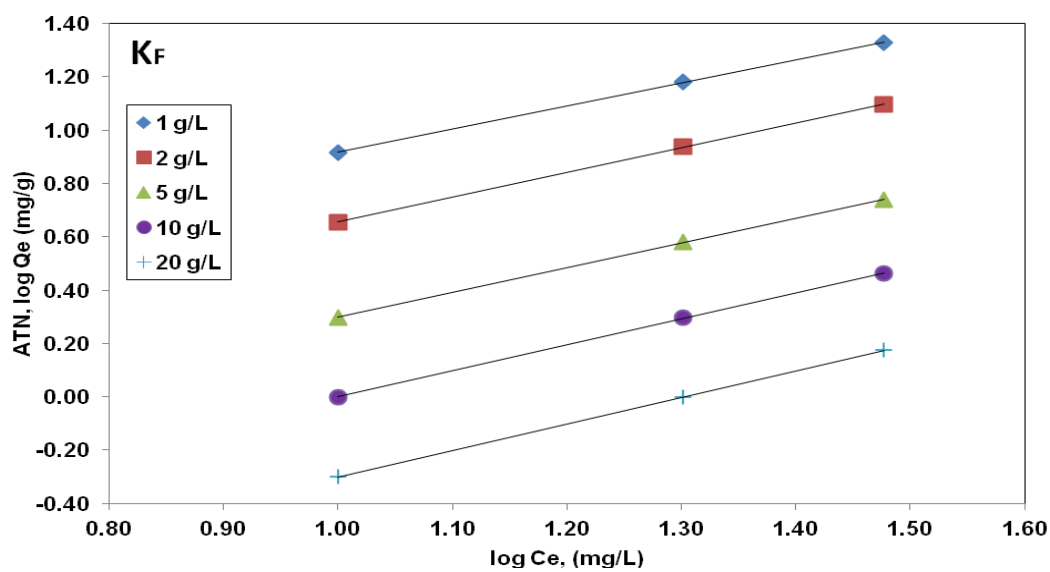


Figure 5.27. Freundlich plot for ATN adsorption onto BC [pH = 9;  $C_o = 10, 20, 30$ mg/L; dosage = 1, 2, 5, 10, 20g/L]

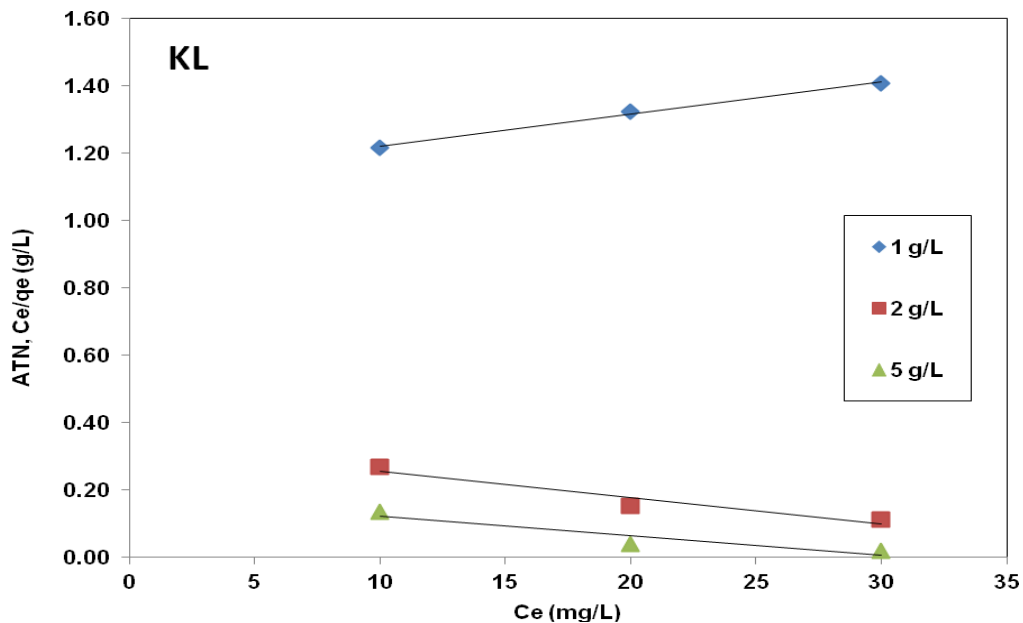


Figure 5.28. Langmuir plot for ATN adsorption onto BC [pH = 9;  $C_o = 10, 20, 30$ mg/L; dosage = 1, 2, 5g/L]

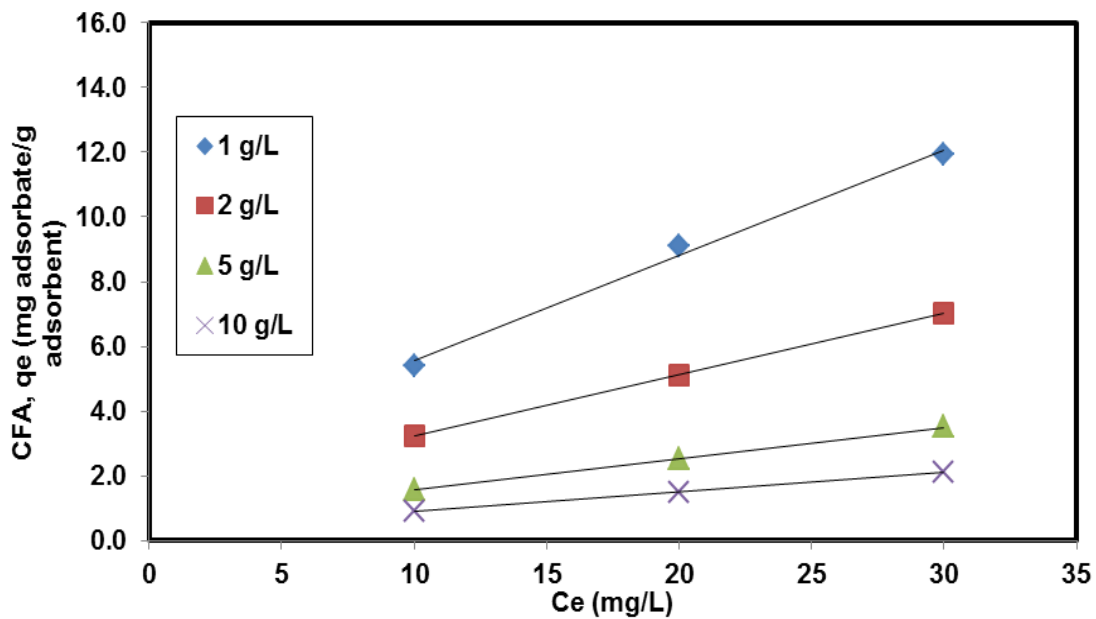


Figure 5.29. CFA equilibrium adsorption isotherm onto BC [pH = 9;  $C_o = 10, 20, 30$ mg/L; dosage = 1, 2, 5, 10g/L]

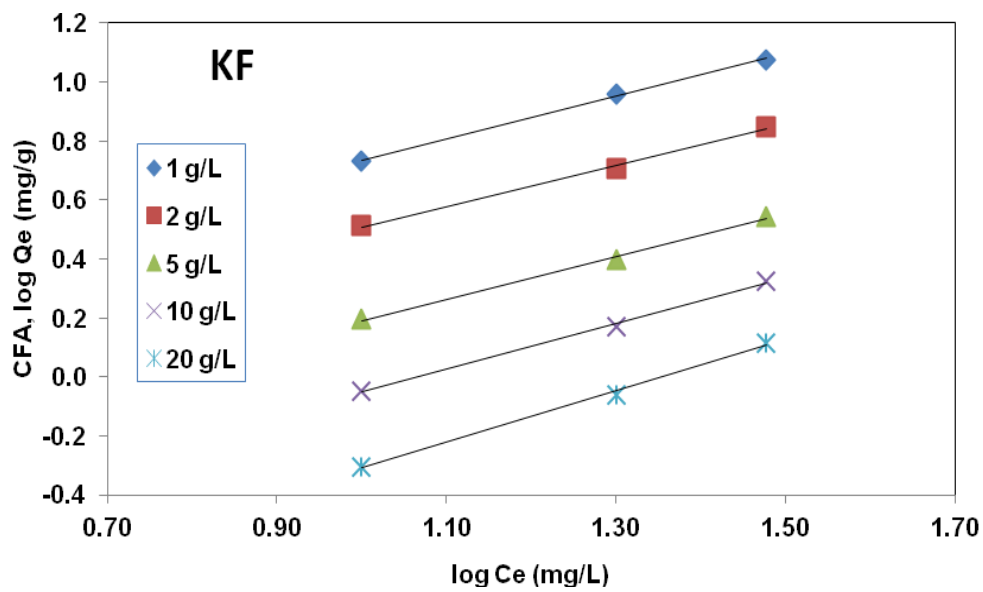


Figure 5.30. Freundlich plot for CFA adsorption onto BC [pH = 9; Co = 10, 20, 30mg/L; dosage = 1, 2, 5, 10, 20g/L]

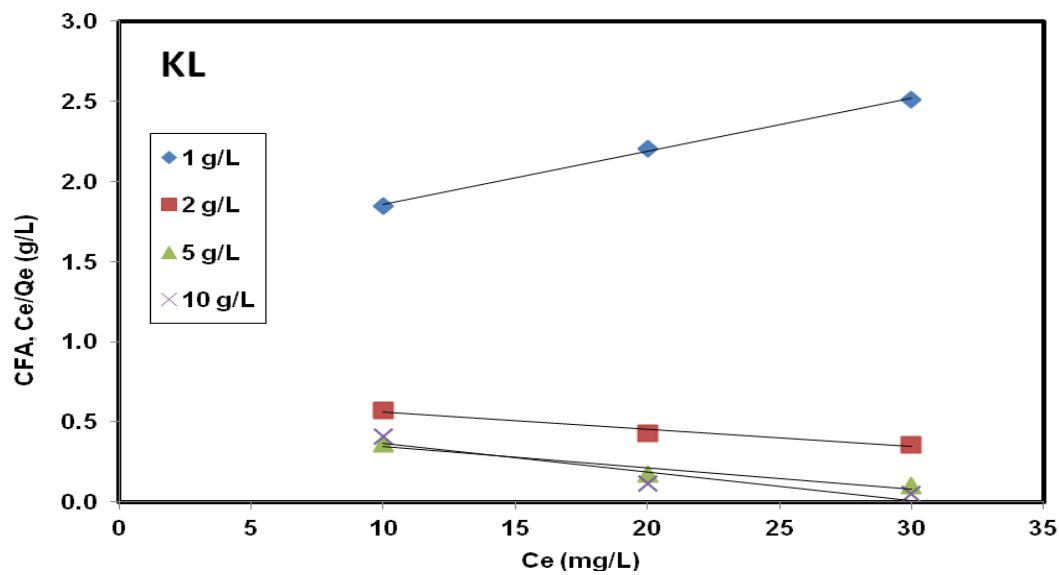


Figure 5.31. Langmuir plot for CFA adsorption onto BC [pH = 9; Co = 10, 20, 30mg/L; dosage = 1, 2, 5, 10g/L]

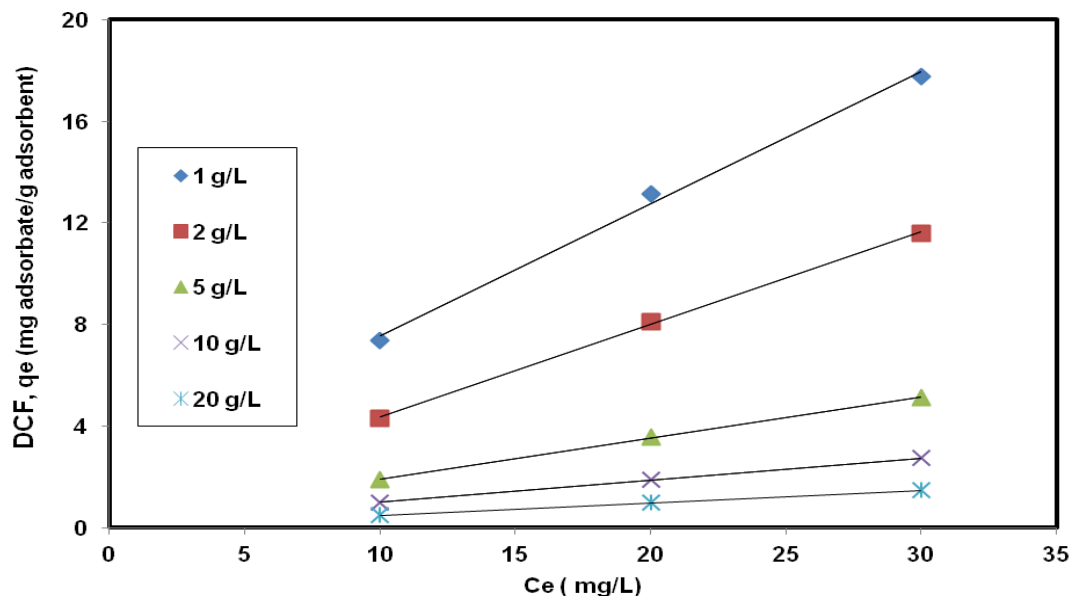


Figure 5.32. DCF equilibrium adsorption isotherm onto BC [pH = 9;  $C_o = 10, 20, 30$ mg/L; dosage = 1, 2, 5, 10, 20g/L]

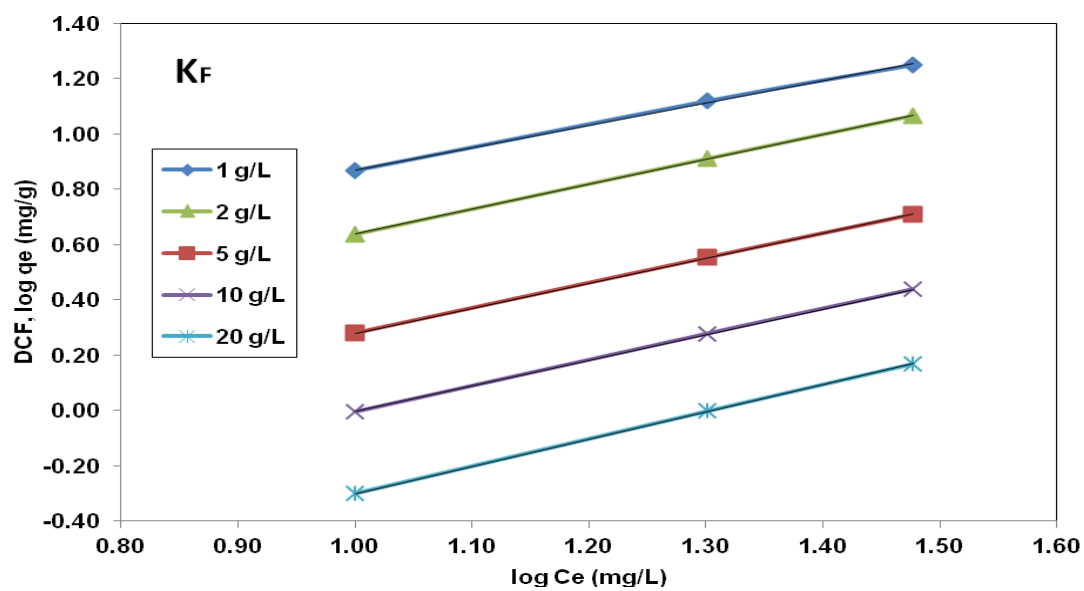


Figure 5.33. Freundlich plot for DCF adsorption onto BC [pH = 9;  $C_o = 10, 20, 30$ mg/L; dosage = 1, 2, 5, 10, 20g/L]

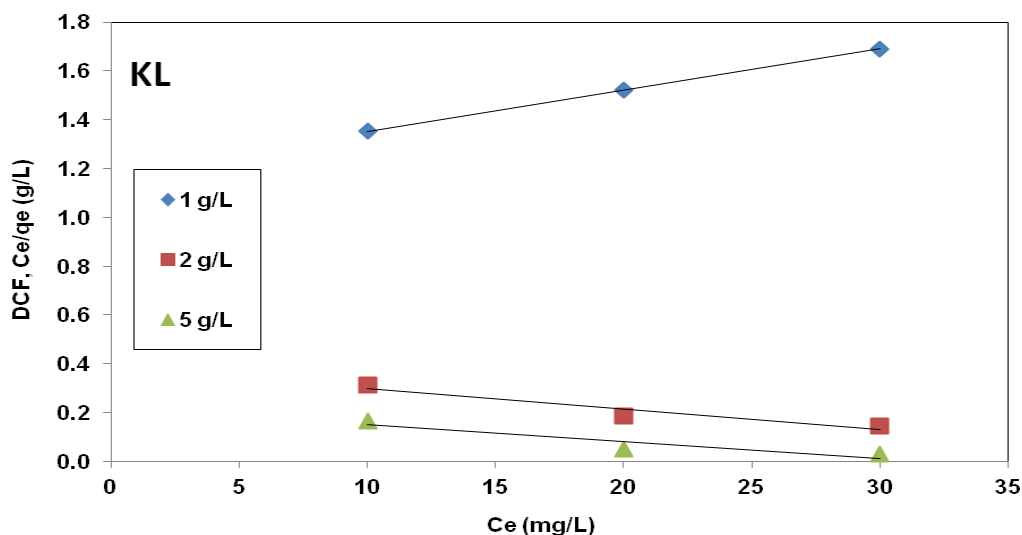


Figure 5.34. Langmuir plot for DCF adsorption onto BC [pH = 9;  $C_o = 10, 20, 30$  mg/L; dosage = 1, 2, 5 g/L]

Table 5.6. Freundlich and Langmuir isotherm constants for ATN adsorption onto BC with their correlation coefficient,  $R^2$  at different dosages

| ATN | Freundlich Isotherm |                                      |        | Langmuir Isotherm |                 |                     |
|-----|---------------------|--------------------------------------|--------|-------------------|-----------------|---------------------|
|     | Dosages,<br>g/L     | $K_F$<br>(mg/g)(L/mg) <sup>1/n</sup> | n      | $R^2$             | $K_L$<br>(L/mg) | $q_{max}$<br>(mg/g) |
| 1   | 1.118               | 1.15                                 | 0.9999 | 0.0085            | 104.2           | 0.9951              |
| 2   | 0.541               | 1.08                                 | 0.9999 | **                |                 |                     |
| 5   | 0.236               | 1.08                                 | 0.9998 | **                |                 |                     |
| 10  | 0.107               | 1.03                                 | 0.9997 | **                |                 |                     |
| 20  | 0.050               | 1.00                                 | 1.0000 | **                |                 |                     |

The slope and intercept were calculated using linearized form of the Freundlich and Langmuir equations and the linear plots obtained with their  $R^2$  values for the adsorption isotherm parameters are given in Table 5.6, 5.7 and 5.8.



Table 5.7. Freundlich and Langmuir isotherm constants for CFA adsorption onto BC with their correlation coefficient,  $R^2$  at different dosages

| CFA | Freundlich Isotherm |                                      |        | Langmuir Isotherm |                 |                     |
|-----|---------------------|--------------------------------------|--------|-------------------|-----------------|---------------------|
|     | Dosages,<br>g/L     | $K_F$<br>(mg/g)(L/mg) <sup>1/n</sup> | n      | $R^2$             | $K_L$<br>(L/mg) | $q_{max}$<br>(mg/g) |
| 1   | 1.026               | 1.38                                 | 0.9993 | 0.022             | 30.211          | 0.9986              |
| 2   | 0.645               | 1.43                                 | 0.9973 | **                |                 |                     |
| 5   | 0.289               | 1.37                                 | 0.9970 | **                |                 |                     |
| 10  | 0.149               | 1.29                                 | 0.9972 | **                |                 |                     |
| 20  | 0.065               | 1.15                                 | 0.9967 | **                |                 |                     |

Table 5.8. Freundlich and Langmuir isotherm constants for DCF adsorption onto BC with their correlation coefficient,  $R^2$  at different dosages

| DCF | Freundlich Isotherm |                                      |        | Langmuir Isotherm |                 |                     |
|-----|---------------------|--------------------------------------|--------|-------------------|-----------------|---------------------|
|     | Dosages,<br>g/L     | $K_F$<br>(mg/g)(L/mg) <sup>1/n</sup> | n      | $R^2$             | $K_L$<br>(L/mg) | $q_{max}$<br>(mg/g) |
| 1   | 1.17                | 1.25                                 | 0.9991 | 0.014             | 59.5            | 1.0000              |
| 2   | 0.55                | 1.11                                 | 0.9999 | **                |                 |                     |
| 5   | 0.24                | 1.11                                 | 1.0000 | **                |                 |                     |
| 10  | 0.12                | 1.08                                 | 0.9999 | **                |                 |                     |
| 20  | 0.05                | 1.01                                 | 1.0000 | **                |                 |                     |

\*\* Not Applicable

From the data it is clear that Freundlich isotherm values fitted more to the experimental data than Langmuir isotherm model in terms of  $R^2$  values. Freundlich isotherm shows that with increase in PPCP concentration, the adsorption will also increase in multilayer rather than single layer.

The  $n$  values between 1 and 10 favours adsorption between adsorbent and adsorbate. From Table 5.6, 5.7 and 5.8 for ATN, CFA and DCF, it is seen that the  $n$  values are above 1 for Freundlich and shows favourable adsorption of PPCPs onto BC. Higher the values of  $n$ , the stronger are the interaction between them. Hence assumption of physical adsorption by multilayer between BC and PPCPs validates to findings.

## 5.4 Conclusions

Adsorption studies with biochar showed that target PPCPs can be effectively and completely removed from secondary effluents by pyrolysis of wood biomass at 700°C. The performance of biochar can be maintained by proper biochar dosage to secondary effluent. The pre-conditioning of biochar by 0.1N NaCl increased the removal efficiency by 1.24 times for ATN and to a lesser extent for CFA and DCF. While chemical activation by KOH for ATN, CFA and DCF showed the maximum removal efficiency of 87.5%, 64% and 81.8% and followed the order by pre-conditioning (86.7%, 57.7%, 75.9%) > biochar (82.3%, 54.1%, 73.9%) > biochar : chabazite (66.1%, 50.9%, 72.4%) respectively at pH 9 and adsorbent dosage of 1 g/L. The sorption was mostly influenced by pH and the percent removal followed the order DCF > CFA > ATN for pH at 3 > 5 > 7 > 9 whereas percent removal followed a reverse trend as observed for ATN at pH 9 > 7 > 5 > 3. Adsorption isotherms favored Freundlich model for ATN, CFA and DCF as the values fitted more to the experimental data than Langmuir isotherm in terms of their  $R^2$  values.

Further work may be needed to pyrolyze the biochar at different temperatures based on type of wood biomass and type of PPCP compound selected and also depends on the type of wastewater. Steam activation can also be used as an alternative for chemical activation of biochar to study the percent removal of PPCs.

## 5.5 References

- Aguera, A., Alba, A.R.F., Piedra, L., Mezcuca, M., and Gomez, M.J., 2003. Evaluation of triclosan and biphenylol in marine sediments and urban wastewaters by pressurized liquid extraction and solid phase extraction followed by gas chromatography mass spectrometry and liquid chromatography mass spectrometry. *Analytica Chimica Acta*. 480 (2), 193–205.
- Ahmad, M., Lee, S.S., Rajapaksha, A.U., Vithanage, M., Zhang, M., Cho, J.S., Lee, S.E., Ok, Y.S., 2013. Trichloroethylene adsorption by pine needle biochars produced at various pyrolysis temperatures. *Bioresour. Technol.* 143, 615–622.
- Ahmad, M., Usman, A.R.A., Lee, S.S., Kim, S.C., Joo, J.H., Yang, J.E., Ok, Y.S., 2012b. Eggshell and coral wastes as low cost sorbents for the removal of  $Pb^{2+}$ ,  $Cd^{2+}$  and  $Cu^{2+}$  from aqueous solutions. *J. Ind. Eng. Chem.* 18, 198–204.
- Ahmad, M., Usman, A.R.A., Lee, S.S., Kim, S.C., Joo, J.H., Yang, J.E., Ok, Y.S., 2012c. Eggshell and coral wastes as low cost sorbents for the removal of  $Pb^{2+}$ ,  $Cd^{2+}$  and  $Cu^{2+}$  from aqueous solutions. *J. Ind. Eng. Chem.* 18, 198–204.
- Asano, T., and Cotruvo, J.A., 2004. Groundwater recharge with reclaimed municipal wastewater: Health and regulatory considerations. *Water Research* 38, 1941–1951.
- Ashton, D., Hilton, M., and Thomas, K.V., 2004. Investigating the environmental transport of human pharmaceuticals to streams in the United Kingdom. *Science of the Total Environment*. 333 (1–3), 167–184.
- Bargmann, I., Rilling, M.C., Buss, W., Kruse, A., Kuecke, M., 2013. Hydrochar and biochar effects on germination of spring barley. *J. Agro. Crop Sci.* 199, 360–373.
- Barnes, K.K., Christenson, S.C., Kolpin, D.W., Focazio, M., Furlong, E.T., Zaugg, S.D., Meyer, M.T., and Barber, L.B., 2004. Pharmaceuticals and other organic waste water contaminants within a leachate plume down gradient of a municipal landfill. *Ground Water Monitoring and Remediation*. 24 (2), 119–126.
- Barrer, R. M., 1948. *J. Chem. Soc.*, 127–132 RSC.
- Barrer, R. M., 1949. *Discuss. Faraday Soc.*, 7, 135–141 RSC.
- Barrer, R. M., and Brook, D. W., 1953. *Trans. Faraday Soc.*, 49, 1049–1059 RSC.
- Barrer, R. M., and Brook, D. W., 1953. *Trans. Faraday Soc.*, 49, 940–948 RSC.
- Barrer, R. M., and Ibbitson, D. A., 1944. *Trans. Faraday Soc.*, 40, 195–206 RSC.
- Barrer, R.M., and Fender, B.E.F., 1961. *J. Phys. Chem. Solids*. 21, 1–11. CrossRef. CAS.

Batt, A.L., Bruce, I.B., and Aga, D.S., 2006. Evaluating the vulnerability of surface waters to antibiotic contamination from varying wastewater treatment plant discharges. *Environmental Pollution*. 142 (2), 295–302.

Batt, A.L., Snow, D.D., and Aga, D.S., 2006. Occurrence of sulfonamide antimicrobials in private water wells in Washington County, Idaho, USA. *Chemosphere*. 64 (11), 1963–1971.

Beesley, L., Jimenez, E.M., Eyles, J.L.G., 2010. Effects of biochar and green waste compost amendments on mobility, bioavailability and toxicity of inorganic and organic contaminants in a multi-element polluted soil. *Environ. Pollut.* 158, 2282–2287.

Bendz, D., Paxeus, N.A., Ginn, T.R., and Loge, F.J., 2005. Occurrence and fate of pharmaceutically active compounds in the environment, a case study: Hoje River in Sweden. *Journal of Hazardous Materials*. 122 (3), 195–204.

Bertanza, G., Pedrazzani, R., Zambarda, V., 2009. I microinquinanti organici nelle acque di scarico urbane: presenza e rimozione. *Ingegneria Ambientale*. 48.

Bhogaraju, A., Nazeer, S., Al-Baghdadi, Y., Rahman, M., Wrestler, F., Patel, N., 1999. Diclofenac-associated hepatitis. *South. Med. J.* 92 (7), 711–713.

Bin C, J., Wen G. H., Lei Z. Y., Zhang, Y., Fei Z. X., Qi L. C., Ping G. H., 2014. Developmental Toxicity of Diclofenac and Elucidation of Gene Regulation in zebrafish (*Danio rerio*). *Scientific Reports*, 4:4841, DOI: 10.1038/srep04841.

Bornemann L.C., Kookana R.S., Welp, G., 2007. Differential sorption behavior of aromatic hydrocarbons on charcoals prepared at different temperatures from grass and wood. *Chemosphere* 67:1033–1042.

Bound, J.P., and Voulvoulis, N., 2005. Household disposal of pharmaceuticals as a pathway for aquatic contamination in the United Kingdom. *Environmental Health Perspectives*. 113 (12), 1705–1711.

Brick, S., 2010. *Biochar: Assessing the Promise and Risks to Guide US Policy*. Natural Resource Defense Council, USA.

Brown, K.D., Kulis, J., Thomson, B., Chapman, T.H., and Mawhinney, D.B., Occurrence of antibiotics in hospital, residential, and dairy, effluent, municipal wastewater, and the Rio Grande in New Mexico, *Science of the Total Environment* 366 (2–3), 772–783, 2006.

Bruchet, A., Hochereau, C., Picard, C., Decottignies, V., Rodrigues, J.M., and Janex-Habibi, M.L., 2005. Analysis of drugs and personal care products in French source and drinking waters: The analytical challenge and examples of application. *Water Science and Technology*. 52 (8), 53–61.

Brun, G.L., Bernier, M., Losier, R., Doe, K., Jackman, P., and Lee, H.B., 2006. Pharmaceutically active compounds in Atlantic Canadian sewage treatment plant effluents and receiving waters, and potential for environmental effects as measured by acute and chronic aquatic toxicity. *Environmental Toxicology and Chemistry*. 25, 2163–2176.

Buyuksonmez, F., and Sekeroglu, S., 2005. Presence of pharmaceuticals and personal care products (PPCPs) in biosolids and their degradation during composting. *Journal of Residuals Science & Technology*. 2 (1), 31–40.

Cabello, F.C., 2006. Heavy use of prophylactic antibiotics in aquaculture: A growing problem for human and animal health and for the environment. *Environmental Microbiology*. 8 (7), 1137–1144.

Camenisch, G., Folkers, G., and Van de Waterbeemd, H., 1997. *International Journal of Pharmaceutics*, 147, 61–70.

Cantrell, K.B., Hunt, P.G., Uchimiya, M., Novak, J.M., Ro, K.S., 2012. Impact of pyrolysis temperature and manure source on physicochemical characteristics of biochar. *Bioresour. Technol.* 107, 419–428.

Carballa, M., Omil, F., Lema, J.M., 2005. Removal of cosmetic ingredients and pharmaceuticals in sewage primary treatment. *Water Res.* 39, 4790–4796.

Chemicalize.org by ChemAxon (<http://www.chemicalize.org>) (date retrieved: 2015/03/07).

Chen, B., Chen, Z., Lv, S., 2011a. A novel magnetic biochar efficiently sorbs organic pollutants and phosphate. *Bioresour. Technol.* 102, 716–723.

Chen, W., Duan, L., Zhu, D., 2007. Adsorption of polar and nonpolar organic chemicals to carbon nanotubes. *Environ. Sci. Technol.* 41, 8295–8300.

Chen, X., Chen, G., Chen, L., Chen, Y., Lehmann, J., McBride, M.B., Hay, A.G., 2011b. Adsorption of copper and zinc by biochars produced from pyrolysis of hardwood and corn straw in aqueous solution. *Bioresource Technology*. Volume 102, Issue 19, Pages 8877-8884.

Choi, K.J., Kim, S.G., Kim, C.W., Kim, S.H., 2005. Effects of activated carbon types and service life on removal of endocrine disrupting chemicals: amitrol, nonylphenol, and bisphenol-A. *Chemosphere*. 58, 1535–1545.

Clara, M., Strenn, B., Gans, O., Martinez, E., Kreuzinger, N., and Kroiss, H., 2005. Removal of selected pharmaceuticals, fragrances and endocrine disrupting compounds in a membrane bioreactor and conventional wastewater treatment plants. *Water Research*. 39 (19), 4797–4807.

Clark, D.E., 1999. *Journal of Pharmaceutical Sciences*. 88, 807–814.

- Clark, D.E., 1999. *Journal of Pharmaceutical Sciences*. 88, 815–821.
- Cora, L., 2012. Two Decades of Negative Thermal Expansion Research: Where Do We Stand? *Materials*. 5(6), 1125-1154; doi:10.3390/ma5061125.
- Cordy, G.E., Duran, N.L., Bouwer, H., Rice, R.C., Furlong, E.T., Zaugg, S.D., Meyer, M.T., Barber, L.B., and Kolpin, D.W., 2004. Do pharmaceuticals, pathogens, and other organic waste water compounds persist when waste water is used for recharge? *Ground Water Monitoring and Remediation*. 24 (2), 58–69.
- Cunningham, V.L., Buzby, M., Hutchinson, T., Mastrocco, F., Parke, N., and Roden, N., 2006. Effects of human pharmaceuticals on aquatic life: Next steps. *Environmental Science & Technology*. 40 (11), 3456–3462.
- de Ridder, D.J., Verberk, J.Q.J.C., Heijman, S.G.J., Amya, G.L., van Dijk, J.C., 2012. Zeolites for nitrosamine and pharmaceutical removal from demineralised and surface water: Mechanisms and efficacy. *Separation and Purification Technology*. 89, 71–77.
- Dietze, J.E., Scribner, E.A., Meyer, M.T., and Kolpin, D.W., 2005. Occurrence of antibiotics in water from 13 fish hatcheries, 2001–2003. *International Journal of Environmental Analytical Chemistry*. 85 (15), 1141–1152.
- Ding, L., Zou, B., Gao, W., Liu, Q., Wang, Z., Guo, Y., Wang, X., Liu, Y., 2014. Adsorption of rhodamine-B from aqueous solution using treated rice husk-based activated carbon. *Colloids Surf. A* 446, 1–7.
- Dodd, M.C. and Huang, C.H., 2004. Transformation of the antibacterial agent sulfamethoxazole in reactions with chlorine: Kinetics mechanisms, and pathways. *Environmental Science & Technology*. 38 (21), 5607–5615.
- Drewes, J.E., Heberer, T., Rauch, T., and Reddersen, K., 2003. Fate of pharmaceuticals during ground water recharge. *Ground Water Monitoring and Remediation*. 23, 64–72.
- Enders, A., Hanley, K., Whitman, T., Joseph, S., Lehmann, J., 2012. Characterization of Biochars to evaluate recalcitrance and agronomic performance. *Bioresour. Technol.* 114, 644–653.
- Fent, K., Weston, A.A., and Caminada, D., 2006. Ecotoxicology of human pharmaceuticals. *Aquatic Toxicology*. 76 (2), 122–159.
- Fini, A., Cavallari, C. and Ospitali, F., 2010. Diclofenac Salts. V. Examples of Polymorphism among Diclofenac Salts with Alkyl-hydroxy Amines Studied by DSC and HSM. *Pharmaceutics*. 2, 136–158; doi:10.3390/pharmaceutics2020136.
- Gallant, J., Prakash, A., and Hogg, L.E.W., 2009. “Removal of Selected Radionuclides and Metal Contaminants by Natural Zeolites from Liquid Effluents”, *Proceedings of 30<sup>th</sup> Annual Conference of the Canadian Nuclear Society*, May 31-June 03, pp.

Glassmeyer, S.T., Furlong, E.T., Kolpin, D.W., Cahill, J.D., Zaugg, S.D., Werner, S.L., Meyer, M.T., and Kryak, D.D., 2005. Transport of chemical and microbial compounds from known waste water discharges: Potential for use as indicators of human fecal contamination. *Environmental Science & Technology*. 39 (14), 5157–5169.

Gros, M., Petrovic, M., and Barcelo, D., 2006. Development of a multi-residue analytical methodology based on liquid chromatography-tandem mass spectrometry (LC-MS/MS) for screening and trace level determination of pharmaceuticals in surface and wastewaters. *Talanta*. 70, 678–690.

Gross, B., Brown, J.M., Naumann, A., and Reinhard, M., 2004. Occurrence and fate of pharmaceuticals and alkylphenol ethoxylate metabolites in an effluent-dominated river and wetland. *Environmental Toxicology and Chemistry*. 23 (9), 2074–2083.

Hapeshi, E., Achilleos, A., Vasquez, M.I., Michael, C., Xekoukoulotakis, N.P., Mantzavinos, D., Kassinos, D., 2010. Drugs degrading photocatalytically: kinetics and mechanisms of ofloxacin and atenolol removal on titania suspensions. *Water Res.* 44, 1737–1746.

Harrison, E.Z., Oakes, S.R., Hysell, M., and Hay, A. 2006. Organic chemicals in sewage sludges. *Science of the Total Environment*. 367 (2–3), 481–497.

Harvey, O. M., Herbert, B. E., Kuo, L. J., and Louchouart, P., 2012. Generalized two-dimensional perturbation correlation Infrared spectroscopy reveals mechanisms for the development of surface charge and recalcitrance in plant-derived biochars, *Environ. Sci. Technol.*, 46, 10641–10650.

Heberer, T., Bäumler, K.S., Stan, H.J., 1998. Occurrence and distribution of organic contaminants in the aquatic system in Berlin. Part I: Drug residues and other polar contaminants in Berlin surface and ground water. *Acta Hydrochim. Hydrobiol.* 26 (5), 272–278.

Heberer, T., Mechlinski, A., Fanck, B., Knappe, A., Massmann, G., Pekdeger, A., and Fritz, B., 2004. Field studies on the fate and transport of pharmaceutical residues in bank filtration. *Ground Water Monitoring and Remediation*. 24 (2), 70–77.

Hernando, M.D., Heath, E., Petrovic, M., and Barcelo, D., 2006. Trace-level determination of pharmaceutical residues by LC-MS/MS in natural and treated waters. A pilot-survey study. *Analytical and Bioanalytical Chemistry*. 385 (6), 985–991.

<http://beggcousland.co.uk/products/gas-cleaning/active-carbon-systems> (Date Retrieved: 7th March, 2015).

<http://www.alternabiocarbon.com/carbonization/carbonization-of-wood> (Date Retrieved: 7th March, 2015).

[http://www.wiley-vch.de/books/sample/3527329544\\_c01.pdf](http://www.wiley-vch.de/books/sample/3527329544_c01.pdf) (Date Retrieved: 25th March, 2015).

- Huang, Y., Li, S., Chen, J., Zhang, X., Chen, Y., 2014. Adsorption of Pb(II) on mesoporous activated carbon fabricated from water hyacinth using H<sub>3</sub>PO<sub>4</sub> activated: Adsorption capacity, kinetic and isotherm studies. *Appl. Surf. Sci.* 293, 160–168.
- Isarain-Chávez, E., Arias, C., Cabot, P.L., Centellas, F., Rodríguez, R.M., Garrido, J.A., Brillas, E., 2010. Mineralization of the drug b-blocker atenolol by electro-Fenton and photoelectron-Fenton using an air-diffusion cathode for H<sub>2</sub>O<sub>2</sub> electrogeneration combined with a carbon-felt cathode for Fe<sup>2+</sup> regeneration. *Appl. Catal. B: Environ.* 96, 361-369.
- Jain, J.S., Snoeyink, V.L., 1973. Adsorption from bisolute systems on active carbon, *J. Water Pollut. Control Fed.* 45 (1973) 2463–2479.
- Ji, Y., Zeng, C., Ferronato, C., Chovelon, J.M., Yang, X., 2012. Nitrate-induced photodegradation of atenolol in aqueous solution: kinetics, toxicity and degradation pathways. *Chemosphere* 88, 644–649.
- Ji, Y., Zhou, L., Ferronato, C., Yang, X., Salvador, A., Zeng, C., Chovelon, J.M., 2013. Photocatalytic degradation of atenolol in aqueous titanium dioxide suspensions: kinetics, intermediates and degradation pathways. *J. Photochem. Photobiol., A: Chem.* 254, 35–44.
- Jodeh, S., Abdelwahab, F., Jaradat, N., Warad, I., Jodeh, W., 2015. Adsorption of diclofenac from aqueous solution using *Cyclamen persicum* tubers based activated carbon (CTAC). *Journal of the Association of Arab Universities for Basic and Applied Sciences*. <http://dx.doi.org/10.1016/j.jaubas.2014.11.002>.
- Jones, A.H., Voulvoulis, N., and Lester, J.N., 2004. Potential ecological and human health risks associated with the presence of pharmaceutically active compounds in the aquatic environment. *Critical Reviews in Toxicology.* 34 (4), 335–350.
- Jones, O.A., Lester, J.N., and Voulvoulis, N., 2005. Pharmaceuticals: A threat to drinking water? *Trends in Biotechnology.* 23 (4), 163–167.
- Joseph, S., Graber, E. R., Chia, C., Munroe, P., Donne, S., Thomas, T., Nielsen, S., Marjo, C., Rutledge, H., Pan, G. X., Li, L., Taylor, P., Rawal, A., and Hook, J., 2013. Shifting paradigms: development of high-efficiency biochar fertilizers based on nanostructures and soluble components. *Carbon Manage.* 4, 323–343.
- Jung, C., Park, J., Lim, K.H., Park, S., Heo, J., Her, N., Oh, J., Yun, S., Yoon, Y., 2013. Adsorption of selected endocrine disrupting compounds and pharmaceuticals on activated biochars. *J. Hazard. Mater.* 263, 702–710.
- Jung, K., Ok, Y.S., Chang, S.X., 2011. Sulfate adsorption properties of acid-sensitive soils in the Athabasca oil sands region in Alberta, Canada. *Chemosphere.* 84, 457–463.



- Kalderis, D., Hawthorne, S. B., Clifford, A. A., and Gidarakos, E., 2008. Interaction of soil, water and TNT during degradation of TNT on contaminated soil using subcritical water. *J. Hazard. Mater.* 159, 329–334, 2008.
- Kelder, J., Grootenhuis, P.D.J., Bayada, D.M., Delbressine, L.P.C., and Ploemen, J.-P., 1999. *Pharmaceutical Research*. 16, 1514-1519.
- Kibbey, T.C.G., Paruchuri, R., Sabatini, D.A., Chen, L., 2007. Adsorption of beta blockers to environmental surfaces. *Environ. Sci. Technol.* 41, 5349–5356.
- Kinney, C.A., Furlong, E.T., Werner, S.L., and Cahill, J.D., 2006. Presence and distribution of wastewater-derived pharmaceuticals in soil irrigated with reclaimed water. *Environmental Toxicology and Chemistry*. 25 (2), 317–326.
- Kinney, C.A., Furlong, E.T., Zaugg, S.D., Burkhardt, M.R., Werner, S.L., Cahill, J.D., and Jorgensen, G.R., 2006. Survey of organic wastewater contaminants in biosolids destined for land application. *Environmental Science & Technology*. 40 (23), 7207–7215.
- Koelmans, A.A., Jonker, M.T.O., Cornelissen, G., Bucheli, T.D., Van Noort, P.C.M., Gustafsson, Ö., 2006. Black carbon: the reverse of its dark side. *Chemosphere*. 63:365–377.
- Kreuzinger, N., Clara, M., Strenn, B., and Vogel, B., 2004. Investigation on the behavior of selected pharmaceuticals in the groundwater after infiltration of treated wastewater. *Water Science and Technology*. 50 (2), 221–228.
- Ku"ster, A., Alder, C. A., Escher, I. B., Duis, K., Fenner, K., Garric, J., Hutchinson, H. T., Lapen, R. D., Pe'ry, A., Ro"mbke, J., Snape, J., Ternes, T., Topp, E., Anne Wehrhan, Y. A., and Knackerk, T., 2009. Environmental Risk Assessment of Human Pharmaceuticals in the European Union: A Case Study with the  $\beta$ -Blocker Atenolol. *Integrated Environmental Assessment and Management — Volume 6, Supplement 1—* pp. 514–523 514, SETAC.
- K"sgens, P., Rose, M., Senkovska, I., Fr"de, H., Henschel, A., Siegle, S., Kaskel, S., 2009. Characterization of metal–organic frameworks by water adsorption. *Microporous Mesoporous Mater.* 120, 325–330.
- Kuzyakov Y., Xu X. 2013. Tansley Review: Competition between roots and microorganisms for N: mechanisms and ecological relevance. *New Phytologist* 198 (3), 656-669.
- Lee, H.B., Peart, T.E., and Svoboda, M.L., 2005. Determination of endocrine-disrupting phenols, acidic pharmaceuticals, and personal-care products in sewage by solid-phase extraction and gas chromatography-mass spectrometry. *Journal of Chromatography A*1094 (1–2), 122–129.

Lee, J. W., Kidder, M., Evans, B. R., Paik, S., Buchanan, A. C., Garten, C. T., and Brown, R. C., 2010. Characterization of biochars produced from cornstovers for soil amendment, *Environ. Sci. Technol.*, 44, 7970–7974.

Lehmann, J., 2007. Bio-energy in the black. *Frontiers Ecol. Environ.* 5, 381–387.

Lehmann, J., Joseph, S., 2009. Biochar for environmental management: an introduction. In: Lehmann, J., Joseph, S. (Eds.), *Biochar for Environmental Management Science and Technology*. Earthscans, UK, pp. 1–12.

Lehmann, M., 2000. Arzneimittel und hormonell wirksame Stoffe in Fließgewässern Baden-Württembergs. In: 25 Jahre LFU. Jahresbericht 1998/1999. LFU Baden-Württemberg.

Lei, O. and Zhang, R., 2013. Effects of biochars derived from different feedstocks and pyrolysis temperatures on soil physical and hydraulic properties. *J. Soil. Sedim.*, 13, 1561–1572.

Li, J., Werth, C.J., 2001. Evaluating competitive sorption mechanisms of volatile organic compounds in soils and sediments using polymers and zeolites. *Environ. Sci. Technol.* 35, 568–574.

Li, W., Lu, S., Qiu, Z., and Lin, K., 2011. Photocatalysis of Clofibric Acid under Solar Light in Summer and Winter Seasons. [dx.doi.org/10.1021/ie1017145](https://doi.org/10.1021/ie1017145) | *Ind. Eng. Chem. Res.* 50, 5384–5393.

Lindqvist, N., Tuhkanen, T., and Kronberg, L., 2005. Occurrence of acidic pharmaceuticals in raw and treated sewages and in receiving waters. *Water Research*, 39 (11), 2219–2228.

Liu, Z. and Zhang, F. S., 2009. Renoval of lead from water using biochars prepared from hydrothermal liquefaction o biomass. *J. Hazard. Mater.* 167, 933–939.

Lohmann, R., 2003. The emergence of black carbon as a supersorbent in environmental Chemistry: the end of octanol? *Environ Forensic*, 4:161–165.

Mackay, D. M., and Roberts, P. V., 1982. The influence of pyrolysis conditions on yield and microporosity of lignocellulosic chars, *Carbon*, 20, 95–105.

Magnan, J.-P., and Ghassem, Y., 1989. Methylene blue Essaiu and geotechnical soil classification. *Geotechnical-Soil Mechanics. Bull link and P. Ch.* 159. Ref. 3378.

Marsh, H., (Editor), 2001. *Activated carbon compendium*, Elsevier Science Ltd, ISBN: 0-08- 044030-4, UK, pp 17-20.

Masters, R.W., Verstraeten, I.M., and Heberer, T., 2004. Fate and transport of pharmaceuticals and endocrine disrupting compounds during ground water recharge, *Ground Water Monitoring and Remediation*, 24 (2), 54–57.

- Matamoros, V., Garcia, J., and Bayona, J.M., 2005. Behavior of selected pharmaceuticals in subsurface flow constructed wetlands: A pilot-scale study. *Environmental Science & Technology*, 39 (14), 5449–5454.
- Matsui, Y., Knappe, D.R.U., Takagi, R., 2002. Pesticide adsorption by granular activated carbon adsorbers. 1. Effect of natural organic matter preloading on removal rates and model simplification. *Environ. Sci. Technol.*, 36, 3426–3431.
- Meteyer, C.U., Rideout, B.A., Gilbert, M., Shivaprasad, H.L., and Oaks, J.L., 2005. Pathology and proposed pathophysiology of diclofenac poisoning in free-living and experimentally exposed oriental white-backed vultures (*Gyps bengalensis*). *Journal of Wildlife Diseases*, 41 (4), 707–716.
- Miao, X.S., Yang, J.J., and Metcalfe, C.D., 2005. Carbamazepine and its metabolites in wastewater and in biosolids in a municipal wastewater treatment plant, *Environmental Science & Technology*, 39 (19), 7469–7475.
- Mimeault, C., Woodhouse, A., Miao, X.S., Metcalfe, C.D., Moon, T.W., and Trudeau, V.L., 2005. The human lipid regulator, gemfibrozil bioconcentrates and reduces testosterone in the goldfish, *Carassius auratus*. *Aquatic Toxicology*, 73 (1), 44–54.
- Mozaz, S. R., de Alda, M.J.L., and Barcelo, D., 2004. Monitoring of estrogens, pesticides and bisphenol A in natural waters and drinking water treatment plants by solid-phase extraction-liquid chromatography-mass spectrometry. *Journal of Chromatography, A* 1045 (1–2), 85–92.
- Muller, G., Radke, C.J., Prausnitz, J.M., 1985. Adsorption of weak organic electrolytes from dilute aqueous solution onto activated carbon. Part 1. Single solute system. *J. Colloid Interface Sci.* 103, 466.
- Munoz, S.M., Garcia, J.L.L., Ramos, M.J., Alba, A.F., and de Castro, M.D.L., 2005. Sequential superheated liquid extraction of pesticides, pharmaceutical and personal care products with different polarity from marine sediments followed by gas chromatography mass spectrometry detection. *Analytica Chimica Acta*, 552 (1–2), 50–59.
- Nandi, B.K., Goswami, A., Purkait, M.K., 2009. Removal of cationic dyes from aqueous solution by kaolin: kinetic and equilibrium studies. *Appl. Clay Sci.* 42, 583.
- Nguyen, T.H., Cho, H.H., Poster, D.L., and Ball, W.P., 2007. “Evidence for a pore-filling mechanism in the adsorption of aromatic hydrocarbons to a natural wood char,” *Environmental Science and Technology*. vol. 41, pp. 1212–1217.
- Nguyen, B. T. and Lehmann, J., 2009. Black carbon decomposition under varying water regimes. *Org. Geochem.* 40, 846–853.
- Noh, J.S., Schwarz, J.A., 1989. Estimation of the point of zero charge of simple oxides by mass titration. *J. Colloid Interface Sci.* 130, 157–164.

Novak, J. M., Lima, I., Xing, B., Gaskin, J. W., Steiner, C., Das, K. C., Ahmedna, M., Rehrh, D., Watts, D. W., Busscher, W. J., and Harry, S.: Characterization of designer biochar produced at different temperatures and their effects on a loamy sand. *Annals. Environ. Sci.* 3, 195–206, 2009.

Ok, Y.S., Yang, J.E., Zhang, Y.S., Kim, S.J., Chung, D.Y., 2007. Heavy metal adsorption by a formulated zeolite–Portland cement mixture. *J. Hazard. Mater.* 147, 91–96.

Overcash, M., Sims, R.C., Sims, J.L., and Nieman, J.K.C., 2005. Beneficial reuse and sustainability: The fate of organic compounds in land-applied waste. *Journal of Environmental Quality*, 34 (1), 29–41.

Palm, K., Luthman, K., Ungell, A.-L., Strandlund, G., Beigi, F., Lundahl, P., and Artursson, P., 1998. *Journal of Medicinal Chemistry*, 41, 5382–5392.

Pedersen, J.A., Soliman, M., and Suffet, I.H., 2005. Human pharmaceuticals, hormones, and personal care product ingredients in runoff from agricultural fields irrigated with treated wastewater. *Journal of Agricultural and Food Chemistry*, 53 (5), 1625–1632.

Pelekani, C., Snoeyink, V.L., 1999. Competitive adsorption in natural water: role of activated carbon pore size. *Water Res.* 33, 1209–1219.

Pierre M. J., Ghassem, Y., 1989. Essai au bleu de methylene et classification geotechnique des sols, *Bull, liaison Labo P. et Ch. Ref.* 3378.

Pomati, F., Castiglioni, S., Zuccato, E., Fanelli, R., Vigetti, D., Rossetti, C., and Calamari, D., 2006. Effects of a complex mixture of therapeutic drugs at environmental levels on human embryonic cells. *Environmental Science & Technology*, 40 (7), 2442–2447.

Qiu, Y., Zheng, Z., Zhou, Z., Sheng, G.D., 2009. Effectiveness and mechanisms of dye adsorption on a straw-based biochar. *Bioresour. Technol.* 100, 5348–5351.

Quintana, J.B., and Reemtsma, T., 2004. Sensitive determination of acidic drugs and triclosan in surface and wastewater by ion-pair reverse-phase liquid chromatography/tandem mass spectrometry. *Rapid Communications in Mass Spectrometry*, 18 (7), 765–774.

Quintana, J.B., Rodil, R., and Reemtsma, T., 2004. Suitability of hollow fibre liquid-phase micro extraction for the determination of acidic pharmaceuticals in wastewater by liquid chromatography-electrospray tandem mass spectrometry without matrix effects. *Journal of Chromatography, A* 1061 (1), 19–26.

Quintana, J.B., Weiss, S., and Reemtsma, T., 2005. Pathways and metabolites of microbial degradation of selected acidic pharmaceutical and their occurrence in municipal wastewater treated by a membrane bioreactor. *Water Research*, 39 (12), 2654–2664.

Ramesh, N., Jayakumar, K., Narayana, K., Vijayasarithi, S.K., 2002. A study on toxicity of diclofenac in dogs. *Indian Vet. J.*, 79, 668–671.

Revai, T., Harnos, G., 1999. Nephrotoxic syndrome and acute interstitial nephritis associated with the use of diclofenac. *Wien.Klin. Wochenschr.* 111 (13), 523–524.

Richards, S.M., Wilson, C.J., Johnson, D.J., Castle, D.M., Lam, M., Mabury, S.A., Sibley, P.K., and Solomon, K.R., 2004. Effects of pharmaceutical mixtures in aquatic microcosms. *Environmental Toxicology and Chemistry*, 23 (4), 1035–1042.

Roberts, P.H., and Thomas, K.V., 2006. The occurrence of selected pharmaceuticals in wastewater effluent and surface waters of the lower Tyne catchment. *Science of the Total Environment*, 356 (1–3), 143–153.

Rule, K.L., Ebbett, V.R., and Vikesland, P.J., 2005. Formation of chloroform and chlorinated organics by free-chlorine-mediated oxidation of triclosan. *Environmental Science & Technology*, 39 (9), 3176–3185.

Saeed, A., Akhter, M.W., Iqbal, M., 2005. Removal and recovery of heavy metals from aqueous solution using papaya wood as a new biosorbent. *Sep. Purif. Technol.* 45, 25–31.

Salih, H.H., Patterson, C.L., Sorial, G.A., Sinha, R., Krishnan, R., 2011. The fate and transport of the SiO<sub>2</sub> nanoparticles in a granular activated carbon bed and their impact on the removal of VOCs. *J. Hazard. Mater.* 193, 95–101.

Sanderson, H., Johnson, D.J., Reitsma, T., Brain, R.A., Wilson, C.J., and Solomon, K.R., 2004. Ranking and prioritization of environmental risks of pharmaceuticals in surface waters. *Regulatory Toxicology and Pharmacology*, 39 (2), 158–183.

Santos, J.L., Aparicio, I., Alonso, E., and Callejon, M., 2005. Simultaneous determination of pharmaceutically active compounds in wastewater samples by solid phase extraction and high-performance liquid chromatography with diode array and fluorescence detectors. *Analytica Chimica Acta*, 550 (1–2), 116–122.

Scheytt, T., Mersmann, P., Leidig, M., Pekdeger, A., and Heberer, T., 2004. Transport of pharmaceutically active compounds in saturated laboratory columns. *Ground Water*, 42 (5), 767–773.

Seitz, W., Jiang, J.Q., Weber, W.H., Lloyd, B.J., Maier, M., and Maier, D., 2006. Removal of iodinated X-ray contrast media during drinking water treatment, *Environmental Chemistry* 3 (1), 35–39.

Shackley, S., Carter, S., Knowles, T., Middelink, E., Haefele, S., Sohi, S., Cross, A., Haszeldine, S., 2012. Sustainable gasification-biochar systems? A case-study of rice-husk gasification in Cambodia, Part 1: Context, chemical properties, environmental and health and safety issues. *Energy Policy*, 42, 49–58.

- Singh, B.P., Cowie, A.L., Smernik, R.J., 2012. Biochar carbon stability in a clayey soil as a function of feedstock and pyrolysis temperature. *Environ. Sci. Technol.* 46, 11770–11778.
- Slack, R.J., Gronow, J., and Vulvulis, N., 2005. Household hazardous waste in municipal landfills: Contaminants in leachate. *Science of the Total Environment*, 337 (1–3), 119–137.
- Slack, R.J., Zerva, P., Gronow, J.R., and Voulvoulis, N., 2005. Assessing quantities and disposal routes for household hazardous products in the United Kingdom. *Environmental Science & Technology*, 39 (6), 1912–1919.
- Snyder, S.A., Leising, J., Westerhoff, P., Yoon, Y., Mash, H., and Vanderford, B., 2004. Biological and physical attenuation of endocrine disruptors and pharmaceuticals: Implications for water reuse. *Ground Water Monitoring and Remediation*, 24 (2), 108–118.
- Snyder, S.A., Westerhoff, P., Yoon, Y., and Sedlak, D.L., 2003. Pharmaceuticals, personal care products, and endocrine disruptors in water: Implications for the water industry. *Environmental Engineering Science*, 20 (5), 449–469.
- Song, W., and Guo, M., 2011. Quality variations of poultry litter biochar generated at different pyrolysis temperatures. *J. Anal. Appl. Pyrol.*, 94, 138–145.
- Spokas, K. A., 2010. Review of the stability of biochar in soils: predictability of O: C molar ratios. *Carbon Manage.* 1, 289–303.
- Stackelberg, P.E., Gibs, J., Furlong, E.T., Meyer, M.T., Zaugg, S.D., Lippincott, R.L., 2007. Efficiency of conventional drinking-water-treatment processes in removal of pharmaceuticals and other organic compounds. *Sci. Total Environ.* 377, 255–272.
- Sulaymon, A.H., Ahmed, K.W., 2008. Competitive adsorption of furfural and phenolic compounds onto activated carbon in fixed bed column, *Environ. Sci. Technol.* 42, 392–397.
- Suriyanon, N., Punyapalukul, P., Ngamcharussrivichai, C., 2013. Mechanistic study of diclofenac and carbamazepine adsorption on functionalized silica-based porous materials. *Chem. Eng. J.* 214, 208–218.
- Swan, G., Naidoo, V., Cuthbert, R., Green, R.E., Pain, D.J., Swarup, D., Prakash, V., Taggart, M., Bekker, L., Das, D., Diekmann, J., Diekmann, M., Killian, E., Meharg, A., Patra, R.C., Saini, M., and Wolter, K., 2006. Removing the threat of diclofenac to critically endangered Asian vultures. *Plos Biology*, 4 (3), 395–402.
- Teixido, M., Pignatello, J.J., Beltran, J.L., Granados, M., Peccia, J., 2011. Speciation of the ionizable antibiotic sulfamethazine on black carbon (biochar). *Environ. Sci. Technol.* 45, 10020–10027.

- Ternes, T.A., 1998. Occurrence of drugs in German sewage treatment plants and rivers. *Water Res.* 32 (11), 3245–3260.
- Ternes, T.A., 2001. Occurrence of pharmaceuticals in surface waters. *Vorkommen Von Pharmaka in Gewässern. Wasser & Boden* 53 (4), 9–14.
- Tom Tague, Bruker Optics Inc., Infrared Spectral Interpretation ([www.bruker.com](http://www.bruker.com)). Date retrieved: 2016/02/11.
- Triebkorn, R., Casper, H., Heyd, A., Eikemper, R., Köhler, H.R., Schwaiger, J., 2004. Toxic effects of the non-steroidal anti-inflammatory drug diclofenac. Part II. Cytological effects in liver, kidney, gills and intestine of rainbow trout (*Oncorhynchus mykiss*). *Aquatic Toxicology*. 68, 151–166.
- Valladares L. R., Quintanilla, V.Y., Li, Z., Amy, G., 2011. Rejection of micropollutants by clean and fouled forward osmosis membrane. *Water Res.* 45, 6737–6744.
- Venkata, S.M., Ramanaiah, S.V., Rajkumar, B., Sarma, P.N., 2007a. Removal of fluoride from aqueous phase by biosorption onto algal biosorbent *Spirogyra* sp. I02: sorption mechanism elucidation. *J. Hazard. Mater.* 141, 465–474.
- Venkata, S.M., Ramanaya, S.V., Rajkumar, B., Sarma, P.N., 2007b. Biosorption of fluoride from aqueous phase onto algal *Spirogyra* sp. and evaluation of adsorption kinetics. *Bioresour. Technol.* 98, 1006–1011.
- Verenitch, S.S., Lowe, C.J., and Mazumder, A., 2006. Determination of acidic drugs and caffeine in municipal wastewaters and receiving waters by gas chromatography-ion trap tandem mass spectrometry. *Journal of Chromatography A*. 1116 (1–2), 193–203.
- Verstraeten, I.M., Fetterman, G.S., Meyer, M.T., Bullen, T., and Seabee, S.K., 2005. Use of tracers and isotopes to evaluate vulnerability of water in domestic wells to septic waste. *Ground Water Monitoring and Remediation*, 25 (2), 107–117.
- Wei, Z., Seo, Y., 2010. Trichloroethylene (TCE) adsorption using sustainable organic mulch. *J. Hazard. Mater.* 181, 147–153.
- Westerhoff, P., Yoon, Y., Snyder, S., and Wert, E., 2005. Fate of endocrine-disruptor, pharmaceutical, and personal care product chemicals during simulated drinking water treatment processes. *Environmental Science & Technology*. 39 (17), 6649–6663.
- Xia, K., Bhandari, A., Das, K., and Pillar, G., 2005. Occurrence and fate of pharmaceuticals and personal care products (PPCPs) in biosolids. *Journal of Environmental Quality*. 34 (1), 91–104.
- Xu, J., Chen, W.P., Wu, L.S., Green, R., Chang, A.C., 2009a. Leachability of some emerging contaminants in reclaimed municipal wastewater irrigated turf grass fields. *Environ. Toxicol. Chem.* 28, 1842–1850.

- Xu, J., Wub, L., Chang, C. A., 2009. Degradation and adsorption of selected pharmaceuticals and personal care products (PPCPs) in agricultural soils. *Chemosphere*, 77, 1299–1305.
- Xu, T., Lou, L., Luo, L., Cao, R., Duan, D., Chen, Y., 2012. Effect of bamboo biochar on pentachlorophenol leachability and bioavailability in agricultural soil. *Sci. Total Environ.* 414, 727–731.
- Yang, H., Yan, R., Chen, H., Lee, H. D., Zheng, C., 2007. Characteristics of hemicellulose, cellulose and lignin pyrolysis. *Science Direct. Fuel* 86, 1781–1788.
- Yang, J.E., Skogley, E.O., Ok, Y.S., 2011. Carbonaceous resin capsule for vapor-phase monitoring of volatile monoaromatic hydrocarbons in soil. *Soil Sediment Contam.* 20, 205–220.
- Yang, K. and Xing, B., 2009. Adsorption of fulvic acid by carbon nanotubes from water. *Environmental pollution*, vol 157, no. 4, pp 1095-1100.
- Yoon, Y., Westerhoff, P., Snyder, S.A., Esparza, M., 2003. HPLC-fluorescence detection and adsorption of bisphenol A, 17 $\beta$ -estradiol, and 17 $\alpha$ -ethynyl estradiol on powdered activated carbon. *Water Res.* 37, 3530–3537.
- Zhang, H., Lin, K., Wang, H., Gan, J., 2010. Effect of Pinus radiata derived biochars on soil sorption and desorption of phenanthrene. *Environ. Pollut.* 158, 2821–2825.
- Zuccato, E., Castiglioni, S., and Fanelli, R., 2005. Identification of the pharmaceuticals for human use contaminating the Italian aquatic environment. *Journal of Hazardous Materials.* 122 (3), 205–209.
- Zuehlke, S., Duennbier, U., Heberer, T., and Fritz, B., 2004. Analysis of endocrine disrupting steroids: Investigation of their release into the environment and their behavior during bank filtration. *Ground Water Monitoring and Remediation.* 24 (2), 78–85.



## Chapter 6

### 6 Conclusions and Recommendations

#### 6.1 Conclusions

The following conclusions can be drawn from this study:

1. Immobilization of Degussa P25 catalyst was achieved successfully as a uniform thickness layer of coating could be obtained with 2%, 4% and 20%.
2. All the optimized conditions were fed into the reactor for degradation of PPCP compounds [ $O_3=2\text{ppm}$ ,  $TiO_2 = 1\text{g/m}^2$ ,  $UV = 13\text{W}$ ] in secondary effluent.
3. A comparison of various AOPs conducted on secondary effluent revealed that  $O_3/UV/TiO_2$  was able to remove 99.9% of ATN in 90 min, 99.5% of CFA in 30min and 99.9% of DCF in 15min respectively. Hence  $O_3/UV/TiO_2$  is considered as the best treatment option for the removal of these PPCP compounds from secondary effluent.
4. 100% ATN removal could be achieved in 60 min by increasing the pH from 7 to 9.
5. The concentration of organic matter and various ions in secondary effluent had negligible effect in percent removal of ATN, CFA and DCF.
6.  $In_2O_3$  microspheres, nanocubes, nanoplates and nano crystals were synthesized successfully as revealed by FE-SEM images.
7. Among the various  $In_2O_3$  nanoparticles synthesized, porous microspheres exhibited the maximum removal efficiency with 99.9% ATN in 60 min compared to 68.5% by  $UV/TiO_2$ , 80.4% by  $O_3/TiO_2$  and 99.3% by  $O_3/UV/TiO_2$  in 90 min at pH 7.

8. Removal efficiency was almost same between MS, NC, NP and O<sub>3</sub>/UV/TiO<sub>2</sub> for DCF as 100% removal was achieved in 15 min except NCY which showed only 98.6% in 15 min.
9. For CFA, the percent removal was 100% by MS in 30min and 100% by O<sub>3</sub>/UV/TiO<sub>2</sub> in 60 min and 99.8% by UV/TiO<sub>2</sub> and 60.4% by O<sub>3</sub>/TiO<sub>2</sub> in 90min.
10. The activity of other nanoparticles such as NC, NP and NCY were almost slightly lower to MS and shows that all these nanoparticles were highly effective in removal of PPCP compounds from secondary effluent.
11. Biochar was prepared successfully by calcining it at 700°C. The surface morphology of BC characterized by FESEM showed honeycomb like structure with several pores of <0.1µm to 20-20µm.
12. Adsorption studies with BC showed that PPCP compounds can be effectively removed from secondary effluents. The removal efficiency was increased by 1.24 times for ATN by pre-conditioning of BC with 0.1N NaCl.
13. ATN removal was 44.1% at pH 3 which increased to 82.3% by increasing the pH to 9 at 1 g/L adsorbent dosage. Similarly, CFA and DCF exhibited higher removal efficiency at 88.2% and 99.2% at pH 3 compared to 54.1% and 73.9% at pH 9 respectively.
14. A mixed adsorbent with 1:1 BC:Chb showed removal efficiency of 34.3% at pH 3 compared to 66.1% at pH 9 whereas for CFA and DCF, 82.1% and 99.5% was observed at pH 3 compared to 50.9% and 72.4% at pH 9 respectively for 1 g/L adsorbent dosage.
15. By pre-conditioning, ATN removal increased after pre-conditioning from 44.1% to 54.9% at pH 3 whereas observed slight increase from 82.3% to 86.7% at pH 9. Similarly, for CFA and DCF, the maximum removal efficiency was found to be 95.2% and 99.4% at pH 3 compared to 88.2% and 99.2% respectively at 1g/L adsorbent dosage.

16. Chemical activation of BC by KOH showed maximum removal efficiency of 87.5%, 64% and 81.8% for ATN, CFA and DCF respectively at pH 9 for 1 g/L adsorbent dosage.
17. The percent removal efficiency for various adsorption methods follows the order as BC-KOH > BC-Pre-conditioned > BC > BC-Chb.
18. Percent removal efficiency followed the order as DCF > CFA > ATN for pH at 3 > 5 > 7 > 9 whereas a reverse trend was observed for ATN at pH 9 > 7 > 5 > 3.

## 6.2 Recommendations

1. Increasing the catalyst loadings to 40 – 50% would reduce the number of dip-coating and drying cycles.
2. Other PPCP compounds that show very low degradation rates can also be studied for their kinetics.
3. Photodegradation rates will provide an insight to the environmental life time of such chemicals in natural water.
4. Increasing the concentration of HA, nitrates and chlorides can be studied further to gather more information on the efficiency of O<sub>3</sub>/UV/TiO<sub>2</sub>.
5. Photocatalytic efficiency of O<sub>3</sub>/UV/TiO<sub>2</sub> can be studied further by increasing the NOM concentration to 25, 50, 100 and 250ppm.
6. Cost-benefit analysis of preparation of immobilized catalyst and use of O<sub>3</sub>/UV/TiO<sub>2</sub> at an industrial scale should be considered.

7. Synthesis of  $\text{In}_2\text{O}_3$  nanoparticles is a lengthy process and lowering the time to autoclave or increasing the reactor temperature may be an alternate procedure to speed up the reaction of synthesis but requires optimization.
8. Efficiency of BC can be improved by altering pyrolysis temperatures of biochar based on the type of wood material chosen, type of PPCP compounds selected and type of wastewater.
9. Steam activation can be an alternative method for chemical activation to study the percent removal of PPCPs.

## Appendices

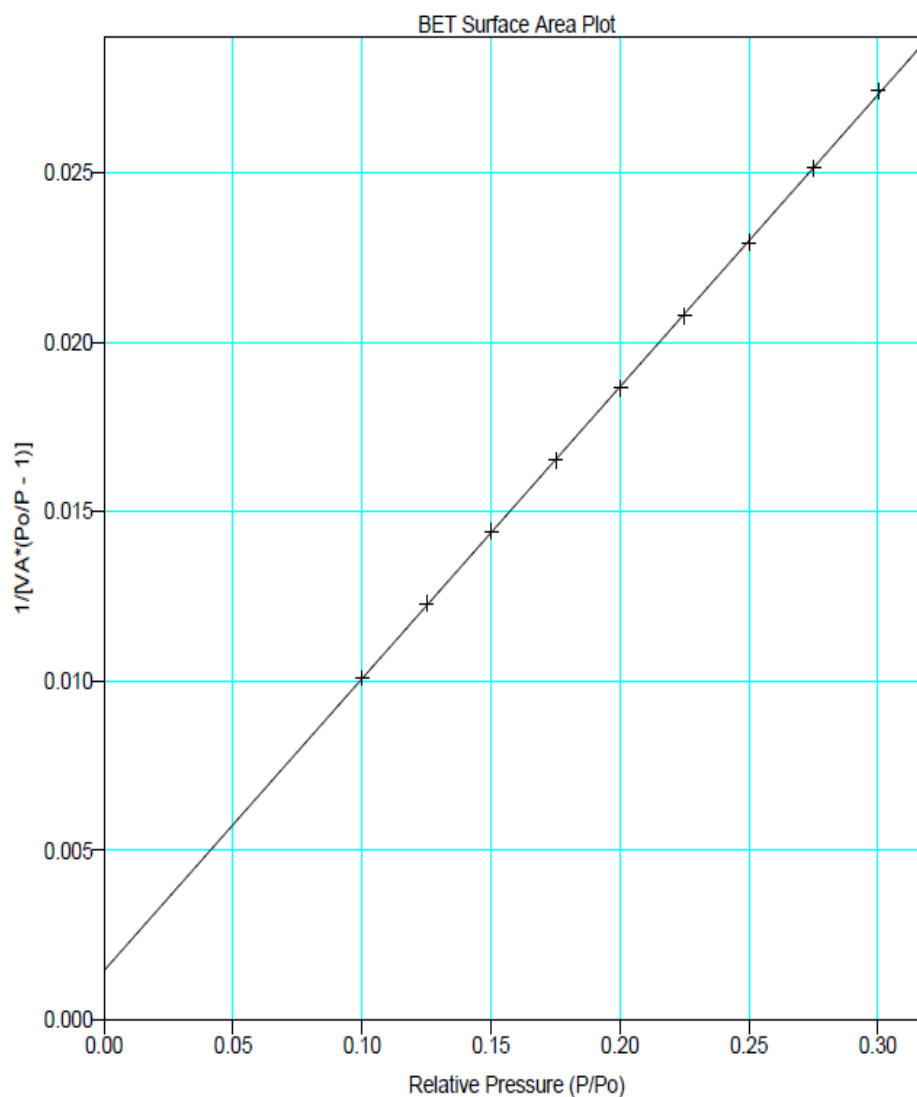
Appendix 1. Average monthly water quality (raw and treated) reported by Adelaide Wastewater Treatment Plant, 2014

| Parameters                              | Results, mg/L | Results, mg/L |
|---|---------------|---------------|
|   | Raw           | UV Channel    |
| pH                                      | 7.5           | 7.3           |
| Temperature, °C                         | 22            | 16.5          |
| E. Coli orgs./100mL                     | NA            | 43            |
| Dissolved Oxygen                        | NA            | 7.4           |
| Biochemical Oxygen Demand               | 129           | 3             |
| Total Suspended Solids                  | 153           | 3             |
| Free Ammonia                            | 18.1          | 0.4           |
| Nitrate as NO <sub>3</sub> <sup>-</sup> | NA            | 16.4          |
| Nitrite as NO <sub>2</sub> <sup>-</sup> | 0.7           | 0.6           |
| Total Kjeldahl Nitrogen (TKN)           | 29.1          | 2.0           |
| Phosphorus                              | 4.2           | 0.59          |
| Alkalinity as CaCO <sub>3</sub>         | 263           | 122           |

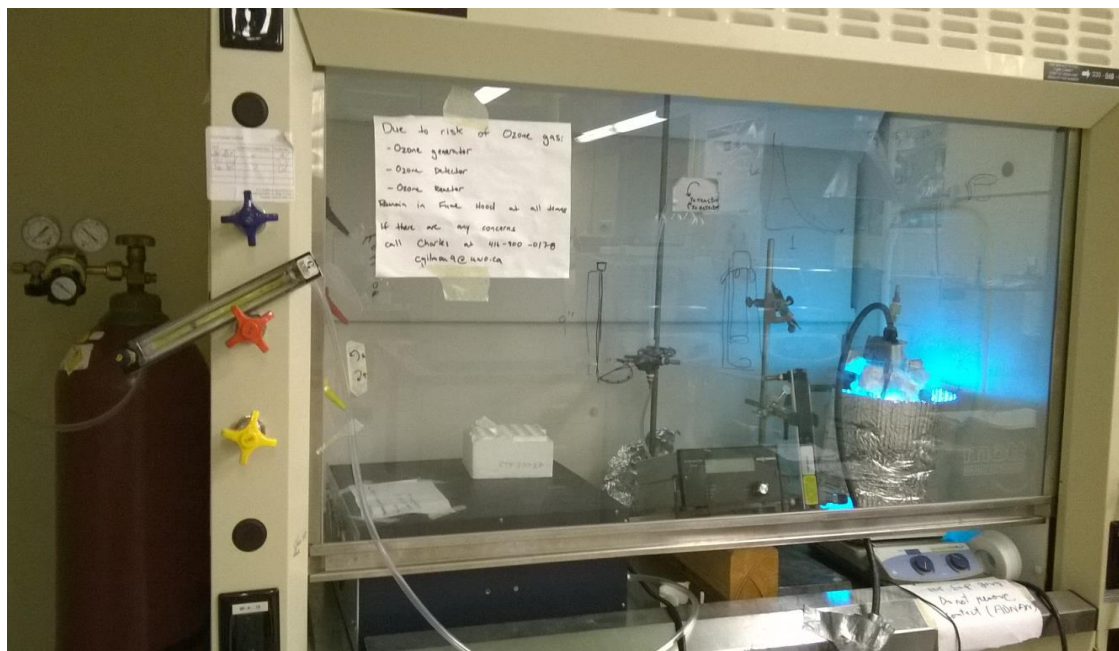
Note: All the above values are reported in mg/L except pH, Temperature and E. Coli  
 NA: Not Available

File Name: C:/STARDRV/DEC8S314.MGD  
Sample ID: 4-3  
Setup Group: None

Started: Sat. Pressure: 760.00 mmHg  
Completed: Meas. Freespace: -0.1445 cm<sup>3</sup>  
Report Time: 12/8/2014 4:39:35PM Sample Weight: 0.3122 g  
Evac. Rate: 500.0 mmHg/min Evac. Time: 3.000000 minutes  
Analysis Mode: Equilibration Equil. Interval: 5 secs



Appendix 2. BET Surface Area for TiO<sub>2</sub> film after calcination



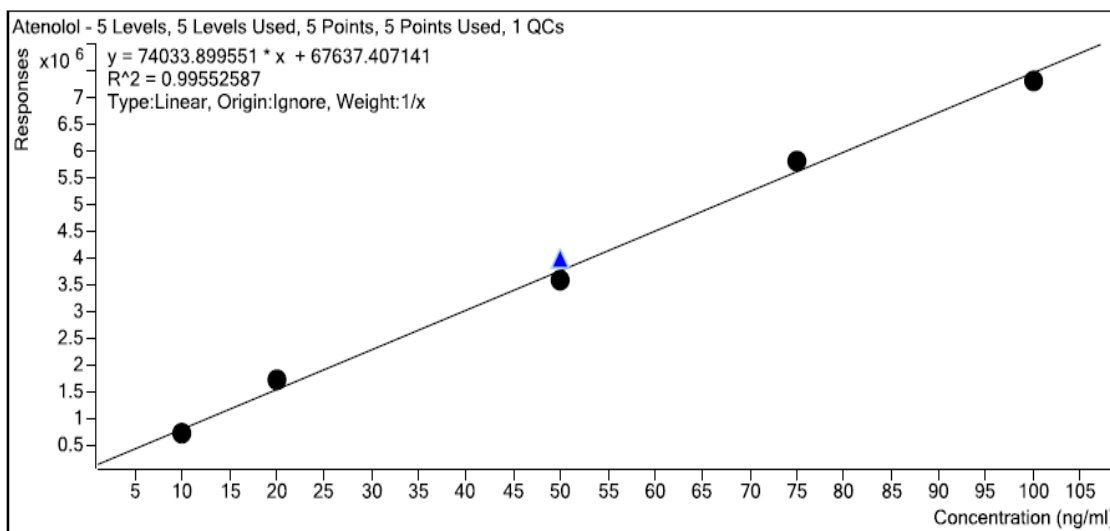
Appendix 3. Reactor setup showing the wastewater spiked with PPCP compounds subjected to  $O_3/UV/TiO_2$



Appendix 4. Agilent 6460 LC-MS/MS (High Resolution)

**Calibration Curve**

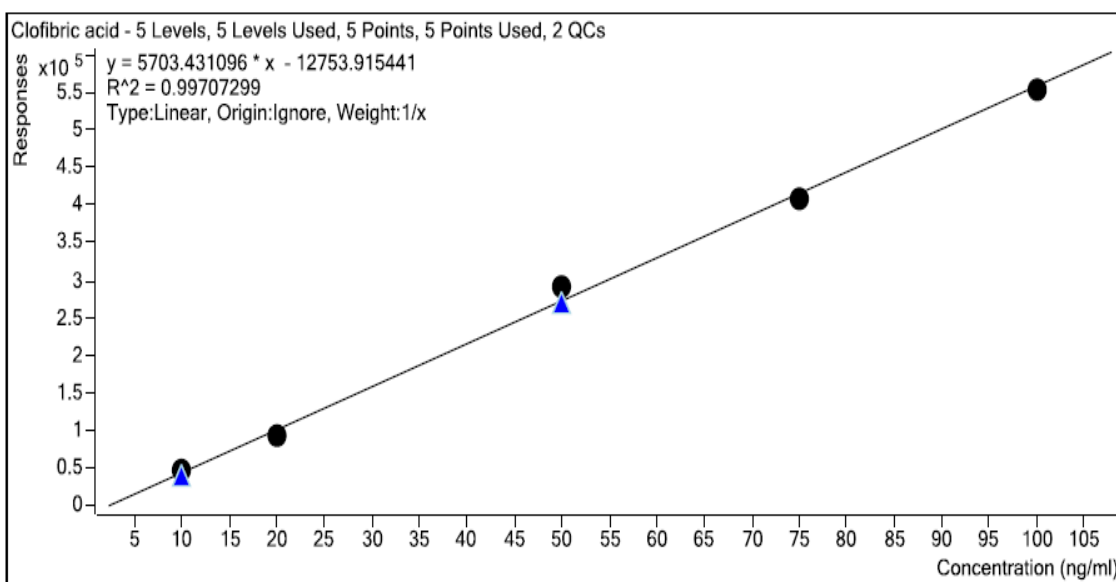
Atenolol



Appendix 5. A five point calibration curve for Atenolol with conc. of 10, 20, 50, 75 and 100 ng/ml

**Calibration Curve**

Clofibric acid

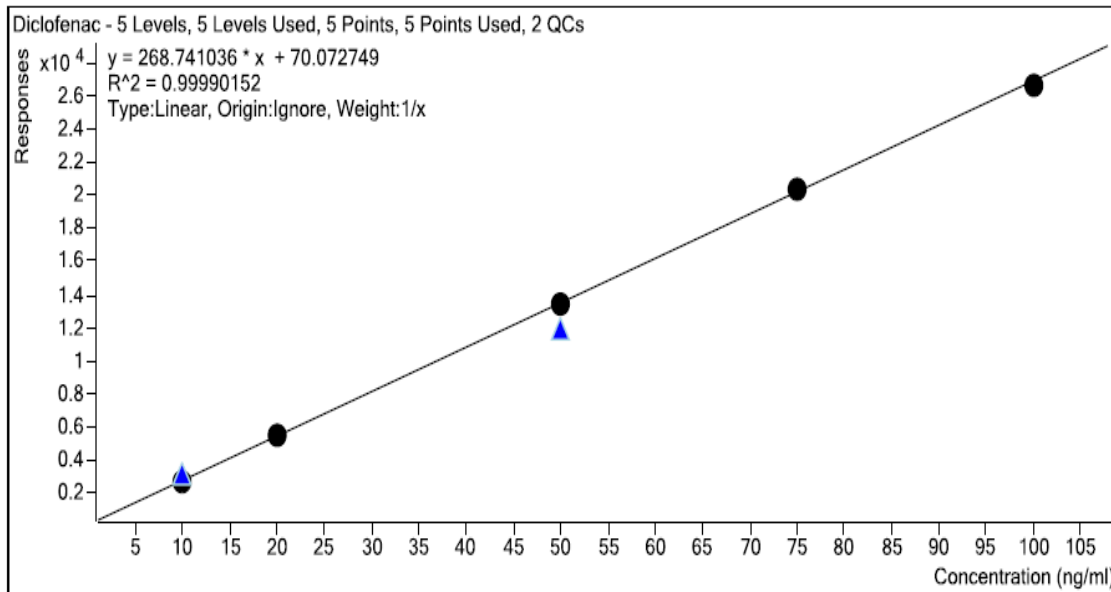


Appendix 6. A five point calibration curve for Clofibric acid with conc. of 10, 20, 50, 75 and 100 ng/ml



### Calibration Curve

Diclofenac



Appendix 7. A five point calibration curve for Diclofenac with conc. of 10, 20, 50, 75 and 100 ng/ml

Appendix 8. A comparison of various AOPs with their percent removal

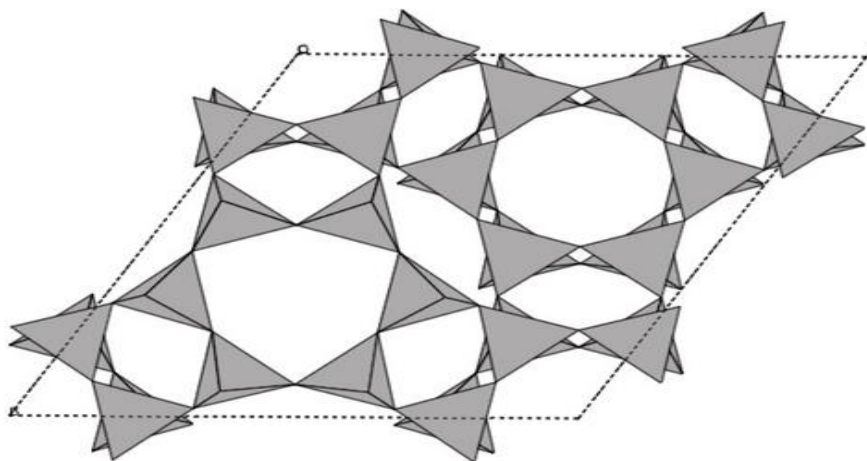
| PPCPs →                             | ATN                 | CFA                 | DCF            |
|-------------------------------------|---------------------|---------------------|----------------|
| AOP↓                                | % Removal in 90 min | % Removal in 90 min | % Removal      |
| UV                                  | 32.2                | 97.3                | 99.9 in 30 min |
| O <sub>3</sub>                      | 52.3                | 13.0                | 100 in 30 min  |
| UV/O <sub>3</sub>                   | 59.0                | 99.4                | 99.4 in 60 min |
| UV/TiO <sub>2</sub>                 | 68.5                | 99.8                | 99.8 in 30 min |
| O <sub>3</sub> /TiO <sub>2</sub>    | 80.4                | 60.4                | 100 in 60 min  |
| O <sub>3</sub> /UV/TiO <sub>2</sub> | 99.9                | 99.5 in 30min       | 99.9 in 15 min |

Appendix 9. Effect of pH on the percent removal of ATN using various AOPs

| PPCPs →<br><br>AOP↓                 | ATN<br>% Removal in 90 min |              |              |
|-------------------------------------|----------------------------|--------------|--------------|
|                                     | pH = 7                     | pH = 8       | pH = 9       |
| UV/TiO <sub>2</sub>                 | 68.5                       | 74.4         | 78.4         |
| O <sub>3</sub> /TiO <sub>2</sub>    | 80.4                       | 91.6         | 92.8         |
| O <sub>3</sub> /UV/TiO <sub>2</sub> | 99.3                       | 100 in 60min | 100 in 60min |

Appendix 10. Comparison of various AOPs on degradation of PPCPs in presence of varying concentrations of NOM and Br

| PPCPs                               | ATN                           |                               | CFA                           |                               | DCF                           |                               |
|-------------------------------------|-------------------------------|-------------------------------|-------------------------------|-------------------------------|-------------------------------|-------------------------------|
|                                     | NOM<br>4ppm +<br>Br<br>0.1ppm | NOM<br>8ppm +<br>Br<br>0.3ppm | NOM<br>4ppm +<br>Br<br>0.1ppm | NOM<br>8ppm +<br>Br<br>0.3ppm | NOM<br>4ppm<br>+ Br<br>0.1ppm | NOM<br>8ppm<br>+ Br<br>0.3ppm |
| UV/TiO <sub>2</sub>                 | 55.4%<br>in 90 min            | 48.4%<br>in 90 min            | 98.6%<br>in 90 min            | 98.4%<br>in 90 min            | 99.5%<br>in 30 min            | 99.8%<br>in 60 min            |
| O <sub>3</sub> /TiO <sub>2</sub>    | 73.5%<br>in 90 min            | 70.4%<br>in 90 min            | 46.3%<br>in 90 min            | 41.0%<br>in 90min             | 99.3%<br>in 60 min            | 99.8%<br>in 90 min            |
| O <sub>3</sub> /UV/TiO <sub>2</sub> | 99.2%<br>in 90 min            | 98.9%<br>in 90min             | 100%<br>in 60 min             | 100%<br>in 90 min             | 99.8%<br>in 15 min            | 99.5%<br>in 15 min            |



### Appendix 11. Crystal Structure of Chabazite

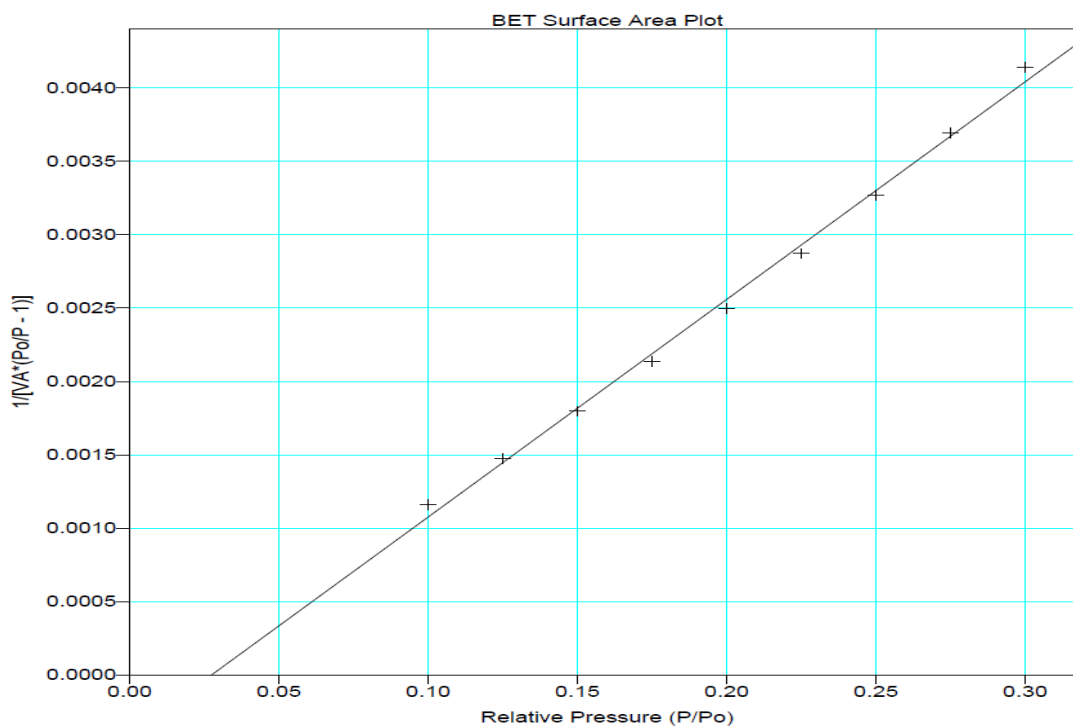
```

File Name: C:/STARDRV/DEC8S114.MGD
Sample ID: Charcoal
Setup Group: None

Started:
Completed: 12/8/2014 2:15:18PM
Report Time: 12/8/2014 2:15:18PM
Evac. Rate: 500.0 mmHg/min
Analysis Mode: Equilibration

Sat. Pressure: 760.00 mmHg
Meas. Freespace: 0.1184 cm³
Sample Weight: 0.5306 g
Evac. Time: 3.000000 minutes
Equil. Interval: 5 secs

```



Appendix 12. BET Surface Area plot for Biochar sample pyrolyzed at 700oC

File Name: C:/STARDRV/DEC8S114.MGD  
 Sample ID: Charcoal  
 Setup Group: None

Started: Sat. Pressure: 760.00 mmHg  
 Completed: Meas. Freespace: 0.1184 cm<sup>3</sup>  
 Report Time: 12/8/2014 2:15:18PM Sample Weight: 0.5306 g  
 Evac. Rate: 500.0 mmHg/min Evac. Time: 3.000000 minutes  
 Analysis Mode: Equilibration Equil. Interval: 5 secs

---

BET Surface Area Report

BET Surface Area: 301.7311 ± 7.2048 m<sup>2</sup>/g  
 Slope: 0.014835 ± 0.000337  
 Y-Intercept: -0.000408 ± 0.000071  
 C: -35.398805  
 VM: 69.312497 cm<sup>3</sup>/g STP  
 Correlation Coefficient: 9.981973e-01

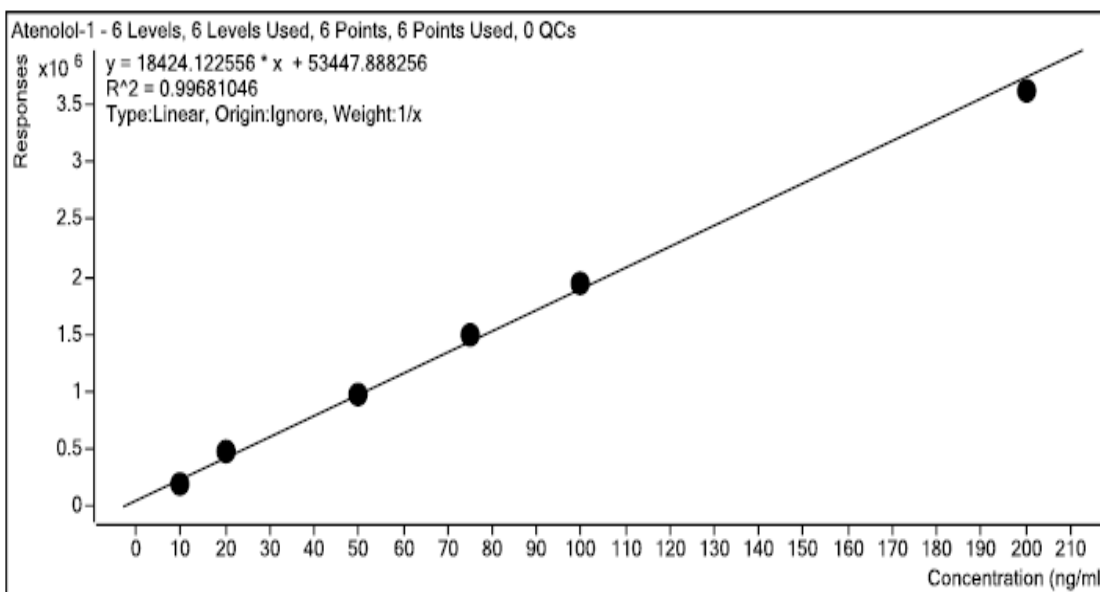
Molecular Cross-section: 0.1620 nm<sup>2</sup>

| Relative Pressure | Vol Adsorbed (cm <sup>3</sup> /g STP) | 1/[VA*(Po/P - 1)] |
|-------------------|---------------------------------------|-------------------|
| 0.100006575       | 95.6243                               | 0.001162          |
| 0.125052633       | 97.0221                               | 0.001473          |
| 0.150046057       | 98.2106                               | 0.001798          |
| 0.175032887       | 99.2757                               | 0.002137          |
| 0.200046057       | 100.2402                              | 0.002495          |
| 0.225052623       | 101.1301                              | 0.002872          |
| 0.250026321       | 101.9361                              | 0.003270          |
| 0.275065793       | 102.7565                              | 0.003693          |
| 0.300052623       | 103.5147                              | 0.004141          |

Appendix 13. BET Surface Area Report with pore volume for Biochar samples

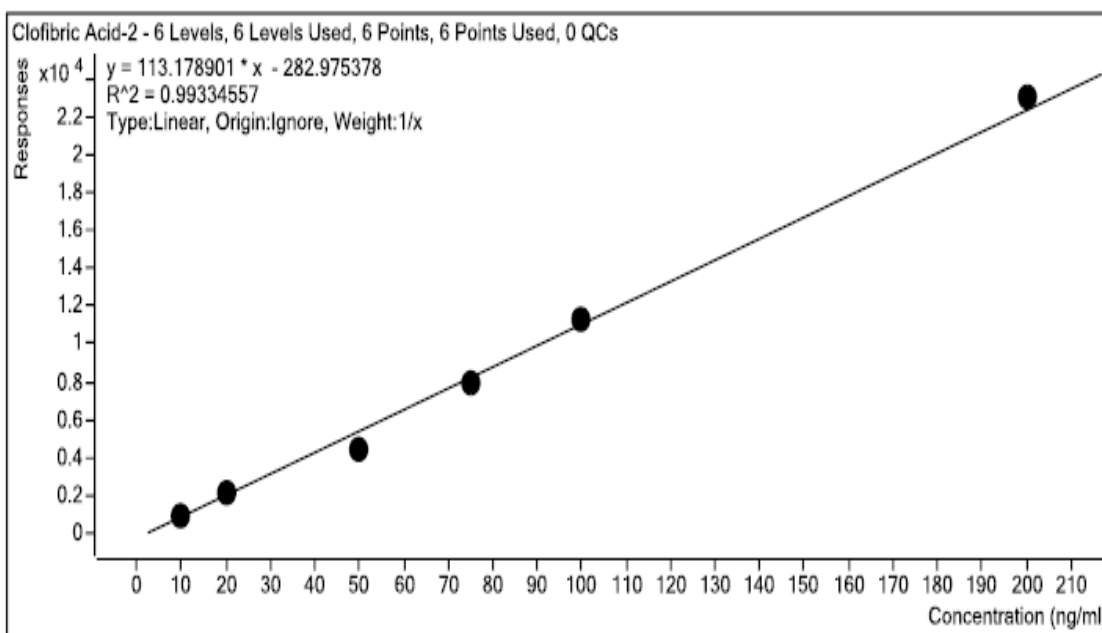
**Calibration Curve**

Atenolol-1

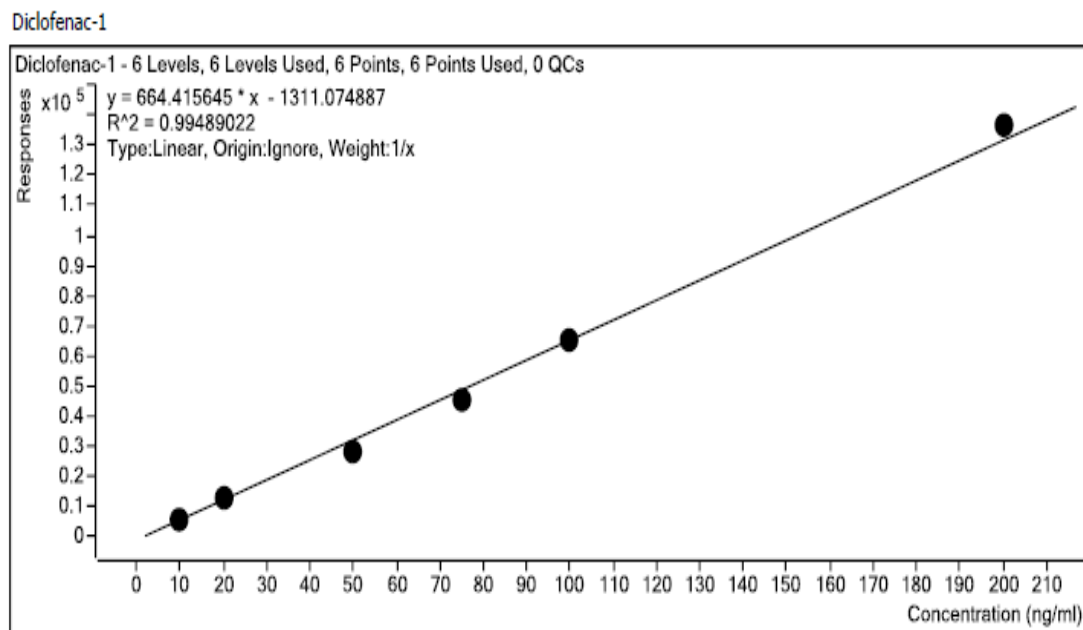


Appendix 14. A six point calibration curve for Atenolol with conc. of 10, 20, 50, 75, 100 and 200 ng/ml

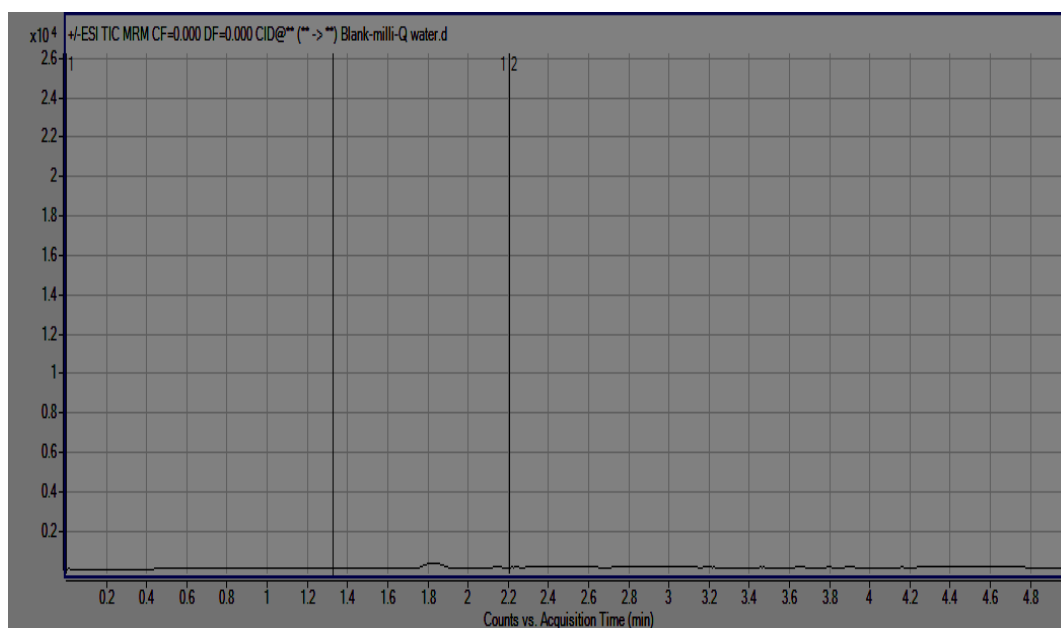
Clofibric Acid-2



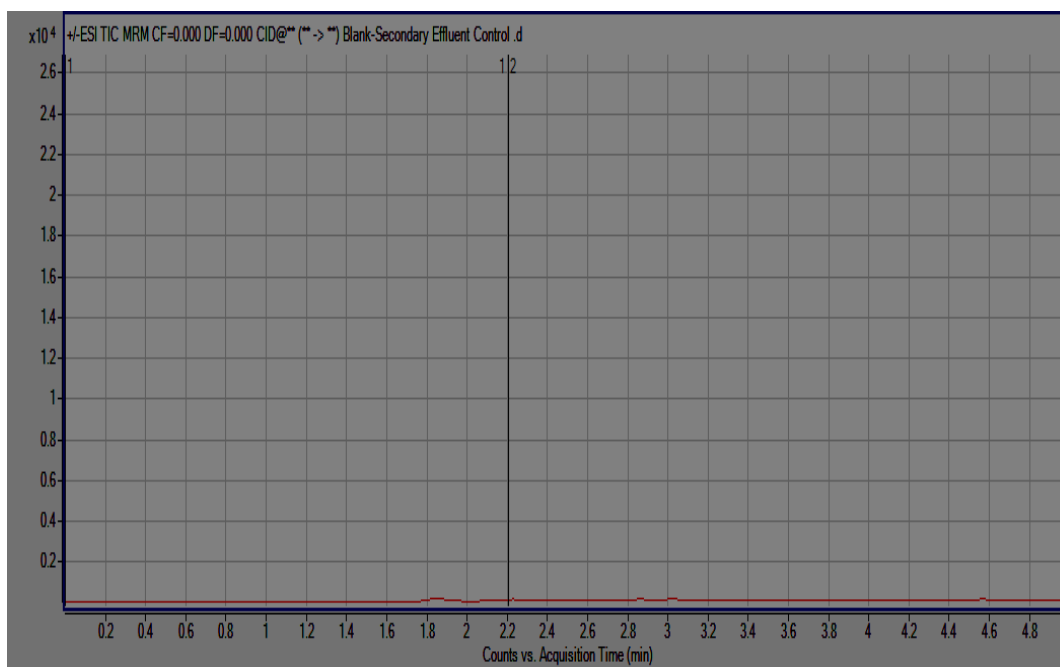
Appendix 15. A six point calibration curve for Clofibric Acid with conc. of 10, 20, 50, 75, 100 and 200 ng/ml



Appendix 16. A six point calibration curve for Diclofenac with conc. of 10, 20, 50, 75, 100 and 200 ng/ml



Appendix 17. Blank Milli-Q water chromatogram by LC-MS/MS



Appendix 18. Secondary Effluent chromatogram by LC-MS/MS (baseline study)

## Curriculum Vitae

Name: Venkateswara Reddy Kandlakuti

Post-secondary Education and Degrees: The University of Western Ontario  
London, Ontario, Canada  
2007-2008 M. Eng.

The University of Western Ontario  
London, Ontario, Canada  
2010-2016 Ph.D.

Related Work Experience: Teaching Assistant  
The University of Western Ontario  
London, Ontario, Canada  
2010-2016

Research Assistant  
The University of Western Ontario  
London, Ontario, Canada  
2010-2016

### Publications:

V.R. Kandlakuti and E.K. Yanful. Preparation of Biochar, its characterization and application in removal of PPCPs from wastewater with comparison to natural zeolites. (To be submitted to Journal of Hazardous Materials).